Assessing anti-tumour immunity and adoptive T cell therapies in solid tumours

Oliver Liang

A thesis submitted in fulfillment of the requirements for the degree of

Master of Philosophy

Supervisors: Dr. Dannel Yeo and Associate Professor Kate Mahon

Faculty of Medicine and Health

The University of Sydney

2025

Statement of originality

This is to certify that the content presented in this thesis is, to the best of my knowledge, my original work, except as acknowledged in the text.

I certify that the intellectual content of this thesis is the product of my own work, and that all assistance received in preparing this thesis and all sources have been acknowledged.

Dr. Amy White performed immunohistochemistry staining for mesothelin on the human pancreatic cancer tissue microarray samples analysed in Chapter 3. Immunohistochemistry staining for CD3, CD8, and CD68 on human pancreatic cancer whole-tissue samples, analysed in Chapter 3, was undertaken at New South Wales Pathology, Royal Prince Alfred Hospital. Dr. Timony Fielder and Dr. Joo-Shik Shin conducted scoring of immunohistochemistry staining on both the human pancreatic cancer tissue microarray and whole-tissue samples analysed in Chapter 3.

The Precision Oncology Program, Centenary Institute established the patient-derived appendiceal cancer organoids and provided the bulk RNA-sequencing data of appendiceal cancer organoids analysed in Chapter 4. Dr. Madeleine Strach provided the single cell RNA-sequencing data of appendiceal cancer analysed in Chapter 4. Dr. Dannel Yeo provided the viral supernatant for the generation of CAR T cells used in Chapter 4. Dr. Chuck Bailey, Ms Rajini Nagarajah, and Dr. Gerard Chu performed the design and synthesis of CAR constructs, as well as the generation of virus-producing cells.

No part of this work has been presented for award of any other degree or diploma at any educational institution.

Oliver Liang

29 September 2025

Acknowledgements

My postgraduate degree has been a journey of learning, and a journey of learning, by itself, is a journey of growth.

I would like to acknowledge sincerely my primary supervisor, Dr. Dannel Yeo. The completion of this thesis would not have been possible without your ongoing support. I am also grateful for the guidance from my auxiliary supervisor, Associate Professor Kate Mahon and mentor, Dr. Sharon Sagnella. Your advice has always been invaluable. Thank you all for your supervision and mentorship.

I would also like to acknowledge the support of individuals who have contributed significantly to the current work. In particular, I want to thank Dr. Amy White, Dr. Timony Fielder, and Dr. Joo-Shik Shin, for staining and scoring the human pancreatic cancer tissue samples; Dr. Madeleine Strach, for kindly providing appendiceal cancer single-cell RNA-sequencing data; and Associate Professor Ulf Schmitz, for offering insightful feedback on my bioinformatic analyses.

To past and current members from the Precision Oncology Lab, my time with you all have filled my research with joy and I cannot express how grateful I am to be in your company, every day. I will miss you all dearly.

To my family and close friends, thank you for always listening to me, through good times and bad. With you, I feel heard, understood, and never alone. Thank you for your unconditional support, it is what allows me to carry on.

Lastly, I would like to thank myself. Thank you for always putting out your best and showing what you are capable of. You have grown so much to become the version you wanted to be. I hope the memories and lessons you gained along the way will guide you well in your journey ahead.

Authorship attribution statement

Chapter 3 of this thesis has been adapted and expanded from a manuscript that was submitted and recently accepted for publication (Liang O, et al., *High mesothelin expression is associated with low cytotoxic T cell infiltration in pancreatic cancer*, submitted to *Frontiers in Immunology* on 22nd June 2025; accepted 25th September 2025). Introduction and methodologies described in the manuscript have also been incorporated into Chapters 1 and 2 of this thesis, respectively. I designed the study, analysed the data, and drafted/revised the manuscript.

In addition to the authorship attribution statements above, in cases where I am not the corresponding author of a published item, permission to include the published material has been granted by the corresponding author.

Student: Oliver Liang

29 September 2025

As supervisor for the candidature upon which this thesis is based, I can confirm that the authorship attribution statements above are correct.

Lead Supervisor: Dannel Yeo

29 September 2025

Generative AI attribution statement

During the preparation of the thesis the author used ChatGPT for the purposes of text enhancement. The use of this generative AI tool includes spelling corrections and minor sentence restructuring. The author confirms that where text was modified by generative AI, the content was reviewed for possible errors, inaccuracies, and bias. The author takes full responsibility for the submitted thesis and ensures the work is their own and has used generative AI within the parameters of use permitted by the University guidelines and policies.

Australian government support statement

This research was supported by an Australian Government Research Training Program (RTP) Fee Offset Scholarship and also by the Postgraduate Research Scholarship in Building Expertise and Capability in Cell and Gene Therapies, funded jointly by New South Wales (NSW) Health and the University of Sydney.

Index of Tables

Index of Figures

List of abbreviations

AA	Appendiceal adenocarcinoma
ALL	Acute lymphoblastic leukemia
AMN	Appendiceal mucinous neoplasm
ANOVA	Analysis of variance
APC	Antigen-presenting cell
Breg	Regulatory B cell
CAF	Cancer-associated fibroblast
CAR	Chimeric antigen receptor
CD	Cluster of differentiation
CP	Cyclophosphamide
CR	Complete remission
CRS	Cytoreductive surgery
CTLA-4	Cytotoxic T-lymphocyte associated protein 4
DAPI	4′,6-diamidino-2-phenylindole
DC	Dendritic cell
DMEM	Dulbecco's Modified Eagle Medium
DMSO	Dimethyl sulfoxide
ECM	Extracellular matrix
ELISA	Enzyme-linked immunosorbent assay
FA	Fludarabine
FACS	Fluorescence-Activated Cell Sorting
FBS	Fetal bovine serum
FFPE	Formalin-Fixed, Paraffin-Embedded
GvHD	Graft-versus-host disease
HIPEC	Hyperthermal intraperitoneal chemoperfusion
HLA	Human leukocyte antigen
ICI	Immune checkpoint inhibitor
IFN-γ	Interferon-gamma
IHC	Immunohistochemistry
IL	Interleukin
IPMN	Intraductal papillary mucinous neoplasm
LNP	Lipid nanoparticles
MDSC	Myeloid-derived suppressor cells
MFI	Median fluorescent intensity
MOI	Multiplicity of infection
MPF	Megakaryocyte potentiating factor
MSI	Microsatellite instability

MSLN	Mesothelin
MUC1	Mucin-1
MUC16	Mucin-16
NMA-LD	Non-myeloablative lymphodepletion
ORR	Objective response rate
OS	Overall survival
PanIN	Pancreatic Intraepithelial Neoplasia
PBMC	Peripheral blood mononuclear cell
PBS	Phosphate buffered saline
PD	Progressive disease
PD-1	Programmed cell death protein 1
PDAC	Pancreatic ductal adenocarcinoma
PFS	Progression-free survival
PMP	Pseudomyxoma peritonei
PR	Progressive disease
PSMA	Prostate-specific membrane antigen
R/R	Relapsed/refractory
REP	Rapid expansion protocol
RFS	Relapse-free survival
RNA-seq	RNA sequencing
RPMI	Roswell Park Memorial Institute
RTCA	Real-time Cell Analysis
scFv	Single chain variable fragment
scRNA-seq	Single-cell RNA sequencing
SEB	Staphylococcal enterotoxin B
SMRP	Soluble mesothelin-related protein
TAM	Tumour-associated macrophage
TAN	Tumour-associated neutrophil
TCR	T cell receptor
TIL	Tumour infiltrating lymphocyte
TLS	Tertiary lymphoid structure
TM	Transmembrane
TMA	Tissue microarray
TMB	Tumour mutational burden
TME	Tumour microenvironment
Treg	Regulatory T cell
WES	Whole exome sequencing

Table of Contents

Abstract

Adoptive T cell therapies have revolutionised the treatment of haematological malignancies, where complete remissions up to 90% have been achieved, paving their translation to solid tumours where standard treatments have failed or remain limited. Two types of adoptive T cell therapies are chimeric antigen receptor (CAR) T cell therapy and tumour infiltrating lymphocyte (TIL) therapy. However, their clinical responses in solid tumours remain modest to date. This thesis focuses on improving the translation of adoptive T cell therapies in two solid tumours of significant unmet need, pancreatic cancer and appendiceal cancer.

Pancreatic cancer has an extremely poor prognosis (<15% five-year survival), and CAR T cell therapies targeting the tumour antigen mesothelin (MSLN) have exhibited limited clinical efficacy. Although MSLN is the most studied CAR target in solid tumours, its role in pancreatic cancer and potential contribution to the poor therapeutic efficacy remain unclear. To improve MSLN-targeted immunotherapies, we aimed to examine the clinicopathological and biological significance of MSLN in pancreatic cancer. MSLN expression in 74 pancreatic cancer patients was evaluated by immunohistochemical staining. Patients with high MSLN expression (H-score ≥ 62) were significantly associated with improved relapse-free survival ($p = 0.021$). Analysis of bulk and single-cell RNA-sequencing datasets found that MSLN-high tumours were associated with an immunosuppressive microenvironment characterised by lower anti-tumour immune reactivity and reduced CD8 T cell abundance, which was further supported by immunohistochemical staining in a small patient cohort ($n = 10$).

Appendiceal cancer is a rare disease with limited treatment options. Immunotherapies were understudied and no adoptive T cell therapies have been examined to date. We aimed, for the first time, to assess CAR T cell and TIL therapies in appendiceal cancer. Using patient-derived appendiceal tumour organoids, common tumour antigens MSLN and mucin-1 (MUC1) were shown to be expressed in 3 of the 4 examined organoids by flow cytometry and transcriptomic analyses. Two anti-MSLN CAR T cell products, SS1 and P4 CAR T cells, demonstrated effective tumour killing of antigen-positive organoids, as measured by impedance-based cytotoxicity assay. TIL expansion was tested and was successfully established from 73% (8 out of 11) appendiceal surgical tissue specimens. Expanded TILs displayed a high (> 95%) CD3% fraction and upregulated functional responses induced by superantigen stimulation, although no

consistent reactivity or killing was observed when co-cultured with their matched tumour organoid.

Overall, the immunosuppressive association of MSLN in pancreatic cancer highlights an underappreciated barrier that should be addressed to improve MSLN-targeting adoptive T cell therapies. In appendiceal cancer, CAR T cells, targeting MSLN or MUC1, could be potentially attractive and effective treatment options, while further optimisation of TIL expansion is required. These findings provide crucial insights that could guide the development of more effective adoptive T cell therapies in these cancers of unmet need.

CHAPTER 1

Introduction

1.1 Overview

Adoptive T cell therapies have emerged as a novel treatment paradigm for cancers, experiencing a rapid growth globally with over 200 clinical trials initiated each year since 2019 (1). These therapies rely on *ex vivo* manufacturing of live T cell products, which are then infused into patients for tumour-directed killing. There exist three main types of adoptive T cell therapies – chimeric antigen receptor (CAR) T cell therapy, T cell receptor (TCR) T cell therapy, and tumour infiltrating lymphocyte (TIL) therapy.

CAR T cell therapy has achieved remarkable success in the treatment of haematological malignancies with complete remissions (CRs) as high as 80 – 90% reported from clinical trials of relapsed and refractory (R/R) B-cell acute lymphoblastic leukemia (B-ALL) (2). Currently, seven CAR T cell products have been approved by the Food and Drug Administration (FDA). Five of these have been used for the treatment of R/R non-Hodgkin lymphomas (NHL) and B-ALL. These include axicabtagene ciloleucel (Yescarta) (3), tisagelecleucel (Kymriah) (4), lisocabtagene maraleucel (Breyanzi) (5), brexucabtagene autoleucel (Tecartus) (6), and obecabtagene autoleucel (Aucatzyl) (7). Two products, idecabtagene vicleucel (Abecma) and ciltacabtagene autoleucel (Carvykti) (8, 9), have been approved for the treatment of R/R multiple myeloma (MM), and are now being tested during earlier lines of treatment (1).

TIL and TCR T cell therapies have recently received FDA-approvals for advanced, treatment-resistant solid tumours. In early 2024, the first TIL product – lilfileucel (Amtagvi), received accelerated FDA approval for advanced (unresectable or metastatic) melanoma, following an objective response rate (ORR) of 31% (48/153) in the pivotal Phase 2 C-144-01 study (10). In late 2024, the first TCR T cell therapy – afamitresgene autoleucel (Tecelra), received FDA approval for advanced synovial sarcoma in HLA-A*02-positive patients with MAGE-4 antigen expression, based on an ORR of 43% (19/44) from the open-label, phase II SPEARHEAD-1 trial (11). Despite these recent successes, the translation of adoptive T cell therapies to other solid tumour types have not achieved comparable levels of clinical efficacy.

This thesis will focus on two types of adoptive T cell therapies: CAR T cell and TIL therapies, in two solid tumours of significant unmet need – pancreatic cancer and appendiceal cancer. In this introduction, we first outline CAR T cell therapy and TIL therapy, specifically detailing the design of CAR T cells and TIL manufacturing as critical components to the success of these

therapies. We then summarise the clinical applications of CAR T cell therapies targeting two antigens of high relevance in solid tumours, mesothelin (MSLN) and mucin-1 (MUC1), along with the clinical trial landscape of TIL therapy. Lastly, we discuss the current challenges and advances in translating these adoptive T cell therapies to solid tumours, to provide insight in their application in pancreatic and appendiceal cancers. In pancreatic cancer, CAR T cell therapy has been extensively tested but further understanding of the antigen expression and disease biology is required to improve clinical efficacy. In appendiceal cancer, adoptive T cell therapies, to the best of our knowledge, have not been studied, providing an ideal avenue to pioneer adoption of CAR T cell therapy and TIL therapy in this rare disease.

1.2 Adoptive T cell therapies

1.2.1 CAR T cell engineering

In CAR T cell therapy, T cells are engineered to express artificial receptors targeting a tumour-bound antigen. This redirects the cytotoxic potential of T cells to promote tumour killing and has proven CAR T cells a powerful tool in cancer treatment. Success of CAR T cell therapy is mainly dependent on the identification of an ideal target antigen as well as design of the CAR construct. Significant advances in CAR structural design, delivery strategies, and understanding of CAR T cell functional responses have been made to improve the efficacy of CAR T cell treatments.

1.2.1.1 Standard manufacturing workflow

To date, the manufacturing process of CAR T cell therapy has not undergone significant modifications and remains relatively standardised (12).

Standard workflow of autologous CAR T cell therapy involves (1) obtaining peripheral blood mononuclear cells (PBMCs) from patient leukapheresis, (2) *ex vivo* activation of the T cell population, (3) CAR delivery, (4) expansion of CAR T cells, (5) harvest and release testing, and (6) reinfusion of CAR T cell product, as illustrated in **Figure 1.1**. Current clinical-scale manufacturing of CAR T cell products costs approximately $40,000 - $60,000 USD per patient and can take 2-6 weeks (13, 14).

The main disadvantages of clinical CAR T cell manufacturing are its high cost, time consumption, and potential for production failures (as high as 14% in lymphoma treatment) (15). Alternative CAR T cell manufacturing workflows, such as the production of "off-the-shelf" allogenic CAR T cells, are also being explored, however none have been clinically approved thus far. Allogeneic CAR T cell manufacturing produces infusion products using T cells derived from a third-party source, such as the blood of healthy donors, in advance of patient demand. Ideally, these allogeneic products could be mass-produced, readily available and universal applicable to all patients, thus overcoming the main challenges in current autologous CAR T cell manufacturing. However, immune incompatibility arising between the donor and the recipient poses two major challenges in allogeneic CAR T cell therapy: graft-versus-host disease (GvHD), which leads to treatment toxicities, and graft rejection by the host immune system, which compromises long-term efficacy of the therapy (16). To overcome this, allogeneic products often exhibit additional modifications to disrupt the expression of endogenous TCR and human leukocyte antigen (HLA) molecules that are responsible for GvHD and graft rejection, respectively. However, knockdown of TCR compromises persistence of allogeneic anti-CD19 CAR T cells in a murine B-ALL model (17), while downregulated HLA class I can render CAR T cells to be susceptible to killing by the host's natural killer cells (18). Clinical trials of allogeneic CAR T cells have not achieved similar levels of therapeutic efficacy observed with autologous CAR T cells, and efforts are ongoing to improve the persistence and safety of allogeneic products (19).

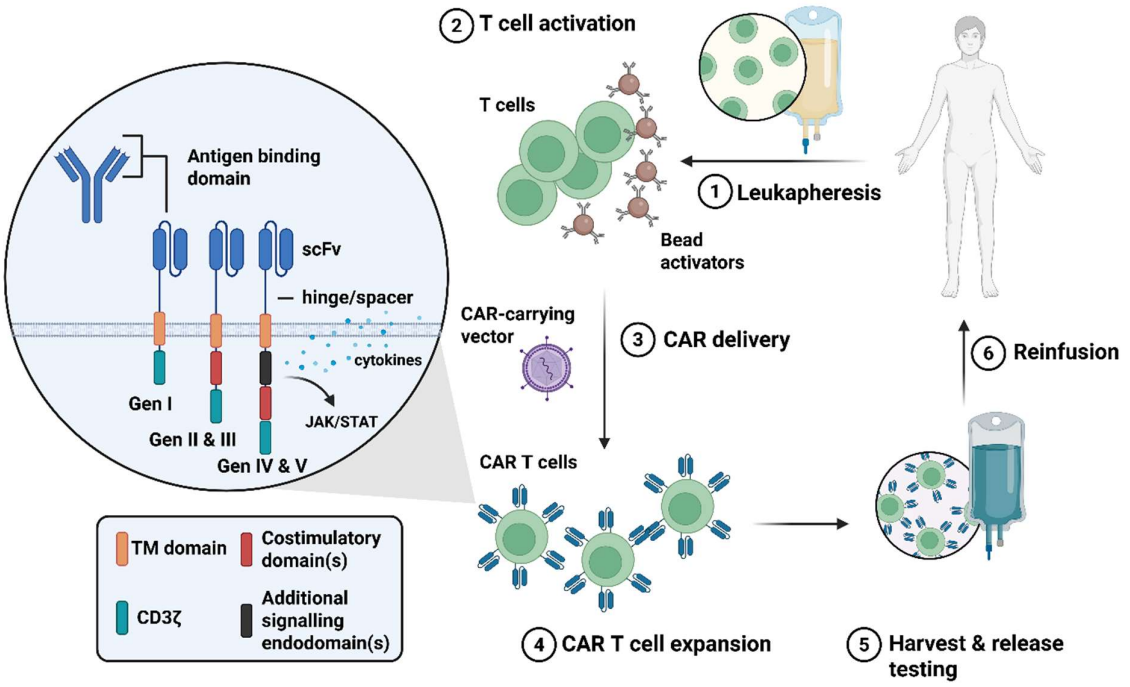

Figure 1.1 Generic workflow of chimeric antigen receptor (CAR) T cell manufacturing and design of CAR constructs. In standard manufacturing workflow, CAR T cells are produced via (1) leukapheresis, followed by (2) bead-based T cell activation, (3) delivery of CAR using a CAR-carrying vector, (4) expansion, (5) harvest and release testing, and (6) reinfusion into the same patient. A CAR construct includes a single-chain variable fragment (scFv) synthesised from the antigen binding domain derived from an antibody, connected to hinge/spacer region, a transmembrane (TM) domain, and intracellular domains for downstream signalling. In first-generation (Gen I) CARs, the intracellular signalling domain consists of a CD3ζ chain only. Second-generation (Gen II) CARs contain one whereas third-generation (Gen III) CARs contain two costimulatory domains. Additional modules are incorporated in fourth-generation (Gen IV) CARs for cytokine release and other coupled signalling pathways in fifth-generation (GEN V) CARs. Figure was generated in Biorender.

1.2.1.2 CAR design

The design of a CAR construct generally consists of an extracellular antigen-binding domain connected by a hinge/spacer region and transmembrane domain to endodomains responsible for CAR T cell activation (**Figure 1.1**).

The antigen binding domain is usually derived from the single-chain variable fragment (scFv) from an antibody, where the variable binding regions of heavy chains (VH) and light chains (VL)

are connected by a short linker sequence. This confers CAR T cells the ability to recognise antigens without HLA restriction, a requirement for physiological activation of T cells.

The hinge/spacer region, mainly derived from CD28 and CD8, confers structural flexibility that enables the CAR to access its target antigen. Compared to CD28-derived hinge, CD8-derived hinge shows increased length and structural flexibility, which is more appropriate for targeting membrane-proximal epitopes or heavily glycosylated antigens (20). Choice of hinge/spacer domain has been shown to influence the formation of immunological synapse and regulate the signalling threshold responsible for CAR T cell activation (21).

The transmembrane domain, mainly derived from CD3ζ, CD4, CD8, and CD28, provides CAR anchorage in the cell membrane through a hydrophobic α-helix structure. This is generally considered an inert component in the CAR construct, although it has also been shown to regulate CAR expression on the cell surface (21),.

Inherent in the endodomains of almost every CAR is the intracellular CD3ζ chain, which stimulates signalling via phosphorylation of its three immunoreceptor tyrosine-based activation motifs upon antigen-recognition. CAR constructs have evolved through several generations, driven by improvements in the design of endodomains. In the first-generation CAR, the antigen-binding domain was joined by the hinge and transmembrane domains to a portion of the CD3ζ chain as the only intracellular signalling module (22). However, these CAR T cells exhibit weak signalling, limited functional persistence, and low efficacy, highlighting the need for additional co-stimulation signals (23).

To improve signalling strength, second-generation CARs inserts a costimulatory domain in between the transmembrane domain and CD3ζ chain, while two costimulatory domains are employed in third-generation CARs (24). Choices of costimulatory domains include CD28, 4-1BB, OX40, CD27, and ICOS, with CD28 and 4-1BB being the most commonly employed in second-generation CARs. To date, all FDA-approved CAR T cell products are second-generation, as well as the majority currently being tested in clinical trials. Nevertheless, when directly compared, third-generation CARs exhibited greater *in vivo* expansion and persistence than second-generation CARs in patients receiving anti-CD19 CAR T cell therapies, highlighting their emerging potential in clinical application (25)

Fourth-generation CAR T cells, known as TRUCK T cells (T cells redirected for antigen-unrestricted cytokine-initiated killing) co-express key cytokines (such as IL-2, IL-5, IL-12, and IL-15) to counteract the immunosuppressive milieu of solid tumours and improve the *in vivo* functionality of CAR T cells (26, 27). Designs of fourth-generation CARs have been extensively tested in preclinical studies and are currently being translated for clinical evaluation.

Lastly, fifth-generation CAR T cells activate additional coupled pathways downstream CAR T cell signalling, such as JAK/STAT3, by incorporating a costimulatory domain responsible for transcription factor binding (i.e. IL2-RB for STAT5 binding). Upon antigen recognition, activation of the coupled JAK/STAT3 pathway provides additional stimulation beyond CD3ζ and CD28 co-stimulation, resulting in enhanced CAR T cell expansion, persistence, and sustained tumour control in murine xenograft models (28). However, fifth-generation CAR T cells are still in preclinical development and have yet to be clinically evaluated.

1.2.1.3 CAR delivery

In the FDA-approved CAR T cell products, CAR delivery into T cells was performed by transduction with a viral vector. In particular, gamma retroviral vectors are used for axicabtagene ciloleucel and brexucabtagene autoleucel, whereas all the other approved CAR T cell products use lentiviral vectors (29). Both types of viral vectors allow for stable, permanent CAR integration into the host T cell genome to ensure sustained CAR expression. Gamma retroviral vectors can only transduce actively dividing T cells, whereas lentiviral vectors can transduce both dividing and non-dividing cells. Additionally, gamma retroviral vectors preferentially insert transgenes in promoter and exon regions, whereas lentiviral vectors preferentially insert transgenes in introns and intergenic regions (30). In both cases, such viral integrations carry inherent risks of insertional mutagenesis. Importantly, cases of secondary T cell lymphomas arising from CAR T cell therapies have been reported (31, 32). However, current evidence does not implicate such secondary malignancies to be associated with viral integration of the CAR construct; instead, reports have suggested that they are more likely to arise from lymphoid clonal haematopoiesis (31, 32). Nevertheless, the FDA has mandated 15-year long-term follow-up to monitor potential secondary malignancies that may develop from insertional mutagenesis in CAR T cell products (33).

While *ex vivo* transduction using a CAR-carrying viral vector remains the mainstream method of CAR modification, other CAR delivery methods are being explored. One of which is transfection of the CAR via electroporation, which circumvents the need to generate costly GMP-grade viral vectors (34). Transient transfection has generally been regarded as a non-toxic alternative to treatment using virally transduced CAR T cells, since any toxicity will be self-limiting due to the short life-span of the transfected CAR T cells (34-36). Transfection of the CAR construct can be done using electroporation of plasmid DNA (37), or more commonly, the messenger RNA (mRNA) (38). Electroporation-based transfection known as nucleofection can also directly deliver nucleic acids into target cell nucleus. This strategy is popular for delivering transposon/transposase systems, such as the PiggyBac and Sleeping Beauty systems, into cells to enable permanent insertion of the transgene into the genome (39, 40). These transposons are simpler and cheaper to manufacture and yields higher efficiency of stable gene transfer (39, 41). However, secondary malignancies arising from PiggBac transposon-manufactured CAR T cells have been reported in 2 out of 8 infusion cases from a Phase I trial, highlighting the safety concerns associated with this approach (42).

Additionally, transfection of the CAR mRNA can be achieved by encapsulating the vector in lipid-based nanoparticles (LNPs), which are endocytosed by target cells and release the mRNA vector into the cytosol for CAR expression (43). Comparing to electroporation, LNP-based delivery is shown to be less damaging to the transfected T cells while retaining similar levels of transfection efficiency (44, 45). This approach has also been utilised for the novel strategy of CAR delivery *in vivo*, which is gaining traction as a cost-effective and broadly applicable method of CAR T cell generation, with significant potential shown from preclinical studies. CAR T cells targeting fibroblast activation protein (FAP) have demonstrated specific killing of fibroblasts to reduce fibrosis and treat cardiac injury *in vivo* (43). Importantly, LNPs were engineered with an antibody-coated surface targeting the T cell marker CD5, which triggers receptor-mediated endocytosis upon contact with T cells. Without such modifications to confer T cell-targeting specificity, the majority of LNPs will be taken up by hepatocytes (46). Although most of the CAR modifications occurred in T cells, a small percentage (<25%) of non-T cells in the spleen (i.e. B cells, dendritic cells, and macrophages) was also modified. In addition to anti-CD5 LNPs, anti-

CD8 LNPs have also been shown to successfully generate anti-CD19 and anti-CD20 CAR T cells from the CD8 T cell population *in vivo* (47). These CAR T cells achieved near-complete tumour clearance in a humanised leukemia xenograft mouse model and induced deep B cell depletion in cynomolgus monkeys, without evidence of significant LNP-mediated toxicities. Further optimisations in dosing, safety profiles, and efficacy remain necessary for the successful clinical application of *in vivo* CAR T cell delivery.

1.2.1.4 Functional responses

Upon engagement of CAR with its ligand, an immunological synapse forms and provides CAR T cells anchorage to the ligand-presenting target cells for subsequent release of cytotoxic granules (48). Unlike the conventional well-organised immunological synapse between CD8 T cells and their targets, the CAR immunological synapse is characterised by loose distribution of adhesion molecules (IFA-1), small actin ring formation, and random micro-clusters of Lck recruited to CARs for downstream signalling (49). This results in CAR T cells exhibiting a convoluted immunological synapse with smaller size, which corresponds to faster signalling, recruitment of cytotoxic granule, and detachment from the dying target cell, compared to conventional CD8 T cells (50).

So far, studies on the downstream signalling pathways following IS formation are limited for first-generation CARs (51). Much of the interest has been on characterising signalling of CARs containing the CD28 and 4-1BB costimulatory domains, as these have been incorporated in the FDA-approved products and are commonly used clinically. CAR T cells bearing the CD28 costimulatory domain were known to have more robust but short-lived proliferation and effector functions than CAR T cells bearing the 4-1BB costimulatory domain, which had higher *in vivo* persistence and more sustained anti-tumour responses instead (24). Both costimulatory domains can activate canonical CD28 and 4-1BB signalling pathways (52). In particular, signalling via the 4-1BB costimulatory domain can phosphorylate endogenous CD28; while signalling via the CD28 costimulatory domain phosphorylates LSP1, a signalling intermediate that can directly bind to endogenous 4-1BB and TRAF2. Downstream signalling is associated with pathways involved in endogenous TCR activation (i.e. MAPK, JAK/STAT, PI3K/AKT, and NF-kB) (53-55). However, CAR T cells bearing the CD28 costimulatory domain generally have faster and greater levels of protein phosphorylation, partially owing to a much stronger recruitment of Lck, and consequently display more effector-like phenotypes (52). In

contrast, CAR T cells bearing the 4-1BB costimulatory domain show higher expressions of memory T cell-associated genes (i.e. FOXO4, KLF2, and IL-7R), and downregulated expression of effector molecules (i.e. IFN-γ, IL-2, granzyme B, and TNF-α). They also selectively upregulate genes involved in fatty acid oxidation and mitochondrial biogenesis, as opposed to the primarily glycolytic metabolism profile adopted by CD28 CAR T cells, and have higher levels of antiapoptotic proteins BCL-2 and BCL-XL (55, 56). Taken together, these factors explain the brisk response of CD28 CAR T cells and the functional persistence of 4-1BB CAR T cells following antigen stimulation, contributing to differences in their clinical performances (57).

Following activation, the anti-tumour activity of CAR T cells is mainly mediated by two types of effector functions: cytotoxicity and cytokine secretion (58). Direct tumour killing by CAR T cells is mostly attributed to the degranulation of perforin and granzyme B. Importantly, activated CARs confer granzyme/perforin-dependent cytotoxic capacity to CD4 T cells, which conventionally do not play a major role in cell killing. Compared to their CD8 counterparts, CD4 CAR T cells secrete lower levels of cytolytic granules (granzyme B and perforin) and participate in killing at a slower rate; but are less susceptible to activation-induced cell death following cytotoxic responses (59-61). When testing the effects of intrapleural infusion *in vivo*, initial cytotoxicity mediated by early CD4 CAR T activation was essential for kick-starting anti-tumour immunity, which led to the eradication of primary and metastasised tumours that were not achievable during conventional systemic CAR T cell administration (62). In addition, a defined CD4:CD8 ratio of 1:1 in the CAR T cell product has been shown to confer synergistic and superior anti-tumour efficacy than CAR T cells derived from CD4 or CD8 T cell subsets alone (63), highlighting the important contribution of CD4 CAR T cell responses in directing treatment successes.

CAR T cells can also mediate cytotoxicity based on the engagement of their death ligands (i.e. FasL, TRAIL) to corresponding death receptors (i.e. Fas, DR4/5, respectively) on target cells. Previously considered to have a minor contribution to CAR-mediated target lysis, the significance of this alternative killing mechanism is being increasingly appreciated. Indeed, one of the factors that hamper long-term persistence of CAR T cells is fratricide, which is attributed to death ligand/receptor-based signalling interactions among CAR T cells (64). Ligation of death receptors on tumour cells enables CAR T cells to perform CAR-independent killing. CAR T cells can eliminate surrounding antigen-negative tumour cells via direct FasL/Fas

interactions, when there is a fraction of antigen-positive tumour cells to provide CAR activation (65). Additionally, impaired death receptor signalling in cancer cells has been associated with rapid tumour progression and poor survival (66). The underlying mechanism was shown to be (a) an initial resistance to death-ligand-based killing by CAR T cells, which results in antigen persistence, and (b) chronic exposure of CAR T cells to target antigens that leads to progressive functional impairments, ultimately ending in treatment failure and disease progression.

Lastly, cytokine release by CAR T cells enhances tumour destruction and orchestrates further anti-tumour immune responses. Generally, CAR T cells have a low activation threshold (defined by antigen density on target cells) for cytotoxic responses, but a higher one for cytokine secretion (67). The exact level of antigen density to trigger each response varies depending on the design of the CAR construct, and CAR T cells are effective *in vivo* only when antigen density sufficient for cytokine secretion is reached during activation (68). IL-2, TNF-α, and IFN-γ are among the most common cytokines secreted by activated CAR T cells (69). IL-2 production is essential for CAR T cell proliferation and survival through autocrine signalling (70). TNF-α is a potent pro-inflammatory cytokine (71), while IFN-γ contributes to solid tumour lysis through direct stromal destruction, polarisation of anti-tumour (M1) macrophages, and activation of IFN-γ receptor-mediated signalling on tumour cells that enhances CAR T cell adhesion and cytotoxicity (72, 73). Other cytokines and chemokines produced include those that promote anti-tumour effects (i.e. MIP-1α), proliferation (i.e. GM-CSF), and immune regulation (i.e. IL-13), as well as novel cytokine secretion pathways (i.e. IL-12 and IL-15) introduced in fourth-generation CAR T cells (26, 27, 74).

Overall, CAR-dependent cytotoxicity, death-ligand-based signalling, and cytokine secretion, are key functional responses that underlie the anti-tumour efficacy and therapeutic outcomes of CAR T cells.

1.2.2 TIL manufacturing

Tumour-infiltrating lymphocyte (TIL) therapy is a form of adoptive T cell therapy where immune cells were selectively expanded *ex vivo* from patient tumours and reinfused into the

same patients for treatment. Although broadly termed as “tumour-infiltrating lymphocytes”, existing TIL therapies rely solely on tumour-reactive T cells for therapeutic efficacy.

In TIL therapy, design of the manufacturing pipeline underlies the successful expansion and efficacy of the infusion product. The general TIL manufacturing workflow is presented in **Figure 1.2**. Standard protocols to produce bulk, unselected TILs consist of a two-stage – pre-rapid expansion protocol (REP) and REP – expansion process. Prior to REP, TIL cultures can also be subjected to further reactivity selection and modifications. Manufacturing of unselected TILs typically takes 2-6 weeks, whereas several months are required to produce selected or modified TILs (75, 76). Cryopreservation can be performed at each stage of clinical expansion. Specific stages of TIL manufacturing are described in the following subsections.

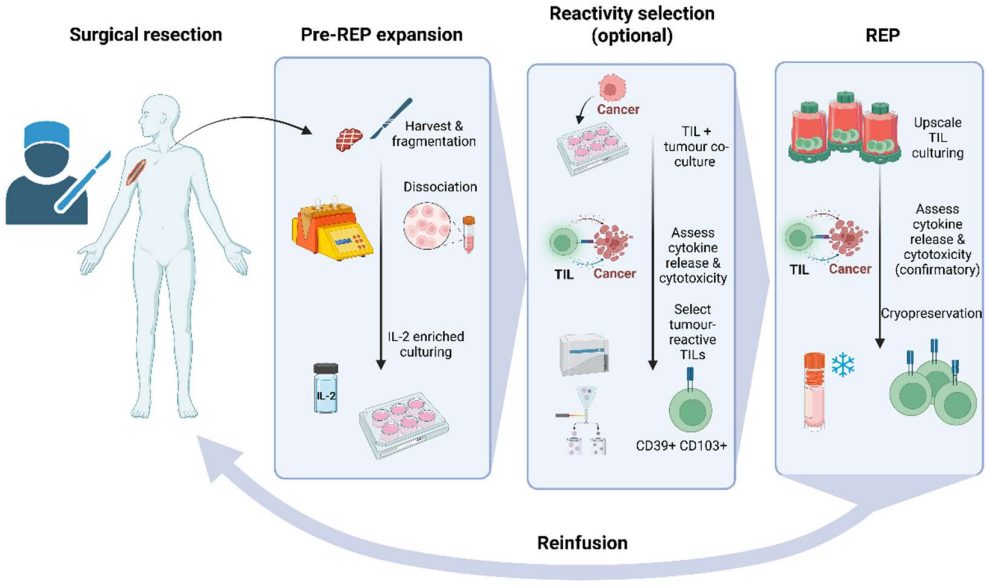

Figure 1.2 Manufacturing pipeline of tumour-infiltrating lymphocyte (TIL) therapy. Tumour specimen was obtained from surgical resection, processed, and expanded using IL-2-enriched media in the first TIL expansion stage (pre-REP). Expanded TILs can undergo additional reactivity selection to enrich tumour-reactive TIL populations, or alternatively proceed directly to the second TIL expansion stage (REP), where large-scale culturing is achieved using bioreactors. Final TIL products are functionally validated and can be cryopreserved for reinfusion into the same patient. REP, rapid expansion protocol. Figure was generated using Biorender.

1.2.2.1 Tumour procurement

Surgical resection is the most common method for obtaining tumour tissues for TIL manufacturing, although samples from core biopsies can also be used (77, 78). Importantly,

guidelines for surgical harvest are similar across different cancer types and locations of resection (79). Because patients receiving TIL therapy typically present with advanced disease, metastatic deposits and lymph nodes are common sites of harvest. Surgery prioritises minimising patient morbidity over therapeutic intent, and does not need to follow traditional margins or achieve complete resections. Exact locations and process of surgical resection for each patient relies on the best decision from collaborating surgical and medical oncologist teams.

Having a diameter of at least 1.5 cm (1.5 cm – 4 cm) is a standard requirement for tumours procured for TIL manufacturing (80). Additionally, necrotic and adipose tissues should be avoided, and any excess should be trimmed off during tumour processing. Patients with brain metastases are excluded from procurement and TIL treatment due to potential concerns of intracranial bleeding. Irradiated and ulcerated tumours are also excluded. Tumours with high risks of bacterial colonization, such as those derived from the gastrointestinal lumen, are excluded or handled with caution to prevent bacterial contamination during *ex vivo* expansion (81). Sterile practices are used for tumour handling similar to organ transplantation procedures. Tissues from procurement, either cryopreserved or stored in cold, antibiotics-enriched media, are transported to TIL manufacturing facility for further processing.

1.2.2.2 Tumour processing & pre-REP expansion

Strategies for processing of tumour on the initial day of TIL expansion include culturing of tumour fragments (1 - 3 mm in size) and culturing of single cell digests.

In tumour fragment cultures, individual tumour fragments are placed in separate wells of a 24-well tissue culture microplate. Cultures are maintained for 1-3 weeks, during which lymphocytes will egress and form a dense carpet around the fragment. Confluent wells will be split and maintained as independent subcultures, by half media exchange or culture splitting every 2-3 days after TIL outgrowth. Fragment cultures can also be initiated in bioreactors, such as the gas-permeable culturing flasks, known as G-rex (Wilson-wolf, Minneapolis, MN) devices, which allows for efficient gas exchange to occur on a membrane where cells settle, with ample nutrient availability provided by the large volume of culturing media loaded on top (82). Bioreactors minimize operator handling and have been utilised across several generations in the proprietary manufacturing of lifileucel products (83, 84). Pre-REP expansion from

Generation 1 (Gen 1) manufacturing takes approximately 21 days. 4 tumour fragments were seeded in 10 G-rex 10 flasks and manual open volume reduction (every 3-4 days) were performed after the initial week. Gen 2 manufacturing employs upscaled bioreactors without interim media exchange and has been used in the majority of lifileucel clinical trials to date. During pre-REP expansion, 40 tumour fragments were seeded in a single G-rex 100-CS and cultured without operator intervention for 11 days, while the entire manufacturing process takes only 22 days. A novel 16-day Gen 3 process shortens the pre-REP expansion to 7-8 days by the addition of anti-CD3 antibody (OKT-3 clone) with optional antigen-presenting feeder cells. This is being assessed in ongoing clinical trials and awaits initial reports on safety and efficacy (85).

In cultures of single cell digests, procured tumours are fragmented and subjected to enzymatic and/or mechanical dissociations. Dissociated mixtures are then filtered to obtain single cell suspensions for expansion similar to tumour fragment cultures. In one melanoma study, enzymatically digested cultures yielded the highest success rate in TIL expansion (94.1%), compared to fragment-derived (69.9%) and mechanically dissociated cultures (90.3%) (86). Enzymatic digestion was performed overnight using a cocktail of collagenase, hyaluronidase, and DNAse under gentle agitation, whereas mechanical dissociation was performed on a sterile homogenizer (Medimachine) followed by density gradient centrifugation (Ficoll) to obtain the lower TIL-enriched fraction. The same overnight enzymatic digestion was tested in renal cell carcinoma, but shown to be inferior compared to the commercial mechanical/enzymatic GentleMACS dissociation system (Miltenyi Biotec), which demonstrated less variability in TIL number and preserved expressions of cell surface antigens (87). Although enzymatic digest cultures have been used in bioreactors and clinical manufacturing (88, 89), fragment cultures are generally preferred due to simpler practices.

Standard expansion of pre-REP cultures is performed in a complete medium (i.e. RPMI-1640 enriched with 10% inactivated human AB serum), supplemented with high IL-2 concentration (3000 – 6000 IU/mL) (83). High IL-2 concentration is critical as stimulated TILs are incapable of producing their own IL-2, unlike T cells from the peripheral circulation (90).

1.2.2.3 Reactivity selection

Selection of pre-REP cultures is not a mandatory procedure in TIL manufacturing. Bulk, unselected TILs, exhibit benefits from accelerated manufacturing such as higher telomere lengths and lower levels of differentiation (89). These features are associated with higher *in vivo* persistence and objective responses in melanoma. Nevertheless, unselected TILs may not display similar therapeutic efficacy in a non-melanoma setting. Lack of responses of unselected TILs from immunogenically cold tumours such as gastrointestinal cancers indicate that manufacturing pipelines of reactive TILs are still essential for translating TIL therapies from melanoma to other solid tumours (91).

The two main types of TIL selection are selection based on cell surface marker expression and selection based on antigen recognition, which are detailed below. Additionally, detection of cytokine production (IFN-γ response) from co-culture assays is a standard requirement for reactivity assessment. This can be evaluated in ELISA assays as an increase in the soluble IFN-γ concentration or in ELISpot assays as an increase in the number of IFN-γ -secreting cells.

1.2.2.3.1 Selection based on cell surface markers

Reactive pre-REP TIL cultures can be identified via upregulations of reactive markers during co-culture with HLA-matched or autologous tumours. Reactive clones can also be sorted, isolated, or selectively enriched based on surface marker expression. This is usually done at the initiation of pre-REP expansion following tumour digestion.

Initial studies identified PD-1 as a marker for tumour reactivity on CD8 TILs (92). Fluorescence-activated cell sorting (FACS) sorting of mouse PD-1+ CD8 TILs led to specific recognition of tumour cells and prolonged survival in micrometastasis murine models of melanoma and colon adenocarcinoma (93). Notably, PD-1+ TILs displayed a fold expansion that was 10 times lower compared to the PD-1- fraction. The outgrowth of PD-1- CD8 TILs could have contributed to the lack of tumour recognition from unsorted CD8 TILs, which initially exhibited high PD-1 expression (70-90%) during tumour harvesting. Despite PD-1 being a well-known exhaustion marker, PD-1+ TILs from FACS sorting or magnetic bead separations of human melanoma digests did not display exhausted phenotypes after 2-weeks of *ex vivo* culture with IL-2 (94). Both bulk and selected CD8 TILs also showed consistent decreases of PD-1 expression over time, indicating that PD-1 is not a reliable marker for reactivity during

prolonged culturing (2-5 weeks). Lifileucel with PD-1 selection (LN-145-S1, by Iovance Biotherapeutics) is being assessed in a melanoma cohort within an ongoing Phase II IOV-COM-202 trial (85).

CD39 (ENTPD1), either alone or in combination with CD103 (ITGAE), have been shown to identify reactive, tumour-resident TIL populations. Following FACS sorting and expansion, CD39+ CD103+ double-positive (DP) CD8 TILs demonstrated reactivity against autologous tumours in all tested patients (n = 6), whereas double-negative or single-positive (CD103+ CD39−) TILs yielded minimal reactivity (95). These DP CD8 T cells cannot be found in the peripheral blood of cancer patients, and were more abundant in immunogenic tumours such as melanoma and microsatellite instability-high (MSI-H) colon cancer than microsatellite stable (MSS) colon cancer. In contrast, tumour reactive CD4 T cells can be recognised by CD39 expression alone (96). At the transcriptomic level, CD39+ CD4 TILs displayed similar activated and tissue-resident phenotypes as CD39+ CD103+ CD8+ TILs. FACS-sorted CD39+ CD4 TILs demonstrated strong reactivity to oncoproteins E6 and E7 in HPV-specific cancers and did not lead to expansion of immunosuppressive regulatory T cells (Tregs). Sorting directly from tumour digests is necessary due to variations in CD39 and CD103 expressions during *ex vivo* expansion.

Tumour-reactive TILs can also be identified by the expression of CD137 (4-1BB), a co-stimulation marker of T cells (97). Magnetic bead isolation of CD137+ TILs have been established using CliniMACS Prodigy (Miltenyi Biotec), a closed and semi-automated platform for GMP-compliant manufacturing. TILs with CD137 expression, following co-culture of pre-REP cultures with autologous tumour cells, were column-isolated using CliniMACS reagents (98). Alternatively, the Tumour Reactive T cell (TRT) Process allows for expansion of CD137-selected TILs on CliniMACS Prodigy within 16 days (99). Automatic magnetic isolation of CD137+ TILs was initiated following a pre-culture phase of tumour digests, and isolated CD137+ TILs were directly fed into an automated REP process. Final CD137+ TILs products showed high reactivity against autologous tumour cell lines, for all tested samples (n =3). However, the TRT Process currently has a maximum output of 5 x 10^9 (5 billion) cells, and requires upscaling to support the larger dose requirements in many clinical trials, which have upper ranges of 100 – 200 billion cells per dose. Urelumab, an anti-CD137 antibody, has also been used for agonist stimulation during pre-REP expansion by the proprietary MDACC TIL

manufacturing process (80, 100). Agonist stimulation of CD137 and CD3 accelerated TIL expansion and improved success rate of TIL establishment in melanoma, with TILs exhibiting low expressions of exhaustion markers PD-1 and TIM3 (80). Reactivity was also displayed in 4 of 5 TIL products against autologous cutaneous melanoma cell lines.

Importantly, surface CD137 expression is also upregulated upon stimulation of TIL with tumour antigens (98). Detection of CD137 expression is a standard reactivity assessment in co-cultures of TILs with tumours. Since CD137 is reliable for identifying tumour-reactive CD8 but not CD4 TILs, another reactivity marker such as CD134 (OX40) is often used in conjunction with CD137 to detect tumour-reactive CD4 TIL subsets (101). Nevertheless, high expression of tumour reactivity markers might not always correlate with TIL responses in cytokine production. This is reflected in one study where renal cell carcinoma TILs exhibited upregulation of CD137 upon co-culture with autologous tumour digest but triggered minimal production of TNF-α and IFN-γ (102). Therefore, both detection of reactive markers and cytokine production responses from TILs should be incorporated for comprehensive assessment of TIL reactivity.

1.2.2.3.2 Selection based on antigen recognition

In antigen-based selection, TILs are co-cultured with autologous or HLA-matched antigen-presenting cells (APCs) that were loaded with specified antigens for recognition. Recognition of HPV antigens E6 and E7 have been used to select reactive TILs for the treatment of HPV-associated cancers (103). Neoantigen-reactive TILs have also been established based on the mutational profiles of individual patients through whole-exome sequencing (WES). Although technically difficult and demanding prolonged manufacturing time, neoantigen-reactive TILs have been tested in a number of clinical trials and achieved positive responses in gastrointestinal cancers (91, 104).

Choices of APCs include autologous dendritic cells (DCs), B cells, and HLA-matched cell lines, such as COS-7 cells transfected with autologous HLA alleles (105, 106). Antigens from pre-defined or WES-predicted epitopes are fragmented into 24-25 mer long peptides and introduced to APCs as peptide pools (PPs) for intracellular processing. Alternatively, a library of tandem minigene (TMG) RNAs derived from the same peptide sequences can be delivered to APCs through transfection or virally transduction. Reactive T cells from the co-culture can then be FACS-sorted for subsequent expansion. This neoantigen selection process has been

employed by the NeoExpand protocols, which has been tested in several recent clinical trials (105). When peptide and TMG libraries from patient-specific neoantigens need to be newly synthesised, the NeoExpand process requires 4-6 weeks. However, selection using common neoantigens that can be prepared ahead of time, such as p53 and KRAS, can accelerate the NeoExpand process to 14-19 days. Compared to bulk, unselected TILs, TILs generated using NeoExpand showed increased diversity of tumour reactive clonotypes and preserved stem-like memory phenotypes. These neoantigen-reactive TILs also outperformed bulk, unselected TILs in controlling tumour growths in xenograft models of colorectal and ovarian cancer harbouring the same *p53* and *KRAS* mutations, which mirrored subsequent clinical experiences (91). However, low yield of autologous APCs and the complex selection process remain challenges that hinder the wide adoption of neoantigen selection in TIL manufacturing.

1.2.2.4 REP expansion

Pre-REP TILs or TILs after reactivity selection will be expanded using the REP process, to obtain cell numbers sufficient for clinical infusion (5- 150 billions) (75). REP accelerates TIL expansion by providing a nutrient-rich media containing high dose IL-2 (3000 – 6000 IU/mL), agonistic CD3 stimulation (via the OKT-3 clone) and irradiated allogeneic feeder cells derived from healthy donor PBMCs, at a 200:1 ratio to TILs. Traditional REP process takes 14 days, with initial seeding in T-175 tissue culture flasks followed by transfer into gas-permeable bags after one week (86). Compared to traditional REP, REP conducted in G-rex bioreactors showed doubled fold expansion (median = 2653 vs median = 1210) in the same 14-day period (107). More recent (Gen 2 and Gen 3) pipelines of lifileucel manufacturing have shortened the REP process to within 11 days using G-rex bioreactors (83). The exact mechanism by which REP accelerates TIL expansion remains unclear. Reductions in frequencies of neoantigen-reactive TILs have been shown following REP of reactivity-selected TIL cultures, likely because of enrichment of non-reactive bystander cells through nonspecific stimulation (105).

The use of allogeneic feeder cells during REP has been a major barrier for the wide implementation of TIL manufacturing. For each treated patient, large numbers (up to 10^{10}) of feeder cells need to be procured, which require pooling PBMCs from 4-6 donor samples (108). Donor heterogeneity also contributes to differences in TIL activation and expansion. An alternative approach is to use artificial antigen presenting cells (aAPCs) as substitution of allogeneic feeders. Initially, magnetic beads attached with anti-CD3 and anti-CD28 monoclonal

antibodies were used as aAPCs to induce T cell activation by receptor crosslinking. These bead-based aAPCs failed to sufficiently expand TILs but showed substantially better expansion of T cells from matched patient PBMCs (90). An underlying reason could be the lower expression of CD28 on TILs compared to matched patient PBMCs. Cell-based aAPCs, such as irradiated K592 cell lines engineered to express molecules including the high affinity Fc receptor CD64 and costimulatory ligand CD137L, were explored. K592-based aAPCs showed comparable expansion of TILs as conventional REP in small-scale and clinical-grade manufacturing (90, 108). Compared to conventional REP, rapid expansion using K592-based aAPCs also exhibited increased CD8 T cell frequency, reductions in Tregs, and similar effector-memory and exhaustion profiles. Furthermore, no differences were observed in clonotype diversity and antitumour reactivity, and a much lower APC to TIL ratio was used (50:1 vs 200:1 in clinical-grade manufacturing). Overall, K592-based aAPCs show similar performance in the rapid expansion of TILs as traditional allogeneic feeders. Their ease for upscaling, lot-to-lot consistency, and capacity for additional engineering make them an attractive alternative source of APCs. Such cell-based aAPCs have not been examined in existing clinical trials but show potential clinical implementations in the future.

1.3 Clinical applications of adoptive T cell therapies in solid tumours

1.3.1 Selection of tumour antigen targets for CAR T cell therapies

In haematological malignancies, successful clinical outcomes from CAR T cell therapy have largely been attributed to the identification of an ideal target antigen such as CD19. CD19 has been considered as one of the most reliable biomarkers for B cells (109). Its expression is restricted to B cells from the pro-B cell lineage until terminal differentiation into plasma cells and is stably regulated (110). Positivity of CD19 is detected in over 90% of B-ALL cases, of which the mean percentage of positive cells from the blast population is close to 80% (111). On-target, off-tumour killing of anti-CD19 CAR T cells depletes CD19-positive, normal B cells, but such B cell aplasia is manageable through antibiotics and antibody infusion treatments (112, 113). Overall, CD19 is highlighted by its high specificity, stability, prevalence, and manageable off-tumour effects as a CAR T cell target in B-cell malignancies.

The heterogeneity of antigen expressions, however, remains one of the major hurdles for the effective translation of CAR T cells to solid tumours. So far, no CAR T cell therapy for solid tumours has progressed beyond Phase II clinical trials. Overall outcomes from existing trials suggest that responses of CAR T cells against solid tumours are modest at best, and complete remissions are rare. Unlike haematological malignancies, solid tumours exhibit strong clonal diversity, and complex tumour microenvironment (TME) supported by a diverse range of stromal cells. On-target, off-tumour toxicities can and have been reported to be life-threatening (113, 114). As such, tumour-associated antigens that are highly upregulated in solid cancers but minimally expressed on normal tissues represent the best target candidates. Some of the most examined targets in clinical trials to date are listed below (**Figure 1.3**). In this review, we will focus on CAR T cells directed against the tumour-associated antigens mesothelin (MSLN) and mucin-1 (MUC1) in solid tumours.

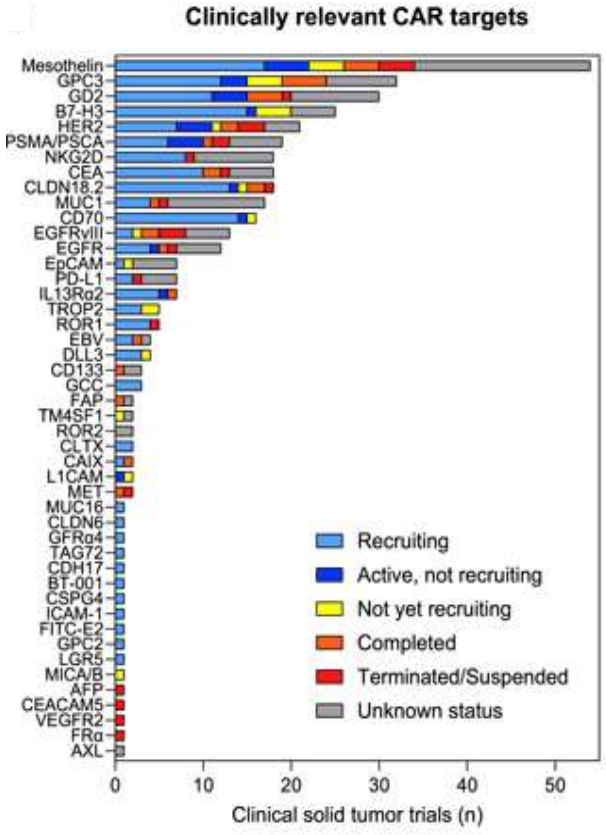

Figure 1.3 Tumour-associated antigens targeted by CAR T cells in solid tumour clinical trials worldwide. Antigens are ranked by the total number of CAR T cell clinical trials in solid tumours and each clinical trial status is represented in the legend. Information was collected

from trials as of July 2024 from clinicaltrials.gov. Figure was reproduced from Tony et al., 2025 (115).

1.3.2 Anti-MSLN CAR T cell therapies

By far, MSLN remains the most studied target for CAR T cell therapy in solid tumours (115). MSLN is a glycosylphosphatidylinositol (GPI)-anchored glycoprotein that was originally discovered on mesothelial linings of the pericardium, peritoneum, and pleura (116). Further characterisation revealed its expression to be mainly confined in normal mesothelial cells, but upregulated in a wide range of solid tumours (117) (**Figure 1.4**). Some of the cancer types with high (over 50%) positivity of MSLN include intestinal cancers, ovarian cancer, pancreatic cancer, endometrial cancer, lung cancer, and mesothelioma. The aberrant expression of MSLN in cancer development and limited physiological expression characterises it as a tumour-associated antigen with high prevalence and specificity. In addition, although the exact function of MSLN remains unclear, mice with MSLN knockout demonstrated no differences in survival, development, and reproduction compared to wild-type mice (118). This highlights advantages for the use of MSLN as a CAR target, as loss of MSLN is not shown to be essential for vital functions. MSLN has also been shown to promote tumorigenesis. In pancreatic cancer cells, MSLN expression increases proliferation through STAT3 activation, and rescues TNF-α-induced apoptosis through autocrine IL-6 production (119-122). During cell-to-cell contact, its interaction with mucin-16 (MUC16), the only identified binding partner of MSLN, facilitates migration and contributes to metastatic dissemination of pancreatic cancer cells (123, 124).

Expression of MSLN is regulated by multiple steps of biological processing (**Figure 1.5**). The MSLN protein is expressed on the cell surface as a 71-kDa precursor protein. Upon furin cleavage, a 31-kDa soluble product is released from the N-terminal known as the megakaryocyte potentiating factor (MPF), which is named after its ability to support colony formation of mouse megakaryocytes in the presence of IL-3 (125). The remaining 41-kDa GPI-anchored protein is the mature form of MSLN. This form of MSLN is recognised by the antigen-binding domains of current anti-MSLN CAR constructs, such as SS1 and P4 (126, 127). Enzymes in the ADAM, MMP, and BACE families can further cleave mature MSLN at the C-terminal domain, which releases the protein into the peripheral circulation as the soluble mesothelin-related peptide (SMRP) (128, 129). Mature MSLN is also responsible for interacting with membrane-bound MUC16 (130, 131). Overall, shedding of MSLN and its binding interactions

with MUC16 can reduce the availability of targetable antigens on tumours to impair CAR T cell recognition.

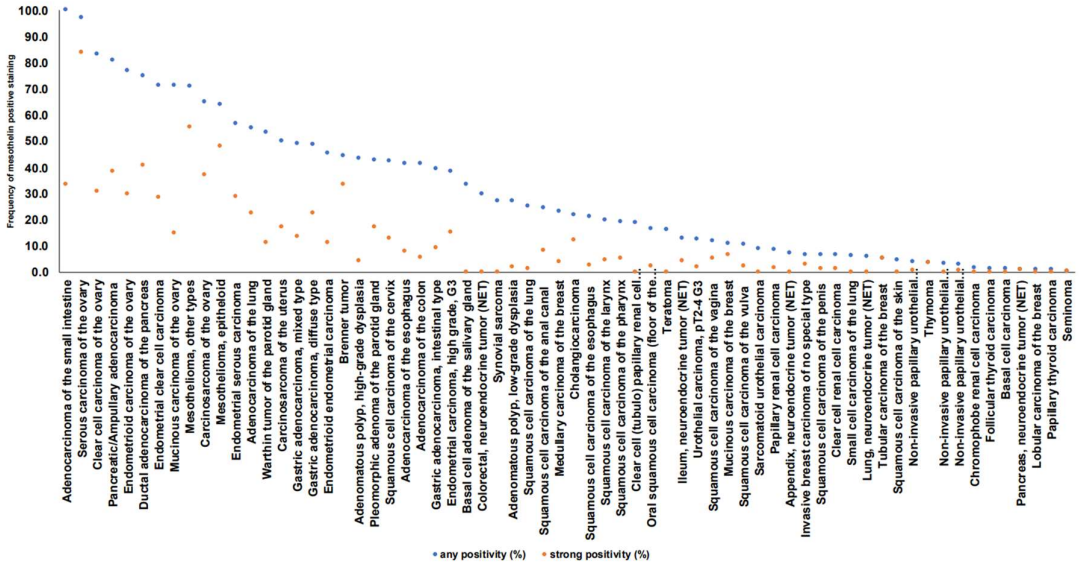

Figure 1.4 Mesothelin (MSLN) expression examined across solid tumours by immunohistochemical staining. Blue dots represent percentages of samples with any positive MSLN staining. Orange dots represent percentages of samples with strong MSLN positivity, defined by >70% of tumour cells exhibiting staining intensity of 2+ or >30% of tumour cells exhibiting staining intensity of 3+. Figure was reproduced from Weidemann et al., 2021 (117).

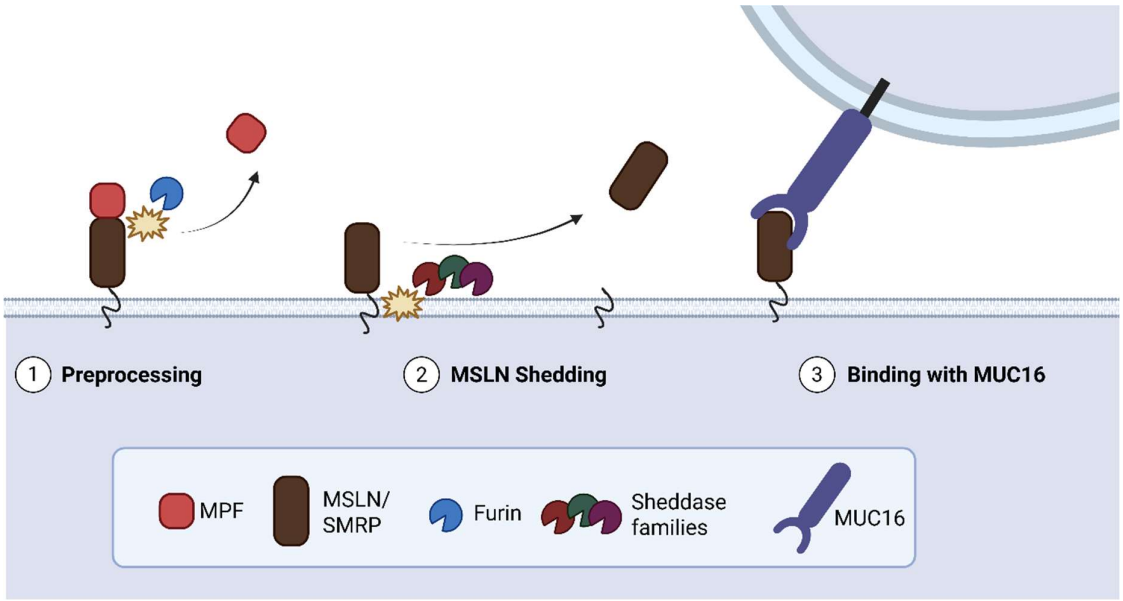

Figure 1.5 Biological processes of mesothelin (MSLN) expression. (1) During preprocessing, a precursor protein is cleaved by furin enzyme into a soluble component (MPF) and mature MSLN. (2) During MSLN shedding, the mature form is cleaved by families of sheddase enzymes to release a soluble protein (SMRP). (3) MSLN can participate in binding interactions with membrane-bound MUC16 on adjacent cells. MPF, megakaryocyte potentiating factor; MSLN, mesothelin; SMRP, soluble mesothelin-related peptide; MUC16, mucin-16. Figure was generated in Biorender.

1.2.4.1 Development and clinical outcomes of anti-MSLN CAR T cell therapies

In early clinical trials, scFv of anti-MSLN CAR T cells employed the antigen recognition domain of a murine anti-MSLN antibody clone known as SS1. This antibody and its immunotoxin derivative SS1P have been widely assessed in Phase I and II clinical trials of solid tumours (132). In preclinical testing, CAR T cells bearing the SS1-derived scFv (hereafter referred to as SS1 CAR T cells) achieved complete eradication of well-established (~ 500 mm^3) tumours in xenograft models of melanoma (133). However, first-in-human study reported severe anaphylaxis and cardiac arrest immediately after third CAR T cell infusion (134). This has been attributed to the long dosing schedule of the multi-infusion regimen (3 infusions over 49 days), which allowed for the development of IgE-mediated allergic reaction. Further studies employed shorter dosing schedules that must be completed within 21 days, so that CAR T cells are administered before isotype switching from IgG to IgE is complete. In Phase I clinical trials, second-generation SS1 CAR T cells bearing the 4-1BB costimulatory domain have been shown to be well-tolerated, both when CAR constructs are expressed transiently by mRNA electroporation and constitutively by lentiviral transduction (34, 135). However, clinical efficacy was suboptimal, with no ORR observed in either trials, and stable disease (SD) was the best response in 73% (11/15) from the lentiviral-transduced SS1 CAR T cells. The issues of CAR T cell-induced anaphylaxis and lack of favourable efficacy have been suggested to be the immunogenicity of the SS1 scFv, which is of murine origin. Antibodies against the murine component of the CAR have been observed in both the anaphylaxis case and 57.1% (8/14) patients in the study with lentiviral-transduced SS1 CAR T cells.

Fully human scFvs have been utilised in other anti-MSLN CAR T cell therapies, to address the issue of xenoreactivity observed with SS1 CAR T cells. The P4 scFv (human-anti-human) was selected from a yeast-display scFv library based on its high binding affinity to recombinant MSLN (127). Antibodies with the P4 antigen binding domain were shown to inhibit MUC16/MSLN-dependent cell adhesion, suggest that the P4 scFv likely recognises an epitope

on MSLN that competes with MUC16 docking. P4 CAR T cells exhibited robust IFN-γ secretion against immobilised MSLN, and were capable of mediating bystander killing of MSLN-negative tumour cells in the presence of MSLN-positive tumour targets (126). Unlike the SS1 CAR T cells, effector functions of P4 CAR T cells were not suppressed in the presence of SMRP (136), highlighting their specificity to the tumour cells and increased resistance to MSLN shedding. Rapid tumour control was observed in xenograft models of ovarian cancer through intratumoural and intravenous injections of second-generation P4 CAR T cells containing the CD28 costimulatory domain. In a Phase I dose-escalation study in MSLN-positive solid tumours, these second-generation P4 CAR T cells were shown to be well-tolerated (137). No autoimmune reactions or dose-limiting toxicities were observed in patients receiving multi-infusion regimens (up to three infusions) or maximal doses (up to 1.1 x 10^7 cells/kg). In addition, CRISPR-Cas9 knockout of PD-1 and T cell receptor alpha subunit (TRAC) were performed on the infusion product in addition to CAR delivery. TCR removal via TRAC knockout was initially expected to improve CAR T cell expansion; however, outgrowth of TCR-positive CAR T cells was observed in 3 patients after infusion. In all patients, CAR T cells did not persist for more than 6 weeks post-infusion, and this limited persistence was confirmed in xenograft models to be due to the TRAC disruption. Clinical efficacy was poor, with SD achieved in 2 from 15 patients as the best overall response. Whether P4 CAR T cells without TRAC disruption would result in favourable persistence and efficacy in patients remains to be tested. P4 CAR T cells have also been modified to reverse functional exhaustion through depletion of the transcription factor BATF (138), and to reduce off-tumour toxicities through tandem expression of a CAR targeting folate receptor 1 (FOLR1) (139, 140). However, these strategies have not been examined clinically.

The m912 and M5 scFvs are two other fully human anti-MSLN domains incorporated in clinical anti-MSLN CAR constructs. The m912 scFv was selected from a phage display assay based on specific recognition of native MSLN, at an epitope that is unaffected by glycosylation (141). The m912 scFv has not been affinity-maturated, and a 30-fold higher concentration of the m912 antibody is required for MSLN detection on MSLN-positive tumour cells, compared to the SS1 antibody. Consistent with this observation, m912 CAR T cells also exhibited lack of targeted killing of cells with low MSLN antigen density (142). However, this confers m912 CAR T cells with minimal off-tumour toxicities, such as against normal mesothelial cells. Increasing

antigen density through inhibition of the MSLN shedding process was able to recover the killing responses of m912 CAR T cells on MSLN-positive tumours (142). When administered regionally via the intrapleural route, pleural tumours in mice were eradicated using second-generation m912 CAR T cells bearing the CD28 costimulatory domain (62). Importantly, compared to intravenous injection, regional injection enabled efficient tumour infiltration, clearance of tumour deposits, and required 30-fold lower dose to achieve long-term remission. The underlying mechanism was attributed to early activation of CD4 CAR T cells, which showed sustained functional persistence and promoted accumulation of T cells in established tumours. These promising results led to the initiation of a Phase I trial assessing intrapleural administration of m912 CAR T cells, with or without PD-1 blockade by pembrolizumab, in patients with pleural tumours (143). CAR T cells used in this trial were second-generation with the CD28 costimulatory domain, same as the preclinical studies. Treatment was well-tolerated, with no dose-limiting toxicities and reversible grade 4 adverse events (AEs) from the preconditioning lymphodepletion only. In pleural mesothelioma patients, 39% (9/23) had detectable CAR T cells in the peripheral blood more than 100 days post-infusion, based on polymerase chain reaction (PCR) analysis. In patients receiving the combination treatment (m912 CAR T cells followed by pembrolizumab) with measurable disease, ORR was 13% (2/16), with 2 partial responses (PR) and 9 SD as the best overall response. Overall, incorporation of the fully human m912 scFv in the CAR construct did not induce severe autoimmune reactions, and on-target, off-tumour toxicities were not observed. Regional delivery, coupled with immune checkpoint blockade, likely contributed to the positive clinical responses and favourable *in vivo* persistence of m912 CAR T cells in the treated patients.

The M5 scFv was selected from a phage display library and exhibited sensitive recognition of low-MSLN expressing cells when used as a CAR antigen binding domain (144). The M5 scFv binds to the membrane-proximal epitope close to the C-terminal of MSLN, and does not interfere with the binding of SS1 scFv, which instead recognises an epitope close to the N-terminal of MSLN. In xenograft models, M5 CAR T cells demonstrated similar regressions of tumours with moderate levels of MSLN expression compared to SS1 CAR T cells, but substantially outperformed SS1 CAR T cells in controlling tumours with low MSLN expression. However, two severe cases of pulmonary toxicities were reported in the treatment of mesothelioma patients in the subsequent Phase I dose-escalation study (144, 145). Both

subjects received intravenous infusion of second-generation M5 CAR T cells with the 4-1BB costimulatory domain at the highest tested dose (1–3 × 10^8 CAR T cells/m^2). Clinical conditions were managed in one patient who did not require intubation, but the second patient succumbed to treatment complications despite medical management. Further analysis revealed low levels of MSLN expression in pulmonary epithelial cells, which were shown to be upregulated during inflammation and lung injury. In addition, the second patient received pembrolizumab prior to CAR T cell therapy, and circulating pembrolizumab was detected at the time of CAR T cell infusion. Residual pembrolizumab could boost CAR T cell responses or induce pulmonary inflammation and potentially exacerbated the pulmonary toxicities. The trial was re-evaluated due to the toxicities and continued with modifications to include a 4-month washout period for prior immune checkpoint blockade therapy. Intrapleural injection of M5 CAR T cells was also tested. Overall, clinical experiences from M5 CAR T cells suggest that, despite the fully human nature, on-target off-tumour toxicities remain a significant concern for scFvs with high potency against targets with low antigen expression.

In a first-in-human testing of another fully humanised anti-MSLN CAR construct (huCART-MESO), infusions were well-tolerated and an ORR of 9% (1/11) was observed in patients with advanced pancreatic cancer, with SD as the best overall response (146). These CAR T cells harbour a second-generation construct with the 4-1BB costimulatory domain; however, the scFv was not specified. Further analysis revealed low tumour infiltration and exhausted phenotypes of infused CAR T cells. Knockout of ID3 and SOX4, two transcriptional factors associated with T cell exhaustion, in these CAR T cells promoted sustained control of disease recurrence in murine xenograft models of pancreatic cancer, but this strategy remains to be clinically assessed.

Other anti-MSLN scFvs have been evaluated in pre-clinical studies or are being tested in clinical trials, but extensive clinical outcomes remain to be reported. The 15B6 scFv binds to a juxtamembrane position on mature MSLN to circumvent loss of antigen recognition due to MSLN shedding (136). 15B6 CAR T cells were not influenced by high levels of SMRP and showed substantial improvement *in vivo* compared to SS1 CAR T cells, achieving complete eradication of ovarian and pancreatic tumours in xenograft mice models. The 15B6 scFv was initially of murine origin but has been humanised subsequently (147). 15B6 CAR T cells remain to be assessed clinically. The hYP218 scFv, derived from the humanized antibody YP218,

represents another antigen binding domain that targets a membrane-proximal region of MSLN (148). Similar to 15B6 CAR T cells, hYP218 CAR T cells demonstrated improved efficacy *in vitro* and *in vivo* compared to SS1 CAR T cells. Additionally, hYP218 CAR T cells showed long-term persistence in the TME and remained functional 40 days post-treatment, with enhanced tumour control from combination treatment with pembrolizumab (149). Safety and efficacy of hYP218 are currently being tested in a Phase I clinical trial (NCT06885697).

In summary, anti-MSLN CAR T cells have been tested in solid tumours with extensive clinical experiences reported to date. Despite being one of the earliest CAR T cells examined in solid tumours, improvements of existing CAR constructs and identification of new anti-MSLN scFv continue to emerge from preclinical studies. Advancement of anti-MSLN CAR T cell therapy over the years has focused on humanisation of the scFv (i.e. P4, m912, M5, 15B6, and hYP218) to prevent potentially life-threatening immune reactions due to xenoreactivity. To avoid impairments from MSLN shedding, scFvs have been designed to bind to the membrane-proximal region of MSLN, such as 15B4. Although this allows for improved potency and efficacy, this does potentially increase on-target off-tumour toxicities, as MSLN expression is observed in physiological conditions, and potentially upregulated during tissue injury, as reported in the fatal pulmonary toxicities from M5 CAR T cells (144). Selection of scFvs that react to antigen density levels compatible from malignant tissues but not the low levels from benign tissues will be an ideal strategy. To date, most of the anti-MSLN CAR T cells in clinical trials are second-generation, with varied results on safety and generally suboptimal clinical efficacy. Additional genetic modifications (i.e. CRISPR-Cas9 knockouts or receptor co-expression) are being explored as novel strategies in next-generation CAR T cells, with potential for clinical translation and improving the clinical outcomes of anti-MSLN CAR T cell therapies in the future.

1.3.3 Anti-MUC1 CAR T cell therapies

MUC1 is a widely tested CAR target in solid tumours (including pancreatic, breast, liver, lung, and gastrointestinal cancers) and may be particularly relevant for mucinous cancers, such as appendiceal cancer.

MUC1 is a member of the transmembrane mucin family and is characterised by its large structure (300 – 600 kDa) and heavy glycosylation (150). Under physiological conditions, MUC1 is abundantly expressed on the apical surface of glandular epithelial cells, forming a

physical covering that provides lubrication and protects against pathogenic invasion (151, 152). The protein is composed of two subunits stabilised by hydrogen bonds (**Figure 1.6**). The short C-terminal subunit contains the transmembrane domain and is responsible for intracellular signalling. The large N-terminal subunit forms an extracellular domain that extends 200 – 500 nm above the cell surface. This subunit is extensively O-glycosylated at the membrane-distal region and N-glycosylated at the membrane-proximal region.

During carcinogenesis, MUC1 shows abnormalities in both expression and glycosylation patterns. Due to loss of polarity, MUC1 expression is no longer confined to the apical surface but can be found on the basal and lateral surfaces as well. A 10-fold increase is observed in MUC1 expression of epithelial tumours, compared to normal physiological expression (153). Positivity of MUC1 expression in solid tumours ranges from 44% - 66% in gastrointestinal and cervical cancers, and from 77% - 100% in liver, thyroid, lung, breast, and ovarian cancer (150). Furthermore, MUC1 is altered structurally in tumour cells and shows exposure of the core peptide in the extracellular domain with incomplete glycosylation of the carbohydrate side chains. Importantly, new carbohydrate side chains are formed. These include the Tn (Thomsen Nouveau), TF (Thomsen-Friedenreich), sTn (sialyl Tn), ST (sialyl T antigen), and sTF (sialyl TF) glycoforms (154).

The biological functions of MUC1 in malignant settings have been well-studied. MUC1 participates in various pathways that regulate inflammation, drug resistance, angiogenesis, cancer migration, tumour growth and apoptosis (151). Additionally, similar to MSLN, the extracellular domain of MUC1 can be proteolytically cleaved by enzymes of the TACE family to mediate MUC1 shedding (155), which can reduce on-tumour recognition by CAR T cells. As a CAR target, it is worthwhile noting that increased antigen expression alone is not sufficient for MUC1 to be a suitable candidate, as its expression on normal epithelial cells would lead to potential obvious on-target, off-tumour toxicities. Given the aberrantly glycosylated nature of MUC1 protein in malignancies, current CAR T cells targeting MUC1 were designed to recognise the various tumour-specific MUC1 glycoforms.

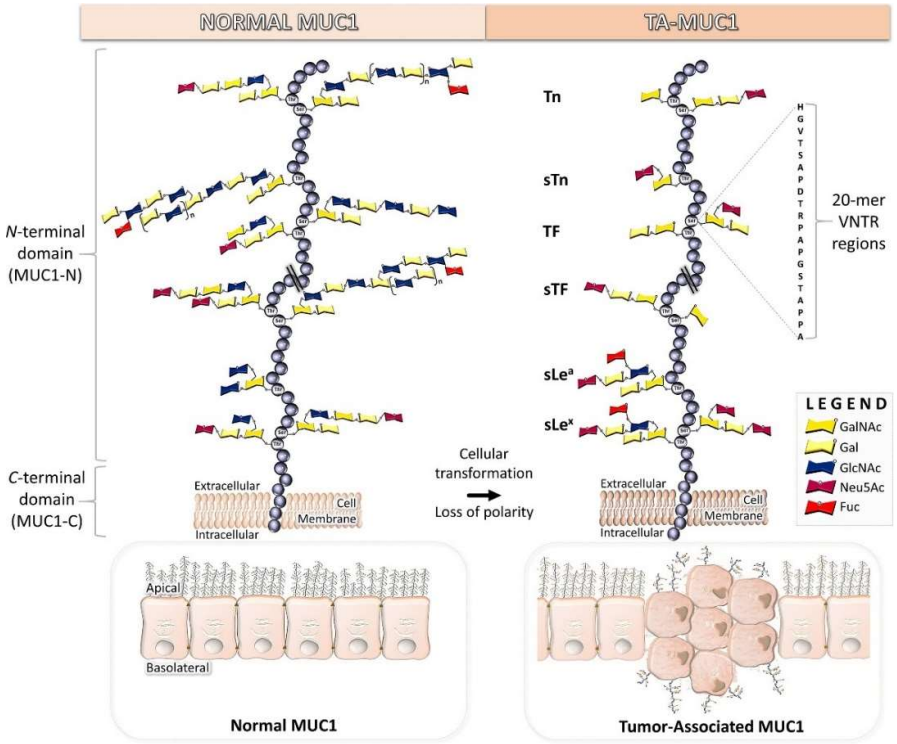

Figure 1.6 Mucin-1 (MUC1) structure in normal physiology and during malignancy. In this illustration, the C-terminal and N-terminal subunits were visualised as a single peptide, and the membrane-proximal N-glycosylation region was not shown. Glycoforms of MUC1 (Tn, sTn, TF, sTF, sLe^a, and sLe^x) were indicated, with the respective glycosylation moieties shown in the legend. Notably, the ST glycoform (Neu5Acα2-3Galβ1-3GalNAc) was not included in this illustration. VNTR, variable number of tandem repeats. Figure was reproduced from Beckwith and Cudic, 2020 (154).

1.2.4.1 Development and clinical outcomes of anti-MUC1 CAR T cell therapies

The initial anti-MUC1 CAR T cells in early development employed scFvs derived from antigen binding domains of murine antibodies, such as SM3 and HMFG2. Both SM3 and HMFG2 were capable of binding to multiple tumour-specific glycoforms (T, sTn, Tn, and additionally ST for HMFG2) as well as unglycosylated core protein (156). SM3 is highly specific to tumour-associated MUC1 glycoforms, however second-generation SM3 CAR T cells (with CD28 costimulatory domain) showed inefficient targeting of MUC1-positive tumour cells, and the reasons have been attributed to steric hinderance imposed by MUC1's size and heavy glycosylation (157). Despite lower surface expression, increasing the hinge length improved recognition and response of the SM3 CARs, resulting in drastically higher proliferation and IFN-

γ responses against MUC1-positive target cells. Phase I clinical trials of SM3 CAR T cells reported the treatment to be well-tolerated, although efficacy was moderate. In patients with advanced oesophageal cancer and non-small-cell lung cancer (NSCLC), no serious adverse events were reported where SM3 CAR T cells were modified with PD-1 knockout (158, 159). Best overall response was 66.7% (6/9) SD in the oesophageal cancer cohort and 55.0% (11/20) SD in the NSCLC cohort. In another study, two patients with metastatic seminal vesicle cancer received intratumoural injections of two third-generation SM3-based CAR T cell therapies (bearing the tandem CD28-41BB costimulatory domain) in separate tumours lesions (160). Since the SM3 scFv is incapable of recognising the MUC1 ST glycoform, the SM3 scFv was mutated in one product to improve binding of this specific glycoform. In the other product, the unmodified SM3 CAR was co-expressed with IL-12 to reduce immunosuppression. Significant tumour necrosis was observed in both patients only in the lesions infused with the mutated SM3 CAR T cells, suggesting that improving the binding capability of SM3 CAR T cells is essential for their clinical efficacy.

Unlike SM3, HMFG2 is a highly potent scFv, exhibiting a 7.4-fold higher affinity than SM3 when binding to unglycosylated MUC1 core protein. Third-generation HMFG2 CAR T cells with tandem OX40 and CD28 co-stimulatory domains showed efficient killing of target cells with low MUC1 expression and significantly delayed tumour growth *in vivo* (157). However, recognition of HMFG2 to MUC1 on normal breast epithelial tissues gave rise to the potential concern of on-target, off-tumour toxicities, hindering clinical translation of this CAR T cell therapy (161).

The 5E5 scFv represents an alternative with high tumour specificity and safety profiles *in vivo* (162). 5E5 selectively binds the tumour-associated Tn glycoform of MUC1, and, to a lower extent, the sTn glycoform as well, without binding of normally glycosylated MUC1 expressed on non-malignant cells (162). The primary epitope bound by 5E5 has been elucidated as the entire GalNAc unit on the MUC1 glycoforms, with direct contact to two of its residues (163). CAR T cells bearing the 5E5 scFv have been tested in xenograft mouse models of T cell leukemia, pancreatic cancer, and cholangiocarcinoma (162, 164). Interestingly, in cholangiocarcinoma, the tumour-specific Tn glycoforms were only recognised by 5E5 on tumour tissues but not found in all examined tumour cell lines (164). As a result, the *C1GALT1* gene had to be knocked out to produce the Tn glycoforms by inhibition of T-synthase, and

consequentially the knockout cell line was used for mouse engraftment. Compared to control CAR T cells, robust tumour control by 5E5 CAR T cells was seen in the pancreatic cancer and cholangiocarcinoma models (100% vs 40% survival at endpoint and 60% vs 0% tumour eradication, respectively), while in the T cell leukemia model survival was significantly increased (median survival: 50 vs 30 days). However, when 5E5 CAR T cells were tested in a syngeneic mouse model of ovarian cancer, no effect of tumour control was observed, although median survival was significantly extended by three other Tn-dependent anti-MUC1 CAR T cells (WE, 237, and TNGK) (165). The lack of efficacy was attributed to basal tonic signalling of the second-generation 5E5 CAR construct (with CD28 costimulatory domain) used, which contributed to lower CAR expression on the cell surface and higher release of immunosuppressive cytokines (IL-10 and IL-4) upon *in vitro* stimulation. In addition, while 237 scFv and its WE and TNGK derivatives were all developed against mouse mucin-family protein podoplanin (Tn-OST8), the cognate antigen used in the syngeneic model, 5E5 was initially designed for binding of the human Tn-MUC1 protein, and exhibited low binding to mouse Tn-OST8. In this instance, the poor responses of 5E5 CAR T cells could be specific to the design of the endogenous murine Tn-OST8 target. 5E5 CAR T cells with PD-1 knockout are being tested in an ongoing clinical trial (NCT05812326), for the treatment of recurrent/metastatic breast cancer, with preliminary results indicating that the treatment was safe and well-tolerated (166). The most serious adverse event was grade 4 lymphopenias which occurred in only one patient, lasting only a day. Preliminary data on efficacy showed 42% (5/12) evaluated patients had SD, and responses were associated with increased circulating CAR copies. It is unknown whether the 5E5 scFv has been humanized in this study, although humanised 5E5 CAR T cells have been used in another active clinical trial (NCT04025216) (165).

To address the issue of MUC1 shedding, the huMNC2 scFv was designed to recognise a specific juxtamembrane region, termed MUC1*, that is retained after enzymatic cleavage of MUC1 (167, 168). The huMNC2 scFv is fully humanised and does not bind to full-length MUC1 on normal epithelial cells. Immunohistochemical staining confirmed recognition of MUC1* by the huMNC2 scFv in 70% - 90% of lung, pancreatic, ovarian, and breast cancers (167, 168). Second-generation huMNC2 CAR T cells with CD28 or 41BB costimulatory domains (huMNC2-CAR28 and huMNC2-CAR44, respectively) both exhibited *in vitro* and *in vivo* efficacy against MUC1*-positive tumours. An ongoing Phase I/II clinical trial (NCT04020575) is currently assessing the

safety and efficacy of huMNC2-CAR44 T cells in patients with metastatic breast cancer (169, 170). 5 patients have been treated, although clinical outcomes have not yet been reported.

Overall, compared with anti-MSLN CAR T cells, anti-MUC1 CAR T cells offer the advantage of selectively recognising tumour-specific glycoforms, thus minimising the potential for on-target, off-tumour toxicities. Progress has been made to humanise scFvs (i.e. 5E5 and huMNC2) and balance the limited efficacy (SM3) or safety concerns (HMFG2) observed with earlier murine-derived scFvs. To date, clinical evaluations of humanised anti-MUC1 CAR T cells remain preliminary. Initial findings with 5E5 CAR T cells suggest favourable safety profiles and early-stage efficacy, although it remains to be confirmed through further clinical investigations. Shedding of MUC1 poses an ongoing therapeutic challenge and is currently being addressed by the huMNC2 scFv targeting the MUC1 cleavage product (MUC1*), which still awaits clinical reporting. Additionally, the limited availability of specific targetable glycoforms in cell line models has complicated the preclinical evaluation of glycoform-targeting CAR T cells. The development of more patient-related tumour models will be crucial for examining the expressions of MUC1 glycoforms, as well as to assess and optimise the therapeutic efficacy of anti-MUC1 CAR T cells.

1.3.4 Clinical trial landscape of TIL therapy

TIL isolation and efficacy were first demonstrated in murine models by Dr. Rosenberg and his group in 1982 (171). Following this, a first-in-human clinical trial was conducted in 1988 for metastatic melanoma, where objective response was observed in 55% (11/20) patients (172). Since this initial clinical success, clinical trials of TIL therapy have expanded over the years, mainly concentrating on melanoma and has led to the FDA approval of lifileucel, with ongoing testing in other solid tumours such as ovarian, pancreatic, lung, and intestinal cancers.

In general, TIL therapy is evaluated to be safe and the toxicities from treatment regimens can be clinically managed. Notably, serious adverse effects from TIL therapy mainly come from the non-myeloablative lymphodepletion (NMA-LD) and high dose of IL-2 administered prior and post TIL infusion, respectively. Standard NMA-LD is delivered as a combination regimen of cyclophosphamide (CP, 60 mg/kg) for 2 days and fludarabine (FA, 25 mg/m^2) for the next 5 days before TIL infusion (75). Common grade 3 or above adverse events related to NMA-LD

are haematological complications such as low white blood cell count and febrile neutropenia, which are the expected consequences of the therapy. High dose of IL-2, usually ranging from 600,000 IU/kg to 720,000 IU/kg, is given at 8-12 hour intervals post-TIL infusion. Most studies employ up to 6 doses of IL-2. Grade 3 or above adverse events related to the IL-2 regimen include hypotension and capillary leakage. Although side effects from NMA-LD and IL-2 are typically temporary and manageable, deaths due to pneumonia, arrhythmia, and acute respiratory failure related to NMA-LD and/or IL-2 have been reported (10). TIL infusion is usually given as a single injection, where less than 5 billion to 150 billion cells per dose have been administered (75). It is generally regarded as well-tolerated, with transient dyspnea, chills and fever as common side effects. However, life-threatening adverse effects, such as anaphylactic reactions, have been reported (10). Such infusion-related reactions occur in less than 4% of patients (173). These can be mitigated by close monitoring and easily accessible emergency medications (i.e. epinephrine and diphenhydramine).

1.3.4.1 Clinical efficacy in melanoma

Favourable outcomes of TIL therapy have been achieved in melanoma, an immunogenic disease where most clinical trials of TIL therapy have been conducted (174). Prior to the approval of immune checkpoint blockade treatments, early studies reported ORR of 34 – 55% from metastatic patients receiving TIL therapy (172, 175). Treatment regimens in these early studies consisted only of CP in NMD-LD and involved multiple cycles of TIL and IL-2 infusions instead of single infusions. While REP expansion was not yet implemented, the transfer to gas-permeable bags from expansion in tissue-culture plates has been explored (175), laying the foundation for the more advanced protocols that are now in clinical use.

Further studies have assessed TIL generations from tumour-reactive cultures (selected TILs) in contrast to bulk, unselected TILs. One type of unselected TILs, known as “young TILs”, were shown to be comparable or superior in efficacy than reactivity-selected TIL products while minimising *ex vivo* culturing time (176, 177). In the expansion of young TILs, microcultures containing lymphocyte outgrowth from tumour fragments were mixed and combined prior to REP expansion. Manufacturing time was significantly shortened while tumour reactivity was retained in cryopreserved aliquots used for infusion (177). In the same study, patients receiving tumour-selected TILs exhibited shorter TIL culturing times in responders than non-responders. This suggested a negative association between manufacturing duration and

clinical response. Nevertheless, young TILs did not show this association, and efficacy was similar between CD8-enriched young TILs and tumour-selected TILs, both at a clinical response rate of ~55% in metastatic patients. In another study on metastatic patients that were refractory to at least one line of therapy, young TIL protocol achieved a significantly higher ORR than the tumour-selected TIL protocol (31% vs 8%) (176). However, substantially more patients were treated with young TILs than tumour-selected TILs (n = 91 vs n = 12). It was unknown whether enrichment of CD8 TIL populations was performed, and if this potential difference contributed to improved efficacy of young TILs over tumour-selected TILs compared to the previous study. Generation of young TILs has also been employed in the manufacturing of lifileucel for melanoma (LN-144, by Iovance Biotherapeutics). In the pivotal Phase II C-144-01 study, lifileucel demonstrated 29% - 35% ORR across two melanoma cohorts (25/87 and 23/66, respectively) (10). Notably, study participants were advanced patients who failed multiple lines of treatment (median = 3 prior lines of therapy), all of which previously received immune checkpoint inhibitors (ICIs) (100% with PD-1/PD-L1 inhibitors and 81.7% with CTLA-4 inhibitors). The Phase III TILVANCE-301 trial assessing lifileucel with pembrolizumab (PD-1 inhibitor) compared to pembrolizumab alone in ICI-naïve, advanced melanoma patients is ongoing (178). Positive results could support the implementation of lifileucel as an earlier line of therapy for patients with metastatic or unresectable melanoma. Preliminary results from a small cohort of ICI-naïve, advanced melanoma patients in the Phase II IOV-COM-202 study have shown an ORR of 88% (7/8), when treated with lifileucel in combination with pembrolizumab (179). Another Phase III randomised trial (M14TIL) compared TIL therapy versus ipilimumab (CTLA-4 inhibitor) as a first or second-line treatment for advanced melanoma (180). TILs were manufactured using a young TIL protocol which is distinct from the manufacturing protocol used for lifileucel. ORR of the young TIL-infused group was 49% (41/84), with 17 (20%) CR and 24 (29%) PR responses. This was in stark contrast with the ipilimumab-infused group where an ORR of 21% (18/84), with 6 (7%) CRs and 12 (14%) PRs, was observed. Progression-free survival was also higher for the TIL-infused group, at 7.2 months, compared to 3.1 months in the ipilimumab-infused group. The majority (87% in TIL-infused group and 85% in ipilimumab-infused group) of patients had prior anti-PD-1 therapy. These results suggest young TILs as a more favourable treatment than ipilimumab monotherapy in advanced patients refractory to frontline anti-PD-1 therapy. Overall, TIL therapy has demonstrated therapeutic success in metastatic melanoma. Its potential to be

used as an earlier line of treatment, in combination or substitution of immune checkpoint inhibitors, is currently being explored in the clinical space.

1.3.4.2 Clinical efficacy in other solid tumours

TIL therapy has also been tested in clinical trials of other solid tumours such as NSCLC, pancreatic cancer, ovarian cancer, cervical cancer, and colorectal cancer, with varying success. In the Phase II IOV-COM-202 trial, lifileucel for non-melanoma solid tumours (LN-145, by Iovance Biotherapeutics) achieved an ORR of 21% (6/28) in a NSCLC cohort (181). Patients had metastatic disease and were heavily pretreated, with 100% having had anti-PD-1/PD-L1 therapy and 96% received one or more lines of systemic chemotherapy. Early results of lifileucel in combination with pembrolizumab had an ORR of 43% (5/12) in head and neck cancer and 50% (5/10) in cervical cancer in ongoing Phase II trials, although small number of patients have been recruited so far (179). All patients had advanced disease but were ICI-naïve, which could have contributed to the high ORRs observed. Similar to LN-144, LN-145 were expanded as young TILs and utilised the same Generation 2 (Gen 2) 22-day manufacturing process employed for LN-144 production in the C-144-01 study (83).

Other studies that used bulk, unselected TILs did not demonstrate comparable clinical responses as LN-145. Instead, tumour-selected TILs have found favourable clinical outcomes. In a Phase II study, unselected TILs yielded a disease control rate (DCR) of 63%, but an ORR of 0%, in a pooled cohort of 16 patients with advanced, treatment-refractory ovarian cancer, colorectal cancer, and pancreatic cancer (80). TILs were generated using the proprietary MDACC manufacturing process, with additional agonist stimulation (anti-CD3 and anti-CD137 antibodies) supplemented in pre-REP expansion to support the early activation of T cells. No manufacturing failure occurred; however, no reactivity assessment using autologous tumour co-cultures was performed. It remains unclear whether the early agonist stimulation preserved sufficient levels of tumour reactivity in the final infusion products, and if it played a role in the inadequate clinical responses.

In another Phase II study, bulk, unselected TILs, generated using the young TIL protocol, yielded no objective clinical responses in a pilot cohort of 18 patients with heavily-pretreated (median = 4 lines of prior therapy), metastatic gastrointestinal cancer (91). Subsequent patients were screened for neoantigen reactivity, of which 57% (95/168) were eligible for

treatment with neoantigen-reactive TILs. Patients received neoantigen-reactive TILs as a monotherapy (the SEL-TIL group) or in combination with pembrolizumab (the SEL-TIL + P group). ORR was 8% (3/39) for the SEL-TIL group and 24% (8/34) for the SEL-TIL + P group. Neoantigen selection was performed using the "NeoExpand" method, where individual TIL microcultures from pre-REP were co-cultured with APCs loaded with mutated neoantigen epitopes identified from WES (105). In the Phase II study, the interval from tumour resection to infusion of neoantigen-selected TILs was 3-5 months, although for several non-responders in both SEL-TIL and SEL-TIL + P groups this period was over 20 months. The high patient dropout during screening and lengthy manufacturing time remain limitations of neoantigen-selected TILs in this study, despite their higher efficacy compared to young TILs.

Viral antigen-selected TILs have also been tested in virus-induced cancers. A phase II study examined TILs for human papillomavirus (HPV)-associated cancers, after an ORR of 33.3% (3/9) was achieved in a preliminary cohort of HPV-positive cervical cancer patients (182). Pre-REP TIL microcultures that showed reactive responses to APCs loaded with oncoproteins E6 and E7 from patient-specific HPV type (HPV-16 or HPV-18) were selected for REP and subsequent infusion. ORR was 28% (5/18) for the cervical cancer cohort and 18% (2/11) for the non-cervical cancer cohort (103). The non-cervical cancer cohort was comprised of patients with oropharyngeal cancer (n = 5), anal cancer (n = 5), and vaginal cancer (n = 1). All patients had HPV-positive, metastatic disease and at least one prior line of systemic chemotherapy. Higher levels of reactivity were shown for responders than non-responders from TIL subcultures. Additionally, there was a positive correlation between clinical response and HPV reactivity from peripheral blood one month post-treatment. However, only 64% (29/45) of patients undergoing surgery received TIL therapy due to high patient-to-patient variability in HPV reactivity. Genetically engineered, HPV-targeted T cells can circumvent this issue, and this is being assessed by the same group in an ongoing phase I/II trial using TCR T cells specific to HPV-16 E7 oncoprotein (NCT02858310).

In addition to antigen-selected TILs, genetic modifications to improve the clinical performance of TILs are also being evaluated for non-melanoma solid tumours. In one completed phase I study, a novel intracellular immune checkpoint, cytokine inducible SH2-containing protein (CISH), was knocked out using CRISPR-Cas9 in neoantigen-selected TILs (104). Patients had metastatic colorectal cancer and were heavily treated with a median of five prior lines of

systemic therapy. ORR was 8% (1/12). The only patient who showed objective response had an ongoing CR that was over 21 months since TIL treatment. This patient had a microsatellite instability (MSI)-high tumour, which likely contributed to a high neoantigen burden that increased reactive T cell repertoire in the infusion product. On average, manufacturing time was 103 days and longer compared to standard young TIL protocols. Despite the genetic modifications, neoantigen-selected, CISH knockout TILs were well-tolerated without severe side effects such as cytokine release syndrome or neurotoxicity. Other trials assessing genetically modified TILs, such as TILs with PD-1 knockout (IOV-4001, Iovance Biotherapeutics) for advanced NSCLC as well as melanoma (NCT05361174), are currently underway. Safety and efficacy of genetically modified TILs remain to be confirmed from these studies.

1.4 Challenges in solid tumours

1.4.1 General challenges and emerging solutions

1.4.1.1 CAR T cell therapy

The identification of an ideal tumour-associated antigen target represents one major challenge of CAR T cells in solid tumours. Other challenges include limited tumour infiltration, poor *in vivo* persistence, and TME-induced hypofunction. Strategies to overcome these challenges have been explored to improve CAR T cell efficacy and achieve long-term remission. In addition, safety of CAR T cells remains hindered by risks of significant toxicities, such as life-threatening on target off-tumour responses, neurotoxicity, and immune reactions to infused CAR T cells. Cytokine release syndrome remains another potential concern for CAR T cells, although its overall incidence and severity are lower in solid tumours compared to haematological malignancies (183). Methods to reduce CAR T cell toxicities and improve treatment safety are also being developed and evaluated.

Locoregional delivery of CAR T cells, in contrast to systemic administration, has been tested in an increasing number of studies as an approach to improve CAR T cell infiltration, persistence, and safety in solid tumours (184, 185). Locoregional delivery refers to administering the CAR T cells intratumourally or in close vicinity of the tumour. Due to the limited trafficking of T cells across the blood brain barrier, intracranial injection has been assessed and considered to be the preferred method of CAR T cell administration for brain tumours, demonstrating

favourable safety and efficacy profiles from a number of clinical trials (186-190). As discussed earlier, for pleural tumours such as mesothelioma, intrapleural injection achieved remarkable improvements in efficacy during preclinical studies, compared to systemic administration of CAR T cells (62). Intrapleural injection has also been well-tolerated when tested clinically and can be a potential method to limit the on-target, off-tumour toxicities of highly potent anti-MSLN CAR T cells (143, 144). Direct intratumoral delivery is also feasible, which can be guided by radiological and/or sonographic imaging for increased precision. In a clinical trial against metastatic breast cancer, intratumoural injection of mRNA-based CAR T cells was well-tolerated and showed necrosis as well as loss of target antigen (c-Met) at the site of injection (191). Use of image guidance, however, was not mentioned. In another head-and-neck cancer trial, intratumoural injection was safe (no severe treatment-related and dose-limiting toxicities), with 60% (9/15) of patients achieving SD as best clinical response. Ultrasound guidance was used during one case of drug administration. CAR T cell leakage into the peripheral circulation was not detected post-injection, which likely contributed to the lack of significant toxicities. Overall, locoregional delivery is a highly clinically applicable technique and has consistently demonstrated to be safe, with potential of enhancing CAR T cell performance compared to systemic delivery.

Combination treatments have also been examined to improve the response of CAR T cell therapies (192). Combination with anti-PD-1 blockade by pembrolizumab has been clinically assessed for CAR T cells in neuroblastoma as well as anti-MSLN (m912) CAR T cells in mesothelioma (143, 193, 194). In both neuroblastoma trials using anti-GD2 and anti-EGFRvIII CAR T cells, combination with pembrolizumab was safe but did not increase CAR T cell expansion, persistence, or efficacy (193, 194). In the mesothelioma trial, more favourable outcomes were seen with complete metabolic responses observed based on radiological evaluation (143). The specific contribution of pembrolizumab administration was unclear, as the CAR T cells were delivered locoregionally and this could have improved treatment responses as well. Nevertheless, in one patient where tumour biopsy was available, PD-L1 expression was increased by 40% eight weeks post-treatment, suggesting evidence of response to pembrolizumab. Further, CAR T cells can be combined with other immunotherapies such as oncolytic viruses and cancer vaccines. Both approaches are capable of promoting an inflammatory TME that facilitates the anti-tumour responses of CAR T cells

in solid tumours (195, 196). An ongoing trial using anti-MSLN (M5) CAR T cells combined with an oncolytic adenovirus (VCN-01) has reported sustained SD in 2 out of 3 treated patients (197). No severe (grade 4 or higher) toxicities occurred, but cytokine release syndrome was observed in one patient, likely because of high potency of M5 CAR T cells. A separate phase I trial testing intratumoural delivery of another oncolytic virus (CAdVEC) with anti-HER2 CAR T cells is currently enrolling (NCT03740256) (198). In the seminal phase I/II BNT211 trial, anti-CLDN6 CAR T cells in combination with CARVac, a cancer vaccine consisting of an RNA-lipid complex amplifying for the CAR target CLDN6, resulted in an ORR of 33% (7/21), with 1 CR and 6 PRs out of 21 patients as the best overall response (199). CARVac administration was well-tolerated, and treatment-related toxicities were mainly attributed to CAR T cell delivery, which were manageable. Transient fever, and increase in CAR T cell frequencies as well as circulating IFN-γ levels were observed upon CARVac infusion, providing preliminary evidence for vaccine-induced effects on immune stimulation and CAR T cell expansion. However, the exact impact of CARVac on CAR T cell engraftment was not characterised extensively. Combination therapies thus provide a multi-faceted approach to overcome the hostile environment that CAR T cells experience in solid tumours.

Although CAR T cell products used in most clinical trials employ second-generation CAR constructs, next-generation CAR T cells have also been employed for solid tumour treatments. Third-generation CAR T cells, such as ones with tandem CD28 and 4-1BB, or CD28 and OX40 costimulatory domains, have achieved increased persistence from xenograft studies (133, 200, 201), although long-term persistence have not been consistently well demonstrated from solid tumour clinical trials (194, 202, 203). Suppressive myeloid populations from the peripheral circulation have been observed as one limitation that inhibited CAR T cell expansion in some of the treated patients. In one case example from a fourth-generation CAR T cell product, complete remission (CR) was demonstrated in an advanced pancreatic cancer patient following intravenous infusion of anti-MSLN CAR T cells co-expressing IL-7 and CCL19 cytokines (204), which also enhanced CAR T cell survival and solid tumour clearance in murine models (205). The patient did receive multiple infusions (6 times in total) for CR to be confirmed radiologically. Although the anti-MSLN scFv was not specified, the patient did not experience significant toxicities and none of the 6 patients in the tested cohort reported grade 2 or above adverse events. Additional genetic modifications, such as CRISPR gene knockout

and overexpression of chemokine receptors, have also been widely tested. The immune checkpoint PD-1 is a common knockout target for reinvigorating the anti-tumour activity of CAR T cells (206). This has been evaluated in clinical trials of both anti-MSLN and anti-MUC1 CAR T cells (137, 159), as mentioned in **section 1.3**. In the case of P4 CAR T cells, the additional TCR-knockout significantly impaired CAR T cell persistence, highlighting the need for extensive preclinical characterisation of intended knockouts prior to clinical translation. Further, co-expression of chemokine receptors (such as CCR2,4,8, and CXCR1,2,6) has been utilised for facilitating homing and infiltration of CAR T cells into solid tumours preclinically, although such strategies await clinical translation (207). In a phase I trial against relapsed/refractory Hodgkin lymphoma, anti-CD30 CAR T cells co-expressing the CCR4 showed enhanced persistence (positive signal at 6-month: 86% vs 22%) and anti-tumour activity (reduction in CCL17 by week 2: 86 ± 13% vs 52 ± 38%) compared to anti-CD30 CAR T cells without CCR4 co-expression (208). Safety and functionality of chemokine receptor co-expression remain to be examined in solid tumour clinical trials.

Progress in synthetic engineering have also sought to improve CAR T cell safety in solid tumours. Dual-targeting CAR T cells can confer greater tumour specificity and reduce the potential for on-target, off-tumour toxicities, when logic-gated by an “AND gate” so that CAR T cells are only activated by simultaneous recognition of both target antigens (209). Dual-targeting CAR T cells can also be logic-gated by an “OR gate”, where recognition of at least one target antigen is sufficient for activation, to counter antigen heterogeneity and improve CAR T cell efficacy. The incorporation of a suicide switch such as the inducible Caspase 9 (iCasp9) enables elimination of CAR T cells in case life-threatening treatment toxicities occur (210). The iCasp9 construct is induced by administration of the pharmaceutical agent AP1903, which leads to apoptosis of CAR T cells within minutes. Suicide switches have been widely employed in CAR T cell clinical trials of CAR T cells, in both haematological and solid tumour settings (209). Clinical experiences indicate that CAR T cells incorporating suicide switches have been well-tolerated, although the suicide switches have been rarely activated. In one instance, activation of iCasp9 successfully terminated severe and steroid-refractory neurotoxicity following CAR T cell administration in a leukemia patient (211). More than 90% of circulating CAR T cells were eliminated 1 day after AP1903 administration. Neurotoxicity immediately improved following AP1903-induced iCasp9 activation and completely resolved by day 4.

Overall, advances in CAR engineering offers promising avenues to combat toxicities and off-target effects of CAR T cell therapies.

In summary, following the success previously seen in the haematological setting, clinical translation of CAR T cell therapy into solid tumours is rapidly expanding. However, the complex architecture, immunosuppression/exclusion, and antigen heterogeneity of solid tumours pose additional challenges. Despite poor to modest responses of CAR T cells in current clinical trials, numerous strategies have been explored in preclinical and clinical settings to enhance the safety and *in vivo* functionality (persistence, infiltration, and anti-tumour responses) of CAR T cells. As addressed above, improvements have been shown in several instances, with locoregional delivery and next-generation CAR T cells being increasingly adopted in more recent trials. The future of CAR T cell therapy in solid tumours awaits to be determined from the outcomes of ongoing clinical trials.

1.4.1.2 TIL therapy

The challenges that TIL therapy faces in solid tumour treatments have largely been outlined in previous sections (**section 1.2.2** and **section 1.3.4**). The main priorities are to optimise TIL manufacturing to ensure successful and timely TIL expansion, as well as to enhance the anti-tumour reactivity of TIL products, especially in other solid tumours besides melanoma.

Current TIL therapy suffers from issues with manufacturing failures and high interpatient variability in TIL performances. The single most important factor for successful TIL establishment is tumour quality (212). As discussed, tumour size specifications (> 1.5 cm greatest diameter) are essential for obtaining sufficient TILs for expansion. For patients who experienced initial TIL manufacturing failure, re-enrolment provides a second chance at manufacturing (104). Manufacturing of reactivity-selected TILs can be aborted if no strong reactivity is observed during reactivity screening. High heterogeneity in TIL expansion and performance is also seen in clinical experience across different solid tumour types. Despite relatively consistent frameworks in TIL generation, individual tumour types have different microenvironment compositions and can differ in the frequency, phenotype, and reactivity of TILs present. For instance, expansion of TILs from gastrointestinal tumours was slower than TILs derived from melanoma due to lower density of TILs within tumours (213). TILs from gastrointestinal tumours also had less number of CD8 T cells and lower reactivity against

autologous tumours compared to TILs from melanoma. Further work is required to characterise the parameters that define successful TIL expansion across different solid tumour settings.

Standardised assays that optimally differentiate between responders and non-responders are still lacking and urgently require development. ELISA assays that detect IFN-γ secreted by TILs in co-culture with autologous tumours remain the gold standard for assessing tumour reactivity during clinical manufacturing (212). However, in cases when autologous tumours were not available and HLA-matched tumour cell lines were used as targets, reactivity from *in vitro* assays has been observed to under-represent clinical reactivities of infused TILs (89). Improvements in potency assays for screening and release testing of TIL products require thorough understanding of the factors governing clinical responses of TIL therapy, which are currently being explored (214).

Genetically modified TILs represent the next-generation TIL therapy for advanced solid tumours. Immune checkpoints that suppress TIL activities can be knocked out using technologies such as CRISPR-Cas9 and TALEN. In one example, CRISPR-Cas9 knockout of the intracellular target CISH enhanced TIL reactivity and was able to restore reactivity that was lost from unedited, control TILs (204). As described earlier, CISH knockout TIL therapy was demonstrated to be safe and CR was achieved in one patient with MSI-H gastrointestinal cancer from an ongoing Phase I trial (104). Current experiences of gene knockouts in TIL studies all showed minimal off-target activities with no detrimental influences on TIL expansion and responses (215, 216) (217), highlighting their safety for clinical delivery. TILs can also be engineered to express transgenes for increased anti-tumour activity. CAR-engineered TILs have also been assessed in preclinical models of colorectal cancer and melanoma, demonstrating improved *in vivo* efficacy over conventional, PBMC-derived CAR T cells (218, 219). However, responses of CAR-engineered TILs remain to be assessed clinically. Transient expression of the pro-inflammatory cytokine IL-12 increased cytotoxicity of TILs injected intratumourally in a murine melanoma model, and led to the elimination of untreated, bilateral tumours (220). In a phase I melanoma trial, a favourable ORR of 63% (10/16) was reported for TILs retrovirally transduced with IL-12 (221). However, the trial was terminated as life-threatening toxicities were observed at the treated dose levels ($0.3 - 3 \times 10^9$ cells per dose), likely due to the unmanaged levels of IL-12 secretion from TILs. The co-expression of

chemokine receptors has also been investigated as a strategy to enhance TIL tumour infiltration, and clinical-grade manufacturing of TILs retrovirally transduced with the chemokine receptor CXCR2 has been established (222). CXCR2 transduction did not affect TIL expansion and retained their cytotoxic capacity. A phase I/II trial in progress is assessing the safety and tumour trafficking ability of CXCR2-transduced TILs in metastatic melanoma (223). Overall, genetic modifications provide strategies to counteract immunosuppression, increase anti-tumour cytotoxicity, and improve infiltration, holding significant potential to enhance the clinical efficacy of TIL therapies in solid tumours.

1.4.2 Solid tumours

While both CAR T cell and TIL therapies have been examined in a wide range of solid tumours, it is essential to recognise that each cancer type presents their own unique set of challenges. Individual cancer types differ in stromal composition, tumour architecture, antigen expression, and profiles as well as immune phenotypes. These can have significant implications on the construct choice for CAR T cell therapy and optimal manufacturing pipelines for TIL therapy. In addition, given the cost and lengthy production process, applications of T cell-based therapies should take into consideration the aggressiveness and complications of the disease, as well as if more cost-effective alternative lines of treatment are available. Given the differences in prevalence and severity of unmet needs, T cell-based therapies have been well-established for clinical testing in some solid tumour types while showing little adoption in others. Below we will describe the challenges faced by T cell-based therapies in pancreatic cancer and appendiceal cancer, where effective treatments are currently lacking. In the former, CAR T cell therapies have been extensively tested but hindered by the hostile tumour microenvironment (TME); in the latter, T cell-based therapies have not been examined so far.

1.4.2.1 Pancreatic cancer

Pancreatic cancer remains a significant global burden of disease, ranking as the 7th cancer-related cause of absolute years of life lost worldwide and the fourth leading cause of cancer deaths in Australia (224, 225). Over 90% of pancreatic malignancies occur as the highly aggressive pancreatic ductal adenocarcinoma (PDAC) subtype (226). Most PDAC cases originate from microscopic dysplastic precursor lesions known as pancreatic intraepithelial neoplasms (PanINs) (227), but other cystic precursor lesions, such as intraductal papillary

mucinous neoplasms (IPMNs) and mucinous cystic neoplasms (MCNs), can also become malignant (228).

The significant disease burden of PDAC is highlighted by its rising incidence rate and high mortality rate, with a five-year survival of less than 10% (225, 229). This is contributed by late diagnosis in the majority of PDAC patients due to both the absence of specific clinical symptoms during early disease and the inherent challenges in imaging and detecting early-stage pancreatic tumours (230, 231). For treatments, surgical resection remains the only potentially curative option, but this is only possible for the 10-15% of patients who have limited local disease (232). The remainder present with locally advanced or metastatic disease that is not amenable to curative intent surgery. Standard systemic chemotherapy and radiotherapy have also shown limited efficacy to date with low response rates and often rapid development of treatment resistance (232-234). Novel treatments are urgently needed to improve the poor clinical outcomes in PDAC.

1.4.2.1.1 Biology of PDAC

PDAC exhibits a highly complex and hostile TME that presents significant therapeutic challenges (**Figure 1.7**). This TME is characterised by pronounced fibrosis, hypoxia, nutrient deprivation, and immunosuppression.

Fibrosis is a significant feature of the PDAC stroma, which can take up more than 90% of the tumour mass (235). This serves as a physical barrier, reducing the penetration of systemic chemotherapies and hindering T cell infiltration into the tumour (236, 237). The fibrotic deposition, known as desmoplasia, is composed of extracellular matrix (ECM) proteins such as collagens, integrins, proteoglycans, and glycoproteins that are predominantly produced by cancer-associated fibroblasts (CAFs) (238). Of these ECM proteins, collagen is the most abundant, with type I collagen considered responsible for most of the desmoplasia in PDAC (239). Production of type I collagen are largely driven by the αSMA+ myofibroblasts (myCAF) subset. Two other subsets, inflammatory CAFs (iCAFs) and antigen-presenting CAFs (apCAFs) contribute to immunomodulation in the TME. iCAFs secrete the pro-inflammatory cytokine IL-6 to promote tumour progression, while apCAFs directly engage with CD4 T cells to induce their differentiation into Tregs, thus inhibiting anti-tumour immunity (240, 241). Interestingly, selective depletion of myCAF to counteract desmoplasia has unexpectedly accelerated PDAC progression and reduced survival in murine models, accompanied by increased

immunosuppression, hypoxia, and epithelial-to-mesenchymal (EMT) transitions (242). As such, stromal modulation approaches that focus on CAF reprogramming, rather than depletion, offer a more effective way to overcome desmoplasia, and have been shown to improve responses of anti-PD-1 therapies in murine PDAC models (236, 243).

Hypoxia in the PDAC TME has been attributed to restricted blood flow due to poor vascularisation. PDAC vasculature is characterised by deficient angiogenesis and markedly elevated interstitial fluid pressure, which is 10-fold higher in pancreas of mice with PDAC than in normal murine pancreas (244). The buildup of high interstitial fluid pressure can induce vascular collapse, limiting effective delivery of therapeutic agents from the peripheral circulation into the TME (244).

Notably, PDAC is considered an immunologically “cold” tumour characterised by a strongly immunosuppressive TME and low infiltrations of effector T cells (245). Diverse myeloid and lymphocyte cell types contribute to this immunosuppressive milieu.

The myeloid populations represent a substantial compartment of the PDAC stroma, and include myeloid-derived suppressor cells (MDSCs), tumour-associated macrophages (TAMs), and tumour-associated neutrophils (TANs). MDSCs engage in contact-dependent cross-talk with Tregs to induce their accumulation within tumours (246). TAMs induce the upregulation of PD-1 expression and the release of immunosuppressive chemokines (CXCL1 and CXCL5) from tumour cells, which promote T cell exhaustion and inhibit T cell infiltration, respectively (247, 248). Additionally, TAMs can be polarised to the immunosuppressive M2 or the pro-inflammatory M1 phenotypes. TAMs in PDAC are predominantly of the M2 phenotype, which produce cytokines such as IL-10 and TGF-β that can inhibit the functional activities of CD8 T cells (249). TAMs have been negatively associated with CD8 T cell infiltration and contribute to T cell exhaustion via upregulation of the immune checkpoint ligand Nectin-2 (250). Blockade of IL-17, a neutrophil-chemoattractant upregulated in the PDAC TME, also improved sensitivity of murine PDAC models to anti-PD-1 immunotherapy (251). Finally, arginase-1 activity from myeloid cells causes local depletion of arginine, an essential metabolite for T cells, leading to a nutrient-poor environment that compromises T cell fitness, survival, and anti-tumour responses (252, 253).

The infiltrating lymphocyte populations in PDAC mainly consist of regulatory B cells and T cells (Bregs and Tregs), and dysfunctional T cells with senescent and exhausted phenotypes (245). IL-18 secreted by PDAC cells has been shown to stimulate the expansion of Bregs and their release of IL-10 (250). Tumour-infiltrating B cells also exert potent immunosuppression via secretion of IL-35, which downregulates effector functions of CD4 and CD8 T cell infiltrates, promotes Treg expansion, and enhances cancer cell proliferation and resistance to apoptosis (254-256). Additionally, these B cells show upregulated PD-L1 expression and interact with TAMs to induce M2 polarisation, which impair anti-tumour responses of CD8 T cells (257, 258). Tregs (identified by CD4+CD25+FOXP3+ expressions) show increased prevalence during PDAC progression and is negatively correlated with CD8 T cell infiltration (259). These cells can contribute to immune evasion through multiple mechanisms, including direct cytotoxicity towards effector T cells, secretion of immunosuppressive cytokines (IL-10 and TGF-β), induction of T cell exhaustion via inhibitory receptor signalling, and deprivation of IL-2 required for effector T cell metabolism and survival (250). In PDAC, Tregs have also been shown to interact directly with CD11c+ dendritic cells (DCs) and suppress the expression of costimulatory ligands (CD40 and CD86), leading to the inhibition of CD8 T cell activation downstream (260). Lastly, the PDAC stroma shows markedly poor infiltration of effector T cells. These effector T cells are uniformly distributed in the PDAC tumour and presented predominantly with dysfunctional phenotypes (261). In particular, single cell transcriptomic profiling revealed that only ~12% of CD8 T cells in PDAC TME showed expression profiles associated with anti-tumour capabilities. The remaining populations are either functionally unresponsive (naïve, senescent or exhausted phenotypes) or immunosuppressive (CD8+FOXP3+ Tregs) (261). In addition, over 40% of CD8 T cells show a terminally differentiated phenotype. Overall, the elevated immune checkpoint expressions within stromal populations, together with a fibrotic, hypoxic, and nutrient-deprived TME enriched in immunosuppressive cytokines, contribute significantly to the low anti-tumour immunity observed in PDAC.

Aside from the PDAC stroma, this low anti-tumour immunity is also partially driven by tumour-intrinsic factors. Compared to other solid tumour types, PDAC exhibits a low tumour mutational burden (TMB) characterised by a few well-defined driver mutations, most commonly in tumour suppressor genes such as *KRAS* (> 95% of all cases), *TP53* (60% - 70%),

CDKN2A (30% - 50%), and *SMAD4* (20% - 50%) (262-264). To date, only a few immunogenic antigens have been identified in PDAC (245). Consequently, the low neoantigen diversity in PDAC constrains the clonality of tumour infiltrating CD8 T cells, which is a critical determinant of anti-tumour immunity (265). Furthermore, downregulations of antigen-presenting molecules (i.e. HLA class I and TAP) have been observed in PDAC tumour tissues and cancer cell lines, presenting a barrier to the generation of tumour-reactive T cell responses (266). PDAC tumour cells can also evade T cell killing by secreting immunosuppressive cytokines (G-CSF and GM-CSF) and developing resistance to death receptor-ligand interactions (267, 268). Their intrinsic aggressiveness and broad chemoresistance further highlight PDAC as a challenging disease for existing therapeutic approaches.

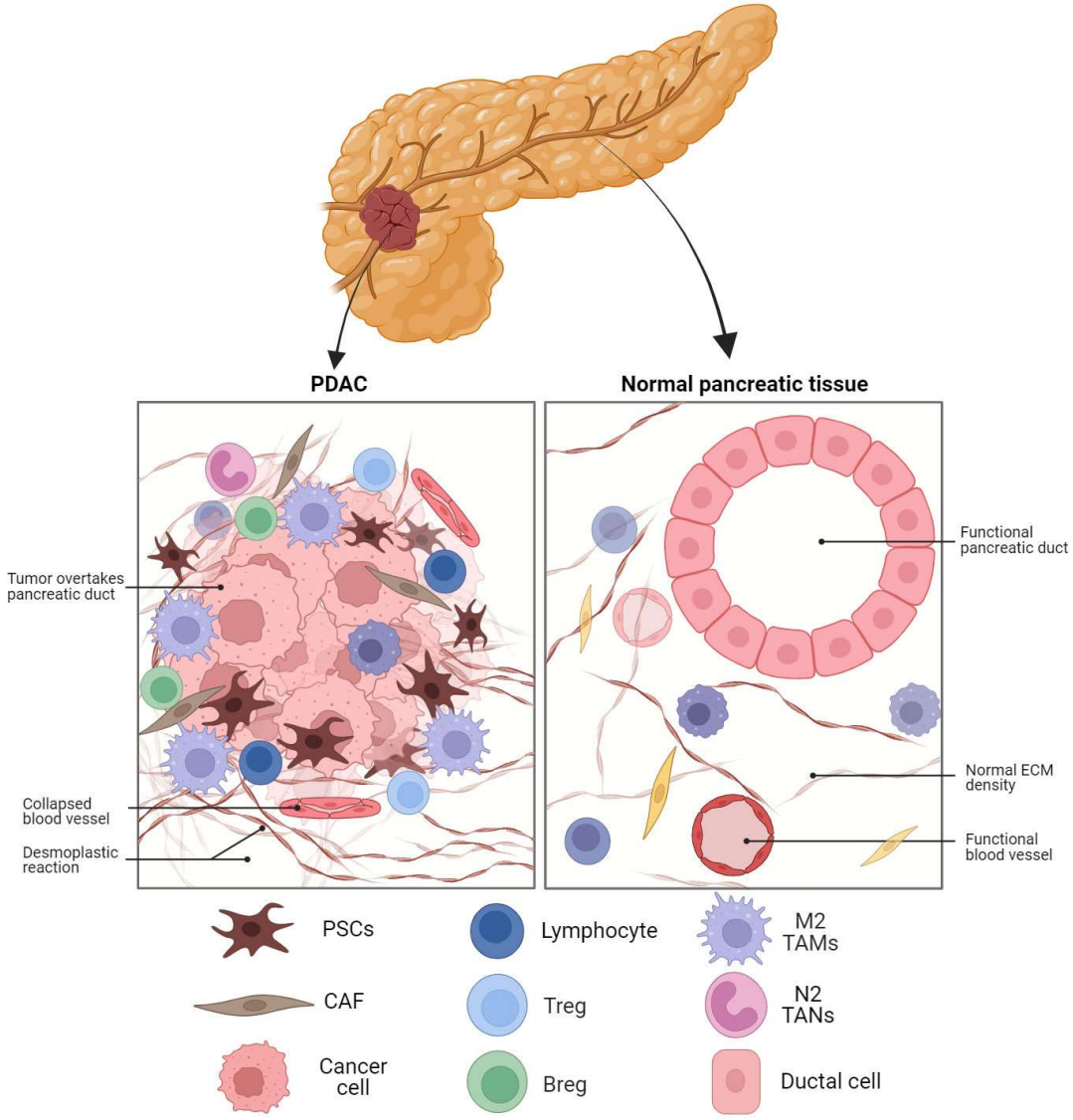

Figure 1.7 Comparison of pancreatic ductal adenocarcinoma (PDAC) pathology versus normal pancreatic tissue. Whereas normal pancreatic tissue (right) shows well-organised vasculature and ductal structure with sparse fibrotic deposition, PDAC tumour (left) is composed of dense tumour cell populations and a heterogenous mixture of stromal cells. The tumour microenvironment also exhibits vascular collapse and substantial amounts of fibrosis (desmoplastic reaction). Figure was reproduced from Joseph et al., 2024 (269). ECM, extracellular matrix; PSCs, pancreatic stellate cells; TAMs, tumour-associated macrophages; CAF, cancer associated fibroblast; Treg, regulatory T cells; TANs, tumour associated neutrophils; Breg; regulatory B cells.

1.4.2.1.2 Limitations of current immunotherapies in PDAC

The low immunogenicity in PDAC has posed significant barriers to the effective translation of immunotherapies. Anti-PD-1 antibodies (pembrolizumab and nivolumab) have only been approved for patients with MSI-H tumours, which represents 2-3% of all PDAC patients, whereas the rest of PDAC patients remain irresponsive (269).

One tumour antigen that shows high on-tumour expression across PDAC populations is MSLN. Due to the lack of effective treatments currently, anti-MSLN immunotherapies have frequently been assessed as a novel treatment for PDAC patients in clinical trials. These include antibody-based therapeutics (i.e. amatuximab, or SS1) (270-272), immunotoxins (i.e. SS1P) (273), antibody-drug conjugates (BMS-986148) (274), and CAR T cells (34, 135). Clinical outcomes, however, remained modest, despite encouraging results from preclinical studies (275, 276). In the case of anti-MSLN CAR T cells, clinical reports were available from completed trials using SS1 CAR T cells, which showed suboptimal efficacy (SDs as best overall response) (34, 135). Similarly, as described earlier, initial clinical testing of anti-MSLN huCART-MESO CAR T cells demonstrated safety but low efficacy, with only 1 SD from 11 advanced PDAC patients as the best overall response (146). In an ongoing phase I trial using M5 CAR T cells combined with an oncolytic virus (VCN-01), infusion was well-tolerated in the three treated patients (197). Measurable disease, however, was not evaluated in the only PDAC patient treated. Further results remain to be reported from trials that have examined combination with B cell depletion (NCT02465983; NCT03497819), locoregional injection (NCT06054308, NCT02706782), PD-1 inhibition (NCT05779917; NCT03182803), improving T cell stemness (NCT06885697), or influences from gut microbiomes (NCT04203459). CAR T cell therapies targeting alternative tumour antigens such as CLDN18.2, CEA, EGFR, and HER2 have also been clinically assessed in small numbers of PDAC patients (<15 from each trial), with PR observed

in selected cases (277). CR responses observed by CAR T cell treatments in haematological malignancies, however, remain to be realised in PDAC.

TIL therapies are also undergoing clinical evaluation in PDAC. However, their application in this disease is still in the early stage, and further optimisation of the manufacturing pipeline remains necessary. In the Phase II clinical trial described in **section 1.3.4.2**, the subset of PDAC patients receiving TIL products demonstrated 60% SD (3/5) as best response, although the number of patients is small (80). One patient was noted to have a prolonged SD that sustained for over 17 months, with reductions in several metastatic lesions, although the primary tumour showed no response. In the other Phase II trial with neoantigen-reactive TILs, ORR was only reported for the pooled gastrointestinal cancer cohort but not specified for the PDAC subpopulation (91). In one example, a PDAC patient demonstrated objective response (PR) with complete resolution of a liver metastasis and 44% of overall tumour shrinkage, but disease still progressed 7 months after treatment, likely due to downregulated antigen presentation (HLA) by tumour cells. Other trials assessing TIL monotherapy (NCT05098197 and NCT03935893) as well as in combination with anti-PD-1 blockade (NCT01174121) are currently ongoing.

Overall, the clinical efficacy of immunotherapies such as checkpoint inhibitors, CAR T cell therapies, and TIL therapies remains to be improved in PDAC. Given the detrimental biology of PDAC, there is an urgent need for deeper characterisation of its tumour composition and immune microenvironment to uncover key factors that could enhance future immunotherapy outcomes.

1.4.2.2 Appendiceal cancer

Appendiceal cancer is a rare disease with an occurrence of about 6 cases per 100,000 people (278). However, its incidence has been recently rising globally (279). Diagnosis can occur incidentally during appendectomy (in about 1% of all appendectomy cases), or more commonly when symptoms develop during peritoneal or systematic dissemination (280).

Historically, classification of appendiceal cancer has been inconsistently applied due to frequent revisions. The current gold standard, the World Health Organisation (WHO) 2019 fifth edition classification system, classifies appendiceal cancer into appendiceal mucinous neoplasms (AMNs) and appendiceal adenocarcinoma (AAs) subtypes (281). AMNs are slow-

growing, indolent tumours characterised by high mucin production and typically low histological grade (282). AAs are usually aggressive diseases with a high histological grade and poor differentiation (283). One AA subtype with signet ring cell histology has high metastatic potential and lethality (284). AAs can also arise from goblet cells, which shows both mucinous and neuroendocrine differentiation in contrast to the glandular epithelial differentiation by typical AAs (285). Prognosis of appendiceal cancer varies depending on disease type. Low-grade AMN has a 10-year survival of 46-63% due to its slow growth (282). AA has a 3-year survival of 15% (283). The current standard of care consists of cytoreductive therapy (CRS) followed by hyperthermic intraperitoneal chemoperfusion (HIPEC). However, recurrent disease following surgery is common and prognosis remains extremely poor once patients develop unresectable disease. Systemic chemotherapy employed in colorectal cancer treatment, such as FOLFOX and FOLFIRI, have also been tested pre-operatively and in unresectable/recurrent patients, but with limited success (281). As such, more effective treatments are urgently needed.

1.4.2.2.1 Biology of appendiceal cancer

Although appendiceal cancer has historically been misclassified as colorectal cancer, accumulating evidence now highlights it as a biologically distinct malignancy.

The mutational landscape of appendiceal cancer is characterised by frequent mutations in *KRAS*, *TP53*, *GNAS*, *SMAD4*, and *BRAF* (286). When compared to the mutational profile of colorectal cancer, AAs demonstrated significantly reduced frequencies in *TP53* (27% vs 68%) and *APC* (9% vs 55%) mutations (287). Early-onset patients were known to have 60% decreasing odds of *GNAS* mutations, when compared to late-onset patients (288). *GNAS* and *TP53* variants were found to be mutually exclusive in appendiceal cancer patients and independently associated with overall survival (OS) (289). In particular, prognosis was improved for patients with *GNAS* mutations (median OS = 115.5 months) but worse for patients with *TP53* mutations (median OS = 37.1 months), when compared to patients carrying the corresponding wildtype genes (median OS = 75.8 months). When MSI status was examined, appendiceal cancer was shown to have a lower MSI-H prevalence (4%) compared to colorectal cancer (15%) (290). Unlike colorectal cancer, where *MLH1* promoter methylation is a canonical driver of MSI, none of the appendiceal cancer patients demonstrated this

alteration, and the underlying mechanism for MSI development in appendiceal cancer remains to be characterised.

Tumour cells often constitute only a small proportion of the volume of appendiceal cancer. From transcriptomic profiling, tumour cells from the AA subtype comprised 2% of total cells, in contrast to the 42% tumour cell abundance in colorectal cancer samples and 29% epithelial cell content in healthy appendiceal tissues (291). The remaining cell populations in AA were composed of fibroblasts (55%), and immune cells such as macrophages/monocytes (25%) and T cells (10%). The precise abundance of tumour cells from the AMN subtype has not been reported; however, low cellularity of samples has long been considered a challenge for the analysis of the AMN tumours (292). Transcriptomic activities of EMT-related pathways and cellular differentiation were upregulated in distinct malignant cell clusters of AA samples (291), while pathways for cell proliferation, reactive oxygen species (ROS) generation, as well as gene sets for secretory mucins (*MUC2*, *MUC5B*, *MUC5A*, *MUC6*, *MUC19*), were elevated in epithelial cells of AMN samples relative to normal appendiceal epithelium (292). Immunohistochemical analysis of appendiceal tumours has revealed high expression of drug resistance proteins, such as BCRP (97%) and MRP1 (81%) (293). Appendiceal tumours were also found to express tumour antigens MSLN, MUC1, MUC16, and EGFR (293-296), which are widely investigated immunotherapy targets, particularly for CAR T cell therapies. Nevertheless, comprehensive profiling of tumour antigen expression has not been performed in appendiceal cancer, partially owning to the rarity of the disease and complex histological subtyping.

Secreted mucins form a crucial feature of appendiceal cancer, especially for the AMN subtype. Under physiological conditions, mucins secreted by epithelial cells provide a barrier for physical protection and against bacterial exposure (297). During appendiceal cancer development, mucin production is upregulated and dysregulated. The buildup of gelatinous deposition, composed primarily of secretory mucins MUC2 and MUC5AC, can result in rupturing of the appendix and dissemination of mucinous deposits throughout the peritoneal cavity, which is manifested clinically as pseudomyxoma peritonei (PMP) (298). This gelatinous deposition is usually acellular or hypocellular. One study demonstrated a lack of immune cell infiltration in perimucinous regions of AMN subtype, whereas this was not observed in the AA subtype (299). The precise biological role of mucin deposition in appendiceal cancer, as well as its influence on therapeutic responses, remain to be determined.

Aside from mucin production, appendiceal cancer also exhibits a complex TME composed of diverse stromal cell populations **(Figure 1.8)**. The appendix harbours rich microbiome populations, and inflammatory conditions such as appendicitis and inflammatory bowel diseases have been shown to substantially alter the microbiome composition (300). Although currently unexplored, the appendiceal microbiota may play a role in the development and progression of appendiceal cancer. TME from peritoneal metastases is known to contain mesothelial cells (from the peritoneal lining), fibroblasts, and immune infiltrates (291, 292). Transcriptomic profiling has identified fibroblasts and macrophages to be the most abundant cell types in AA peritoneal metastases samples (291). Lymphocyte infiltration, in the form of tertiary lymphoid structures (TLS) have also been observed in both AMN and AA subtypes (299). As previously mentioned, these lymphocyte infiltrates show a lack of perimucinonous distribution in AMN. AA samples, in comparison, show a lack of intratumoural infiltration of lymphocytes but increased infiltration in perimucinous and/or peritumoural regions. In general, AMN shows higher density of T cell infiltrates compared to AA, and ratio of CD8:CD3 lymphocyte infiltrates has been shown to be a positive prognostic marker for appendiceal cancer (301). In the case of AMN, transcriptomic expressions of cytotoxic gene signatures in CD8 T cell infiltrates were lower compared to CD8 T cells from matched normal tissues (292). The abundance of exhausted CD8 T cells, however, was not significantly different. It is unclear whether the anti-tumour immunity in AMN was suppressed, due to the decreased cytotoxic gene expressions, or if such observations were caused by non-tumour-reactive, bystander T cell populations. Further understanding of tumour immunogenicity in appendiceal cancer would be crucial to provide insights for novel immunotherapy treatments, such as adoptive T cell therapies, in this rare disease.

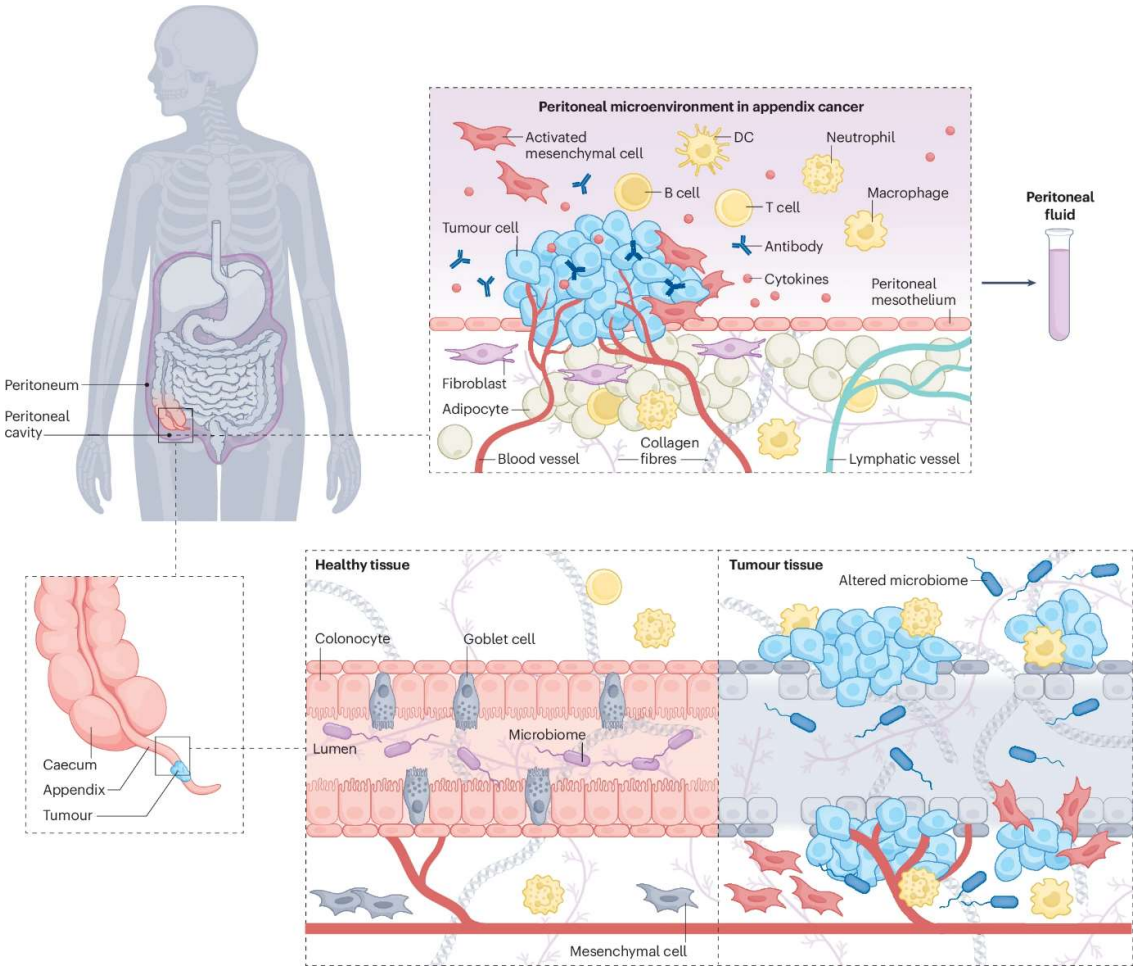

Figure 1.8 Comparison of appendiceal cancer biology versus healthy appendiceal tissue. The healthy appendiceal tissue is composed of well-organised epithelial and mesothelial linings and rich microbiome population within the luminal cavity. During appendiceal cancer development, linings and vasculature are disrupted by tumour cell proliferation, with potential alterations in the microbiome composition. As the tumour disseminates into the peritoneal cavity, it constructs a complex tumour microenvironment involving mesothelial cells, mesenchymal tissues, extracellular matrix, lymphovascular structures, as well as immune infiltrates from the peritoneal fluid. Figure reproduced from Holowatyi et al., 2025 (297). DC, dendritic cells.

1.4.2.2.2 Novel therapies in appendiceal cancer

Current treatment recommendations for appendiceal cancer are informed primarily by experiences from retrospective studies, and are largely based on treatment paradigms for colorectal cancer (281). The rarity of appendiceal cancer has also posed significant challenges on performing large-scale clinical trials to evaluate novel treatments, and existing clinical trials

often require multi-centre collaboration to ensure sufficient patient recruitment (297). To date, no Phase III trial has been conducted.

Clinical trials examining the potential use of systemic chemotherapies have not demonstrated convincing clinical efficacy to inform changes in existing treatment regimens. From a retrospective setting, preoperative chemotherapy was associated with poorer clinical outcomes, while post-operative chemotherapy demonstrated some degree of clinical benefit, especially for patients with high-grade disease (281). A Phase II trial investigated chemotherapy combination, mitomycin C and metronomic capecitabine, with bevacizumab, an anti-angiogenic agent against vascular endothelial growth factor (VEGF), in 15 unresectable appendiceal cancer patients with PMP (302). Progression-free survival (PFS) was 17.5 months, and safety profile was manageable, although three patients discontinued bevacizumab due to thrombosis. 93% (13/14) SD was achieved in evaluable patients, all of which had radiologically evidence of PD prior to treatment, and most patients showed stabilisation of circulating tumour markers (CEA and CA 19.9). However, ORR was 0%. In another randomised crossover trial, 24 patients with inoperable low-grade AA were randomised to receive fluoropyrimidine-based chemotherapy before or after 6 months of observation alone (303). Safety outcomes and tumour growth were similar between treatment and observation. No survival differences were observed between the treatment-first and observation-first groups. Of the 18 patients who received chemotherapy treatment, 78% SD (14/18) was achieved, although ORR remained 0%.

The limited responses from systemic chemotherapies highlight the need to investigate novel therapeutic approaches in appendiceal cancer. Common mutations identified in appendiceal cancer provide avenues for targeted therapies. A retrospective study reported an ORR of 11% (1/9) in AA patients with *BRAF*^{V600E} mutation treated with targeted BRAF^{V600E} inhibition (304). Among the 9 evaluated patients, the best radiographic responses comprised 1 PR and 6 SD cases; however, the sample size was limited. In a trial including 16 patients with *GNAS*-mutant peritoneal mucinous carcinomatosis, 13 of which originated from primary appendiceal tumours, the cyclin-dependent kinase (CDK) 4/6 inhibitor palbociclib was evaluated (305). 50% (8/16) SD was observed 12 months after treatment, and median PFS, at a follow-up of 17.6 months, was not reached, although no objective response was observed. Desired clinical outcomes have also not been achieved from trials assessing immunotherapies. A Phase II trial

assessed autologous tumour-loaded type-1 polarised dendritic cell (αDC1) vaccine with cytokine modulation treatment in patients undergoing CRS/HIPEC for peritoneal metastases (306). A total of 46 patients were recruited, with 24 originating from appendiceal primaries. Treatment was well-tolerated, but did not demonstrate sufficient improvement in PFS, and the trial was terminated early. Similarly, another trial (NCT03693846) assessing immune checkpoint blockade (ipilimumab and nivolumab) in patients with mucinous colorectal and appendiceal tumours was terminated early due to slow enrolment and lack of efficacy. Clinical outcomes of the study, however, have not been reported. Further clinical evaluation of novel therapies in appendiceal cancer remains necessary.

To improve the current clinical outcomes, patient-derived organoid models have been established in appendiceal cancer to recapitulate patient-specific disease biology and allow for evaluation of personalised therapeutic regimens. Organoids harbour patient-specific genetic heterogeneity and antigen expressions from the parental tumour samples (307, 308). This highlights them as particularly useful *in vitro* models in appendiceal cancer, given that no commercially available cell lines exist for this rare disease. The growth of organoids is supported by maintenance of cancer stem cells in a 3-dimensional hydrogel rich in ECM proteins, along with the enrichment of growth factors in culture media. In appendiceal cancer, organoids were usually generated from resected specimens from CRS procedures, with high success rate reported from one study (75%; 9/12 samples) (308). Expressions of cancer-associated markers (CK20, CDX-2, and SATB2) and mutational profiles were consistent between the original tumours and the established organoids (309). In addition, organoids show high expression of CD44, a cancer stem cell marker (310). Sensitivity of organoids to chemotherapeutic reagents and targeted therapies (tyrosine kinase inhibitors) have been shown to correlate with patient responses (308, 309).

Current organoid platforms lack stromal components, due to their lack of self-renewal capacity. In one study, to examine responses of immune checkpoint inhibitors (pembrolizumab, ipilimumab and nivolumab), organoids were enriched with patient-matched immune cells derived from blood, spleen, or lymph nodes (307). Following immunotherapy treatment, cytotoxic responses from CD8 T cells and tumour cell viability were examined. Positive responses were seen with both pembrolizumab and nivolumab, but not the ipilimumab treatment. Available clinical responses from 2 patients mirrored their sensitivity to

pembrolizumab from organoids. Overall, the organoid platform enables screening and assessing the responses of personalised therapies, providing a powerful tool for pioneering the development of adoptive T cell therapies.

1.5 Aims and hypotheses

The current project aims to improve the translation of T cell-based therapies in two solid tumours of unmet need: pancreatic and appendiceal cancers. In pancreatic cancer, CAR T cell therapy targeting the tumour antigen MSLN has been assessed but efficacy remains limited, partially due to a lack of comprehensive understanding of the biology of MSLN in the disease. In appendiceal cancer, effective treatments are needed but adoptive T cell therapies, such as CAR T cell therapy and TIL therapy, have not been studied to date. The specific aims of the project that will be explored are:

Aim 1: To investigate the clinicopathological and biological significance of MSLN in PDAC to improve response to MSLN-directed immunotherapy

Aim 2: To explore and evaluate the efficacy of CAR T cell and TIL therapies as a potential treatment in appendiceal cancer

In aim 1, we hypothesize that MSLN is associated with clinicopathological features (including prognosis) in PDAC. MSLN is a widely investigated immunotherapy target but its prevalence in Australian PDAC populations has not yet been studied. We will perform immunohistochemical analysis on an Australian PDAC cohort to examine MSLN expression and its clinicopathological associations, with the goal of informing patient selection strategies to achieve optimal clinical outcomes. We also hypothesise that patients with high MSLN expression will exhibit altered TMEs compared with those with low MSLN expression. Transcriptomic profiles of human and murine PDAC with high and low MSLN expressions will be compared to identify key biological differences that could guide the future development of personalised MSLN-directed immunotherapies.

In aim 2, we hypothesise that CAR T cells targeting tumour-associated antigens will elicit antigen-dependent functional responses against patient-derived appendiceal cancer organoids. Specifically, we will examine the expression of MSLN and assess the responses of anti-MSLN CAR T cells, given their extensive application in solid tumours. Due to the

upregulated mucin production, we will also examine the expression of MUC1 in appendiceal cancer as a potential target for CAR T cell therapy. We hypothesise that tumour-specific isoforms of MUC1 is expressed on appendiceal cancer organoids. Finally, as a proof-of-concept, we will generate TILs and evaluate their functions *in vitro*. We hypothesise that TILs from patient tumours can be successfully expanded and will exhibit anti-tumour activities against matched appendiceal organoids. Assessments of CAR T cell and TIL therapies will inform the potential of adoptive T cell therapies in in this rare disease, where there is a significant gap in immunotherapy development.

Overall, findings from this project will provide crucial insights to advance future immunotherapies in PDAC and pave the way for the adoption of CAR T cell and TIL therapy in appendiceal cancer, both of which urgently require novel treatments to improve clinical outcomes.

CHAPTER 2

Methods

2.1 List of materials

Table 2.1 List of essential reagents

Reagent	Catalog #	Supplier
4’,6-diamidino-2-phenylindole (DAPI)	D1306	ThermoFisher Scientific
Amphotericin B	A242-20ML	Sigma-Aldrich
Antibody Diluent	S0809	Dako
BD CompBead Anti-Mouse Ig, κ/Negative Control Particles Set	552843	BD Biosciences
Bluing Buffer	CS702	Dako
CHIR99021 (GSK inhibitor)	SML1046-5MG	Sigma-Aldrich
Cultrex Organoid Harvesting Solution	3700-100-01	R&D Systems
Dynabeads Human T-cell Expander CD3/CD28	11141D	ThermoFisher Scientific
ELISA MAX^{TM} Deluxe Set Human IFN-γ	430115	BioLegend
ELISA MAX^{TM} Deluxe Set Human Mesothelin	438604	BioLegend
EnVision+ System-HRP Labelled Polymer, Anti-mouse	K4001	Dako
FcR Blocking Reagent, Human	130-059-901	Miltenyi Biotec
Fetal bovine serum (FBS)	F42306	Cell Sera

GolgiPlug™ Protein Transport Inhibitor	55029	BD Biosciences
GolgiSTOP™ Protein Transport Inhibitor (containing Monensin)	554724	BD Biosciences
Human IL-2 Recombinant Protein	200-02	ThermoFisher Scientific
Liquid DAB + Substrate Chromogen System	K3468	Dako
Matrigel® Basement Membrane Matrix, Phenol Red-free	356231	Corning
Normocin	ant-nr-05	InvivoGen
Nystatin	N9150-20ML	Sigma-Aldrich
Protein Block (serum-free)	X0909	Dako
RBC Lysis Buffer	786-1701	Astral Scientific
Retronectin (r-Fibronectin, CH-296)	T100B	Takara Bio Inc
SPHERO™ AccuCount Blank Particles, ~1E6 Particles/mL, 7.5 um	ACBP-70-10	Spherotech
Staphylococcal enterotoxin B (SEB)	S4881	Sigma-Aldrich
Target Retrieval Solution, pH 9 (10X)	S2367	Dako
TrypLE™ Express	12605-028	Thermo Fisher Scientific
Tumor Dissociation Kit, human	130-095-929	Miltenyi Biotec

Y-27632 (ROCK inhibitor)	Y0503-5MG	Sigma-Aldrich

Table 2.2 Buffer and media compositions

Name	Composition	Used for
Sample processing media	Advanced Dulbecco's Modified Eagle Medium (DMEM) media/F12	Tissue processing
Antimicrobial-enriched sample processing media	Sample processing media supplemented with Normocin (0.2%), amphotericin B (1%), and nystatin (0.625%)	Antibiotics and antifungal treatment
Organoid media	Advanced DMEM supplemented with growth factors – A83-01 (5 µM), B-27 (1x), EGF (50 ng/mL), FGF 10 (100 ng/mL), N acetylcysteine (1 mM), N2 supplement (1x), nicotinamide (100 mM), Noggin (25 ng/mL), prostaglandin E2 (3 µM), Rspo1 (500 ng/mL), and Wnt3a (100 ng/mL)	Organoid culturing
ROCK/GSK inhibitor-enriched organoid media	Organoid media supplemented with ROCK inhibitor Y-27632 (10 µM) and GSK inhibitor CHIR99021 (5 µM)	Promoting organoid survival and proliferation during early establishment phase
T cell media	Roswell Park Memorial Institute (RPMI) 1640 supplemented with β-mercaptoethanol (54 µM), FBS (10%), glutaMAX^{TM} supplement (1X), Penicillin & Streptomycin (1%), and HEPES (25 mM)	TIL and CAR T cell culturing
Cryopreservation media	Sample processing media (for tumour samples) or T cell media (for T cells) with FBS (10%) and DMSO (10%)	Cryopreserving tumour samples or T cells
FACS buffer	Phosphate-buffered saline (PBS) with FBS (2%) and EDTA (2 mM)	Flow cytometry

Table 2.3 Antibodies for flow cytometry

Target	Clone	Fluorophore	Supplier	Catalog #
Primary antibodies				
CD3	UCHT1	AF647	BioLegend	300416
CD3	UCHT1	FITC	Beckman coulter	A07746
CD4	RPA-T4	APC	BD Biosciences	555349
CD8	RPA-T8	BV786	BD Biosciences	563823
CD107a (LAMP-1)	REA792	PE	Miltenyi Biotec	130-111-621
CD134 (OX40)	ACT35	PE-Cy7	BD Biosciences	563663
CD137 (4-1BB)	4B4-1	PE	BD Biosciences	555956
CD227 (MUC-1)	REA448	PE	Miltenyi Biotec	130-120-056
CD227 Tn/STn glycoforms	5E5	Unconjugated	Antibody System	FHD14210
CD326 (EpCAM)	9C4	PE	BioLegend	324206
MSLN	SS1	APC (conjugated in the laboratory)	Unconjugated SS1: Creative Biolab APC Conjugation kit: Abcam	Unconjugated SS1: TAB-201 APC Conjugation kit: ab201807
Isotype controls				
Isotype human IgG1, REAfinity™	QA16A12	APC	BioLegend	403505
Isotype human IgG1, Recombinant	REA293	PE	Miltenyi Biotec	130-113-462
Secondary antibody				
Goat-anti-human IgG (Fc Cross-Adsorbed)	Polyclonal	Dylight650	ThermoFisher Scientific	SA5-10137

2.2 Ethics

Ethics for obtaining human pancreatic cancer tissue microarrays (TMAs) were approved by the University of Sydney Human Research Ethics Committee (2018/730). Ethics for obtaining formalin-fixed paraffin-embedded (FFPE) sections of PDAC patients, and the use of healthy donor PBMC for CAR T cell generation were approved by the Sydney Local Health District Human Ethics Committee (2020/ETH02321 and 2019/ETH07394 respectively). Ethics for the collection of resected appendiceal cancer samples for organoid and TIL generation were approved by the St Vincent's Hospital Human Research Ethics Committee (2020/ETH00687).

Approval for accessing the human PDAC bulk RNA-seq data and associated clinical data from the European Genome-phenome Archive (EGA) database was granted by the International Cancer Genome Consortium (ICGC) (DACO-7197).

2.3 Transcriptomic analysis

Transcriptomic (bulk and single cell RNA-seq) analyses were performed using R Statistical Software (ver. 4.4.2, Vienna, Austria). Data visualisation were conducted in both R Statistical Software and GraphPad Prism (ver 10.4.1, San Diego, California, USA). A summary of the essential R packages used is provided in **Table 2.4**. Transcriptomic and survival analysis scripts used can be found on Github (https://github.com/Oliver-Liang-1999/PDAC_MSLN).

Table 2.4 R packages used for transcriptomic data analysis

Package	Version	Purpose	Reference
clusterProfiler	4.7.1	Gene Ontology analysis of differentially expressed genes from RNA-seq data	Yu et al., 2012 (311)
DESeq2	1.38.2	Normalisation and differential expression analysis of RNA-seq data	Love et al., 2014 (312)
enrichplot	1.18.4	Treeplot visualisation of GO results from RNA-seq data	Bioconductor package
ggplot2	3.5.1	Data visualisation	CRAN package

ggpubr	0.6.0	Data visualisation (specifically for balloon plots)	CRAN package
GSVA	1.46.0	Gene set variation analysis for RNA-seq data	Hanzelmann et al., 2013 (313)
ProjecTILs	3.5.1	Annotation of scRNA-seq data by projection to a TIL atlas	Andreatta et al, 2021 (314)
scaper	0.2.0	Cytokine signalling pathway analysis for scRNA-seq data	Jiang et al., 2021 (315)
SCINA	1.2.0	Cell type annotation of scRNA-seq data using reference markers	Zhang et al., 2019 (316)
Seurat	4.3.0	Processing, clustering, annotation, and visualisation of scRNA-seq data	Hao et al., 2021 (317)
survival	3.8.3	Univariate and multivariate survival analysis tool	CRAN package
survminer	0.5.0	Optimal cutpoint identification for survival analysis	CRAN package
UCell	2.10.1	Gene signature scoring for scRNA-seq data	Andreatta, & Carmona, 2021 (318)

RNA-seq, RNA-sequencing; scRNA-seq, single cell RNA-sequencing; TIL, tumour infiltrating lymphocyte

2.3.1 Bulk RNA-seq analysis

2.3.1.1 PDAC

Two human PDAC bulk RNA-seq datasets were accessed from the EGA database containing a total of 316 samples: 97 samples from ICGC PACA-AU (EGAD00001003298) and 219 samples from ICGC PACA-CA (EGAD00001003945). Patients with missing clinical information were excluded as well as those with a diagnosis not classified as PDAC. To standardise read alignments across datasets, samples were converted from BAM to FASTQ format using

bedtools (ver.2.30.0)(319) and then realigned to the human genome assembly (GENCODE, release 35, GRCh38.p13) using STAR aligner (ver. 2.7.1a) (320). Raw gene counts were enumerated via featureCounts (ver.2.4.2) (321). Batch effects were corrected using the Combat_seq function from sva (ver. 3.50.0) and only counts from protein-coding genes defined by the Human Genome Organisation Gene Nomenclature Committee (HGNC) were retained for analysis (322).

Publicly available, previously published (323), mouse PDAC bulk RNA-seq data (n=37 samples) were obtained from the Gene Expression Omnibus (GEO) database (GSE109933). Seven samples with unknown T cell infiltration status were excluded from downstream analysis. Raw read count data was filtered to remove non-protein coding genes.

Normalisation of raw gene counts and differential expression analysis were conducted via DESeq2 (ver. 1.38.2) (312). For the human PDAC dataset, samples in the top and bottom tertiles of *MSLN* expression were compared. Due to small sample size (n = 30), the mouse PDAC dataset was split based on median *Msln* expression and compared. Upregulated and downregulated genes were identified based on significance (adjusted P-value < 0.05) and expression changes (absolute log2 fold change > 0.58). Over-representation analysis of upregulated and downregulated genes was conducted separately via Gene Ontology (GO) enrichment analysis in clusterProfiler (ver 4.7.1.003) (311). Results were visualized using the treeplot function via enrichplot (ver 1.18.4).

Tumour reactivity was evaluated for human and mouse PDAC datasets using the tumour reactive gene signatures (TRS) (324), which has been validated in melanoma and several other solid tumours including hepatocellular carcinoma, non-small cell lung cancer, melanoma, and colorectal cancer. For the mouse PDAC dataset, TRS genes were converted to mouse Ensembl IDs and TRS scores calculated using GSVA (ver 1.46.0) with default parameters as previously described (313).

To estimate cell type proportions, gene expressions from the human PDAC dataset were converted into Transcripts Per Million (TPM) values and analysed using the “Immune Estimation” algorithm from TIMER2.0 (325).

2.3.1.2 Appendiceal cancer

RNA-seq data of appendiceal cancer organoids (n= 4 samples) were provided in FASTQ format in-house. Reads were aligned to the human genome assembly (GENCODE, release 48, GRCh38.p14) using STAR aligner. Raw gene counts were obtained via featureCounts and normalised in DESeq2.

2.3.2 scRNA-seq analysis

2.3.2.1 PDAC

Human PDAC single-cell RNA-seq (scRNA-seq) data were sourced from a published study (326). Data from 24 samples were collected as normalised gene expression matrices (Cancer Single-Cell Expression Map (CancerSCEM): https://ngdc.cncb.ac.cn/cancerscem/downloads), on the Genome Sequence Archive (CNCB-NGDC; PRJCA001063). Filtering was performed to retain only high-quality cells, as defined by cells with ≥ 500 detectable genes, ≥1500 unique molecular identifiers (UMI), > 0.8 cell complexity (log10 genes per UMI), and <10% of transcripts from mitochondrial genes.

Integration, clustering, and dimensionality reduction of PDAC scRNA-seq samples were performed via Seurat (ver 4.3.0) (317). Elbow plots were used to determine the optimal number of principal components (PCs), and PCs 1 to 30 were used for clustering at resolution = 0.5. Annotation was performed at single cell level via SCINA (ver 1.2.0) (316), using cell type identification markers in the original study from which the data was derived (326). Marker expression in each cell type was verified after cell annotation. Samples were assigned to high and low MSLN expression groups based on median cutoff of *MSLN* normalized counts per cell. For analysis of specific subtypes within annotated cell types, cell populations were isolated from the integrated dataset and re-clustered at optimal resolution determined from a range of 0.5, 0.1, and 0.05. Manual annotation was performed for each cluster based on the expression of representative markers, which were identified using the FindAllMarkers function. UMAP (Uniform Manifold Approximation and Projection) plots were generated to illustrate cell clusters and specific marker expression across clusters using the DimPlot and FeaturePlot functions, respectively. A balloon plot of *MSLN* expression in annotated cell types across samples was generated using the ggballoonplot function in ggpubr (ver 0.6.0). For the

macrophage population, M1 and M2 polarization scores were evaluated for each sample via UCell (ver 2.10.1), based on previously established M1 and M2 gene signatures (318, 327).

Differential gene expressions of CD8 T cell clusters from the MSLN-high and MSLN-low groups were assessed using the FindMarkers function based on default thresholds (adjusted P-value < 0.05 and absolute log2 fold change > 0.25). Upregulated and downregulated genes were used in downstream GO enrichment analysis and visualised. Phenotypic profiling was performed using ProjecTILs (ver 3.5.1), with phenotypes inferred by projecting CD8 T cells onto the reference atlas of tumor-infiltrating CD8 T cells provided within the package (314). Cytokine signaling activities in CD8 T cells from each sample were evaluated using the CytoSig database via scaper (ver 0.2.0) (315). Expression levels of memory and exhaustion markers, as well as all chemokine and chemokine receptors, were averaged for CD8 T cells from each sample and compared between the MSLN-high and MSLN-low groups.

2.3.2.2 Appendiceal cancer

Annotated scRNA-seq data of appendiceal cancer (processed in Seurat) was kindly provided by Dr. Madeleine Strach, Chris O'Brien Lifehouse, Sydney, Australia. Expression of specific markers were visualised using the FeaturePlot function. Comparisons of marker expressions across cell types were visualised as box plots in ggplot2.

2.4 Immunohistochemical staining

2.4.1 Sample acquisition

Immunohistochemical (IHC) staining was performed on formalin-fixed paraffin-embedded (FFPE) slides of human pancreatic cancer TMAs, and whole-tissue sections of human PDAC and appendiceal cancer. The human pancreatic cancer TMAs were obtained through the Australian Pancreatic Cancer Genome Initiative (APGI) Bioresource and contain 74 PDAC patients as well as 14 patients with precursor lesion (13 PanIN and 1 IPMN). Whole-tissue sections were obtained from patients treated at the Royal Prince Alfred Hospital (RPA), consisting of 10 PDAC cases and 2 appendiceal cancer cases.

2.4.2 Immunohistochemistry (IHC)

TMA and whole-tissue FFPE slides were deparaffinised in histolene and rehydrated through sequential rounds of decreasing ethanol gradient (100%, 100%, 95%, 70%). Slides were

incubated in antigen retrieval solution (pH 9.0) at 95 °C for 20 minutes. Slides were then treated with 3% hydrogen peroxide for 5 minutes to block endogenous peroxidase activity, followed by protein block for 15 minutes to prevent non-specific binding. MSLN staining was performed using an anti-MSLN mouse antibody (clone MN-1, Rockland Immunochemicals, Pottstown, PA, USA, Cat#200-301-A88) at 13.3 ug/mL at 4 °C overnight. Additionally, CD3 (clone LN10, Novocastra, Leica Microsystems, Deer Park, IL, USA), CD8 (clone C8144B, Dako, Santa Clara, CA, USA), and CD68 (clone KP1, Dako, Santa Clara, CA, USA) staining were undertaken on the whole-tissue PDAC sections. Anti-mouse horseradish peroxidase (HRP)-conjugated secondary was added for 1 hour at room temperature. For visualisation, diaminobenzidine (DAB) and chromagen were added for 6 minutes, and slides were counterstained using haematoxylin solution and bluing buffer, prior to dehydration in ethanol, cleared using histolene, and cover slipped.

2.4.3 Visualisation and scoring

IHC staining was scored independently by two pathologists: Dr. Timony Fiedlder and Dr. Joo-Shik Shin, NSW Health Pathology, and final scores were calculated as the average score for each core and the average score of the patient's cores from the two pathologists. MSLN staining on PDAC TMA and whole-tissue slides were assessed using the H-score system, which evaluated scores based on staining intensity and percentage of positive tumour cells (328). CD3, CD8, and CD68 scores were evaluated as percentage of stained cells within the tumour stromal area, as previously described (329). Representative bright-field images of IHC staining were acquired using a digital microscope (Olympus DP73, Olympus, Shinjuku City, Japan) at 20 x magnification, with white balance background correction.

2.5 Cell culture

Culturing of patient-derived organoids (from tumour specimens) as well as immune cells (isolated from healthy donor PBMCs) were undertaken. General reagents and media used for cell culture are listed in **Table 2.1** and **Table 2.2.**

2.5.1 Establishment and culturing of patient-derived organoids

For the establishment of patient-derived organoids, tumour specimens were harvested from surgical resections and subjected to tissue processing, as described under **section 2.5.3.1**. The

resulting cell suspension was incubated in antimicrobial-enriched sample processing media for 15 minutes at 37 ^{o}C to provide antibiotic and antifungal treatment. After washing with sample processing media, cells were embedded in a commercial basement membrane matrix, Matrigel, and seeded onto low-attachment 24-well plates in domes supplemented with ROCK/GSK inhibitor-enriched organoid media to promote organoid growth and survival. Plates were monitored 2-3 times per week under the light microscope for evidence of successful organoid establishment, characterised by tumour cell aggregation and the formation and progressive enlargement of spheroid structures. Regular media exchange was performed every 3 to 4 days and organoids were reseeded if morphological disruption, blebbing, or substantial accumulation of dead cells was observed.

For routine culturing of established organoids, organoids were passaged or harvested for experimental use prior to confluency (indicated by disrupted morphology or blebbing). During passaging, domes were dislodged mechanically and incubated in TrypLE^{TM} Express Enzyme solution for 5 – 15 minutes for Matrigel dissolution and cell dissociation. Cell suspension was resuspended in fresh Matrigel and incubated at 37 ^{o}C for 10 minutes to allow for solidification. Organoid media was added thereafter, and plates were incubated at 37 ^{o}C and 5% CO_2 with regular media exchange every 3 to 4 days.

2.5.2 CAR T cell generation

Schematic of the CAR constructs is summarised in **Figure 2.1.** Two mesothelin-targeting CAR constructs with the SS1 and P4 antigen-binding domains (hereafter referred to as SS1 and P4) and a prostate-specific membrane antigen (PSMA)-targeting CAR construct with the J591 antigen binding domain (hereafter referred to as J591) were used. All three CAR constructs are second-generation, each containing a human CD3 hinge domain, CD8 transmembrane domain, CD28 co-stimulatory domain, and CD3 intracellular signalling domain, as well as an mCherry tag, which is separated from the CAR sequence by a P2A self-cleaving peptide.

CAR T cells were generated from the PBMCs of three independent healthy donors. Each donor PBMC was transduced with each of the three CAR constructs. Data on CAR T cell expansion, mCherry expression, and *in vitro* functional validation can be found in the Appendix (**Supplementary Figure 1**).

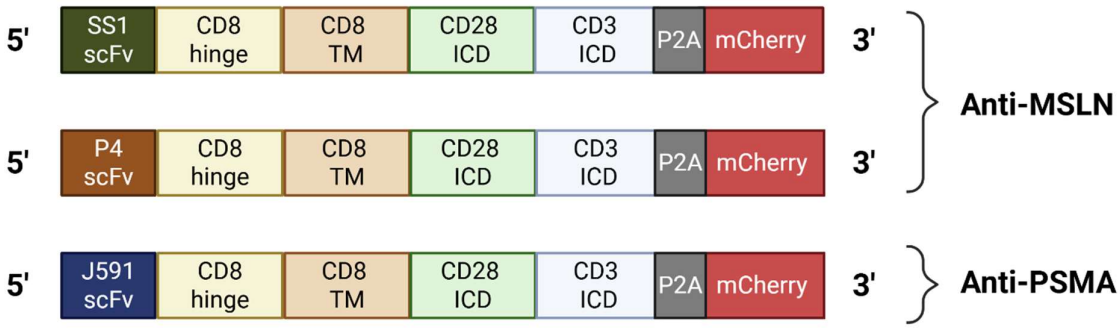

Figure 2.1 Chimeric antigen receptor (CAR) constructs used in the current study. All three CAR constructs are second-generation and co-express a fluorescent tag (mCherry) as a surrogate measure of CAR expression. The top two CAR constructs (with SS1 and P4 scFvs, respectively) target the tumour antigen mesothelin (MSLN) while the bottom CAR construct (with J591 scFv) target the tumour antigen prostate-specific membrane antigen (PSMA). scFv, single chain variable fragment; TM, transmembrane; ICD, intracellular domain.

2.5.2.1 T cell activation

Cryopreserved PBMCs were defrosted and cell counting was performed using the automated cell counter Nucleocounter® NC-202 (Chemometec, Allerod, Denmark) on day 1. PBMCs were seeded in 6-well plates at a density of 1 million cells per mL in T cell media supplemented with 100 IU/mL of human IL-2. Percentage of T cells was determined by flow cytometry by staining with an FITC-conjugated anti-CD3 antibody (clone UCHT1) (see **section 2.6.2**). For T cell activation, Dynabeads™ Human T-Expander CD3/CD28 was added to the culture at a ratio of 1:1 bead to T cells. Seeded plates were incubated at 37 °C and 5% CO_2 and observed daily under the light microscope for the first two days for signs of T cell activation (cell clustering).

2.5.2.2 CAR transduction

Transduction was performed two days after T cell activation using high-titre CAR-containing retroviral supernatant derived from gibbon ape leukemia virus (Galv) producer cells, generated by transduction with replication-defective vesicular stomatitis virus (VSV)-pseudotyped CAR constructs in the SFG retroviral backbone (142). For virus collection, Galv producer cells were seeded in 15 cm plates for 72 hours, after which the culturing medium (DMEM + 10% FBS) was exchanged. Viral supernatant was harvested 24 hours later, passed through a 0.45 µM PVDF filter, and snap-frozen for preservation.

T cells were seeded at 1 million per mL on retronectin-coated 6-well plates, which were prepared via overnight incubation with 15 ug/mL of RetroNectin® at 4 ^{o}C. Retroviral supernatant from Galv producer cells were diluted using fresh T cell media and added to T cells at 1:1 v/v ratio and a multiplicity of infection (MOI) of 3. Plates were spinoculated at 524 x g for 90 mins and subsequently incubated at 37 ^{o}C and 5% CO_2. After 72 hours, cells were reseeded in fresh media at a density of 0.5 million to 1 million T cells per mL with 100 IU/mL IL-2 and cultured for another 2 days.

2.5.2.3 Post-transduction expansion

Cells were transferred to G-Rex®6M culture plates (Wilson Wolf Manufacturing, Saint Paul, Minnesota, USA, Cat#80660M) for continued expansion. A minimum of 5 million cells was seeded in each well. Media was topped up to a final volume of 100 mL using fresh T cell media with 100 IU/mL IL-2. Cultures were incubated at 37 ^{o}C and 5% CO_2 for 7 days, with an additional 100 IU/mL IL-2 supplementation on the fifth day. On the final day, cells were harvested, de-beaded, and cryopreserved for future experiments.

2.5.3 TIL generation

The overall workflow for TIL generation was established as in **Figure 2.2.** An example of sample processing and TIL expansion from one appendiceal cancer sample (PB316, AMN) is also shown in **Figure 2.3.** In this workflow, tumour tissues were processed and phenotyped by flow cytometry on day 1, followed by one week of culturing with T cell activation induced by Dynabeads™ Human T-Expander CD3/CD28. Media exchange or culture splitting was performed every 2-3 days to maintain a cell density of 0.25 – 1 million cells/mL, with IL-2 re-supplementation (3000 IU/mL in the first week and 1000 IU/mL thereafter). Beads were removed on day 7 and cells were further expanded until harvest between days 15 to 30, once a minimum of 15 million cells was obtained, then phenotyped prior to cryopreservation.

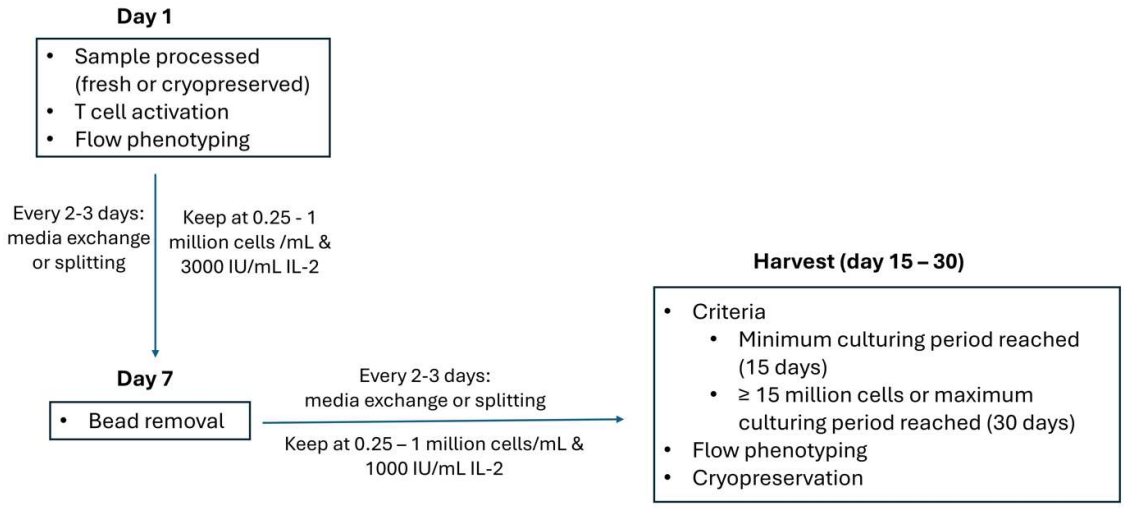

Figure 2.2 Workflow for *in vitro* expansion of tumour-infiltrating lymphocytes from surgical resection specimens of appendiceal cancer. IL-2, interleukin-2.

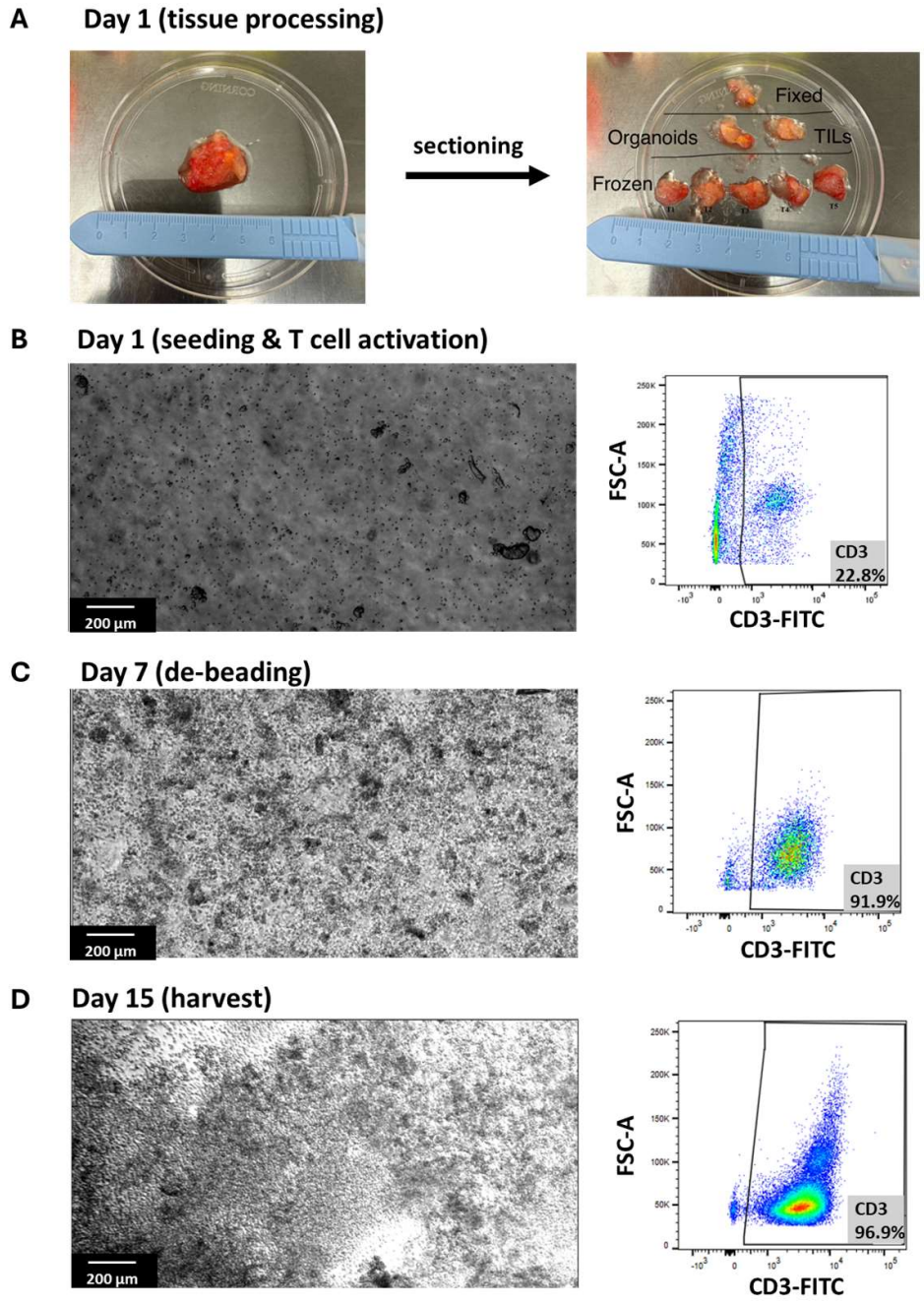

Figure 2.3 TIL establishment from an appendiceal cancer surgical specimen (PB316, appendiceal mucinous neoplasm). (A) Fresh tumour obtained from surgical resection (left) and when sectioned into smaller equal-sized pieces (right). Allocation of tumour pieces was annotated and the piece labelled "TIL" was used for immediate processing. **(B)** Microscopic image of TIL cultures on day 1, after the addition of anti-CD3/CD28 superparamagnetic beads for T cell activation. Uniformly distributed beads and tumour residuals from processing can be observed. A small population of T cells (CD3+%) was observed from flow cytometry. **(C)** On day 7 after bead removal, necrotic tumour cells and lymphocyte aggregates were detected. T cell population has become significantly enriched (22.8% to 91.9%). **(D)** On the day of harvest (day 15), lymphocytes have expanded into a dense carpet covering the bottom surface of the

plate. T cells constitute the majority (96.9%) of live cell population. For **(B)**, **(C)**, **(D)**, scale bar was indicated. Dot plot of CD3 expression was gated on live cell population from flow cytometry. TIL, tumour infiltrating lymphocyte; FSC-A, Area of forward scatter; FITC, fluorescein isothiocyanate.

2.5.3.1 Tissue processing

Surgical resection specimens of appendiceal cancer were collected from the Royal Prince Alfred Hospital (RPA), Sydney, Australia. Necrotic and fatty tissues were removed, and the remaining specimens were sectioned into smaller equal-sized pieces (approximately 1 cm in diameter). For cryopreservation, pieces of tissue were washed with sample processing media and suspended in cryopreservation media in a cryovial for cryostorage in liquid nitrogen. Processing was performed immediately or on defrosted tumour pieces after cryopreservation. The tumour piece was mechanically minced into 1 mm^3 fragments in approximately 500 µL – 1 mL of sample processing media (RPMI). Tissue dissociation was undertaken as per manufacturer's instructions using the Human Tumour Dissocation Kit (Miltenyi Biotec). Samples were incubated in gentleMACS™ C Tubes (Miltenyi Biotec, Cat#130-093-237) on the gentleMACS™ Octo Dissociator (Miltenyi Biotec, Cat#130-134-029) at 37 °C for 1 hour using the in-built program "37C_h_TDK_3". Dissociated tissue was filtered through a 70 µM pluriStrainer® (pluriSelect, Leipzig, Germany, Cat#43-50070-51). Red blood cell (RBC) lysis was performed using the RBC Lysis Buffer, according to the manufacturer's instructions.

2.5.3.2 Culture maintenance and expansion

Following RBC lysis, cell suspensions were supplemented with 3000 IU/mL of human IL-2, and seeded in tissue-culture-treated 24-well plates at a density of 0.5 million cells/mL. T cell activation was performed using Dynabeads™ Human T-Expander CD3/CD28, at 1:1 bead to live cell ratio, immediately after seeding. Cultures were observed daily for signs of TIL outgrowth and maintained as described under **section 2.5.3**.

2.6 Flow cytometry

Flow cytometry analysis on organoids, T cells, and co-cultures of organoids and T cells were undertaken. Antibodies used for flow cytometry analysis are listed in **Table 2.3**. All antibody staining, unless otherwise specified, were performed for 45 minutes at 4 °C in the dark, followed by viability staining, flow cytometry acquisition, and analysis.

2.6.1 Detection of tumour antigen expression on organoids

Flow cytometry was performed on organoids to examine surface expression of tumour antigens, MSLN and MUC1. Organoids were seeded in Matrigel for 24 hours, after which media was removed and Matrigel domes were mechanically dislodged in 400 µL of Cultrex Organoid Harvesting Solution and incubated at 4 ^{o}C for 45 minutes.

For detection of MSLN, cells were stained with 0.2 µg/mL APC-conjugated SS1 (generated in-house using MORAb-009 and APC Conjugation Kit – Lightning-Link) or 0.2 µg/mL of APC-conjugated anti-human IgG1 isotype control antibody (clone QA16A12) as negative control. For detection of MUC1, samples were stained with 20 µL/mL PE-conjugated anti-MUC1 antibody (clone REA448) or 20 µL/mL PE-conjugated human IgG1 isotype control antibody (clone REA293) as negative control. For the detection of tumour-specific MUC1 glycoforms (Tn/sTn), cells were stained with 10 µg/mL of a humanised anti-MUC1 antibody (clone 5E5) or an equivalent volume of FACS buffer as negative control. Samples were then washed and stained with 2.5 µg/mL of Dylight650-conjugated anti-human IgG secondary antibody before proceeding to viability staining.

2.6.2 T cell phenotyping

Abundance of T cell subsets (CD3+, CD4+, and CD8+) were phenotyped via flow cytometry to characterise CAR T cell and TIL products. For T cells cultured with magnetic beads, de-beading was performed using the DynaMag™-2 Magnet (Thermo Fisher Scientific, Cat#12321D). For TIL samples, FcR blocking was undertaken to prevent non-specific staining of tumour and stromal components using FcR Blocking Reagent for 10 minutes at 4 ^{o}C.

Staining was performed using a mixture of 50 µL/mL FITC-conjugated anti-CD3 (clone UCHT1), 0.65 µg/mL APC-conjugated anti-CD4 (clone RPA-T4), and 0.5 µg/mL BV786-conjugated anti-CD8 (clone RPA-T8) antibodies.

2.6.3 Assessment of TIL reactivity

Expressions of reactivity markers, CD134 (OX40) and CD137 (4-1BB), were evaluated on TILs after SEB stimulation or co-cultures with patient-matched organoids. TILs were seeded in T cell media at 0.1 million cells per well on non-tissue-culture-treated 96-well plates. For wells with SEB stimulation, SEB was added at 1 µg/mL. For co-cultures with patient-matched organoids, organoids were dissociated as per **section 2.5.1** and added to TILs at an effector-

to-target ratio of (E:T) ratio of 20:1 (equivalent to 5000 organoid cells per 0.1 million TILs), in an equal volume of organoid culturing media.

After 24 hours, cells were washed with FACS buffer and stained with a 5-marker flow cytometry panel. Staining was performed using a mixture of 10 µg/mL PE-Cy7-conjugated anti-CD134 (clone ACT35), 5 µg/mL PE-conjugated anti-CD137 (clone 4B4-1), 50 µL/mL FITC-conjugated anti-CD3 (clone UCHT1), 0.65 µg/mL APC-conjugated anti-CD4 (clone RPA-T4), and 0.5 µg/mL BV786-conjugated anti-CD8 (clone RPA-T8) antibodies.

2.6.4 Assessment of SEB-induced TIL degranulation

Expression of TIL degranulation marker CD107a was evaluated by flow cytometry after SEB stimulation.

TILs were seeded and stimulated with SEB for 24 hours as per **section 2.6.3**. 20 µL/mL PE-conjugated anti-CD107a antibody (clone REA792) or 20 µL/mL PE-conjugated human IgG1 isotype control antibody (clone REA293) was then added, and cultures were incubated for 1 hour at 37 ^{o}C and 5% CO_2. To block cytokine release, cultures were incubated with 0.67 µL/mL GolgiSTOP^{TM} (BD Biosciences, Cat#554724) and 1 µL/mL GolgiPlug^{TM} (BD Biosciences, Cat#55029) for another 4 hours at 37 ^{o}C and 5% CO_2.

Cells were washed with FACS buffer and stained further with 50 µL/mL FITC-conjugated anti-CD3 (clone UCHT1), 0.65 µg/mL APC-conjugated anti-CD4 (clone RPA-T4), and 0.5 µg/mL BV786-conjugated anti-CD8 (clone RPA-T8) antibodies.

2.6.5 Quantification of TIL-mediated cytotoxicity against dissociated tumour organoid cells

To evaluate TIL cytotoxicity, TILs were co-cultured with patient-matched organoids and alive tumour cell populations were quantified in a bead-based flow cytometry assay.

TILs were co-cultured with patient-matched organoids as per **section 2.6.3**, for 72 hours. Cells were harvested and added with 15 µL of SPHERO^{TM} AccuCount Blank Particles. After washing with FACS buffer, cells were stained with 0.67 µg/mL AF647-conjugated anti-CD3 (clone UCHT1) and 2.5 µg/mL PE-conjugated anti-EpCAM (clone 9C4) antibodies.

2.6.6 Viability staining

Viability staining was performed using 1 µg/mL DAPI on all samples after antibody-staining. Cells were then incubated on ice and immediately proceeded to flow cytometry acquisition.

2.6.7 Flow cytometry acquisition and analysis

Samples were acquired on a LSRFortessa (BD Biosciences) or a LSRFortessa X-20 flow cytometer (BD Biosciences), Sydney Cytometry. To account for spectral spillover for flow cytometry panel in **section 2.6.3**, fluorescence settings were compensated using BD™ CompBeads prior to acquisition, according to the manufacturers' instructions.

Analysis was performed using the FlowJo™ software (ver 11, BD Biosciences). Quantification of viable tumour cell populations in **section 2.6.5** was performed using the following formula, which has been adapted and modified based on a previous study (330):

$$Viable\ tumour\ cells\ per\ bead\ = \frac{Acquired\ counts\ of\ DAPI\ negative,\ EpCAM\ positive\ cells}{Acquired\ counts\ of\ counting\ beads}$$

2.7 Impedance-based cytotoxicity assay

CAR T cell cytotoxicity against appendiceal cancer organoids was assessed using the xCELLigence Real-Time Cell Analysis (RTCA) platform (Agilent Technologies, Santa Clara, California, USA), Cell and Molecular Therapies, RPA Hospital, where electric impedance is used to measure adherent target cell viability (**Figure 2.4**).

Organoids were dissociated using TrypLE™ Express Enzyme as per **section 2.5.1**. Dissociated organoids were seeded in organoid culture media at an optimised density of 10,000 cells per well to allow for cell attachment and proliferation. Before CAR T cell addition, the adherence of cancer organoids was microscopically confirmed, as shown in the Appendix (**Supplementary Figure 2**). After 96 hours, CAR T cells were added at an E:T ratio of 3:1, in an equal volume of fresh T cell media. Control wells were added with T cell media alone. Co-culture was run for 72 hours and cell index was recorded every 15 minutes in the RTCA Software Pro (ver 2.8.1, Agilent Technologies). Cell index was normalised to the time of CAR T cell addition and cancer cell viability at each timepoint was calculated based on the following formula, adapted from previous studies (142, 331):

$$Viability\ (\%)\ at\ time\ X\ = \frac{Normalised\ cell\ index\ of\ coculture\ at\ time\ X}{Normalised\ cell\ index\ of\ cancer\ cells\ alone\ at\ time\ X} \times\ 100\%$$

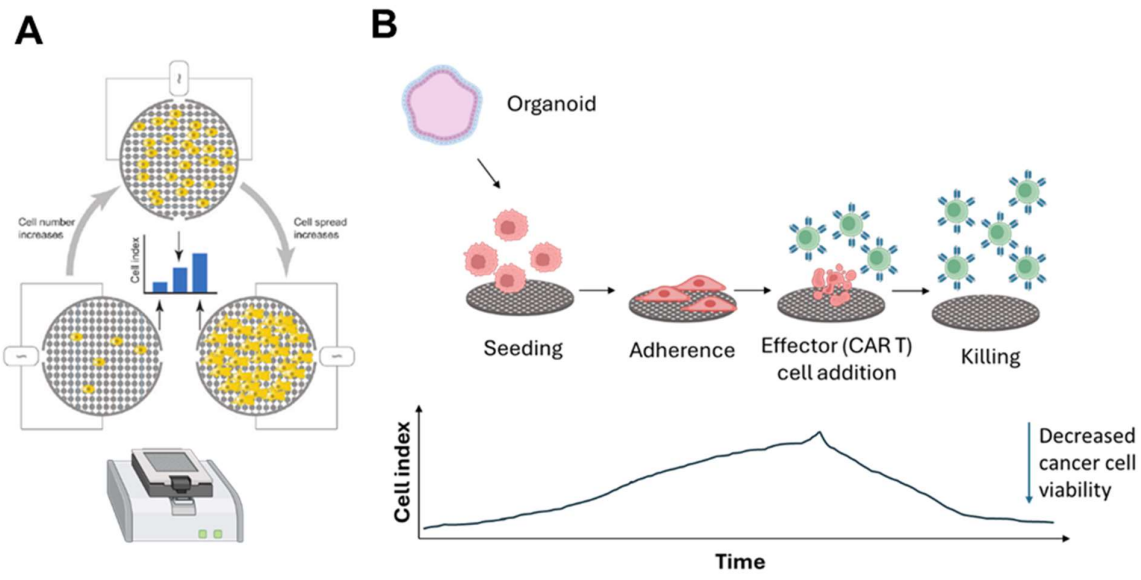

Figure 2.4 Assessing chimeric antigen receptor (CAR) T cell cytotoxicity against appendiceal cancer organoids via the xCELLigence Real-Time Cell Analysis (RTCA) platform. (A) On the RCTA platform, adherent cells (yellow) attach to the plate surface and proliferate. The degree of cell coverage is monitored in real time via electric impedance and reported as the cell index. Image was adapted from Limame et al., 2012 (332). **(B)** In the CAR T cell cytotoxicity assay, organoid cells were seeded to attach and proliferate. Upon CAR T cell-mediated killing, target cells undergo apoptosis, reducing cell attachment and thereby decreasing the cell index. Analysis of cell index values shows the changes in cancer cell viability over time, with higher cell index indicating greater viability.

2.8 ELISA

SMRP concentrations in organoid culture supernatant and IFN-γ concentrations from CAR T cell cytotoxicity and TIL reactivity assay supernatant were evaluated via ELISA.

For SMRP analysis, culture media, from organoids that were maintained for 1 week and reached 70% – 80% confluency, were taken. Samples were spun at 500 x g for 5 minutes to remove debris, and cryopreserved at -80 °C. Quantification of SMRP from defrosted culture supernatant was performed using a commercial ELISA kit – ELISA MAX™ Deluxe Set Human Mesothelin, according to the manufacturers' instructions.

For IFN-γ analysis, cell suspensions were spun at 500 x g for 5 minutes and the supernatant was cryopreserved at – 80 ^{o}C. Defrosted samples were analysed via the ELISA MAX^{TM} Deluxe Set Human IFN-γ kit, according to the manufacturers' instructions.

Absorbance measurements were analysed at 450 nm and 570 nm (as background) on a FLUOstar Omega plate reader (BMG Labtech, Ortenberg, Baden-Württemberg, Germany). Standard curves were generated using serially diluted standard controls from the ELISA kits, and background-corrected values (450 nm – 570 nm readings) were fitted with a four-parameter logistic model to determine analyte concentrations.

2.9 Statistical methods

All statistical testing were performed using GraphPad Prism (ver 10.4.1) and R Statistical Software (ver. 4.4.2).

Associations of clinicopathological characteristics were evaluated using the Mann-Whitney U test for continuous variables, and the chi-squared test for categorical variables. Survival data was analysed using Kaplan-Meier curves with the log-rank test. Optimal H-score cutoff for survival using the exact distribution of maximally selected rank statistic was used, as previously described (333), using the surv_cutpoint function from survminer (ver 0.5.0). Univariate and multivariate analyses were performed using Cox proportional hazards regression models for estimating hazard ratios (HR) with 95% confidence intervals (CIs). For multivariate analysis, effects of covariates (age, sex, and tumor stage) were accounted for when evaluating survival differences.

Student's t-tests were used to compare conditions in transcriptomic analyses. Pearson correlation analysis was used to assess relationships between IHC staining for CD3, CD8, CD68, and MSLN on PDAC whole-tissue sections. For other *in vitro* assays, data was analysed from at least three independent experiments. Where appropriate, statistical comparisons were performed using Student's t-tests for two conditions, or one-way analysis of variance (ANOVA) with Turkey's multiple comparison tests for three or more conditions, as indicated in each experiment.

In all cases, two-tailed tests were used. Statistical significance was assigned at $\alpha = 0.05$ (not significant (ns), $p > 0.05$; $*p < 0.05$; $** p < 0.01$; $*** p < 0.001$).

CHAPTER 3

High mesothelin expression is associated with low cytotoxic T cell infiltration in pancreatic cancer

3.1 Introduction

MSLN is a prominent therapeutic target for CAR T cell therapy and other immunotherapeutic strategies in PDAC. The clinical relevance of MSLN expression has been examined in PDAC and across various other malignancies, including colorectal cancer (334, 335), ovarian cancer (336, 337), breast cancer (338, 339), gastric cancer (340, 341), lung cancer (342, 343), and mesothelioma (328, 344). However, there are conflicting results on the prognostic potential of MSLN due in part to differences in cohorts and methodologies used. Cohorts from the United States and Japan have reported an unfavourable association with tumour pathology and/or survival outcomes based on MSLN transcript (345, 346) and protein (347, 348) levels. Although no survival analysis was undertaken, no association was found between MSLN expression in PDAC tissues and clinicopathological factors (age, sex, disease stage, and tumour differentiation) in one cohort from China (349). No studies, to date, have performed immunohistochemical evaluation of MSLN in an Australian PDAC cohort.

Beyond its clinical associations, the biological role of MSLN has not been fully understood. Aside from a lack of physiological function and promotion of tumourigenesis, recent transcriptomic studies found MSLN was associated with anti-tumour immunity. Studies in ovarian cancer and colorectal cancer demonstrated an association between high *MSLN* expression and an immunosuppressive tumour TME (350, 351). In PDAC, high *MSLN* expression was associated with an increased stromal *CD274* (PD-L1) expression in classical B and basal-like subtypes, which could play a role in immune evasion (352, 353). Another study found that PDAC tumours with high *MSLN* expression had decreased infiltration scores of immune cell subsets (CD4 T cells, CD8 T cells, B cells, and dendritic cells) (346). These findings warrant further characterisation of the PDAC tumour landscape to understand the role that MSLN plays in immune regulation.

In this study, we evaluated novel associations between MSLN expression patterns (at both transcript and protein levels) with clinical outcomes and the composition of the immune microenvironment in PDAC patients, to understand the clinicopathological and biological significance of MSLN in PDAC. These findings will provide important insights to guide patient selection and support the development of adoptive T cell therapies for future PDAC patients.

3.2 Methods

Methodologies used in this chapter have been addressed in the Materials & Methods chapter (specifically under sections **2.3.1.1**, **2.3.2.1**, **2.4**, and **2.9**).

3.3 Results

3.3.1 High MSLN expression in the PDAC TMA cohort is associated with increased prognosis

MSLN expression was examined in an Australian TMA cohort via IHC. The clinical characteristics of the 74 PDAC patients from the cohort are summarised in **Table 3.1**. Twelve of the patients (16.2%) received chemotherapy, as adjuvant (n = 7), neoadjuvant (n = 2), and/or palliative (n = 3) treatment. Our dataset also included 14 patients with precursor lesions (PanINs and IPMNs) and no difference in MSLN H-score was observed between the PDAC and the precursor lesion cohorts (**Figure 3.1A**).

To investigate the relationship between MSLN expression and survival outcomes, the PDAC cohort was stratified into two groups based on an optimal MSLN H-score cutoff of 62, determined from the exact distribution of maximally selected rank statistics **(Figure 3.1B)**. 32% (n = 24) of patients were classified as MSLN-low and 68% (n = 50) were classified as MSLN-high (**Figure 3.2A**). The MSLN-high group demonstrated significantly higher relapse-free survival (RFS) with a median of 14.5 months (95% CI: 10.0 – 21.6 months), compared to a median RFS survival of 8.5 months (95% CI: 6.9 – 13.9 months) in the MSLN-low group (p = 0.021) (**Figure 3.2B**). Univariate Cox regression analysis revealed a significantly reduced hazard ratio (HR) for RFS in the MSLN-high group, compared to the MSLN-low group (HR = 0.571; 95% CI: 0.343 – 0.951; p = 0.031). Although a similar trend in HR reduction was observed from multivariate analysis adjusted for age, sex, and tumour stage, the result was not statistically significant (HR = 0.618, 95% CI: 0.332 – 1.147, p = 0.127).

Clinicopathological associations with MSLN expression found that the MSLN-high group exhibited a positive association with increased age (p = 0.036) (**Table 3.2**). No significant differences in MSLN expression were observed with respect to other clinicopathological

parameters including sex, tumour characteristics (stage, size, location, differentiation, and residual tumour), invasion (in peritoneum, and vasculature) and lymph node involvements.

In contrast to the PDAC TMA data, no significant difference in survival outcomes (overall and relapse-free survival) was observed in relation to *MSLN* expression levels in an RNA-seq dataset of PDAC (**Figure 3.3**). The MSLN-high group also did not correlate with any of the clinicopathological parameters examined, including age, sex, tumour characteristics (stage, location, and differentiation), treatment type, response, and relapse status (**Table 3.3**).

Table 3.1 Demographic and clinicopathological characteristics of PDAC patients in the tissue microarray cohort

Parameter	Patients, n (%)
Total	74 (100.0)
Age (years)	74 (100.0)
< 65	36 (48.6)
≥ 65	38 (51.4)
Sex	74 (100.0)
Male	39 (52.7)
Female	35 (47.3)
Tumour stage	72 (97.3)
IA	3 (4.2)
IB	8 (11.1)
IIA	20 (27.8)
IIB	38 (52.8)
IV	3 (4.2)

PDAC, pancreatic ductal adenocarcinoma.

Table 3.2 Associations between clinicopathological features and MSLN expression in PDAC patients from the tissue microarray cohort

Parameter	Total (n=74)	MSLN-high (n=50)	MSLN-low (n=24)	p-value
Age (years), median (range)	65 (40-83)	66.5 (44-79)	60.5 (40-83)	0.036

Sex, n (%) 74 (100.0)	Male	39 (52.7)	29 (58.0)	10 (41.7)	0.188
	Female	35 (47.3)	21 (42.0)	14 (58.3)	
Tumour stage*, n (%) 72 (97.3)	IA-IB	11 (15.3)	9 (18.4)	2 (8.7)	0.567
	IIA	20 (27.8)	13 (26.5)	7 (30.4)	
	IIB - IV	41 (56.9)	27 (55.1)	14 (60.9)	
Tumour size, n (%) 64 (86.5)	≤ 3.5 cm	42 (65.6)	31 (68.9)	11 (57.9)	0.398
	> 3.5 cm	22 (34.4)	14 (31.1)	8 (42.1)	
Tumour location, n (%) 55 (74.3)	Head	42 (76.4)	28 (73.7)	14 (82.4)	0.779
	Body	4 (7.3)	3 (7.9)	1 (5.9)	
	Tail	9 (16.4)	7 (18.4)	2 (11.8)	
Tumour differentiation, n (%) 72 (97.3)	Well differentiated	8 (11.1)	6 (12.5)	2 (8.3)	0.868
	Moderately differentiated	41 (56.9)	27 (56.3)	14 (58.3)	
	Poorly differentiated	23 (31.9)	15 (31.3)	8 (33.3)	
Residual tumour, n (%) 57 (77.0)	No residual tumour	32 (56.1)	18 (52.9)	14 (60.9)	0.554
	Residual microscopic tumour	25 (43.9)	16 (47.1)	9 (39.1)	
Peritoneal invasion, n (%) 54 (73.0)	Absent	9 (16.7)	8 (20.0)	1 (7.1)	0.267
	Present	45 (83.3)	32 (80.0)	13 (92.9)	
Vascular invasion, n (%) 35 (47.3)	Absent	14 (40.0)	11 (42.3)	3 (33.3)	0.636
	Present	21 (60.0)	15 (57.7)	6 (66.7)	
Lymph nodes involved, n (%) 59 (79.7)	0	26 (44.1)	19 (47.5)	7 (36.8)	0.618
	1-3	24 (40.7)	16 (40.0)	8 (42.1)	
	4-7	9 (15.3)	5 (12.5)	4 (21.1)	

*Stages IA and IB were combined, as were stages IIB and IV, due to the small sample sizes in stages IB (*n* = 3) and IV (*n* = 3), respectively. MSLN, mesothelin; PDAC, pancreatic ductal adenocarcinoma; ns, not significant.

Table 3.3 Associations between clinicopathological features and *MSLN* expression in PDAC patents from the RNA-sequencing dataset

Parameter		Total (n=126)	MSLN-high (n=63)	MSLN-low (n=63)	P-value
Cohort, n (%) 126 (100)	Australian	55 (43.7)	26 (41.3)	29 (46.0)	0.590
	Canadian	71 (56.3)	37 (58.7)	34 (54.0)	
Age, n (%) 125 (99.2)	< 70	75 (60.0)	39 (61.9)	36 (58.1)	0.661
	≥ 70	50 (40.0)	24 (38.1)	26 (41.9)	
Sex, n (%) 124 (98.4)	Male	68 (54.0)	39 (61.9)	29 (46.0)	0.058
	Female	57 (45.2)	23 (36.5)	34 (54.0)	
Tumour stage, n (%) 66 (52.4)	I	37 (36.3)	25 (37.9)	12 (33.3)	0.304
	II	56 (54.9)	34 (51.5)	22 (61.1)	
	III	5 (4.9)	5 (7.6)	0 (0.0)	
	IV	4 (3.9)	2 (3.0)	2 (5.6)	
Tumour location, n (%) 68 (54.0)	Head	51 (75.0)	23 (79.3)	28 (71.8)	0.625
	Body	8 (11.8)	2 (6.9)	6 (15.4)	
	Tail	5 (7.4)	3 (10.3)	2 (5.1)	
	Duct*	1 (1.5)	0 (0)	1 (2.6)	
	Other parts	3 (4.4)	1 (3.4)	2 (5.1)	
Tumour differentiation, n (%) 123 (97.6)	Well differentiated	15 (12.2)	7 (11.1)	8 (13.3)	0.638
	Moderately differentiated	68 (55.3)	33 (52.4)	35 (58.3)	
	Poorly differentiated	39 (31.7)	22 (34.9)	17 (28.3)	
	Undifferentiated*	1 (0.8)	1 (1.6)	0 (0)	
Treatment, n (%) 110 (87.3)	Surgery	28 (25.5)	14 (24.6)	14 (26.4)	0.676
	Chemotherapy	35 (31.8)	21 (36.8)	14 (26.4)	
	Chemotherapy + radiation therapy	14 (12.7)	7 (12.3)	7 (13.2)	
	No treatment	33 (30.0)	15 (26.3)	18 (34.0)	
Response, n (%) 117 (92.9)	Complete remission/NED	22 (18.8)	10 (17.5)	12 (20.0)	0.657
	Stable disease	17 (14.5)	10 (17.5)	7 (11.7)	
	Progressive disease/relapses	78 (66.7)	37 (64.9)	41 (68.3)	

Relapse type, n (%) 73 (57.9)	Local recurrence	14 (19.2)	9 (25.7)	5 (13.2)	0.140
	Distant recurrence/metastasis	48 (65.8)	19 (54.3)	29 (76.3)	
	Local recurrence & distant metastasis	11 (15.1)	7 (20.0)	4 (10.5)	

*Group was excluded from chi-squared analysis due to small sample size (*n* = 1). MSLN, mesothelin; PDAC, pancreatic ductal adenocarcinoma; NED, no evidence of disease; ns, not significant.

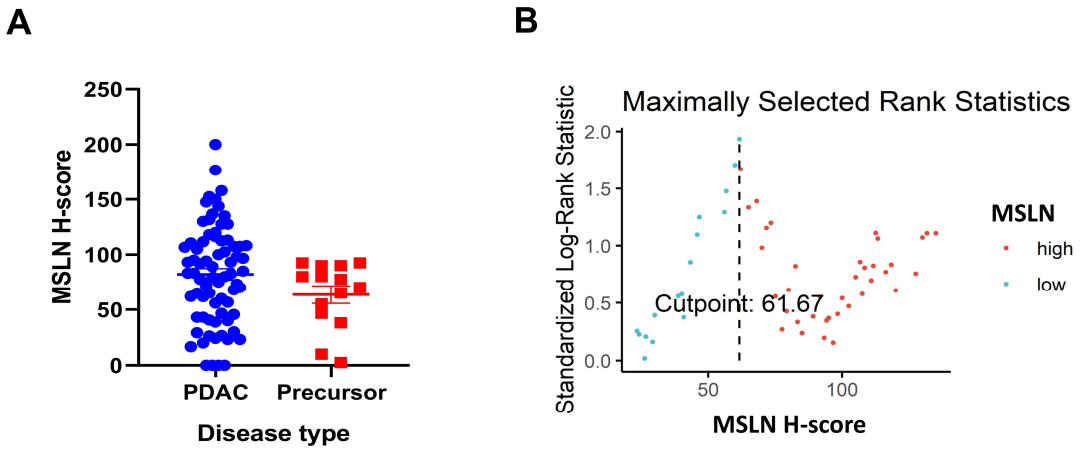

Figure 3.1 Mesothelin (MSLN) expression distribution and determination of optimal H-score cutoff from the tissue microarray cohort. (**A**) MSLN expression, evaluated as H-scores, across pancreatic cancer subtypes – pancreatic ductal adenocarcinoma (PDAC) and precursors. Precursor group includes pancreatic intraepithelial neoplasms (PanINs) and intraductal papillary mucinous neoplasms (IPMNs). Statistical testing was performed using unpaired student's t-test and non-significance ($p > 0.05$) is not shown. Data is presented as mean ± SEM. (**B**) In the PDAC group, the optimal H-score cutoff providing the highest standardized log-rank statistics was evaluated based on maximally selected rank statistics and indicated.

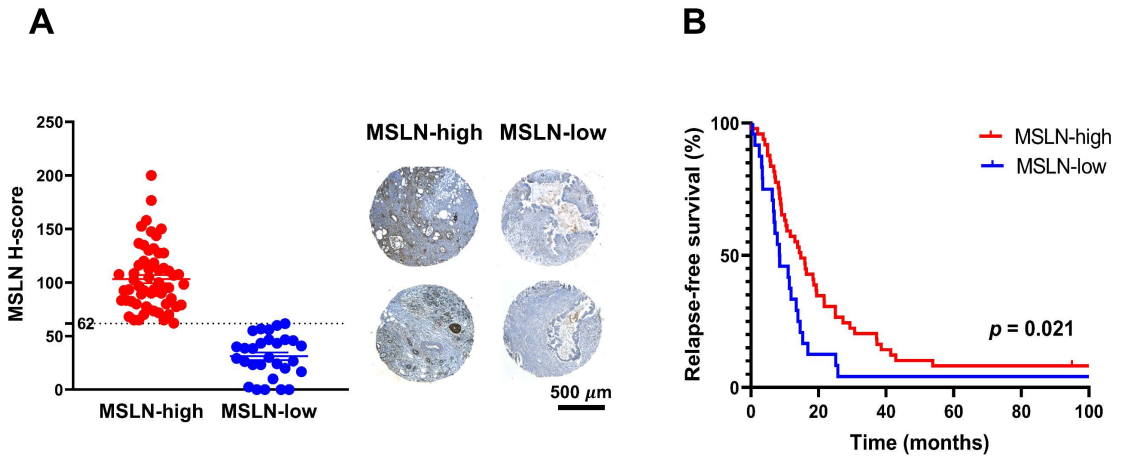

Figure 3.2 High mesothelin (MSLN) level is associated with increased relapse-free survival (RFS) in the pancreatic ductal adenocarcinoma (PDAC) tissue microarray cohort. (A) Distribution of MSLN expression across the cohort based on H-score cutoff of 62 (dotted line) (left). Data is shown as mean ± SEM. Representative images of tissue microarray samples from the MSLN-high and MSLN-low groups (right). Scale bar = 500 µm. **(B)** Kaplan Meier curves of RFS of MSLN-high and MSLN-low groups. Censored events were indicated. Statistical testing was performed by log-rank test and p-value was indicated.

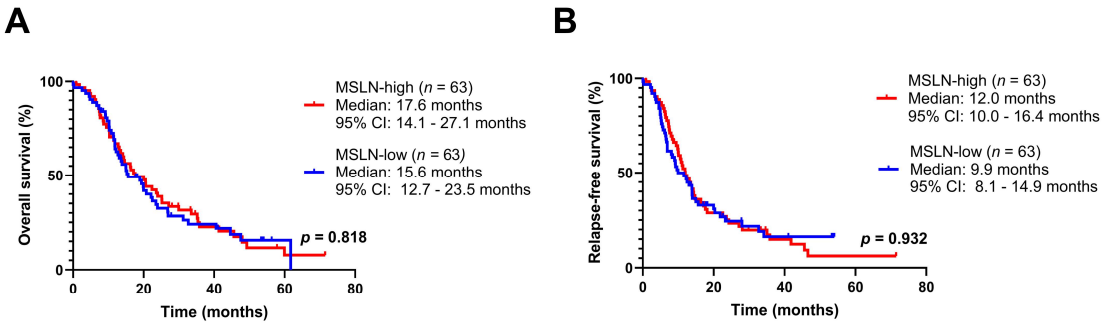

Figure 3.3 Survival outcomes are not associated with mesothelin (*MSLN*) level in the human pancreatic ductal adenocarcinoma (PDAC) RNA-sequencing dataset. Top and bottom tertiles of *MSLN* expression were used to establish the MSLN-high and MSLN-low groups. Kaplan-Meier curves of relapse-free survival (RFS) (**A**) and overall survival (OS) (**B**) were shown. Censored events were indicated, along with median survival and 90% confidence interval (CI). Statistical testing was performed by log-rank tests and p-values were indicated.

3.3.2 High MSLN expression in human and mouse PDAC tumours is associated with reduced immune activity

To investigate the biological significance of MSLN, transcriptomic analysis was conducted on human and mouse PDAC RNA-seq datasets to compare samples with high and low MSLN expressions (**Figure 3.4A-B**). In both datasets, the MSLN-high group exhibited consistent downregulation of genes associated with immune-related pathways, including those involved in the regulation of leukocyte adhesion, proliferation, and migration/chemotaxis (**Figure 3.4C-D**). In addition, pathways related to T cell activation and broader adaptive immune response were suppressed in the MSLN-high group. Among the top 30 downregulated pathways, the human RNA-seq dataset also included two clusters of pathways participating in bone development and peptide secretions, although these were not observed in the mouse RNA-seq dataset, which was comprised only of immune-associated clusters.

To assess anti-tumour responses, tumour reactivity was estimated using tumour reactive CD8 T cell signature (TRS) scores from a previous study (324), which has been validated using hepatocellular carcinoma, non-small-cell lung cancer, melanoma, and colorectal cancer datasets. In both human and mouse datasets, the MSLN-high group showed significantly lower TRS scores, indicating high MSLN expression is potentially associated with reduced anti-tumour immune activity (**Figure 3.4E-F**).

To investigate if immune cell infiltration into tumours also decreased, the relative proportions of key immune cell infiltrates (CD8 T cells and macrophages) were estimated via cell type prediction algorithms and compared between the MSLN-high and MSLN-low groups in the human RNA-seq dataset. However, considerable discordance was observed across the different algorithms used (**Figure 3.5**). For the mouse RNA-seq dataset, T cell infiltration status of the implanted tumour clones, described in the study from which the mouse data was derived (323), was not associated with *Msln* expression. Specifically, *Msln* expression did not differ significantly between “T cell high” and “T cell low” clones, nor did tumours in the MSLN-high group have higher proportions of “T cell high” clones (**Figure 3.6**).

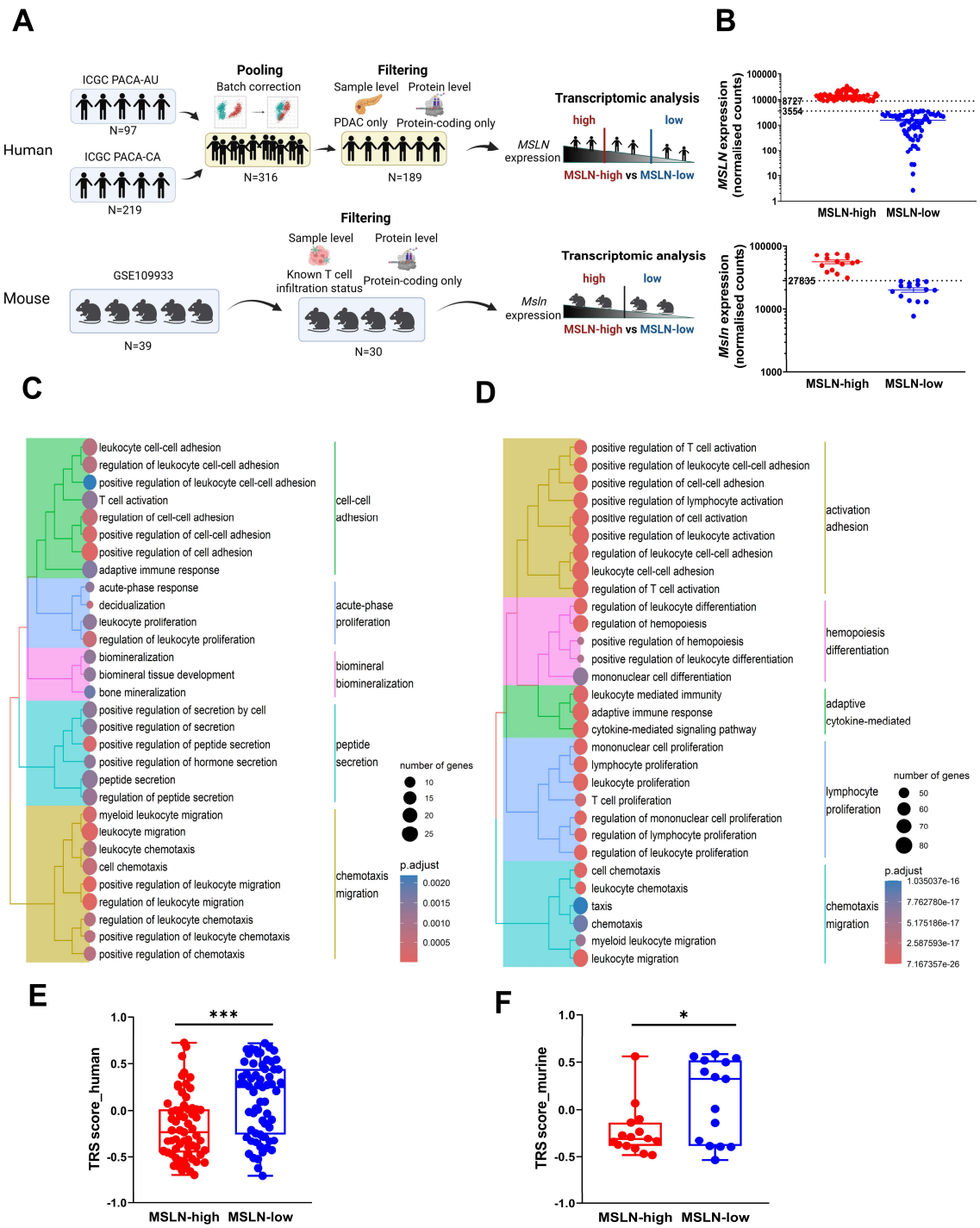

Figure 3.4 High mesothelin (human: *MSLN*; mouse: *Msln*) expression is associated with suppressed transcriptomic signatures of immune functions and tumour reactivity. (**A**) Workflow for transcriptomic analysis of human (top) and mouse (bottom) pancreatic ductal adenocarcinoma (PDAC) RNA-sequencing datasets. **(B)** Human (top) and mouse (bottom) datasets were separated into MSLN-high and MSLN-low groups based on $\log_{10}$-transformed normalized read counts of *MSLN*/*Msln*, quantified via DESeq2. Expression thresholds for stratification are indicated (dashed lines). Top 30 biological processes from gene ontology

enrichment analysis of downregulated genes in MSLN-high vs MSLN-low groups from the human **(C)** and mouse **(D)** datasets. Predicted tumour-reactive T cell signatures (TRS) scores for MSLN-high and MSLN-low groups from the human (**E**) and mouse (**F**) datasets. Data are presented as mean ± SEM. Statistical testing was performed via unpaired student's t-tests, with significance indicated (*p < 0.05; ***p < 0.001).

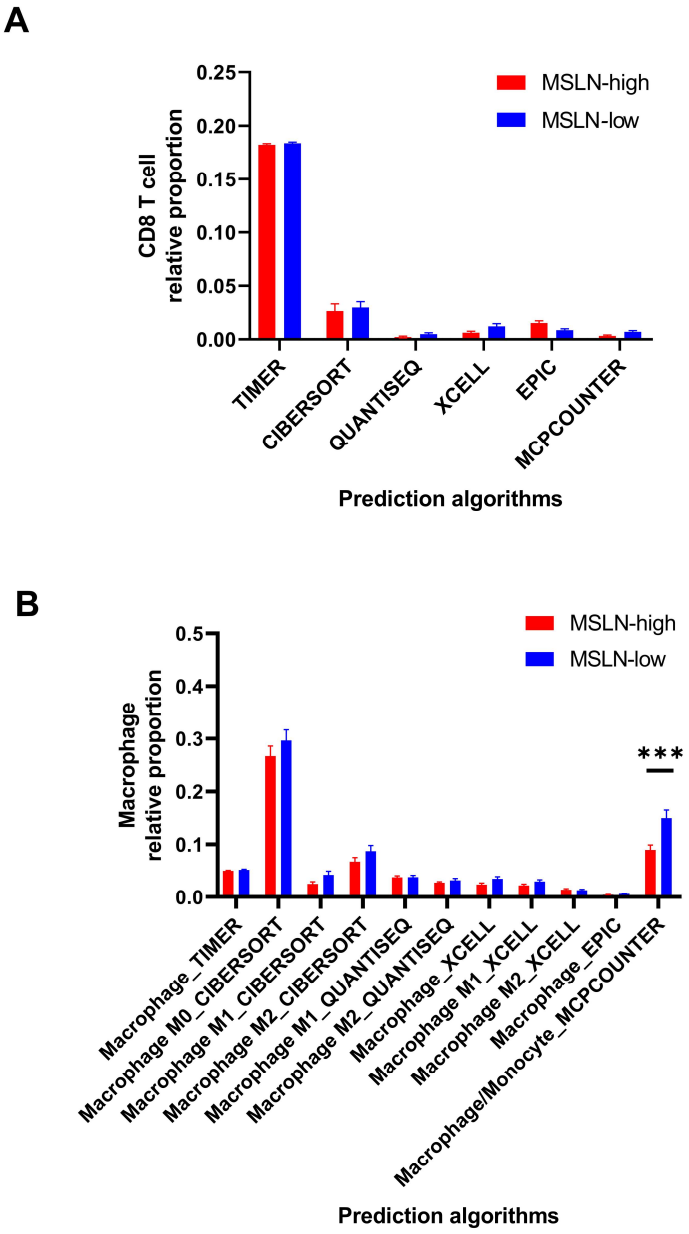

Figure 3.5 Immune cell infiltration predictions on the human pancreatic ductal adenocarcinoma (PDAC) RNA-sequencing dataset are highly inconsistent. Relative proportions of CD8 T cells (**A**) and macrophage populations (**B**) in the MSLN-high and MSLN-low groups of the human pancreatic ductal adenocarcinoma RNA-sequencing dataset were estimated via different cell type prediction algorithms. Data are shown as mean ± SEM.

Statistical testing was performed by unpaired student's t-tests, with significance indicated (***$p < 0.001$).

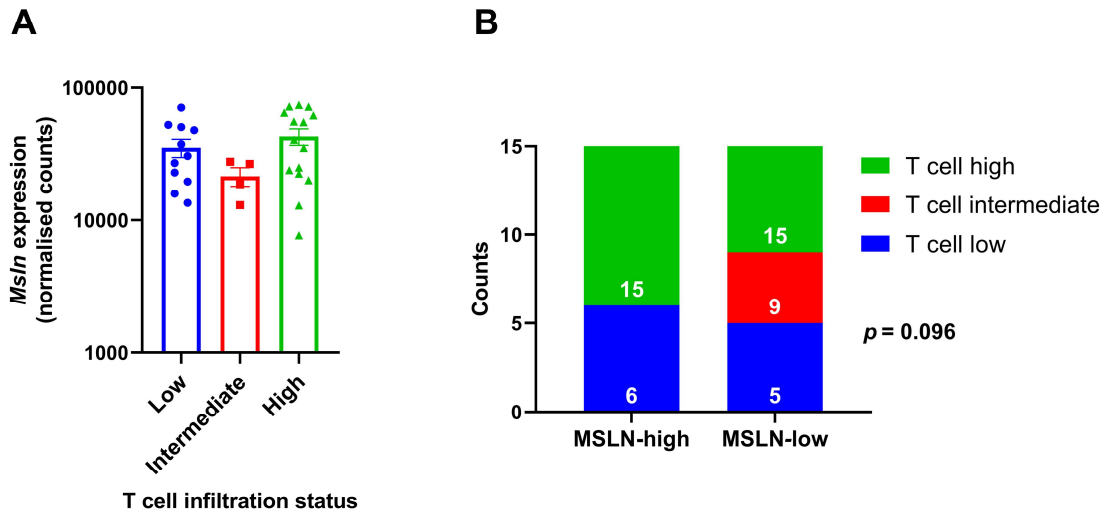

Figure 3.6 Mesothelin (*Msln*) expression was not associated with the T cell infiltration status in the mouse pancreatic ductal adenocarcinoma RNA-sequencing dataset. (**A**) Relationship between predefined T cell infiltration status of implanted tumour clones and *Msln* expression in harvested tumour samples. *Msln* expression was shown as log_{10}-transformed DESeq2-normalized counts. Data was presented as mean ± SEM. Statistical testing was performed using one-way ANOVA followed by Turkey's post hoc test for multiple comparisons and non-significance ($p > 0.05$) is not shown. **(B)** Breakdown of samples with different T cell infiltration status in MSLN-high and MSLN-low groups, stratified based on median *Msln* expression. Statistical testing was performed using chi-squared test, with p-value indicated.

3.3.3 scRNA-seq profiling reveals elevated *MSLN* expression in PDAC to be associated with reduced CD8 T cell abundance

To further investigate the associations of MSLN with the cellular composition of PDAC, a publicly available human PDAC scRNA-seq dataset was profiled and analysed (326). *MSLN* expression was primarily localised in the ductal cell 2 compartment, which was shown to be a malignant population based on the original study from which the dataset was obtained (**Figures 3.7A-B**) (326). From individual samples, the ductal cell 2 population also consistently exhibited the highest MSLN expression, both in terms of expression intensity and percentage (of total cells) (**Figure 3.7C**).

To assess changes in cellular compositions associated with *MSLN* expression, samples were stratified into MSLN-high and MSLN-low groups based on median *MSLN* expression. The MSLN-high group exhibited a significantly higher percentage of ductal cell 2 population (mean ± SEM: 31.2% ± 5.5% vs 7.6% ± 2.2%) and lower percentage of endothelial cells (mean ± SEM: 7.0% ± 2.2% vs 16.0% ± 2.1%), compared to the MSLN-low group (**Figure 3.8A**). Further characterization revealed a *MUC1*-positive cluster to be the predominant subset of ductal cell 2; however, both the *MUC1*-positive cluster and one of the *MUC1*-negative clusters showed increased percentages in the MSLN-high group (**Figure 3.8B**). The endothelial cells were comprised of three clusters representing an arterial population and two (*PLVAP*+/*POSTN*+) venous populations (**Figure 3.8C**). Reductions in percentage were observed only in the *PLVAP*+ venous subset, which comprised the majority (65%) of endothelial cells in MSLN-high versus MSLN-low groups.

To better examine the relationship between MSLN expression and immune cell infiltration, we performed subclustering analysis on T cells, B cells, and macrophages compartments in the PDAC immune microenvironment. Although no differences were observed in the overall abundance of T cell infiltrates, the CD8 T cell subset showed significantly reduced percentage in the MSLN-high group compared to the MSLN-low group (mean ± SEM: 5.5% ± 1.0% vs 9.5% ± 0.8%), representing more than 40% reduction in total CD8 T cell populations (**Figure 3.7D**). Other T cell, B cell, and macrophage subsets did not show any significant difference in percentage between MSLN-high and MSLN-low groups (**Figure 3.9C-D**). However, within the macrophage population, the MSLN-high group demonstrated a shift towards an M2-polarised phenotype (**Figure 3.10**).

Within the CD8 T cell subset, gene ontology analysis revealed downregulations of differentially expressed genes involved in immune-associated activity pathways, in the MSLN-high group compared to the MSLN-low group (**Figure 3.11**). These pathways participate in adaptive immune responses, immune activation, and chemotaxis, consistent with the results from bulk RNA-seq analysis. The memory and exhaustion phenotypes, as well as cytokine and chemokine profiles, of CD8 T cells were further characterized. No significant differences were observed in the memory or exhaustion phenotypes between MSLN-high and MSLN-low groups (**Figure 3.12**). When compared to the MSLN-low group, CD8 T cells from MSLN-high group showed enrichment of GMCSF, HGF, IL-1, IL-2, and TNFSF12 signalling pathways (**Figure**

3.13). These cells also showed downregulated expressions of chemokines *CCL2*, *CCL4*, *XCL1*, and *XCL2*, as well as the chemokine receptor *CXCR6* (**Figures 3.14**). However, expression of *CXCL5*, a neutrophil chemoattractant known to impair CD8 T cell-mediated anti-tumour immunity, was upregulated (354). These findings suggest that high *MSLN* expression is associated with reduced abundance and an altered transcriptomic profile of CD8 T cell infiltrates in PDAC.

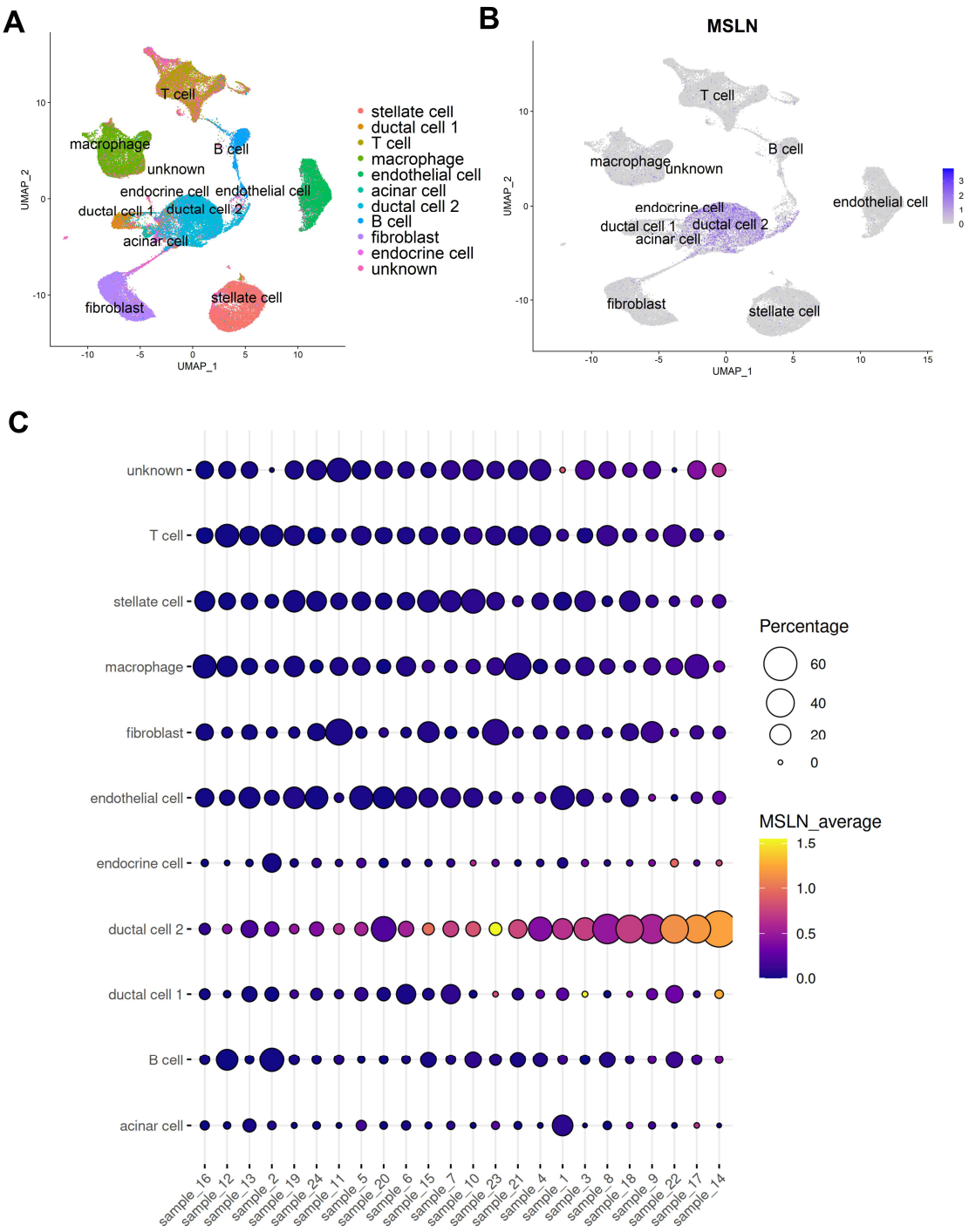

Figure 3.7 Ductal cell 2 population exhibits the highest mesothelin (*MSLN*) expression in the human pancreatic adenocarcinoma (PDAC) single-cell RNA-sequencing dataset. (A) UMAP plot showing clustering of integrated single-cell transcriptomes across all patient samples, annotated by cell type. **(B)** Feature plot visualising *MSLN* expression across annotated cell types. Colour intensity corresponds to the magnitude of expression. **(C)** Balloon plot illustrating the average *MSLN* expression (colour gradient) and relative abundance (dot size) of each annotated cell type across individual samples. Samples were ordered by ascending mean MSLN expression across all cell types.

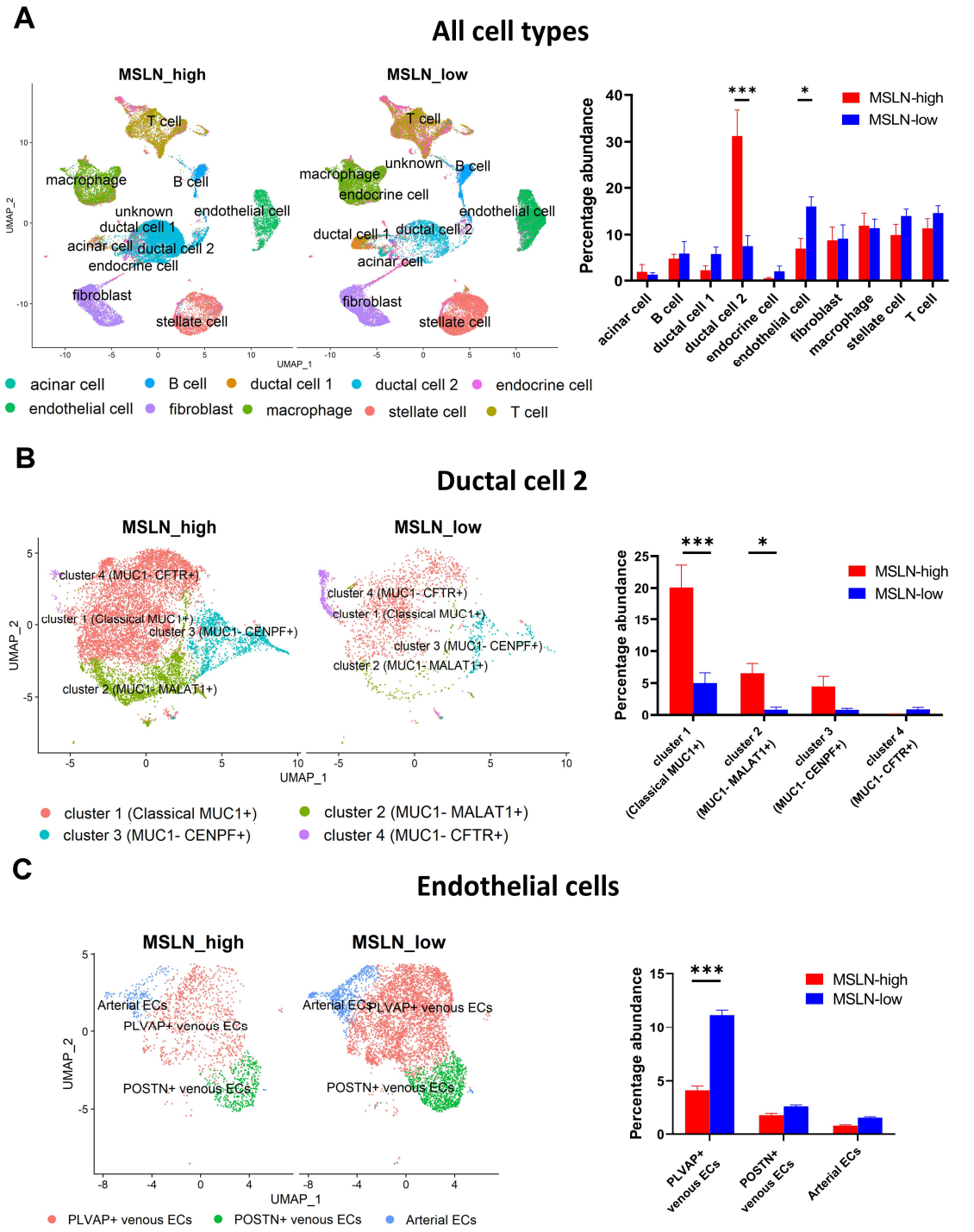

Figure 3.8 High mesothelin (*MSLN*) expression is associated with increased ductal cell 2 and reduced endothelial populations in human pancreatic adenocarcinoma (PDAC). (A) UMAP visualisation of annotated cell types across MSLN-high and MSLN-low groups in the human PDAC single-cell RNA-sequencing dataset, stratified by median MSLN expression. Bar graph (right) quantifies the percentage abundance of each cell type relative to total cells. **(B)** Subclustering of the ductal cell 2 compartment (left) and percentage abundance of each subset (right) **(C)** Subclustering of the endothelial cell compartment (left) and subset percentage abundance (right). Data in bar graphs are presented as mean ± SEM. Statistical

testing was performed via unpaired student's t-tests, with significance indicated (*$p < 0.05$; ***$p < 0.001$).

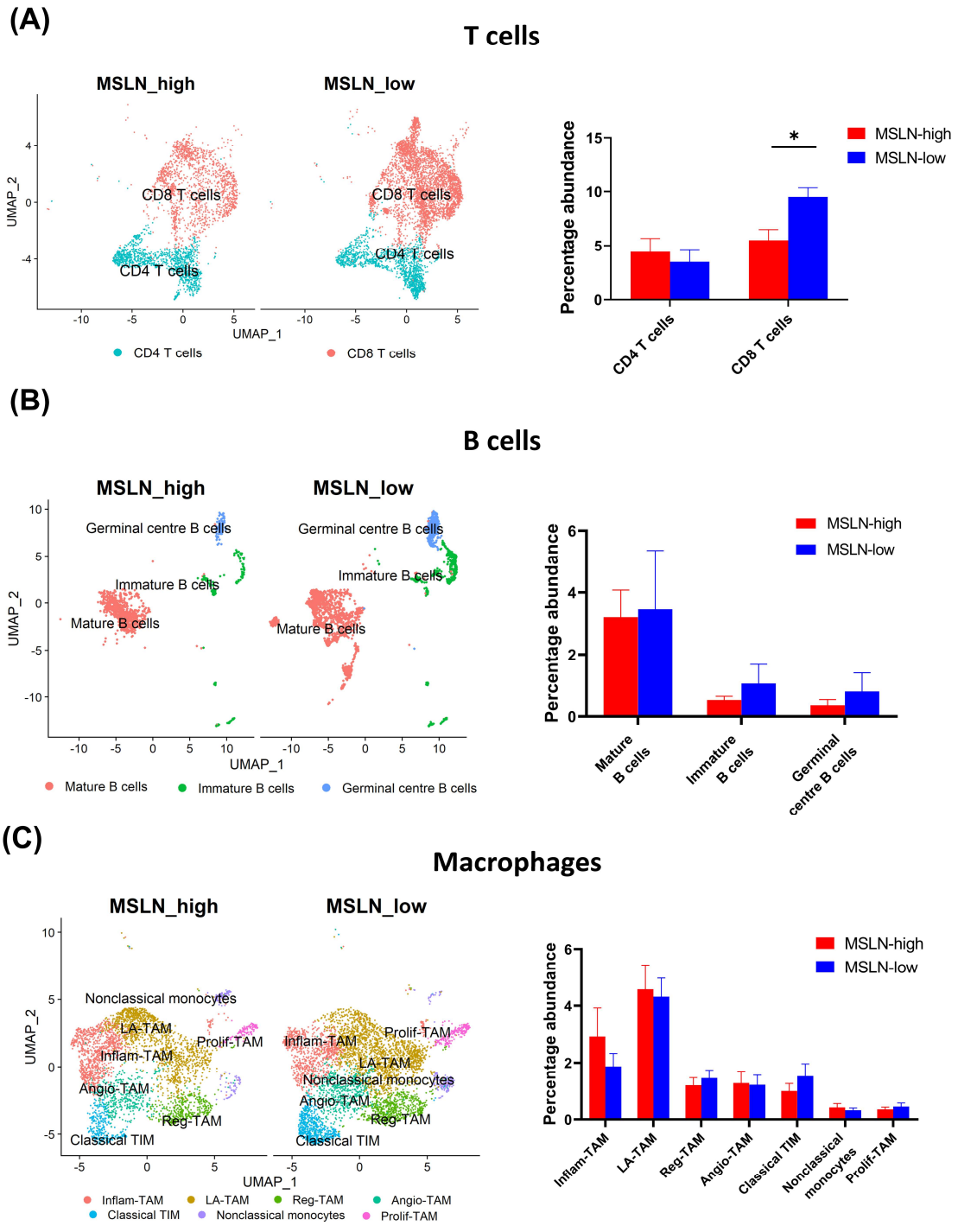

Figure 3.9 Subtype analysis of the immune microenvironment identifies reduced CD8 T cell abundance in human pancreatic ductal adenocarcinoma (PDAC) samples with high mesothelin (*MSLN*) expression. Cells in T cell **(A)**, B cell **(B)**, and macrophage **(C)** compartments were isolated from the human PDAC single-cell RNA-sequencing dataset, re-

clustered, and annotated manually into distinct subsets. Data were visualized as comparisons of UMAP plots between MSLN-high and MSLN-low groups (left) and differences in subset abundances were quantified in bar graphs (right). Data in bar graphs are presented as mean ± SEM. Statistical testing was performed via unpaired student's t-tests, with significance indicated (*p < 0.05).

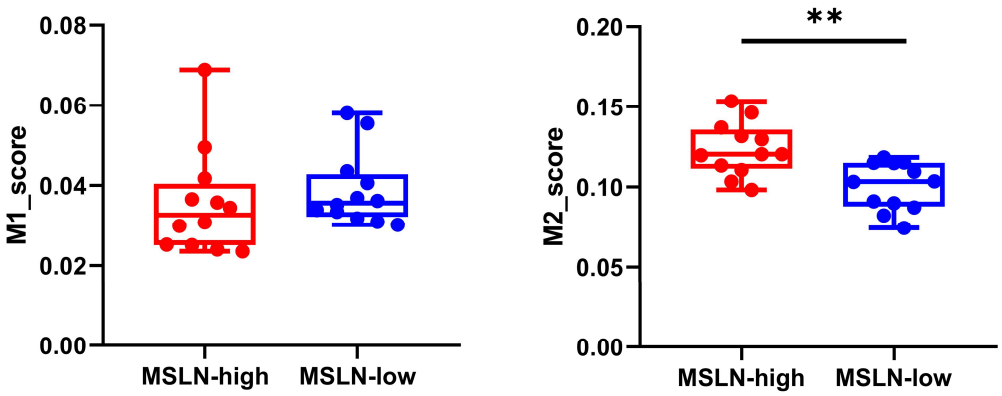

Figure 3.10 High mesothelin (*MSLN*) expression was associated with increased M2 polarisation score of macrophages from the human pancreatic ductal adenocarcinoma (PDAC) single cell RNA-sequencing dataset. M1 (left) and M2 (right) polarisation scores of the macrophage population were evaluated for each sample via UCell using M1 and M2 gene signatures, respectively. Scores were compared between MSLN-high and MSLN-low groups. Statistical testing was performed via unpaired student's t-tests, with significance indicated (**p < 0.01).

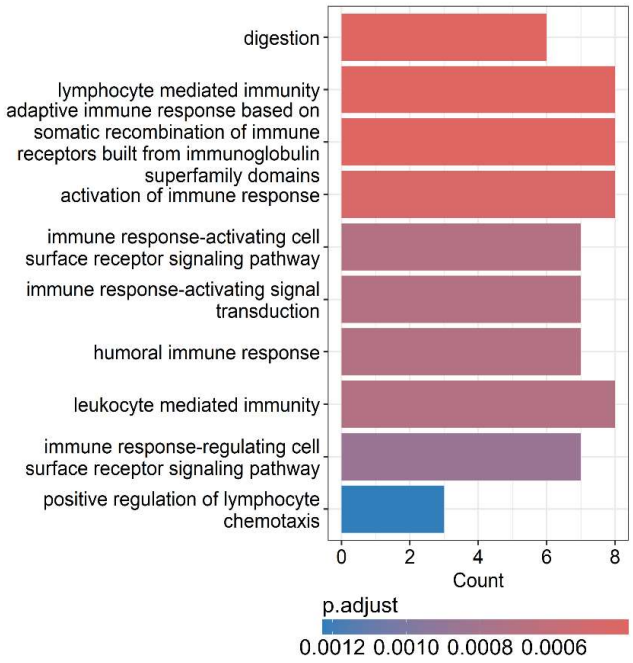

Figure 3.11 CD8 T cells exhibit suppressed transcriptomic signatures of immune activity in human pancreatic ductal adenocarcinoma (PDAC) with high mesothelin (*MSLN*) expression. CD8 T cell subset was isolated from the human PDAC single-cell RNA-sequencing dataset, and gene ontology analysis was performed between cells in the MSLN-high versus the MSLN-low group. The top 10 downregulated biological processes were visualised in the bar plot, ranked based on adjusted p-value (colour gradient).

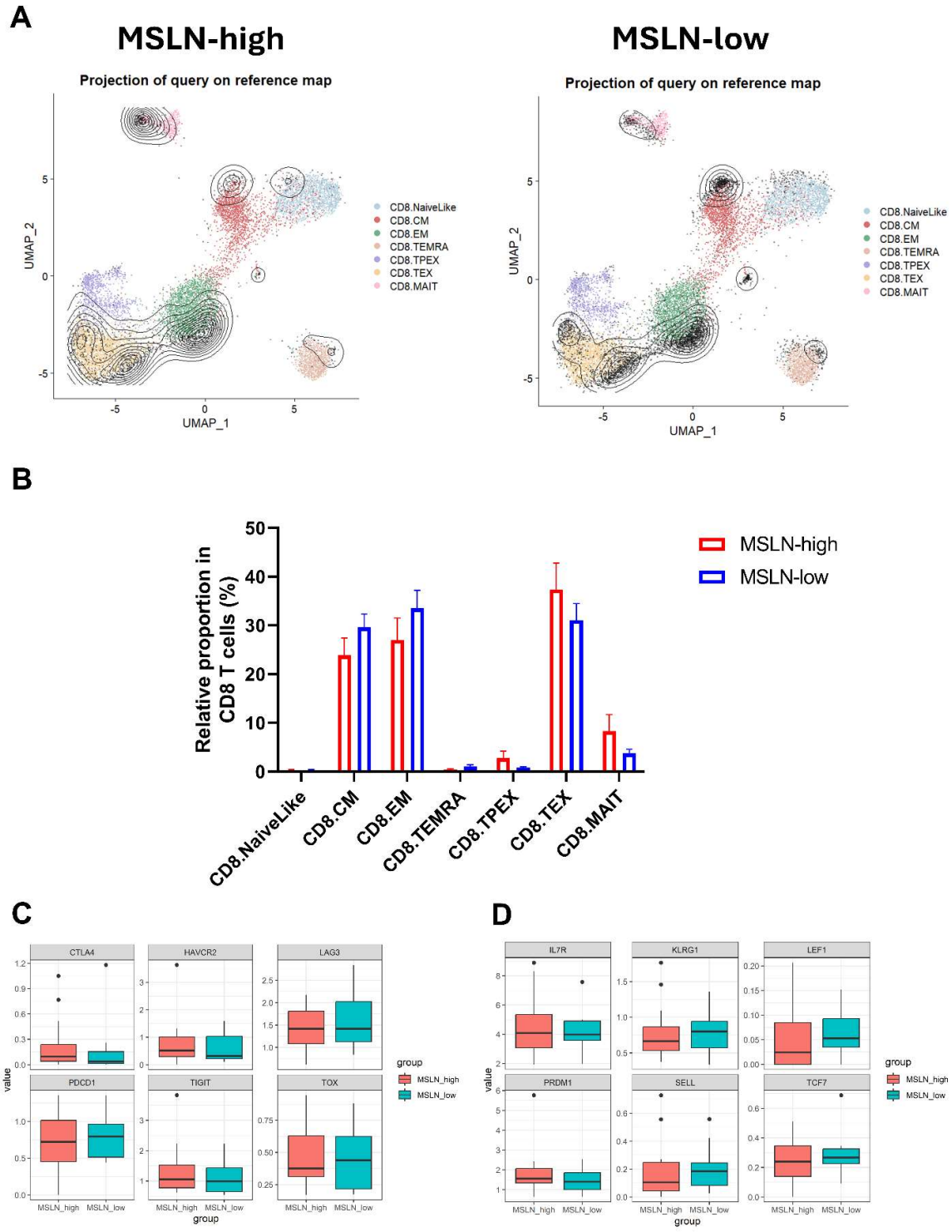

Figure 3.12 Exhaustion and memory phenotypes of CD8 T cells from the human pancreatic ductal adenocarcinoma (PDAC) single-cell RNA sequencing dataset. (A) UMAP comparison of CD8 T cells from MSLN-high (left) and MSLN-low (right) groups, when projected onto a reference CD8 T cell atlas. **(B)** Differences in the relative proportion of projected CD8 T cell subsets between the MSLN-high and MSLN-low groups. Expression of phenotypic markers for exhaustion **(C)** and memory **(D)** between MSLN-high and MSLN-low groups. Expression was

quantified as normalised counts per cell via Seurat. Data in bar graphs are presented as mean ± SEM. Statistical testing was performed via unpaired student's t-tests and non-significance ($p > 0.05$) is not shown.

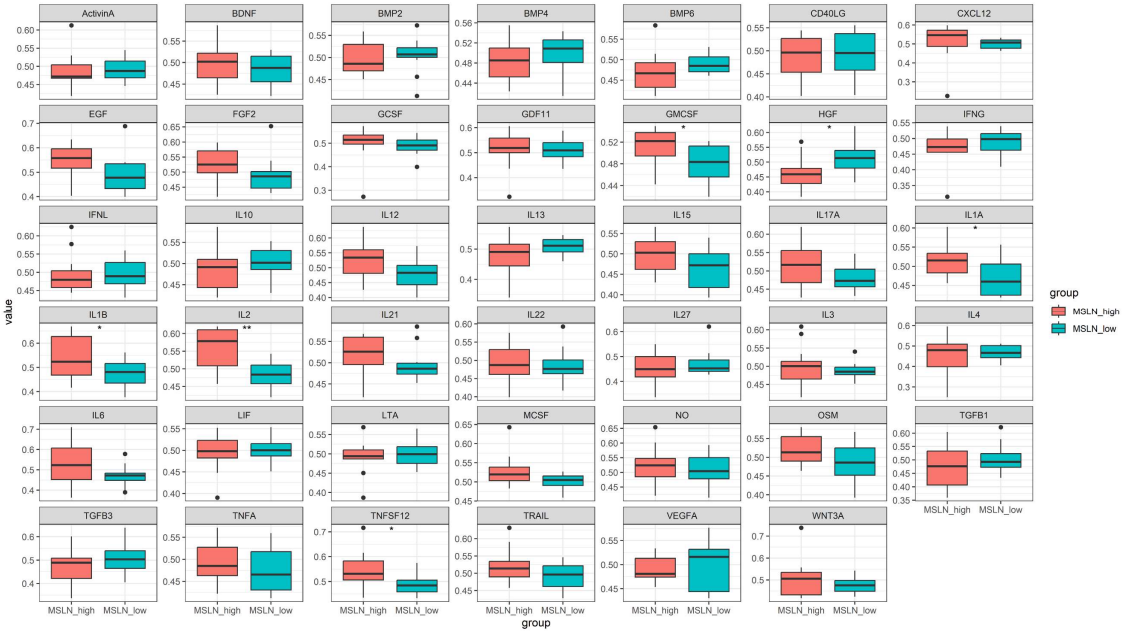

Figure 3.13 Cytokine signalling profiles of CD8 T cells from the human pancreatic ductal adenocarcinoma (PDAC) single-cell RNA sequencing dataset. Predicted activities of 41 cytokine signalling pathways were inferred for each sample using the CytoSig platform, and compared between CD8 T cells from the MSLN-high and MSLN-low groups. Statistical testing was performed via unpaired student's t-tests, with significance indicated (*$p < 0.05$; **$p < 0.01$).

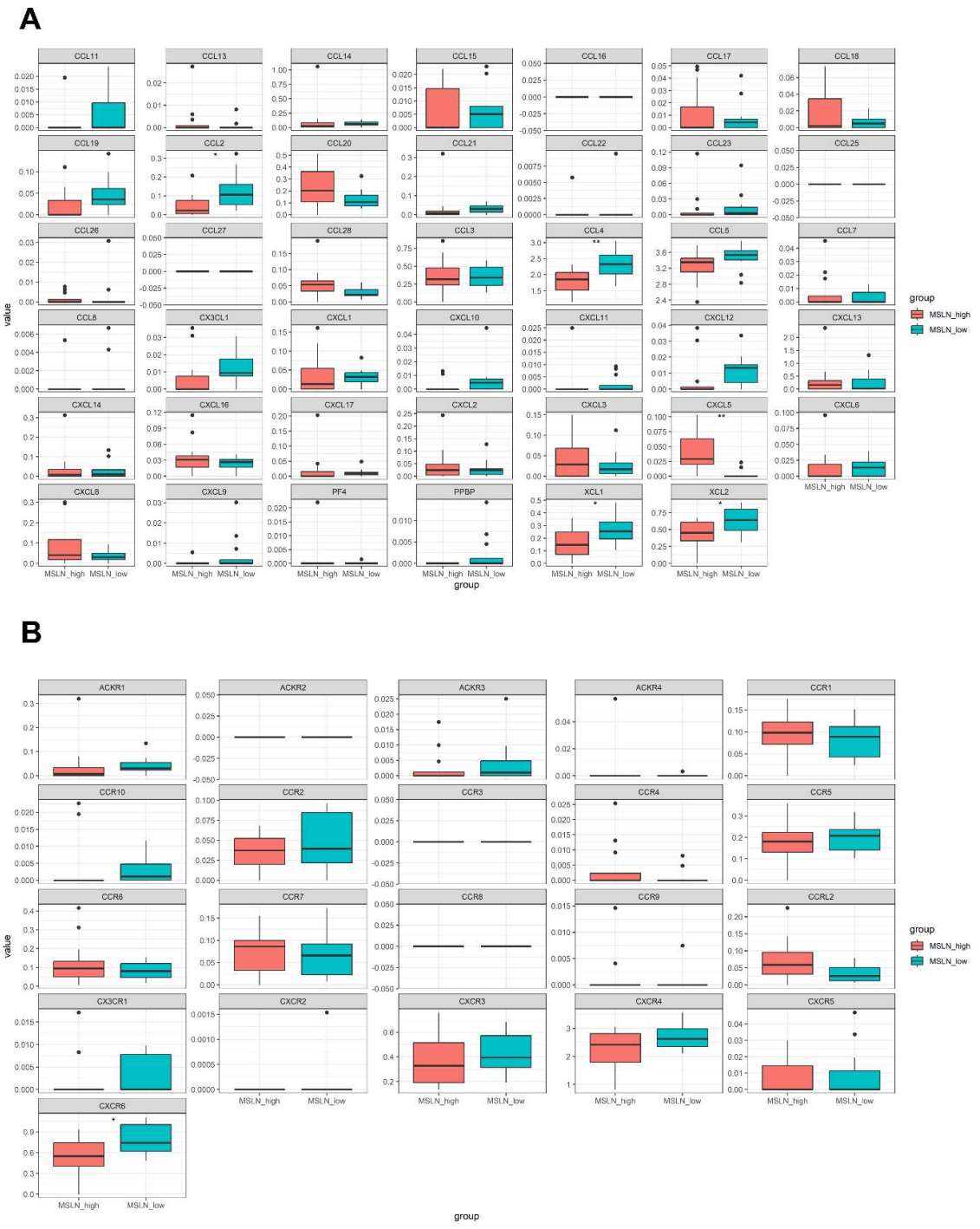

Figure 3.14 Chemokine profiles of CD8 T cells from the human pancreatic ductal adenocarcinoma (PDAC) single-cell RNA sequencing dataset. Expression of all human chemokines **(A)** and chemokine receptors **(B)** were examined for each sample. Expression was quantified as normalised counts per cell via Seurat. Differences were compared between samples in the MSLN-high and MSLN-low groups. Statistical testing was performed via unpaired student's t-tests, with significance indicated (*p < 0.05; **p < 0.01).

3.3.4 Immunohistochemical evaluation shows a trend towards reduced CD8 T cell stromal infiltration in PDAC with high MSLN expression

To validate the transcriptomic relationship between MSLN expression and T cell infiltration, IHC staining was undertaken on whole-tissue FFPE sections of 10 surgically resected PDAC tumours. MSLN expression was evaluated by H-scoring and showed a range from 0.5 to 210 **(Figure 3.15A)**.

Stromal immune cell infiltration was also examined via IHC staining and independently scored as the percentage of positively stained cells. When stratified based on the H-score cutoff of 62 – established in **section 3.3.1** from the PDAC TMA cohort – the MSLN-high group (n=3) exhibited less intense, albeit not significant, staining of CD8 (mean ± SEM: 3.2 ± 0.8 vs 5.4 ± 1.2, p = 0.272) and CD3 (mean ± SEM: 5.3 ± 1.5 vs 7.6 ± 1.6, p = 0.409) in the tumour stroma (**Figure 3.15B-C**). CD68, a macrophage and monocyte marker used as a negative control (355), showed comparable staining between MSLN-high and MSLN-low groups (mean ± SEM: 6.000 ± 2.000 vs 7.143 ± 1.366, p = 0.656).

Across all samples, CD8, CD3, and CD68 scores showed a negative trend with increasing MSLN H-score (**Figure 3.15D**). However, no significance was reported from correlational analysis (CD8: p = 0.174; CD3: p = 0.266; CD68: p = 0.432), likely due to low sample numbers (n = 10). In summary, a decreased trend in CD8 T cell infiltration was observed in MSLN-high tumours, although further confirmation in larger independent cohorts is required.

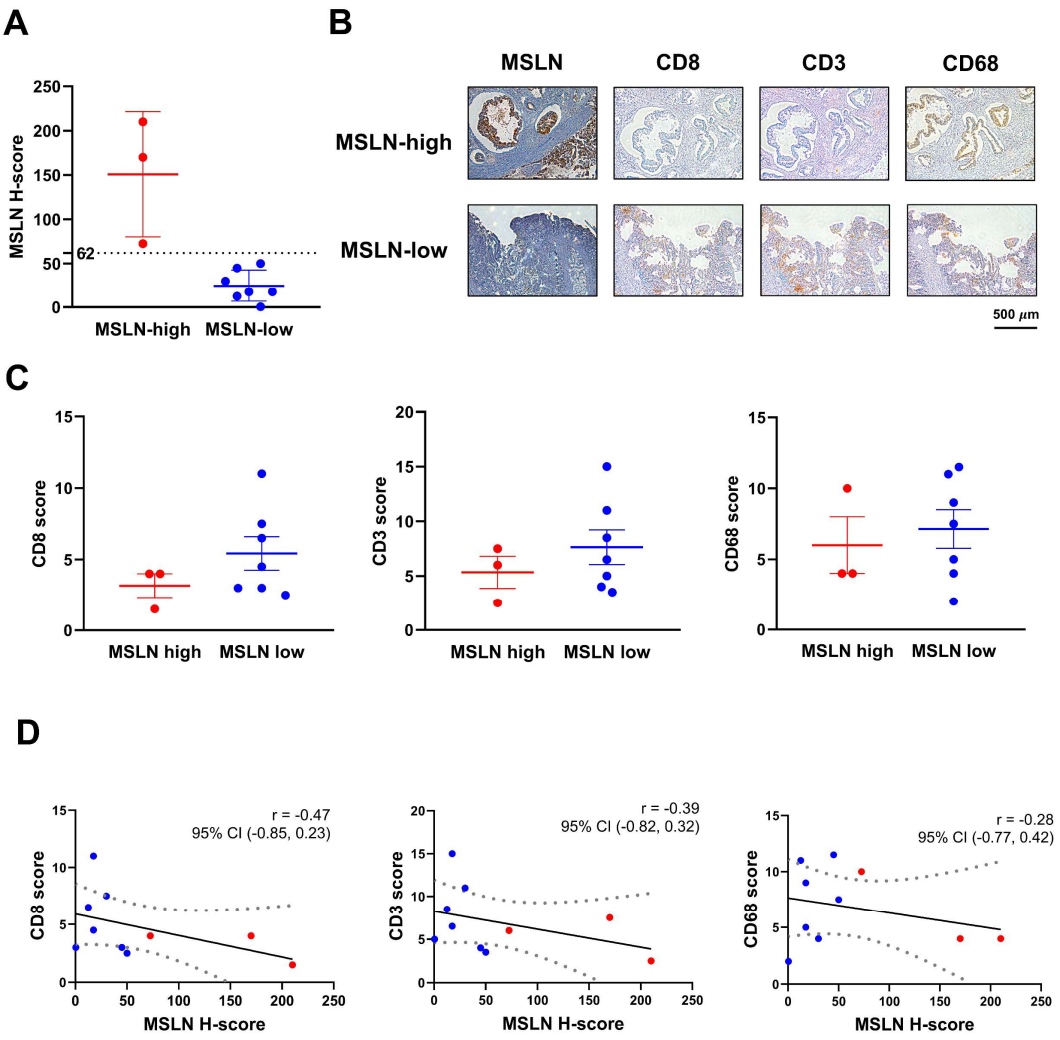

Figure 3.15 Associations of mesothelin (MSLN) expression with T cell infiltration in the stroma of pancreatic ductal adenocarcinoma (PDAC). (**A**) H-score distribution of MSLN staining on whole-tissue sections from surgical specimens. Samples were stratified into MSLN-high and MSLN-low groups based on the H-score cutoff of 62. (**B**) Immunohistochemical (IHC) staining of representative serial sections in the MSLN-high and MSLN-low groups. Scale bar = 500 µm. **(C)** Differences in CD8, CD3, and CD68 scores between the MSLN-high and MSLN-low groups. Scores were assessed independently by pathologists based on IHC staining of corresponding serial sections. Data is presented as mean ± SEM. Statistical testing was performed via unpaired student's t-tests. Non-significance ($p > 0.05$) is not shown. **(D)** Correlational analysis of MSLN H-score with CD8, CD3, and CD68 scores. Linear regression model was fitted (solid line), with dashed boundaries representing the 95% confidence interval (CI). Samples classified as MSLN-high (red) and MSLN-low (blue) groups were highlighted. Correlation coefficient (r) and its 95% CI were indicated for each pair-wise analysis.

3.4 Discussion

This study identified high MSLN expression (H-score ≥ 62 from IHC staining) in PDAC to be associated with improved RFS and age. Transcriptomic analysis found a link between MSLN expression and an immunosuppressive tumour landscape. Specifically, CD8 T cells had reduced immune reactivity and reduced percentage abundance in PDAC tumours with high MSLN expression. In subsequent IHC validation, PDAC tumours with high MSLN expression demonstrated a trend towards reduced infiltration of CD8 T cells in the stroma, although confirmations in larger independent cohorts are necessary.

3.4.1 MSLN as a prognostic biomarker in Australian PDAC patients

In our analysed TMA patient samples, MSLN expression was associated with improved prognosis. Previous studies have found high MSLN expression to be correlated with worse survival outcome in PDAC (123, 347, 348). This discrepancy could be due to the different methodological classification and scoring used. Only one other study in PDAC used the H-score system for stratification. Using a median MSLN H-score cutoff of 180, they found poor survival in patients with high co-expression of MSLN and MUC16 (123). Other studies established cutoffs either based on the percentage of MSLN-positive cells alone (348) or the percentage of positive cells with the staining intensity analysed separately (347). Antibody clones for MSLN staining also varied in studies. Two studies used anti-MSLN antibody clone 5B2 (123, 347), in contrast to the MN-1 clone used in the current study. The 5B2 clone has been found to have lower affinity and staining positivity in PDAC compared to the MN-1 clone (356). Staining patterns also differ between MN-1 and 5B2 clones, likely due to differential expression of epitopes for MSLN recognition, where the exact binding site for 5B2 has not been characterized (328).

Underlying patient-specific differences can potentially contribute to the observed findings as well. Our TMA cohort is relatively small (n = 74), with only a limited number of individuals receiving adjuvant chemotherapy (n = 7) and having resection margin data available (n = 56). Consequently, the effects of surgical resection and adjuvant chemotherapy on RFS could not be robustly examined in this cohort and were therefore excluded from the multivariate analysis. It is unknown if such treatment interventions will affect the positive association between MSLN expression and RFS observed in this study. Further investigation using biopsy

specimens and in cohorts with more balanced distributions of adjuvant chemotherapy and other treatment regimens is warranted.

Our study is the first study to examine MSLN expression in an Australian PDAC population via IHC. Interestingly, high MSLN expression, in tumours of an Australian mesothelioma patient cohort, was also associated with improved patient outcomes, marking MSLN as a good prognostic biomarker in mesothelioma (328). In mesothelioma, the epithelioid subtype shows higher MSLN expression and a more favourable prognosis than the less differentiated sarcomatoid and biphasic subtypes (357). Although MSLN was not associated with the histological grade (**Table 3.2**), relationship of MSLN expression with molecular subtypes of PDAC have not been examined in this Australian cohort and requires further investigation. Additionally, multiple proteases in the ADAM, MMP, and BACE families have been known to shed MSLN from cancer cells (128). Tumours with high MSLN expression could potentially be more resistant to antigen shedding, thus enabling greater surface antigen availability for immune surveillance, as MSLN-specific CD4 and CD8 T cells have been detected in the peripheral circulation of PDAC patients (358). Conversely, tumours with low cell-surface MSLN expression and high shedding activity may release elevated levels of soluble MSLN into the circulation, where sustained exposure could contribute to T cell anergy over time (359), potentially leading to poorer prognosis. Notably, MSLN shedding and other post-translational processing such as antigen maturation may result in discrepancies of MSLN expression at the RNA and protein levels, hence explaining the different prognostic outcomes from the IHC and bulk RNA-seq data. Furthermore, the differences in prognosis may also be attributed to the separate cohorts used. Further validation using an independent Australian cohort is needed to determine whether the positive prognostic value of MSLN is reproducible and reflects a generalizable biological phenomenon or is influenced by population-specific genetic and/or environmental factors. The Australian population is racially and ethnically diverse and a comparison with other populations could be of interest.

3.4.2 Associations of MSLN expression with an immunosuppressive PDAC TME

Our finding that MSLN expression is associated with an immunosuppressive microenvironment is consistent with previous RNA-seq analyses (346, 352). In one study, a positive correlation between tumour *MSLN* expression and stromal *CD274* (PD-L1) expression

was found using the deconvoluted ICGC RNA-seq data and validated *in vitro* (352). PD-L1, upon binding to the PD-1 receptor, is known to suppress T cell activating signals and inhibit anti-tumour responses (360). Although our study did not directly examine PD-1/PD-L1 signalling pathways, transcriptomic analyses of both mouse and human RNA-seq datasets revealed that MSLN-high tumours exhibited decreased T cell activation signatures and suppressed tumour reactivity scores. However, in scRNA-seq, even though the MSLN-high group showed an overall decrease of memory phenotypes (CM, EM, and TEMRA) and increase of exhaustion phenotypes (TPEX and EX), the differences were not statistically significant across samples. In addition, no differences were observed in expressions of memory and exhaustion markers on CD8 T cells across the MSLN-high group and MSLN-low groups. One limitation is the variability of CD8 T cell abundances across samples, which could confound the association with MSLN expression, especially since only a small sample size (n=12 per MSLN-high and MSLN-low groups) was examined in the scRNA-seq dataset. As such, these observations remain to be cross-validated from other independent scRNA-seq cohorts, or from RNA-seq data of bulk-sorted CD8 T cell infiltrates from PDAC tumours, where larger sample sizes can be more conveniently obtained. Downregulation of other immune-related pathways (such as leukocyte adhesion, proliferation and chemotaxis) was also observed in this study and suggests that additional immunosuppressive mechanisms could exist in MSLN-high tumours. In particular, we confirmed that expressions of chemokines and chemokine receptors that promote T cell migration and anti-tumour activities were suppressed in CD8 T cells from MSLN-high tumours, whereas expression of the immunosuppressive cytokine, *CXCL5*, was elevated. Furthermore, a reduced proportion of endothelial cells in the *PLVAP+* venous subtype was observed in the scRNA-seq dataset. PLVAP is known to regulate vascular permeability and facilitates leukocyte trafficking (361-363). Thus, decreased abundance of *PLVAP*+ endothelial cells could be linked to reductions in CD8 T cell infiltration as well.

In ovarian cancer, MSLN activates Wnt/β-catenin signalling to induce protumorigenic macrophage polarization via CD24 upregulation (364). While CD24 upregulation has not been observed in our bulk RNA-seq and scRNA-seq data, we did detect the macrophage population of MSLN-high tumours to exhibit an increased polarisation towards the tumorigenic M2 phenotype. MSLN overexpression has been shown to promote autocrine IL-6 signalling in PDAC cells (121); however, its association with cytokine signalling in T cells has not been

specifically investigated. In our scRNA-seq analysis, we observed increased activities of pro-inflammatory cytokine signalling in CD8 T cells from MSLN-high tumours. Notably, this association was not revealed from bulk RNA-seq datasets, where such upregulated cytokine signalling activities may potentially be obscured by reduced infiltration of CD8 T cells. These suggest that high MSLN expression may be linked to broader immunomodulation within the PDAC TME, while the exact biological pathways underlying the observed functional changes in these immune infiltrates remain to be fully characterised.

High *MSLN* expression has been associated with reduced CD8 T cell infiltration in PDAC tumours in two independent human RNA-seq cohorts (TCGA and GSE62452) (346). Cell type compositions and immune activities were inferred based on the xCell algorithm (365). Although cohort-specific variations in multiple immune cell types, such as dendritic cells, were also observed, only CD8 T cells showed a consistent decrease in both RNA-seq cohorts. Suppressed immune responses (in lymphocyte infiltration, T-cell receptor richness, and cytolytic activity scores) were also associated with high *MSLN* expression. Nevertheless, cell type estimates and immune response predictions remain limited from bulk RNA-seq, as *bona fide* immune cell populations cannot be isolated for independent characterization. In the current study, estimates of cell type compositions from human RNA-seq samples demonstrated large discrepancies across the prediction tools used. Consequently, we confirmed CD8 T cell infiltration by scRNA-seq analysis as well as by IHC staining. Convincingly, as determined by scRNA-seq, CD8 T cells were the only immune subset that exhibited a significant reduction in abundance (~4% of total cells per sample) when comparing MSLN-high to MSLN-low tumours. The IHC validation also found a trend toward reduced CD8 T cell stromal infiltration. However, significance was not reached through correlational analysis ($p = 0.272$), likely reflecting the small sample size of this exploratory cohort ($n = 10$). Similarly, assessment of CD8 T cells using the MSLN cutoff defined in **section 3.3.1** (H-score = 62) showed an overall reduction in the MSLN-high group, but did not reach significance, likely due to the very limited number of cases remaining in this group after stratification ($n = 3$). The consistent inverse relationship between MSLN expression and CD8 T cell infiltration observed across multiple datasets warrants histopathological validation in larger independent cohorts in future studies.

It remains to be addressed whether there is a causative effect between MSLN expression and immunosuppression in PDAC. Our analysis on mouse RNA-seq data suggested that there was a lack of association between T cell infiltration status of the implanted tumour clones and tumour *Msln* levels. This suggests that immunosuppressive tumours did not cause upregulations of *Msln* expression. These findings, and whether high MSLN expression induces immunosuppression, remain to be tested in human-based experimental models. MSLN expression and CD8 T cell infiltration may also be specific to PDAC. Analyses in other MSLN-expressing tumours, such as mesothelioma, have interestingly indicated an opposite relationship where high MSLN expression was associated with high CD8 T cell density in TMAs (366). Transcriptomic analysis in ovarian and colorectal cancer also found higher CD8 T cell infiltration and higher T cell inflamed score, respectively, despite an overall positive association with an immunosuppressive tumour landscape (350, 367). Further studies to elucidate the mechanisms for MSLN and immuno-modulation are required, and to confirm whether this is a direct causative effect.

3.4.3 Significance to adoptive T cell therapies

To date, anti-MSLN CAR T cell therapies have failed to achieve favourable clinical efficacy in PDAC. In this study, we uncovered an association between MSLN overexpression and an immunosuppressive TME in PDAC, which may present a currently underappreciated barrier to effective anti-MSLN CAR T cell treatments.

Based on the current findings, the immunosuppressive association of MSLN was mainly linked to a pronounced reduction of CD8 T cell infiltration, which may contribute to poor CAR T cell trafficking into PDAC tumours. To improve CAR T cell trafficking and enhance long-term efficacy, various methods have been assessed. Locoregional delivery (via intrapleural infusion) has enabled efficient trafficking of anti-MSLN CAR T cells in both mesothelioma preclinical models and patients (368, 369). In PDAC, however, locoregional delivery (via intraperitoneal and intra-hepatic artery infusions) resulted in limited intratumoral infiltration of anti-MSLN CAR T cells and did not improve clinical efficacy in a Phase I study (146). Although anti-MSLN CAR T cell trafficking was confirmed after intrahepatic artery infusion, levels of tumour infiltration were lower than reports from other solid tumour clinical trials. The same study also observed low endogenous T cell infiltration and an immunologically cold TME at baseline. These findings were consistent with the associations of MSLN-high PDAC tumours with

immunosuppression and CD8 T cell exclusion described in the current study. We speculate that the lack of improved CAR T cell trafficking in PDAC could be due to underlying biological mechanisms (such as chemokine signalling) that restrict effective tumour homing and infiltration, even when CAR T cells were delivered in close proximity through locoregional injection. In contrast, the positive association between CD8 T cell density and MSLN expression in mesothelioma may foster a TME more conducive to CAR T cell infiltration (366), thereby enabling substantial benefit from intrapleural injection. Direct intratumoural injection can circumvent the need for tumour homing and infiltration. The feasibility of this approach has been demonstrated through endoscopic ultrasound-guided injections of immunotherapies such as allogeneic mixed lymphocyte cultures (MLCs) (370, 371). In one case study, one PDAC patient received 2 doses of intratumoural injections of mRNA-engineered anti-MSLN CAR T cells following 8 doses of intravenous injections (372). Although safety was demonstrated, disease relapsed in this patient after the intratumoural delivery regimens, and a decreased level in CAR T cell infiltration was observed from CAR transcripts detected in tumour biopsy. Whether intratumoural injection can improve therapeutic efficacy by overcoming T cell exclusion and supporting retention of anti-MSLN CAR T cells in PDAC tumours remains to be determined in larger independent cohorts. The feasibility of ultrasound-guided injection of anti-MSLN CAR T cells as a neoadjuvant treatment in PDAC is currently being investigated in an ongoing clinical trial (NCT06054308).

Our transcriptomic analyses also revealed wide suppressions of chemokine and chemokine receptor expressions on CD8 T cells, in addition to overall downregulations in activities associated with leukocyte migration and chemotaxis pathways, from MSLN-high tumours. Enhancing the chemotaxis of CAR T cells represents another approach to improve CAR T cell trafficking. For instance, CXCR6, which was downregulated on CD8 T cells from MSLN-high tumours in the present study, has been co-expressed in anti-MSLN CAR T cells to enhance tumour infiltration in PDAC (373). These CXCR6-transduced CAR T cells efficiently penetrated pancreatic cancer organoids. In subcutaneous and orthotopic PDAC xenograft models, CXCR6-transduced CAR T cells achieved over 90% long-term remission, compared to the 20% and 53% remission rates from control (CXCR6-unmodified) CAR T cells, respectively. In a syngeneic mouse model, increased efficacy of CAR T cells co-expressing CXCR6 was associated with an increased intratumoral accumulation of T cells. The safety and efficacy of CXCR6 co-expression

remains to be clinically examined for future anti-MSLN CAR T cell therapies in PDAC. Co-expression of XCL1, along with IL-7, has also improved anti-tumour efficacy of CAR T cells targeting carcinoembryonic antigen (CEA) in colorectal cancer models (374). The underlying mechanism was found to be XCL1-induced recruitment of highly potent conventional type-I dendritic cells (cDC1s), which subsequently promoted the generation of endogenous tumour-reactive CD8 T cells. This highlights XCL1 co-expression as a potential strategy for enhancing the efficacy of anti-MSLN CAR T cells in PDAC. It is also worth investigating if the same XCL1-based chemokine signalling is responsible for the reduced CD8 T cell infiltration and the downregulated anti-tumour reactivity seen in MSLN-high PDAC tumours.

From scRNA-seq analyses, macrophages in the MSLN-high tumours were polarised towards an immunosuppressive M2 phenotype. The exact relationship between this and the reduced infiltration of CD8 T cells has not been determined from this study, and cross-validations in additional datasets are still needed. Nevertheless, M2-polarised macrophages were known to suppress CAR T cell cytotoxicity (375). Reprogramming macrophages thus represents a potential strategy to enhance the efficacy of anti-MSLN CAR T cells in PDAC. Combination treatment with PD-L1 blockade has been shown to induce a shift in macrophages from M2 to M1 phenotypes and restore CAR T cell cytotoxicity *in vitro*. Similarly, pharmacological inhibition of CSF1R modulated macrophages towards an immunostimulatory phenotype, subsequently enhancing endogenous tumour-reactivity T cell responses and their sensitivity to immune checkpoint inhibitors (376). Additionally, macrophage reprogramming can be targeted through CAR T cell engineering. Co-expression of an inducible IL-12 (iIL-12) in anti-CEA CAR T cells increased infiltration of macrophages that exhibited an activated phenotype, which was responsible for the elimination of antigen-negative tumour cells in a murine model of colon cancer (377). In glioblastoma, TGF-β signalling responsible for M2 macrophage polarisation was inhibited using dual-targeting IL-13Rα2/TGF-β CAR T cells, resulting in reduced infiltration of immunosuppressive macrophages and increased abundance of M1-like microglia (378). Overall, reprogramming macrophages through combination treatments and CAR T cell engineering offers a potential avenue to overcome the immunosuppressive TME of MSLN-high tumours and improve CAR T cell efficacy in PDAC.

Importantly, our TMA data revealed that PDAC patients with low MSLN expression by IHC had poorer prognosis, underscoring the need to optimise treatment strategies for this patient

subset. In contrast to the immunosuppressive TME shown in MSLN-high tumours, MSLN-low tumours were characterised by increased CD8 T cell infiltration and tumour reactivity scores from transcriptomic analyses. These features may favour the successful generation and effectiveness of TIL therapy. In metastatic melanoma, tumours with extensive lymphocyte infiltration ("brisk TILs") had 100% TIL expansion success, whereas tumours with an absence of TILs showed a success rate of 0% (379). In head and neck cancer, percentage of stromal TILs assessed via histological evaluation was significantly associated with successful TIL expansion, as well as the number of expanded TILs per tumour fragment (380). In breast cancer, the number of cultured TILs was also correlated with increased percentage of TILs and TLS formations from histological evaluations (381). Notably, over 85% of tumour samples with at least 10% TILs from initial tumour fragments achieved sufficient yields during pre-REP expansion ($\geq 1.0 \times 10^5$ TILs per fragment within 2 weeks) for proceeding to REP. In our analysis, none of the MSLN-high tumours showed over 10% stromal T cell infiltration (CD3 score ≥ 10) based on histological evaluation, although sample size was limited (n = 3). This may suggest poorer TIL expansion from MSLN-high, as compared to MSLN-low, PDAC tumours. However, the exact association between T cell infiltration and TIL expansion outcomes have not been specifically examined in PDAC. Moreover, current studies have not examined associations of TIL expansion with infiltration of CD8 T cells in particular. It remains to be tested whether the selective enrichment of CD8 T cells in MSLN-low PDAC tumours positions these cases as better candidates for successful TIL expansions.

In PDAC, the percentage of tumour-reactive T cells from expanded TIL cultures has been shown to be as low as less than 1% (382). This highlights the importance of improving tumour reactivity, which is a key determinant of effective TIL therapy (383). In both human and mouse RNA-seq datasets, the MSLN-low tumours showed enriched tumour-reactive CD8 T cell signatures, suggesting potentials for generating TIL products with higher levels of tumour reactivity. A high CD8:CD4 ratio has also been correlated with improved clinical efficacy of TIL therapy (214). In PDAC, CD8 TILs have demonstrated tumour-specific IFN-γ release against HLA-matched tumour cell lines (384). As such, TIL expansion from MSLN-low PDAC tumours might benefit from increased anti-tumour efficacy due to the selective enrichment of tumour infiltrating CD8 T cells. Nevertheless, it should be noted that the TIL composition can shift dramatically during *ex vivo* expansion. Significant reductions in TCR repertoire diversity have

been observed during TIL expansion from PDAC, characterised by the loss of tumour-dominant clones and outgrowth of newly emerged clones from *in vitro* culturing (382). Therefore, the TIL manufacturing process is also crucial in shaping the composition and functional reactivity of the final infusion product, aside from tumour-intrinsic characteristics. Our finding that MSLN-low PDAC tumours possess high CD8 T cell infiltration provides valuable insights for guiding the design and optimisation of TIL manufacturing. Combination with PD-1 blockade and 4-1BB agonist stimulation have substantially improved the expansion of CD8 TILs from PDAC tumours (384). In the case of PD-1 blockade, IFN-γ release against HLA-matched pancreatic tumours was also enhanced. These strategies may be applied to further improve TIL expansion and efficacy for patients with MSLN-low tumours. Additionally, they could be used to determine whether the low abundance and reactivity of CD8 T cells from MSLN-high patients could be rescued.

In summary, this study investigated the clinicopathological and prognostic significance of MSLN expression at the protein level in an Australian PDAC cohort. High MSLN expression, assessed by immunohistochemical evaluation, was associated with improved RFS. A significant association between high MSLN expression and an immunosuppressive landscape was also identified in PDAC based on transcriptomic analyses. This immunosuppression was characterised by reduced anti-tumour reactivity, M2-polarisation in tumour-infiltrating macrophages, and a reduction in tumour-infiltrating CD8 T cells. Immunohistochemical validation also indicated a trend towards reduced stromal infiltration of CD8 T cells in MSLN-high tumours, but requires further confirmation in larger independent cohorts. By elucidating the relationship between MSLN expression and the immune contexture in PDAC, our work provides a foundational understanding of MSLN biology that could inform the development of personalised treatment strategies, such as adoptive T cell therapies, to improve patient outcomes in the future.

CHAPTER 4

Exploring adoptive T cell therapies in appendiceal cancer

4.1 Introduction

Appendiceal cancer is a rare disease with limited therapeutic options. Immunotherapies in appendiceal cancer have been underexplored. In particular, adoptive T cell therapies, such as CAR T cell and TIL therapies, have not, to our knowledge, been examined in appendiceal cancer.

Recent evidence supports the rationale for investigating these adoptive T cell therapies in appendiceal cancer. A previous study detected the tumour-associated antigen, MSLN, was highly expressed in peritoneal metastases of appendiceal cancer (294). Although this was in a small cohort (n = 8), MSLN expression was detected on both the AMN and AA subtypes, with staining intensity and patterns comparable to those observed in peritoneal metastases of colorectal cancer. Appendiceal cancer is also characterised by high mucin production. In a study profiling mucin expression on appendiceal carcinomas, MUC1 expression was detected on 47.2% (51/108) cases, with predominantly membranous staining (296). Since MSLN and MUC1 are highly expressed in appendiceal cancer, they may serve as ideal therapeutic targets for anti-MSLN and anti-MUC1 CAR T cell therapies, which are already in clinical testing for other solid tumours. Furthermore, scRNA-seq analyses have examined T cell populations in appendiceal cancer, with higher abundance of infiltrating T cells observed in the AMN subtype compared to AA (6-8). This provides a basis for the development of TIL therapy, which relies on the successful expansion of infiltrating T cells from tumour specimens.

In this study, we investigated the application of adoptive T cell therapies in appendiceal cancer. We examined the expression of CAR antigens, MSLN and MUC1, in our patient samples and evaluated the efficacy of anti-MSLN CAR T cells on organoids derived from patients with appendiceal cancer. We also demonstrated the feasibility of TIL expansion from patient samples and assessed their reactivity responses induced by superantigen stimulation and against patient-matched organoids. Findings have the potential of laying the groundwork for further development of adoptive T cell therapies as a novel treatment option in this rare disease, where current treatment options are limited.

4.2 Methods

Methodologies used in this chapter have been addressed in the Materials & Methods chapter (sections **2.3.1.2, 2.3.2.2, 2.4, 2.5, 2.6, 2.7, 2.8** and **2.9**).

4.3 Results

4.3.1 MSLN is expressed in appendiceal cancer tissue and tumour-derived organoids

To confirm previous studies, we stained for MSLN via IHC in both AMN and AA samples of appendiceal cancer and detected positive expression in both subtypes (**Figure 4.1A-B**) (294). Cytoplasmic and membranous staining patterns were observed in MSLN staining in both subtypes, whereas acellular spaces, likely representing mucin deposition, remained unstained.

At the transcriptomic level, MSLN was expressed in both AMN and AA samples based on scRNA-seq (**Figure 4.1C-D**). For both subtypes, *MSLN*-positive cells were present in the tumour cell populations. Apart from tumour cells, *MSLN* was also detected in mesothelial cells and fibroblasts (CAFs) in AMN, and mainly in mesothelial cells in AA.

The expression of MSLN was further confirmed using appendiceal cancer organoids. Our group has established four organoids from surgically resected samples of appendiceal cancer peritoneal metastases **(Table 4.1)**. Of the four organoids, one was derived from an AMN patient (PB252), while the remaining three were from AA patients (PB245, PB280, and PB295). MSLN expression at the transcriptomic and protein (cell surface) levels were found in the AMN organoid (PB252) and two of the three AA organoids (PB245 and PB280), whereas expression from the remaining AA organoid (PB295) was negligible **(Figure 4.2A-B).** Soluble MSLN (SMRP) levels from organoid culture media found significantly higher SMRP concentrations in cultures of the MSLN-positive organoids (PB245, PB252, and PB280), compared to the MSLN-negative organoid (PB295) **(Figure 4.2C)**.

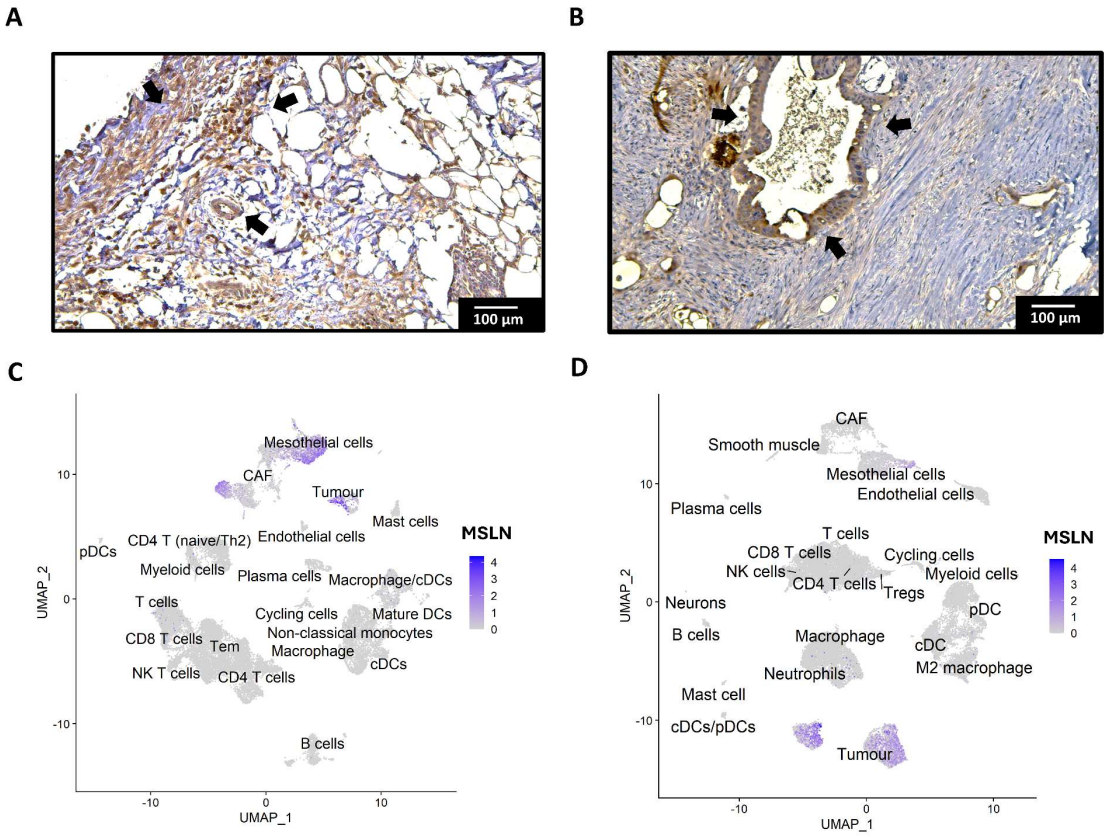

Figure 4.1 Mesothelin (MSLN) is present in appendiceal tumour tissues. Immunohistochemical staining revealed MSLN expression in tissue sections of surgically resected appendiceal tumours of appendiceal mucinous neoplasm (AMN) **(A)** and appendiceal adenocarcinoma (AA) **(B)** subtypes. Positive MSLN expression was indicated by the black arrows. Scale bars were as indicated. Single-cell RNA-sequencing analysis showed *MSLN* expression in both AMN **(C)** and AA **(D)** subtypes of appendiceal tumours. Cells were pooled from three patient samples for each subtype.

Table 4.1 Clinicopathological features of patient-derived organoids

Identifier	Patient sex	Patient age	Tumour stage	Disease subtype
PB245	Female	27	T4N0	AA (goblet cell adenocarcinoma)
PB252	Male	44	TisN0	AMN (low-grade appendiceal mucinous neoplasm)
PB280	Female	70	T4N0	AA (signet ring cell adenocarcinoma)
PB295	Male	67	T4N1	AA (mucinous adenocarcinoma)

Tis, tumour *in situ*; AA, appendiceal adenocarcinoma; AMN, appendiceal mucinous neoplasm.

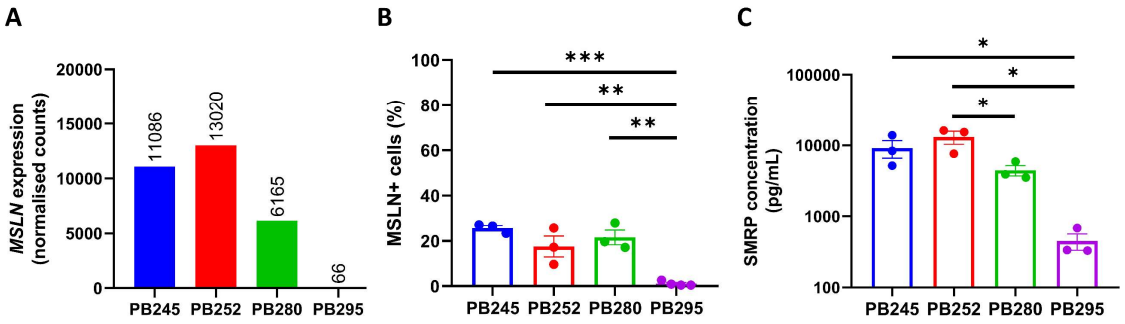

Figure 4.2 Mesothelin (MSLN) was found on three of the four appendiceal cancer organoids tested. (A) *MSLN* expression from RNA-sequencing analysis of appendiceal cancer organoids. Normalised counts were quantified via DESeq2. **(B)** Percentage of organoid cells with positive MSLN expression, evaluated by flow cytometry. **(C)** Soluble mesothelin-related peptide (SMRP) concentration (on $\log_{10}$-scale) from supernatant of organoid cultures, analysed using ELISA. Data from **(B, C)** are presented as mean ± SEM from at least three independent experiments. Statistical testing was performed by one-way ANOVA followed by Turkey's post hoc test for multiple comparisons, with significance indicated (*p < 0.05; **p < 0.01; ***p < 0.001).

4.3.2 Anti-MSLN CAR T cells show cytotoxicity and cytokine secretion against MSLN-positive organoid-derived monolayer cells

Effectiveness of CAR T cell therapy was evaluated on the three MSLN-positive organoids (PB245, PB252, and PB280), which were seeded as monolayer cells, using the xCELLigence RTCA assay and IFN-γ ELISA analysis.

For all three organoids, both anti-MSLN (SS1 and P4) CAR T cells significantly reduced cancer cell viability compared to anti-PSMA (J591) CAR T cells, which were used as the negative control since all appendiceal cancer organoids in the current study lacked *PSMA* expression (**Figure 4.3A-C; Supplementary Figure 3A**). Notably, both SS1 and P4 CAR T cells demonstrated complete cell killing of PB252 and PB280 organoids. For the PB245 organoid, cancer cell viability increased again from 48 hours to 72 hours in co-cultures with P4 CAR T cells, indicating organoid regrowth, but not in co-cultures with SS1 CAR T cells. However, difference in viability did not reach statistical significance at the 72-hour endpoint (mean ± SEM: 36.7% ± 9.2% vs 75.2% ± 13.0%, p = 0.150). No other statistically significant differences in cancer cell viability were observed in SS1 and P4 CAR T cell treatments at 24-hour, 48-hour, and 72-hour timepoints during each organoid co-culture.

ELISA analysis at the endpoint of cytotoxicity assays showed substantially higher IFN-γ concentrations from co-cultures of organoid-derived monolayers with SS1 and P4 CAR T cells, compared with J591 CAR T cells (**Figure 4.4**). Between P4 and SS1 CAR T cells, IFN-γ secretion was comparable in response to PB280 organoid (mean ± SEM: 2461.0 ± 14.0 pg/mL vs 1859.0 ± 294.4 pg/mL, p = 0.319), but significantly higher for P4 CAR T cells against PB245 (mean ± SEM: 7877.0 ± 241.6 pg/mL vs 899.1 ± 517.6 pg/mL, p = 0.003) and PB252 (mean ± SEM: 7754.0 ± 196.1 pg/mL vs 4542 ± 489.4 pg/mL, p = 0.032) organoids.

To our knowledge, this is the first evidence to show the efficacy of CAR T cells in appendiceal cancer. Responses of anti-MSLN CAR T cells on the MSLN-negative organoid (PB295) have not yet been evaluated and remain to be examined in future experiments.

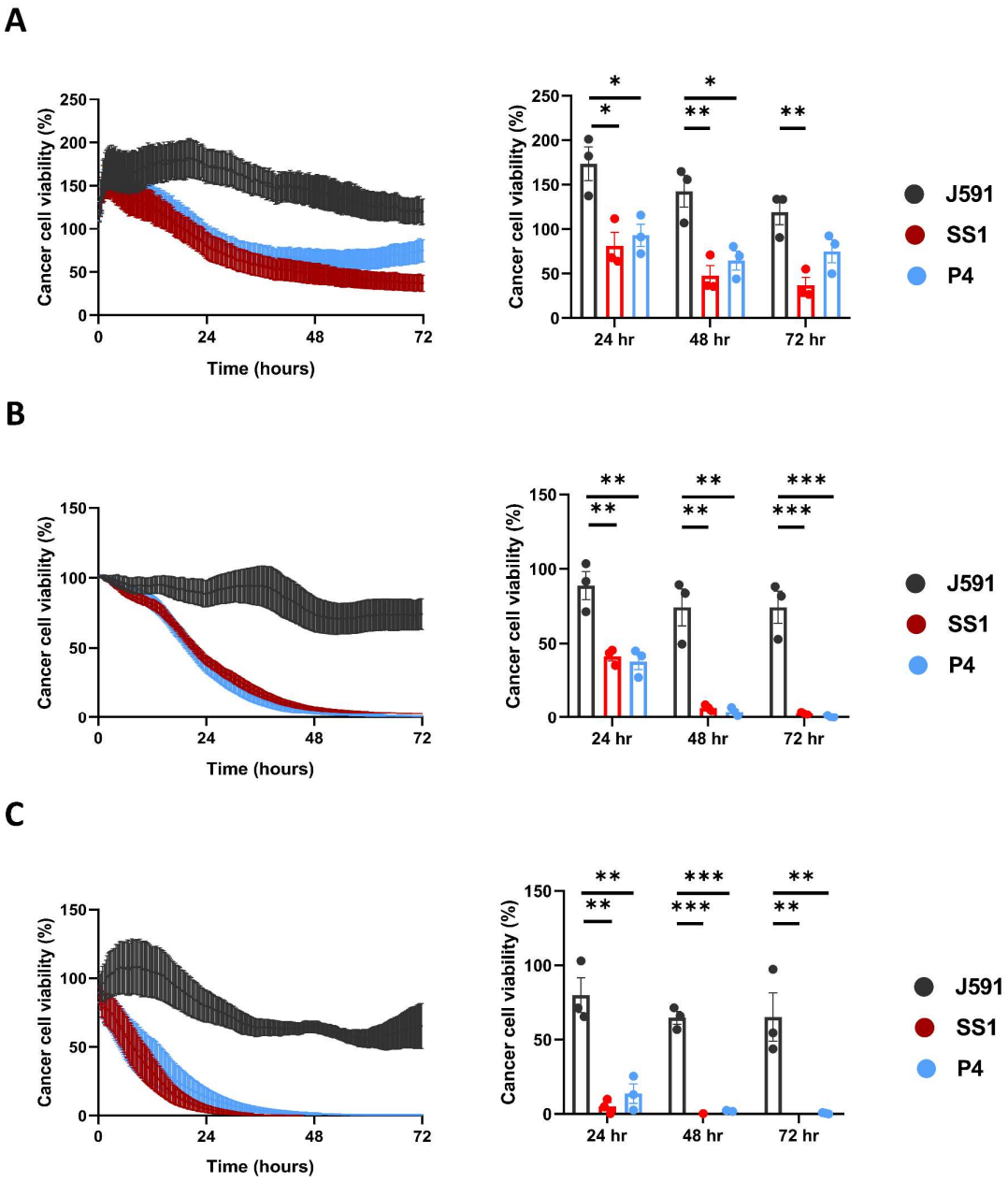

Figure 4.3 SS1 and P4 chimeric antigen receptor (CAR) T cells elicit effective killing responses against mesothelin (MSLN)-positive appendiceal cancer organoid-derived monolayer cells. Cancer cell viability was evaluated from CAR T cell co-cultures with **(A)** PB245, **(B)** PB252, and **(C)** PB280 organoid cells seeded as monolayers, using the xCELLigence real-time cell analysis (RTCA) platform. For each co-culture, viability throughout the time course (left) and at 24, 48, and 72-hour timepoints (right) were shown. Data are presented as mean ± SEM using CAR T cells derived from three independent donors. Statistical testing was performed via repeated measures one-way ANOVA (matched based on CAR T cell donors) followed by Turkey's post hoc test for multiple comparisons, with significance indicated (*p < 0.05; **p < 0.01; ***p < 0.001).

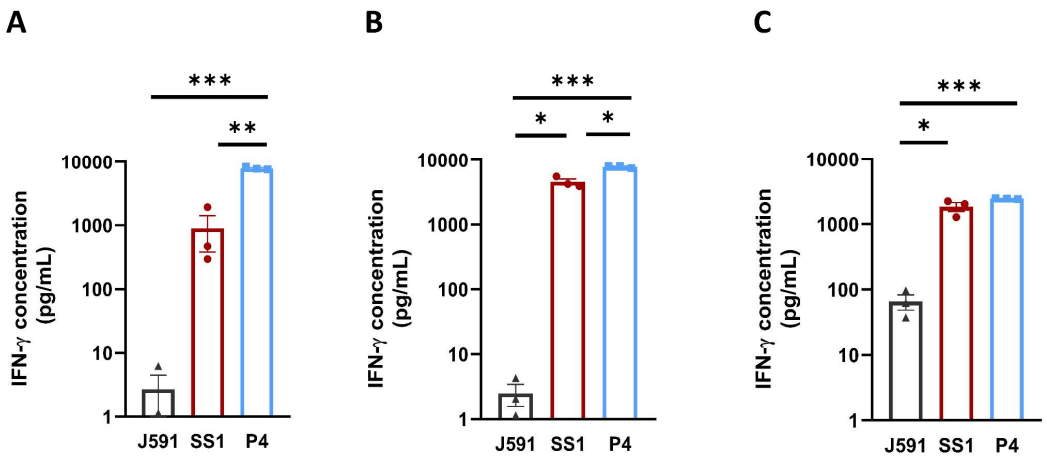

Figure 4.4 SS1 and P4 chimeric antigen receptor (CAR) T cells exhibit high interferon-γ (IFN-γ) release in co-culture with mesothelin (MSLN)-positive appendiceal cancer organoid-derived monolayer cells. IFN-γ concentration (on log_{10}-scale) was measured via ELISA from supernatant of CAR T cell co-cultures with **(A)** PB245, **(B)** PB252, and **(C)** PB280 organoids seeded as monolayers, at the 72-hour endpoint of the xCELLigence cytotoxicity assay. Data are present as mean ± SEM using CAR T cells derived from three independent donors. Statistical testing was performed via repeated measures one-way ANOVA (matched based on CAR T cell donors) followed by Turkey's post hoc test for multiple comparisons, with significance indicated (*p < 0.05; **p < 0.01; ***p < 0.001).

4.3.3 MUC1 is highly expressed in appendiceal cancer

MUC1 expression was assessed due to its potential as a CAR T cell target. scRNA-seq analysis revealed *MUC1* expression in both AMN and AA tissues (**Figure 4.5A-B**). Comparative analysis was conducted between tumour antigens MSLN and MUC1 to evaluate the specificity and level of RNA expression. In both AMN and AA, *MUC1* expression was significantly higher than *MSLN* in the tumour cell populations (**Figure 4.5C-D**). Additionally, *MUC1* showed lower expression than *MSLN* in mesothelial cells, which accounted for 8.3% and 6.8% of total cells in AMN and AA, respectively. In AA, high *MUC1* expression was also detected in a small population of neurons, representing 0.1% of the total cell population.

MUC1 expression was further evaluated on the four appendiceal cancer organoids previously established. PB245, PB252, and PB280 organoids showed positive MUC1 expression at the transcriptomic and cell surface protein level, whereas expression in the PB295 organoid was negligible **(Figure 4.6A-B)**. Interestingly, these MUC1-positive organoids also showed positive

MSLN expression, as indicated previously in **section 4.3.1**. Among the MUC1-positive organoids, MUC1 expression was significantly lower on the PB245 organoid compared to PB252 and PB280 organoids.

As clinically tested anti-MUC1 CAR T cell therapies recognise the aberrant glycoforms of MUC1 during tumour development, we assessed the expression of tumour-specific MUC1 glycoforms (Tn/sTn) using an antibody with the 5E5 antigen binding domain. In all three MUC1-positive organoids, Tn/sTn glycoforms were detected but at lower levels than their overall MUC1 expression (mean ± SEM; PB245: 4.5% ± 0.9% vs 4.7% ± 1.5%; PB252: 37.9% ± 6.6% vs 69.3% ± 12.2%; PB280: 21.9 ± 1.8 vs 79.4% ± 9.5%) (**Figure 4.6B-C**). PB252 and PB280 organoids again showed significantly higher expression than the PB245 organoid. Expression of the Tn/sTn glycoforms remained non-detectable on the MUC1-negative PB295 organoid.

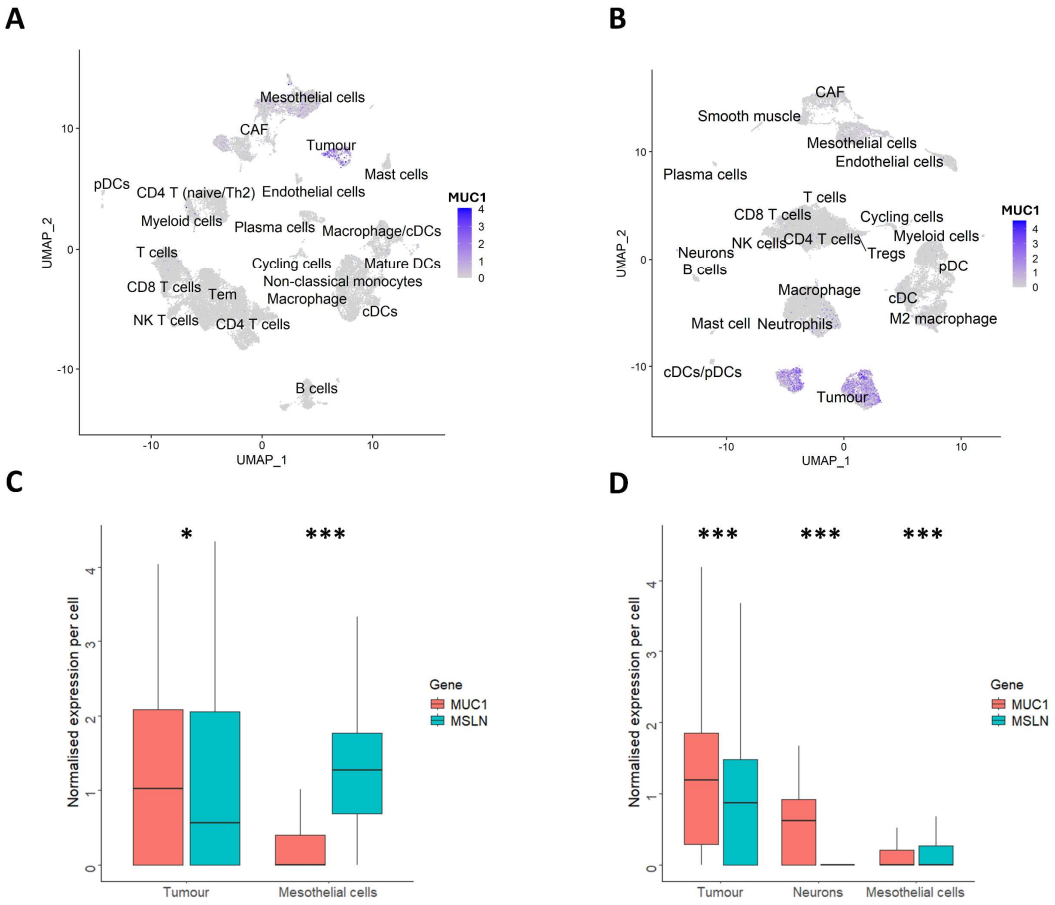

Figure 4.5 Mucin-1 (MUC1) shows high tumour cell expression in appendiceal tumour tissues as determined by single-cell RNA-sequencing. Distribution of *MUC1* expression in both subtypes of appendiceal cancer – appendiceal mucinous neoplasm (AMN) **(A)** and appendiceal adenocarcinoma (AA) **(B)** was shown. Data for each subtype were derived from cells pooled across three patient samples. Tumour antigen specificity analysis was performed for AMN **(C)** and AA **(D)**. *MUC1* expression across each cell type was compared with another tumour antigen, mesothelin (*MSLN*). Outliers and cell types with no expression of *MUC1* and *MSLN* based on interquartile range (IQR) were excluded from the visualisations. Normalised expressions were quantified via Seurat. Statistical testing was performed via paired t-test (matched based on patient sample) for each cell type, with significance indicated (*p < 0.05; **p < 0.01; ***p < 0.001).

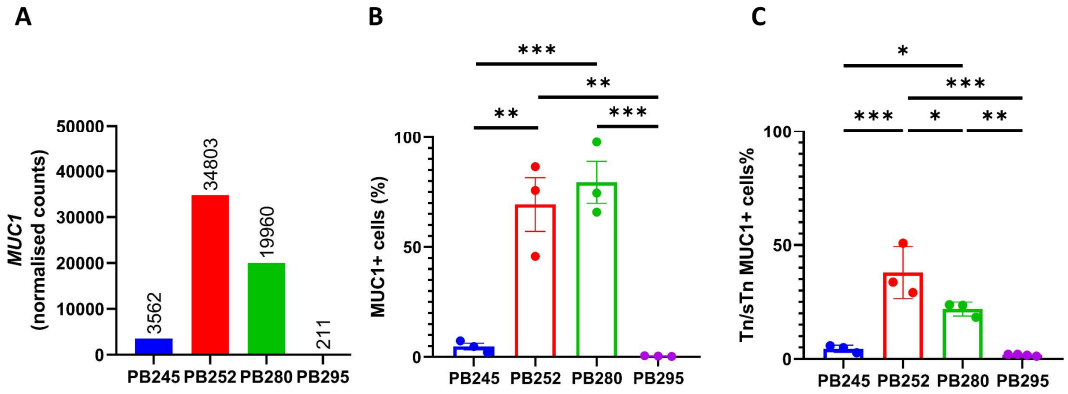

Figure 4.6 Mucin-1 (MUC1) and its tumour-specific (Tn/sTn) glycoforms are present on appendiceal cancer organoids. (A) *MUC1* expression in appendiceal cancer organoids, quantified as DESeq2 normalised counts from RNA-sequencing analysis. **(B)** Percentage of MUC1+ organoid cells evaluated via flow cytometry. **(C)** Percentage of organoid cells positive for tumour-specific MUC1 glycoforms, evaluated by the anti-Tn/sTn antibody (clone: 5E5), via flow cytometry. Data from **(B, C)** are presented as mean ± SEM from three or more independent experiments. Statistical testing was performed by one-way ANOVA followed by Turkey's post hoc test for multiple comparisons, with significance indicated (*p < 0.05; **p < 0.01; ***p < 0.001).

4.3.4 Expanded TILs from appendiceal tumours had high CD3 purity

The feasibility of TIL therapy has not been explored in appendiceal cancer. To address this, we established a pipeline for TIL expansion from appendiceal tumours (**Figure 2.2**), based on the pre-REP process used in clinical TIL manufacturing. Samples were obtained from surgical resection of peritoneal metastatic samples, and TIL expansion was performed either on fresh or cryopreserved specimens. A summary of all 11 TIL expansions from appendiceal tumour specimens is shown in **Table 4.2**.

Out of the 11 tumour samples, 8 had successful TIL expansion (achieving a threshold of 15 million cells within 15 – 30 days of culturing) (**Figure 4.7**). There was no difference in the success rate of TIL expansion between AMN and AA subtypes (**Table 4.3**). 100% (3/3) of the samples that failed TIL expansion were from cryopreserved samples. The possible reasons for failed TIL expansion include: additional freeze-thawing after tumour processing (PB249); low cell viability after tumour processing (PB295); and small tumour sample resulting in low cellular yield (PB317) (**Table 4.2**). The median yield and duration of successful TIL expansions were 23 million cells and 18.5 days, respectively (**Table 4.3**). Notably, 80 million TILs were harvested from one AMN sample (PB315) within 15 days of culture.

Compared to cryopreserved tumour samples, fresh tissue samples yielded faster expansion of TILs (**Figure 4.8A**). All TILs expanded from fresh tissues were harvested on day 15 of culture, at which time they exhibited significantly higher fold expansion than TILs expanded from cryopreserved tissues (mean ± SEM: 40.3 ± 11.4 vs 5.3 ± 2.1, p = 0.006) (**Figure 4.8B**). Additionally, TIL cultures processed from fresh tissues trended to increased viability on day 1 compared to those from cryopreserved tissues, although the difference was not statistically significant (mean ± SEM: 90.1% ± 2.6% vs 54.4% ± 12.0%, p = 0.057) (**Figure 4.8C**).

At the time of harvest, successfully expanded TILs were phenotyped with all samples exhibiting over 95% CD3 positivity, demonstrating high purity of T cells (**Figure 4.9A**). No difference was shown between the CD3 positivity of TILs expanded from AMN and AA samples (mean ± SEM: 98.9% ± 0.1% vs 98.0% ± 0.6%, p = 0.309). Between day 1 and on the day of harvest, no difference was observed in the CD4:CD8 ratio of expanded TILs (mean ± SEM: 2.2 ± 0.5 vs 2.3 ± 0.9, p = 0.935) (**Figure 4.9B**). However, when examining expanded TIL samples individually, noticeable shifts in the CD4:CD8 ratio were observed in some samples, with PB319 TIL exhibiting a dramatic increase (2.9 to 8.3) and PB245 TIL showing a substantial decrease (6.0 to 1.8).

Table 4.2 Appendiceal tumour samples tested for TIL expansion

Identifier	Subtype	Preservation (fresh/cryo-preserved)	Successful expansion?	Comments
PB245	AA	Cryopreserved	Yes	36 million cells harvested on day 22
PB249	AMN	Cryopreserved	No	Additional cryopreservation after tumour processing
PB252	AMN	Cryopreserved	Yes	25 million cells harvested on day 25
PB270	AA	Cryopreserved	Yes	15 million cells harvested on day 22
PB280	AA	Cryopreserved	Yes	21 million cells harvested on day 29
PB295	AA	Cryopreserved	No	Substantial amount of dead cells and debris after tumour processing
PB315	AMN	Fresh	Yes	80 million cells harvested on day 15
PB316	AMN	Fresh	Yes	15 million cells harvested on day 15
PB317	AA	Cryopreserved	No	Low cell number (<0.1 million) on day 1
PB319	AA	Fresh	Yes	16 million cells harvested on day 15
PB324	AA	Fresh	Yes	25 million cells harvested on day 15

TIL, tumour infiltrating lymphocyte; AMN, appendiceal mucinous neoplasm; AA, appendiceal adenocarcinoma

Table 4.3 Summary of TIL expansion parameters

Parameter	Total (*n*=11)	AMN (*n*=4)	AA (*n*=7)	P-value
Preservation, *n* (%)				
Fresh	4 (36.4)	2 (50.0)	2 (28.6)	0.576
Cryopreserved	7 (63.6)	2 (50.0)	5 (71.4)	
Expansion outcome, *n* (%)				
Successful	8 (72.7)	3 (75.0)	5 (71.4)	0.999

Unsuccessful	3 (27.3)	1 (25.0)	2 (28.6)	
Duration of successful expansion (days), median (range)				
	18.5 (15 - 29)	15 (15-25)	22 (15 – 29)	0.821
Yield of successful expansion (days), median (range)				
	23 (15-80)	25 (15-80)	21 (15 – 36)	0.714

TIL, tumour infiltrating lymphocyte; AMN, appendiceal mucinous neoplasm; AA, appendiceal adenocarcinoma

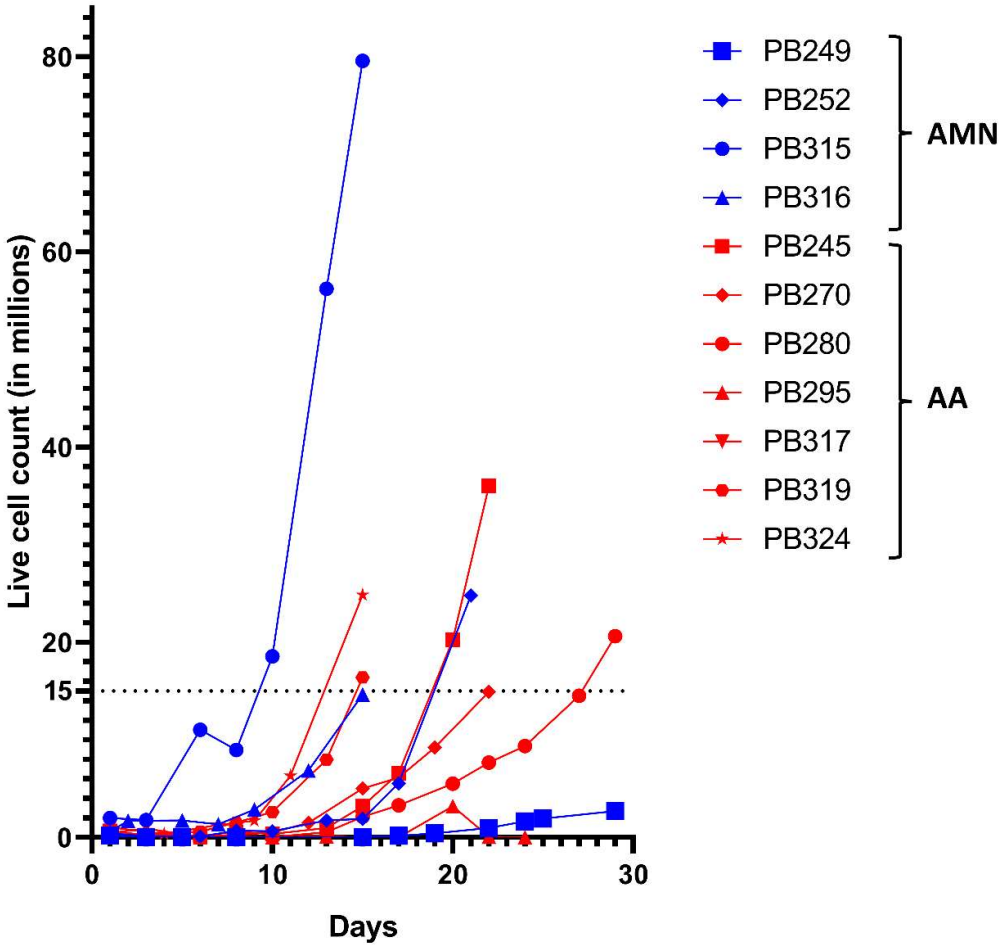

Figure 4.7 Tumour infiltrating lymphocytes (TILs) can be expanded from surgically resected appendiceal peritoneal metastases. Live cell count was monitored during TIL expansion and shown for each tested tumour sample. Samples were derived from the appendiceal mucinous neoplasm (AMN; blue) or appendiceal adenocarcinoma (AA; red) subtypes, as indicated. Successful expansion was defined as achieving at least 15 million live cells (dashed line) within 15 – 30 days of expansion.

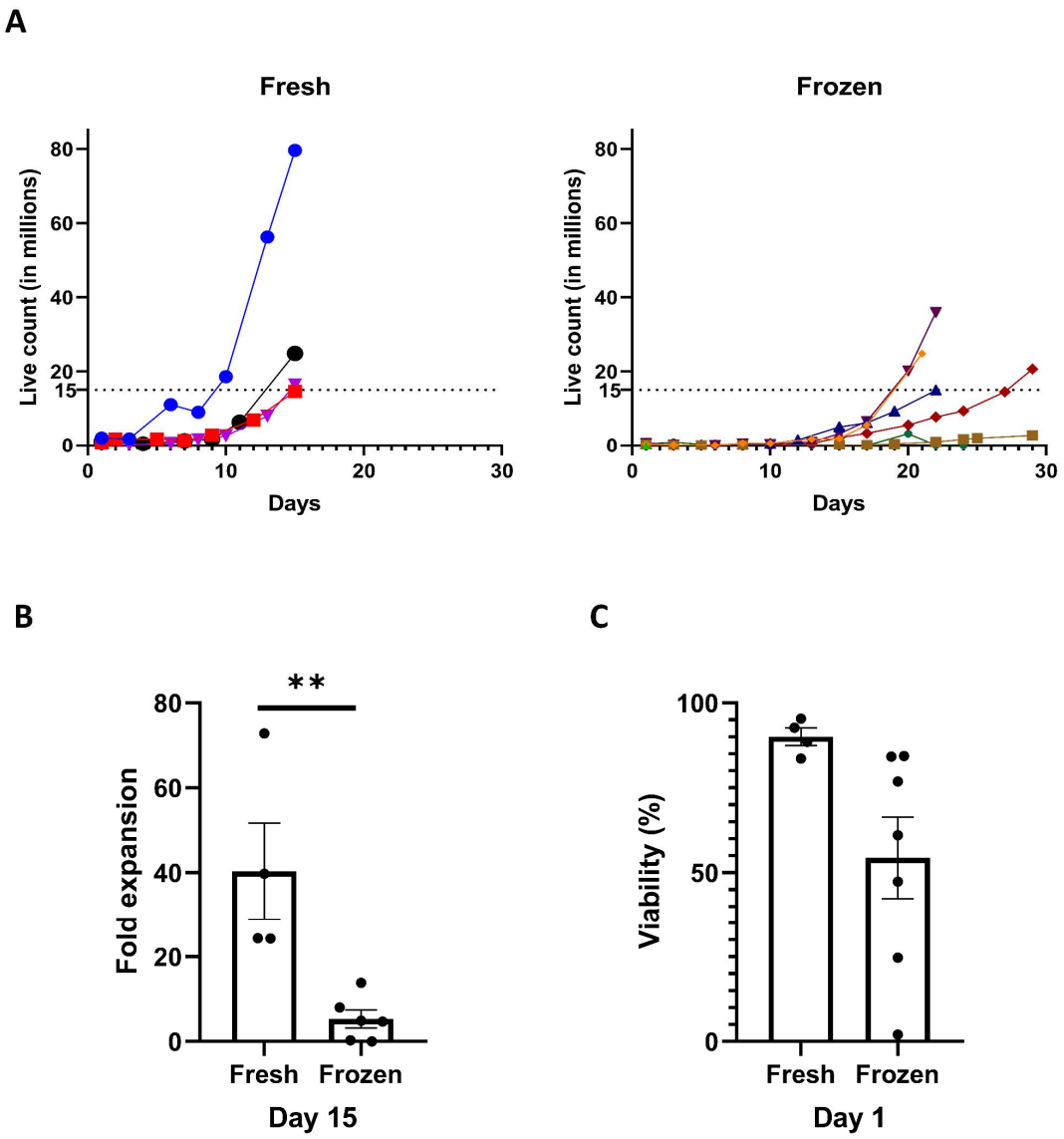

Figure 4.8 Fresh tissues show faster tumour-infiltrating lymphocyte (TIL) expansion and increased viability compared to cryopreserved tissues. (A) Live cell count of TIL expansion from fresh (left) and cryopreserved (right) tumour samples. Threshold for harvesting (dashed line) was indicated. Individual TIL samples were represented by different coloured symbols, as indicated. **(B)** Fold expansion of TIL samples on day 15 relative to day 1, based on ratio of live cell count. **(C)** Viability of TIL cultures on day 1 following tumour processing. Data in **(B, C)** are presented as mean ± SEM. Statistical analysis was performed using unpaired t-tests in **(B, C)**, with significance indicated (**p< 0.01).

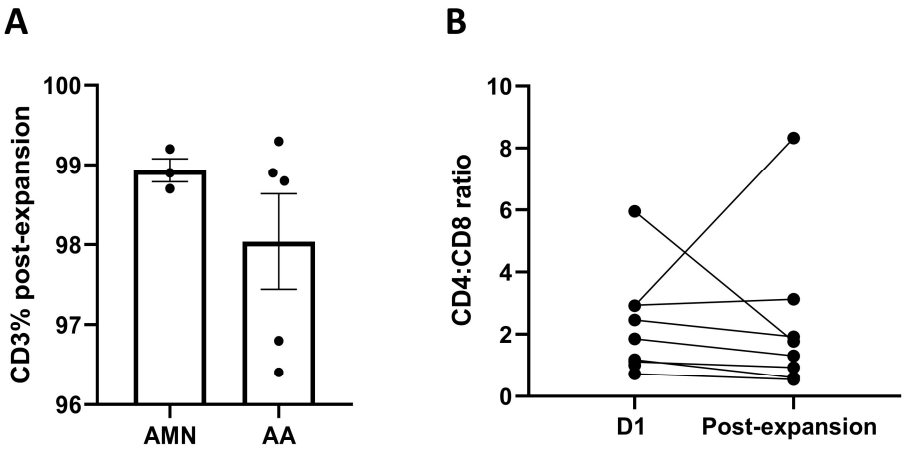

Figure 4.9 Expanded tumour infiltrating lymphocytes (TILs) show high CD3 purity and no consistent changes in CD4:CD8 ratios. (A) Percentage of T cells (CD3+) in TILs expanded from appendiceal mucinous neoplasm (AMN) and appendiceal adenocarcinoma (AA), assessed by flow cytometry. **(B)** CD4:CD8 ratios (CD3+ CD4+ CD8-/CD3+ CD4- CD8+) of expanded TILs, evaluated by flow cytometry on day 1 and at the time of harvest (post-expansion). Data in **(A)** are shown as mean ± SEM. Statistical testing was performed via unpaired t-tests in **(A)** and paired t-tests in **(B)**. Non-significance ($p > 0.05$) is not shown.

4.3.5 Superantigen stimulation induces upregulated functional responses from TILs

To assess functional responsiveness, a selection of the expanded TILs (PB245 TIL, PB252 TIL, and PB280 TIL) with matched (autologous) tumour organoids available were stimulated by SEB, a superantigen that activates T cells irrespective of antigen specificity (385). SEB stimulation induced significant upregulations of reactivity markers (4-1BB and OX40) and the degranulation marker CD107a in T cell subsets from PB245 and PB280 TIL samples (**Figure 4.10A, C**). For PB252 TIL, expression of reactivity and degranulation markers showed an increased trend upon SEB stimulation, although the difference was not shown to be statistically significant, likely due to inconsistencies across experimental repeats.

To study responses of cytokine secretion, IFN-γ release from the three expanded TILs was detected via ELISA after SEB stimulation. IFN-γ secretion was significantly increased after SEB stimulation in PB252 TIL (mean ± SEM: 2615.0 ± 426.5 pg/mL vs 229.5 ± 63.6 pg/mL, $p = 0.036$) (**Figure 4.11**). Upregulated production of IFN-γ was also observed from SEB-stimulated PB245 (mean ± SEM: 2838.0 ± 978.1 pg/mL vs 360.2 ± 122.0 pg/mL, $p = 0.105$) and PB280 (mean ±

SEM: 1738.0 ± 327.8 pg/mL vs 104.7 ± 101.8 pg/mL, p = 0.088) TIL samples, although the differences did not reach statistical significance.

The overall increase in 4-1BB, OX40, and CD107a expression, as well as IFN-γ release upon stimulation indicates that expanded TILs tested were functionally responsive.

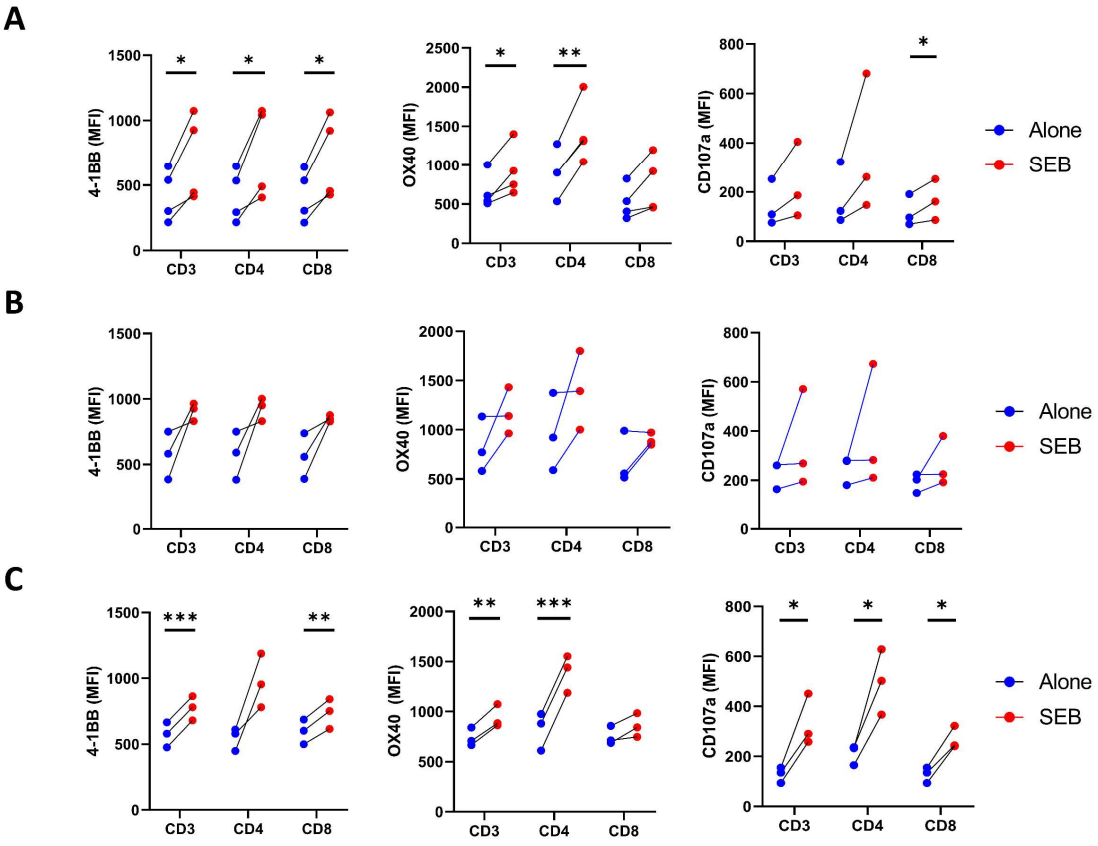

Figure 4.10 Tumour infiltrating lymphocytes (TILs) upregulate reactivity and degranulation markers upon superantigen stimulation. Expression of reactivity markers 4-1BB (left), OX40 (middle), and degranulation marker CD107a (right) for **(A)** PB245 TIL, **(B)** PB252 TIL, and **(C)** PB280 TIL, with or without stimulation by Staphylococcal enterotoxin B (SEB). Expression was evaluated as median fluorescent intensity (MFI) in T cell subsets from flow cytometry. Data represents three or more independent experiments. Statistical testing was performed using paired t-tests, with significance indicated (*p < 0.05; **p < 0.01; ***p < 0.001).

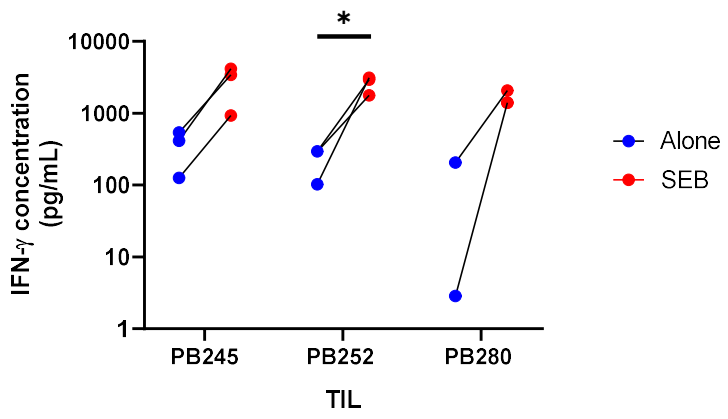

Figure 4.11 Tumour infiltrating lymphocytes (TILs) increase interferon-γ (IFN-γ) release upon superantigen stimulation. IFN-γ concentration (on log_{10}-scale) was analysed via ELISA from supernatant of TIL culture with or without stimulation by Staphylococcal enterotoxin B (SEB). Data represents two or more independent experiments. Statistical testing was performed using paired t-tests, with significance indicated (*$p < 0.05$).

4.3.6 Expanded TILs do not demonstrate consistent evidence of responses against dissociated autologous tumour organoids

To examine anti-tumour responses, the same TIL selection (PB245 TIL, PB252 TIL, and PB280 TIL) were co-cultured with dissociated, patient-matched tumour organoids. Cytotoxic killing of TILs was assessed via a flow cytometry-based quantification assay, where cancer cell viability was evaluated based on the number of live tumour cells relative to the number of counting beads recorded (**Figure 4.12A**). Co-cultures of PB245 TILs with matched organoid led to a slight but significant reduction in cancer cell viability (mean ± SEM: 0.428 ± 0.113 cells per bead vs 0.466 ± 0.119 cells per bead, $p = 0.040$). A slight significant increase in cancer cell viability was observed in co-cultures of PB252 TILs with matched organoid (mean ± SEM: 0.453 ± 0.144 cells per bead vs 0.278 ± 0.133 cells per bead, $p = 0.034$), and no difference was observed in co-cultures of PB280 TILs with matched organoid (mean ± SEM: 0.336 ± 0.070 cells per bead vs 0.366 ± 0.052 cells per bead, $p = 0.293$).

To complement the cytotoxicity results, IFN-γ release was examined in TILs co-cultured with dissociated, patient-matched organoids. TILs co-cultured with matched organoids did not show significant changes in IFN-γ release, compared to TILs cultured alone **(Figure 4.12B)**. Similarly, when reactivity markers were examined, no significant changes in 4-1BB and OX40

expressions were shown from all three TILs (PB245, PB252, and PB280) co-cultured with their matched organoids, when compared to TILs cultured alone (**Figure 4.13A-C**). In conclusion, the expanded TILs tested did not exhibit consistent evidence of anti-tumour functional responses.

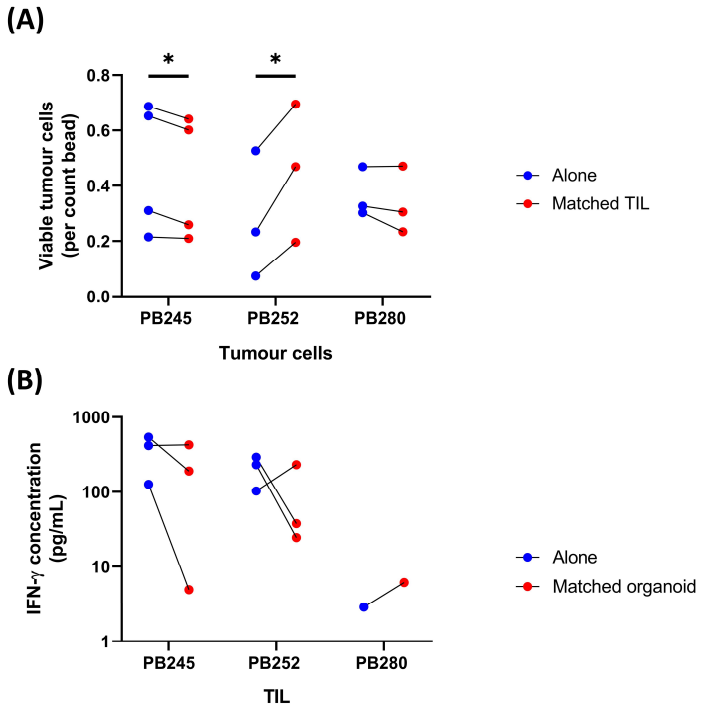

Figure 4.12 Tumour infiltrating lymphocytes (TILs) did not exhibit consistent evidence of functional responses against dissociated matched tumour organoids. (A) TIL cytotoxicity was assessed using a flow cytometry-based killing quantification assay. Viability of dissociate tumour organoid cells alone or in co-culture with matched TILs was evaluated based on number of live tumour cells relative to the number of counting beads recorded. **(B)** Interferon-γ (IFN-γ) concentration (on $\log_{10}$-scale) was assessed via ELISA from culture supernatant of TILs in the absence or presence of matched tumour organoids. Data represents one to four independent experiments. Statistical testing was performed using paired t-tests, with significance indicated (*$p < 0.05$).

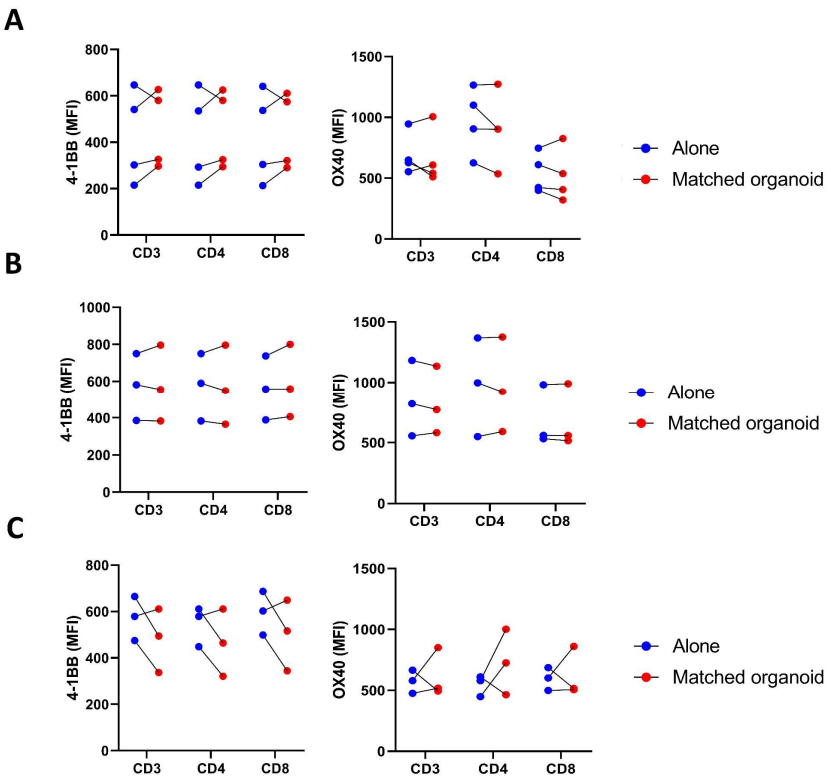

Figure 4.13 Tumour infiltrating lymphocytes (TILs) did not upregulate reactivity markers when co-cultured with dissociated matched tumour organoids. Expression of reactivity markers 4-1BB (left) and OX40 (right) for **(A)** PB245 TIL, **(B)** PB252 TIL, and **(C)** PB280 TIL, in the absence or presence of dissociated, patient-matched tumour organoids. Marker expression was evaluated via flow cytometry as median fluorescent intensity (MFI) on T cell subsets. Data represents three or more independent experiments. Statistical testing was performed using paired t-tests and non-significance ($p > 0.05$) is not shown.

4.4 Discussion

Due to the rarity of the disease, therapeutic options for appendiceal cancer remain limited, particularly for patients who are ineligible or failed to benefit from the current standard-of-care treatment of CRS with HIPEC. As adoptive T cell therapies have not been explored in appendiceal cancer, this chapter investigated the potential applications of CAR T cell and TIL therapies for future appendiceal cancer treatments. Our findings demonstrate that appendiceal cancer expresses the tumour antigens MSLN and MUC1, and anti-MSLN CAR T cells showed effective killing responses against appendiceal tumour organoids. Successful expansion of TILs from appendiceal tumour specimens was also established. TIL samples post-

expansion responded to SEB stimulation, although there was no consistent evidence of responses against autologous tumour cells.

4.4.1 Translation of CAR T cell therapy

In our study, MSLN was detected in both AMN and AA subtypes of appendiceal cancer. Positive MSLN staining from peritoneal metastases of AA and AMN reported from a previous study was concordantly observed in our samples (294). Expression of MSLN at the transcriptomic level from mesothelial cells, which forms the peritoneal lining, was also consistent with the physiological expression in this cell type (386). On-tumour MSLN expression was confirmed in 3 out of 4 (75%) organoids, with the detection of SMRP indicative of an underlying shedding process that has been previously described in other cancer types (128). Nevertheless, due to the limited number of samples, direct comparisons of MSLN expression between AMN and AA subtypes, as well as the overall prevalence of this antigen in appendiceal cancer patients were unable to be examined. To address this, core biopsies can be taken from appendiceal cancer cohorts to construct TMAs for IHC staining. MSLN staining can be evaluated using H-scores to inform stratification of patient populations and their suitability for potential anti-MSLN immunotherapies in the future.

The two clinically tested anti-MSLN CAR T cell therapies, SS1 and P4 CAR T cells, were both effective against MSLN-positive appendiceal cancer organoids *in vitro*, with complete tumour eradication observed in 2 out of 3 organoid models seeded as monolayers. High IFN-γ secretion (> 500 pg/mL) was also observed for both SS1 and P4 CAR T cells. IFN-γ has been shown to enhance solid tumour lysis through alternative signalling via the IFN-γ receptor (IFNγR) pathway (72), independent of direct CAR-mediated cytotoxicity. The substantial IFN-γ release could have contributed to the observed effective killing responses, although IFNγR expression remains to be confirmed on these organoid models.

Functional evaluations of SS1 and P4 CAR T cells have not been compared in parallel. Both SS1 and P4 antigen binding domains have similar affinities (K_d: 0.72 nM vs 1-10 nM, respectively) (126, 387). However, previous studies have shown that the functional responses of SS1, but not P4, CAR T cells were inhibited by MSLN shedding via binding of SMRP to the CAR construct, which decreases the availability of CAR for on-tumour target recognition (126, 136). In the current study, although shed MSLN (SMRP) was detected in our organoid models, SS1 and P4

CAR T cells showed similar cytotoxic responses against appendiceal cancer organoids. The lack of substantial SS1 CAR T cell inhibition by MSLN shedding could be because SMRP concentrations present in current organoid cultures were much lower (in the range of 1 – 10 ng/mL based on ELISA assays) compared to the physiological concentrations (0.3 – 10 ug/mL) used to achieve 50% reductions in SS1 CAR T cell cytotoxicity from previous literature (136). Additionally, P4 CAR T cells showed higher IFN-γ secretion, particularly in co-cultures with the PB245 organoid, compared to SS1 CAR T cells. Previous reports suggest that cytokine secretion by P4 CAR T cells was unaffected by SMRP at both low (25 ng/mL) and physiological (5 ug/mL) levels (126). A higher threshold of CAR molecule engagement with antigen (~10 fold more) on tumour surface is required for cytokine release compared to cytotoxicity (388, 389). It is possible that IFN-γ release can be downregulated in SS1 CAR T cells if SMRP binding sufficiently reduced CAR availability for cytokine secretion but not cytotoxicity. The exact effect of SMRP on SS1 CAR T cell cytokine secretion has not been tested and remain to be examined in future experiments.

In vivo models of appendiceal cancer would be essential for confirming the *in vitro* efficacy of SS1 and P4 CAR T cells. Stromal components cannot be preserved in organoid models, but can be partially recapitulated using mouse xenograft models. Several studies have established xenograft models of AMN and AA using patient-derived tumour fragments or organoids (390-394). Xenografts were implanted either subcutaneously or intraperitoneally (via a midline laparotomy), with intraperitoneal implantation showing higher establishment success, growth rate, and metastatic potential. These models retained the histopathological and molecular features of parental tumours, including production of mucinous ascites, oncogenic mutations, expression of tumour markers, and therapeutic resistance. Previously, SS1 CAR T cells demonstrated poor tumour infiltration and replication within tumours from xenograft models of pancreatic and ovarian cancers (147). Lack of tumour control was attributed to significant binding of SS1 CAR T cells to SMRP present at very high concentrations in the ascites fluid (in the ug/mL range). Given the extensive peritoneal metastases, a similar issue could be present in appendiceal cancer, although SMRP concentrations in ascitic fluid remains to be characterised *in vivo*. Additionally, T cell infiltration was not inhibited by mucin pools in mucinous rectal cancer (395). In appendiceal cancer, it remains to be addressed whether the

high mucin production will influence the infiltration as well as the anti-tumour responses of CAR T cells administered *in vivo*.

Severe on-target, off-tumour toxicities have not been observed for SS1 and P4 CAR T cells clinically. However, possible targeting of mesothelial cells is a potential concern due to their abundance, close proximity, and positive MSLN expression in appendiceal cancer. Low-avidity CARs, such as the m912 construct, could present a safer alternative by selectively recognising MSLN levels upregulated on tumour cells but not the lower, physiological levels from mesothelial cells (142). Another strategy is by logic-gating with a coreceptor against particular subtypes of HLA class I, such that tumour cells with selective loss of HLA class I molecules will be targeted for MSLN-directed killing whereas normal mesothelial cells can be spared (396). Finally, co-expression of a suicide switch, such as iCas9, would enable immediate *in vivo* inhibition of CAR T cell activity in the event of life-threatening toxicities (210).

One mucin family protein, MUC1, was shown to have high on-tumour expression in our AMN and AA samples. Importantly, MUC1 also had low RNA expression in mesothelial cells. It was known that MUC1 RNA is lowly expressed in brain tissues (397), which could explain the MUC1 positivity we observed in a small population of neuronal cells from scRNA-seq. Nevertheless, expression of MUC1 protein and tumour-associated glycoforms have not been reported on healthy neuronal cells. These indicate MUC1 as a therapeutic target with high tumour specificity and low risks of on-target, off-tumour toxicities. Similar to MSLN, the overall prevalence and expression differences between AMN and AA subtypes requires further confirmation in larger appendiceal cancer cohorts to identify patient populations that can best benefit from potential anti-MUC1 immunotherapies.

The effectiveness of anti-MUC1 CAR T cell therapy remains to be tested in appendiceal cancer. Antigen shedding represents one limitation of current anti-MUC1 CAR T cell therapies. MUC1 shedding can downregulate antigen availability for CAR T cell recognition, and shed MUC1 can potentially inhibit the functions of anti-MUC1 CAR T cells. To determine the significance of MUC1 shedding in appendiceal cancer, soluble MUC1 can be detected from organoid cultures via ELISA. Pharmacological inhibition of MUC1 sheddases, such as ADAM17 (155), might present an avenue for improvement if poor CAR T cell responses are observed. The issue of MUC1 shedding can also be circumvented by adopting a CAR that binds to a juxtamembrane region retained after MUC1 cleavage, such as the huMNC2 construct (167).

Further characterisation is needed to discover other tumour-associated antigens in appendiceal cancer that might serve as potential targets for CAR T cell therapies. Aside from MUC1, other mucin family proteins, such as MUC16, have also been shown to be upregulated in appendiceal cancer, although clinical development of anti-MUC16 CAR T cells is not as advanced as anti-MSLN and anti-MUC1 CAR T cell therapies (115, 296). Aside from MUC16, tumour antigens such as CLDN18.2, HER2, EpCAM, CEA, and EGFR, have also been commonly tested as therapeutic targets by CAR T cells in gastrointestinal tumours, and showed positive expressions at the transcriptomic level in at least one of the organoids established in the current study, as shown in the Appendix (**Supplementary Figure 3B-F**). Lastly, the discovery of novel antigens remains understudied in appendiceal cancer, likely due to the rarity of this disease. Profiling the expression of tumour-associated antigens is a key step towards finding the ideal target for the translation of CAR T cell as well as other targeted immunotherapies in appendiceal cancer.

4.4.2 Feasibility of TIL therapy

The current study investigated small-scale expansion of TILs from appendiceal tumours, establishing an overall success rate of 73%. This forms the basis for pre-REP expansion, although further optimisations would be essential to adapt the process for clinical manufacturing. First, due to sample availability, only one sectioned tumour piece per specimen was used to test expansion. Consequently, a relatively low cell number (15 million) was set as the threshold for successful expansion. In a clinical setting, the entire tumour specimen would be used for processing. Given that appendiceal cancer metastases are often procured as large, bulky tumours during peritectomy, 5 – 10 tumour pieces could generally be obtained per tumour specimen, substantially multiplying the number of TIL microcultures for downstream expansion. A higher threshold for cell number (~ 60 million based on experiences in melanoma) would be appropriate to evaluate successful TIL expansion and ensure TIL number is sufficient if REP is to be initiated. Second, stringent criteria should be established for tumour procurement, including standardisation of specimen size (greater than 1.5 cm in diameter) and avoiding areas with significant mucin production, fat tissues, and tissue necrosis. In the current study, a mucinous layer is often observed after centrifugating AMN samples during tumour processing. The interface between this mucinous layer with the cell pellet can hardly be distinguished, which presented difficulty in harvesting the cell pellet for subsequent

TIL expansion at specified cell densities. When processing of highly mucinous samples is unavoidable, cells can be seeded with the mucinous fraction to avoid cell loss, despite lower culturing density. Alternatively, the use of mucolytic agents can be considered. Combination of bromelain (300 - 600 μg/mL) with N-acetylcysteine (3% or 250 mM) has been used for mucolysis of appendiceal tumours (398, 399). However, since cytotoxic effect from bromelain treatment has been observed in appendiceal cancer organoids, the potential effect of mucolytic treatment on TIL growth should be carefully assessed. Fat tissues can be trimmed off and were generally removed early during tumour processing via centrifugation. This has not caused significant challenges for TIL expansion, although high abundance of fat tissue can potentially reduce the available tumour material responsible for TIL production. Necrotic tumour fragments would significantly reduce cell viability in the starting culture. This is likely the reason that led to failed expansion of the PB295 TILs, which showed extremely low cell viability (2%) and was present with abundant debris after tumour processing. Importantly, the debris was unable to be removed via centrifugation and cell viability remained low (<10%) throughout culturing.

Additional considerations should be given to the regimen of IL-2 supplementation and potential use of antibiotic treatment to avoid bacterial contamination. The current study uses a gradient reduction of IL-2 supplementation (from 3000 IU/mL to 1000 IU/mL) for TIL expansion. This IL-2 supplementation regimen has previously been employed for TIL expansion with anti-CD3/CD28 stimulation (87, 400), although standard protocols in clinical manufacturing typically use IL-2 supplementation at 3000 IU/mL or 6000 IU/mL throughout the pre-REP expansion process (212). Different concentrations of IL-2 supplementation (from 1000 – 6000 IU/mL) have not been directly compared during the pre-REP process and warrants further investigation to support optimal TIL expansion. Appendiceal tumours have been known to harbour enteric bacteria (401). No bacterial contamination was observed in the expansions performed in the current study, likely due to antibiotic supplementation (1% penicillin/streptomycin) in the culturing media. Nevertheless, further precautionary measures should be taken in a clinical manufacturing setting, such as by incubating tumour specimens in antibiotic-enriched media (with hypothermosol, amphotericin B, and gentamicin) during transport, and adherence to high sterility standards at all times (173).

Lastly, the expansion protocol in the current study was adapted based on traditional pre-REP culturing of TILs in plate-bound wells. Recent advances in clinical manufacturing have utilised bioreactors, such as the G-rex system, for pre-REP expansion. The use of G-rex bioreactors would reduce the need for frequent media exchanges, minimizing operator handling in a clinical setting (82). In the Gen 2 manufacturing process for FDA-approved lifileucel production, initiating TIL cultures in a single G-rex 100-CS bioreactor has accelerated the pre-REP expansion to within 11 days (83). Given the initial success via the traditional method, TIL expansion in bioreactors can be tested in a Gen 2-like process to streamline pre-REP expansion for clinical manufacturing.

In this study, TILs were expanded from both subtypes of appendiceal cancer (AMN and AA). Compared to AA, AMN was known to possess an increased number of infiltrating T cells, which is consistent with the higher percentage of T cells observed in our scRNA-seq data (AMN vs AA: 47.9% vs 24.1%). It remains to be established whether the proportions of T cells or specific T cell subtypes in the initial tumour can predict outcomes of TIL expansion. To address this, flow cytometry characterisation on single cell suspensions obtained after tumour processing can be used to quantify T cell abundances and correlate with subsequent TIL expansion performances. Slower TIL expansion was also observed from cryopreserved tumour specimens, compared to specimens that were processed fresh after surgery. From previous literature, the effect of cryopreserving tumour samples on TIL production has been inconclusive. In one study, cryopreserved colorectal tumours showed reduced leukocyte counts (mainly by a significant decrease in neutrophils) and induced lower IFN-γ responses from TILs upon polyclonal stimulation, although TIL expansion was not evaluated (402). The cryopreservation media (90% FBS + 10% FBS) was shown to be essential for cell recovery after thawing. Another study comparing lifileucel production from four matched fresh and frozen melanoma tissues has shown no differences in cell number, viability and T cell phenotypes (403). The cryopreservation method, however, was proprietary and not disclosed. The choice of cryopreservation media should be carefully evaluated to ensure optimal TIL expansion from cryopreserved appendiceal tumours. To improve post-thaw recovery, the use of controlled-rate freezers and thawers can also be evaluated, as cooling rates during cryopreservation are known to influence cell viability (404). Overall, improving TIL expansion from cryopreserved samples would be highly beneficial for clinical manufacturing, as tumour specimens can be

delivered from distant procurement centres, withstand long shipping, and be used for TIL expansion at a time optimal for manufacturing workflows.

Expanded TIL products demonstrated consistently high percentage abundance of (CD3+) T cells, with all samples exceeding 95%. However, comprehensive phenotypic characterisation of T cell populations in expanded TIL products remain to be studied. Persistent IL-2 stimulation and prolonged TIL culturing have been shown to increase T cell exhaustion (405, 406). TILs with minimal culturing, such as the young TILs derived from melanoma, also exhibit higher levels of co-stimulatory molecules (CD27 and CD28) and longer telomere lengths (89). It is not known if the varying duration of TIL culture is associated with changes in the memory and exhaustion profiles of T cells. To address this, expression of memory and exhaustion markers of TILs can be examined via multiparameter flow cytometry, or evaluated at a transcriptomic level via RNA-seq or scRNA-seq.

Functional responses of expanded TIL products were upregulated upon polyclonal stimulation with SEB. Polyclonal stimulation offers a general evaluation of TIL functional capacity, and is essential when autologous tumours are not available for assessing tumour-specific responses. One limitation with the use of SEB for stimulation is that it only activates T cells with specific TCR V beta (Vβ) chain subtypes (Vβ 3, 12, 14, and 17) (407). As the TCR subtypes in our expanded TILs have not been studied, a better alternative for polyclonal stimulation would be via the phorbol 12-myristate 13-acetate (PMA) and ionomycin combination, which bypasses the TCR complex to activate T cells non-specifically (408). PMA/ionomycin is commonly used to test the functional capacity of TIL products, and represents a more appropriate method for polyclonal stimulation in future experiments.

The anti-tumour responses of TIL products require further investigation and improvement. None of the TIL products currently tested demonstrated consistent reactivity against dissociated autologous tumour organoids, despite functional responses elicited from polyclonal stimulation. Although immune profiling of appendiceal tumours remains limited, one possibility is the presence of non-tumour-reactive, bystander T cell clones that can outgrow tumour-reactive clones during expansion. As no selection or sorting of tumour-reactive T cells has been performed with the current expansion protocols, the resulting TIL products may instead be dominated by bystander T cell clones with no detectable anti-tumour activity. From the TIL cytotoxicity results, patient-derived cancer cells showed increased,

decreased, and no difference in viability across their three matched TILs respectively. Given the absence of 4-1BB and OX40 upregulations and the lack of IFN-γ release from TILs, the observed changes in cancer cell viability were likely independent from responses induced by tumour-reactive T cell clones. Instead, they could potentially arise from currently uncharacterised interactions between tumour cells and bystander T cell clones. Bystander T cells can contribute to increased cancer cell viability by secreting pro-tumorigenic cytokines, such as IL-4, IL-17, and IL-35, that support tumour cell survival (409, 410). Alternatively, the presence of TILs can indirectly lead to lower cancer cell viability by competing for nutrients and growth factors in the media. The significance of bystander T cells can be studied through further characterisations of TIL cytokine profiles and TIL-tumour interactions across individual TIL products.

Additional experimental designs can assist in validating the lack of anti-tumour reactivity of TIL products. Autologous tumour cell suspension (from initial processing) might show increased heterogeneity in antigen expression than dissociated organoids, and co-cultures of TILs with autologous tumour cell suspension may broaden the repertoire of detectable tumour antigens for TIL recognition. However, assay reproducibility might be limited by sample availability, and killing of stromal versus tumour cells cannot be distinguished. TIL reactivity can also be assessed via enzyme-linked immunospot (ELISpot) assays, where individual spots can be quantified to represent the number of cytokine-secreting cells. Compared to ELISA, ELISpot is highly sensitive and capable of detecting reactive TIL clones at single-cell resolution. As such, ELISpot (for the detection of IFN-γ-secreting TILs) can be used as confirmatory assays for TIL reactivity.

Several strategies to improve the reactivity of TIL products have been clinically evaluated and can be considered for optimisation here. Due to spatial heterogeneity, TIL cultures derived from non-adjacent fragments of the same tumour were found to exhibit substantial differences in TCR repertoire (382). To increase the likelihood of detecting tumour-reactive TILs, the number of tumour fragments for TIL expansion can be increased, and TIL cultures can be screened for upregulated functional responses in co-culture with autologous tumours. This reactivity selection approach is common in clinical manufacturing and the tumour-reactive cultures can be selectively expanded downstream (i.e. via the REP process). Alternatively, as in the “young TIL” protocols, individual TIL cultures can be pooled to achieve

sufficient yield while preserving a consistent level of functional reactivity (177). Neoantigen-specific TIL products can also be generated by co-culturing TILs with autologous or HLA-matched APCs presenting patient-specific neoantigens, as demonstrated in protocols such as NeoExpand (105). Lastly, single tumour-reactive T cell clones can be isolated from TIL cultures by FACS sorting based on reactivity markers such as PD-1, CD39, CD103, and CD137 (92, 95, 97), for subsequent expansion and characterisation. Importantly, TCR sequencing of such tumour-reactive clones can potentially provide insights for the development of other novel therapies, such as TCR T cell therapy, where T cells are engineered to express a personalised TCR construct for tumour-directed cytotoxicity.

In summary, the current study successfully expanded TILs from appendiceal cancer, although a small number of samples (n = 11) was assessed. Improving the reactivity of TIL products and adopting the expansion protocols for clinical manufacturing remain areas for ongoing investigations. In addition, the REP process, utilising irradiated feeder cells, high dose IL-2 (3000 IU/mL) and culturing in bioreactors, would have to be established to upscale the cell number of TIL products to high levels (~10^{10} cells) suitable for clinical infusions. In appendiceal cancer, the common recurrence after CRS/HIPEC (~32%) allows for repeated surgical interventions and provides ideal therapeutic windows for tumour procurement and TIL manufacturing (411). By demonstrating the feasibility of TIL therapy, our study lays the foundation for a novel therapeutic approach aimed at improving outcomes of patients with appendiceal cancer who show limited responses to standard treatments.

4.4.3 Clinical potential to address current unmet needs

Overall, the current study presents pioneering work on the application of adoptive T cell therapies in appendiceal cancer, a rare disease with limited treatment options. Although alternative treatment options are being explored, systemic chemotherapies have not demonstrated adequate clinical efficacy, while immunotherapy options remain scarce and are still in the early stages of clinical testing. The development of new therapies is further hindered by unfavourable cost-benefit considerations given the rarity of the disease. In such a setting, the translation of existing adoptive T cell therapies, such as CAR T cell and TIL therapies, presents a favourable approach to address the critical unmet need for novel treatments in appendiceal cancer. As described in Chapter 1, both CAR T cell and TIL therapies

have been widely assessed in other solid tumours, and these extensive clinical experiences are valuable for guiding their design and implementation in appendiceal cancer.

Comparing CAR T cell and TIL therapies, it remains to be determined which adoptive T cell therapy option would be the most beneficial for appendiceal cancer patients to be considered for clinical translation. Current clinical trial experiences have generally indicated better therapeutic outcomes of TIL therapies in solid tumours than CAR T cell therapies. From our preliminary *in vitro* findings, however, we conclude that anti-MSLN CAR T cell therapies are effective against the antigen-positive appendiceal cancer tumours tested in this study, whereas TIL therapy shows successful expansion but limited anti-tumour efficacy. However, we have not yet performed reactivity selection of our TIL products. In a Phase II study including patients with gastrointestinal cancer, positive ORRs were obtained when neoantigen selection was performed (8% or 24% with or without pembrolizumab, respectively), as opposed to using bulk, unselected "young TIL" protocol that observed no objective responses (91). Although most patients in the trial had colorectal cancer, which is increasingly recognised as biologically distinct from appendiceal cancer, this highlights the importance of performing reactivity selection to achieve clinical efficacy of TIL therapy in a gastrointestinal setting. Favourable clinical responses of unselected TILs in melanoma are partially attributable to tumour immunogenicity (412). Appendiceal cancer is known to have a low MSI-H prevalence (4%), although abundant immune cell infiltration has been observed in the peritoneal metastases of appendiceal cancer in the present studies and from previous literature (291, 292). Evidence on the immunogenicity of appendiceal tumours is limited, and further characterisation could provide important insight into the suitability of unselected TIL therapy.

Lastly, although CAR T cell and TIL killing were performed on the same set of tumour organoids (PB245, PB252, and PB280), we were unable to directly compare the cytotoxic responses of the two approaches due to the different assays used. Following further optimisation in TIL manufacturing, it would be ideal to directly compare TIL and CAR T cell killing using the same standardised system, such as via the xCELLigence RCTA platform, which remains the gold standard for CAR T cell cytotoxicity assessment. Nevertheless, one limitation of the xCELLigence RTCA platform is the need for organoids to be seeded as a monolayer, which does not preserve the native three-dimensional (3D) architecture of organoids. Similarly, in the TIL-organoid co-culture assays used in the current study, the 3D structure of organoids was lost

due to dissociation of organoids into single-cell suspensions. Further investigations can explore the use of fluorescent imaging techniques to study T cell killing responses on intact 3D organoids (413), which can be leveraged using high-throughput 3D imaging platforms such as the Opera Phenix High-Content Screening System (PerkinElmer) or the Incucyte® Live-Cell Analysis System (Sartorius) (414-416). Successful evaluation would enable identification of the adoptive T cell therapy approach with optimal efficacy for further *in vivo* validation. Our results establish the groundwork for adoptive T cell therapies in appendiceal cancer and with ongoing advances, have the potential to significantly improve future patient outcomes.

CHAPTER 5

Concluding Remarks

Adoptive T cell therapies represent an emerging immunotherapy modality for solid tumours that currently lack effective treatments. In principle, CAR T cell and TIL therapies can be applied across diverse malignancies, provided that targeted antigens are expressed or TIL populations can be successfully expanded, respectively. However, while remarkable clinical results have been shown by CAR T cell therapies in CD19-positive B-cell malignancies, their translation in solid tumours has been challenged by limited therapeutic efficacy. Similarly, despite encouraging clinical outcomes in metastatic melanoma, efficacy of TIL therapies in other types of solid tumours remains variable. The lack of clinical success in these settings highlights that adoptive T cell therapies are not truly disease-agnostic. Instead, each cancer type presents unique biological barriers, and a deeper understanding of tumour-specific context is essential for achieving successful therapeutic outcomes.

PDAC, the most common form of pancreatic cancer, carries a significant global burden due to its high incidence and extremely poor prognosis. Although high expression of the tumour antigen MSLN has prompted clinical evaluation of anti-MSLN CAR T cell therapies, their efficacy remains suboptimal. In Chapter 3, the clinicopathological and biological significance of MSLN in PDAC was examined. High MSLN expression was associated with poor prognosis in an Australian patient cohort and an immunosuppressive landscape characterised by reduced CD8 T cell reactivity and abundance. This may shed light on previously underappreciated challenges that are currently hindering the effective responses of anti-MSLN CAR T cell therapies. Immunosuppression, and in particular, T cell exclusion, are shown to be more significant barriers for patients with high antigen expression, who would otherwise be more likely to benefit from these therapies. Additionally, in the MSLN-low population, the increased tumour reactivity and abundance of CD8 T cells are advantageous for the development of TIL therapies, where successful expansion of tumour-reactive T cell lymphocytes is essential for this treatment approach.

It must be noted that the current study only shows associations of MSLN expression with immunosuppression in PDAC, and the biological mechanisms that underly the observed relationships are unclear. Secondly, the implications of these findings for adoptive T cell therapies have not been experimentally tested. *In vitro* and *in vivo* validations are essential future directions for the current work. For *in vitro* studies, TILs could be isolated from MSLN-high and MSLN-low tumours to confirm if there were reductions in the abundance and

reactivity levels of CD8 T cells. For *in vivo* studies, tumour cells with high and low MSLN expression could be implanted to examine if increased MSLN expression promotes an immunosuppressive TME with low CD8 T cell infiltration. Given the consistent transcriptomic activities observed across the human and mouse RNA-seq datasets, such investigations could be conducted in immunocompetent or humanised murine models orthotopically engrafted with tumours, to ensure that a physiologically relevant TME is recapitulated and tumour immune infiltrates are preserved. These models could also be used to evaluate CAR T cell and TIL responses, as well as to determine whether strategies that promote T cell infiltration and resistance to the immunosuppressive TME can improve therapeutic efficacy in PDAC.

In addition, the associations of MSLN with immunosuppression highlight that alternative tumour-associated antigens might be considered better targets for CAR T cell therapies in PDAC. Our group has successful experiences establishing PDAC organoids from primary surgical specimens. Similar to appendiceal cancer, patient-derived PDAC organoids enable profiling of clinically relevant tumour antigens and evaluation of adoptive T cell therapy regimens. Currently, no standard cytotoxicity assay exists for co-cultures of CAR T cells with cancer organoids (417). Given the positive results observed with anti-MSLN CAR T cell therapies on appendiceal cancer organoids, the xCELLigence cytotoxicity assay shows potential for examining the killing responses of adoptive T cell therapies in PDAC organoids as well. The peritoneum represents the second-most common site of metastasis in PDAC (418). However, the biology of peritoneal metastases in PDAC have not been well-characterised, and no studies have reported TIL generation from PDAC peritoneal metastases. It remains to be tested whether the current TIL expansion protocols established for peritoneal metastases of appendiceal cancer could provide a generalisable framework to evaluate TIL expansion from peritoneal metastases of PDAC as well as of other solid tumour origins.

Despite its rarity, the incidence of appendiceal cancer is increasing and prognosis remains poor for patients who fail standard CRS/HIPEC treatments. The expression of solid tumour antigens, such as MSLN and MUC1, and the presence of T cell infiltrates in appendiceal cancer provides a rationale for exploring adoptive T cell therapies in this disease. In Chapter 4, the translation of CAR T cell and TIL therapies in appendiceal cancer was examined for the first time. Anti-MSLN CAR T cells showed robust efficacy against patient-derived organoids of appendiceal cancer with positive MSLN expression. TILs have also been successfully expanded

from patient tumours. However, expanded TILs were only responsive to superantigen stimulation but not matched tumour organoids, suggesting that further optimisation to improve therapeutic efficacy is required. Importantly, a small number of organoid models and tumour specimens was used in the study, partially owning to the rarity of the disease. Further validation will require expanded patient recruitment to enable the establishment of additional organoid models and procurement of tumour specimens for TIL generation. The preliminary results presented here lay the foundation for larger-scale assessments of adoptive T cell therapies in appendiceal cancer.

In vivo validation of anti-MSLN CAR T cell responses using patient-derived xenograft (PDX) or organoid engraftment models will be crucial to identify the most effective CAR T cell product for clinical translation. Moreover, appendiceal cancer may express additional tumour antigens that are targetable by CAR T cell therapies from existing solid tumour clinical trials. As one example, we demonstrated expression of tumour-specific MUC1 glycoforms (Tn/sTn), using the 5E5 antibody from which the antigen-binding domain of anti-MUC1 5E5 CAR T cells was derived. These organoid models can be used to discover novel antigens for designing CAR T cell therapies, although translation of existing CAR T cell treatments likely remains the most cost-effective option given the small size of the patient population. Ideally, future CAR T cell clinical trials would include the recruitment of advanced (unresectable or relapsed/refractory) appendiceal cancer patients, if successful results are shown from these assessments.

While the current study demonstrated pre-REP TIL expansion from appendiceal tumours, further development of the TIL manufacturing pipeline is required. This would involve (1) adaption of the current expansion protocols for clinical manufacturing, (2) optimisation and enrichment of the anti-tumour reactivity of TILs, and (3) establishment of the REP phase. In a clinical setting, the standard CRS procedure provides an appropriate window for procuring the debulked tumours for TIL manufacturing. In advanced disease, the high disease recurrence rate also highlights the potential for multiple tumour procurement procedures and TIL manufacturing runs in patients undergoing repeat CRS. The feasibility of TIL expansion shown in the current study provides the pivotal basis for the continued establishment of TIL therapy that may expand the currently limited therapeutic options for appendiceal cancer patients.

Lastly, the immunogenicity of appendiceal tumours has not been fully characterised. Given that MSLN is expressed in appendiceal tumours, it is worth investigating if high expression of MSLN in appendiceal cancer is similarly associated with immunosuppression and particularly reduced T cell infiltration and activity, as demonstrated in PDAC in Chapter 3. This may have significant implications for optimising the therapeutic efficacy of anti-MSLN CAR T cells and TIL therapies examined in the current work. However, profiling MSLN expression and stratifying patients based on MSLN expression levels could be limited by small sample sizes due to the rarity of the disease and complexity of histological subtyping. Establishing cross-institutional multi-omics database or biobank would be crucial for comprehensive characterisation of appendiceal cancer biology, which could provide relevant insights to inform future immunotherapy development.

In conclusion, this thesis has investigated the challenges of translating adoptive T cell therapies in two solid tumours, pancreatic cancer and appendiceal cancer. In pancreatic cancer, high MSLN expression was discovered to be associated with immunosuppression and reduced CD8 T cell infiltration, highlighting a potential barrier that limits the clinical efficacy of anti-MSLN CAR T cell therapies to date. In appendiceal cancer, *in vitro* efficacy of anti-MSLN CAR T cell therapies and feasibility of TIL expansion have been examined and successfully demonstrated for the first time. These results lay the foundation for advancing adoptive T cell therapies in the solid tumour landscape to improve the currently dismal clinical outcomes faced by patients who desperately need more effective treatments.

References

1. Saez-Ibanez AR, Upadhaya S, Partridge T, Winkelman D, Correa D, Campbell J. The changing landscape of cancer cell therapies: clinical trials and real-world data. Nat Rev Drug Discov. 2024;23(10):736-7.
2. Testa U, Sica S, Pelosi E, Castelli G, Leone G. CAR-T Cell Therapy in B-Cell Acute Lymphoblastic Leukemia. Mediterr J Hematol Infect Dis. 2024;16(1):e2024010.
3. Neelapu SS, Locke FL, Bartlett NL, Lekakis LJ, Miklos DB, Jacobson CA, et al. Axicabtagene Ciloleucel CAR T-Cell Therapy in Refractory Large B-Cell Lymphoma. N Engl J Med. 2017;377(26):2531-44.
4. Maude SL, Laetsch TW, Buechner J, Rives S, Boyer M, Bittencourt H, et al. Tisagenlecleucel in Children and Young Adults with B-Cell Lymphoblastic Leukemia. N Engl J Med. 2018;378(5):439-48.
5. Abramson JS, Palomba ML, Gordon LI, Lunning MA, Wang M, Arnason J, et al. Lisocabtagene maraleucel for patients with relapsed or refractory large B-cell lymphomas (TRANSCEND NHL 001): a multicentre seamless design study. Lancet. 2020;396(10254):839-52.
6. Wang M, Munoz J, Goy A, Locke FL, Jacobson CA, Hill BT, et al. KTE-X19 CAR T-Cell Therapy in Relapsed or Refractory Mantle-Cell Lymphoma. N Engl J Med. 2020;382(14):1331-42.
7. Lee A. Obecabtagene Autoleucel: First Approval. Mol Diagn Ther. 2025;29(3):419-23.
8. Munshi NC, Anderson LD, Jr., Shah N, Madduri D, Berdeja J, Lonial S, et al. Idecabtagene Vicleucel in Relapsed and Refractory Multiple Myeloma. N Engl J Med. 2021;384(8):705-16.
9. Berdeja JG, Madduri D, Usmani SZ, Jakubowiak A, Agha M, Cohen AD, et al. Ciltacabtagene autoleucel, a B-cell maturation antigen-directed chimeric antigen receptor T-cell therapy in patients with relapsed or refractory multiple myeloma (CARTITUDE-1): a phase 1b/2 open-label study. Lancet. 2021;398(10297):314-24.
10. Chesney J, Lewis KD, Kluger H, Hamid O, Whitman E, Thomas S, et al. Efficacy and safety of lifileucel, a one-time autologous tumor-infiltrating lymphocyte (TIL) cell therapy, in patients with advanced melanoma after progression on immune checkpoint inhibitors and targeted therapies: pooled analysis of consecutive cohorts of the C-144-01 study. J Immunother Cancer. 2022;10(12).
11. D'Angelo SP, Araujo DM, Abdul Razak AR, Agulnik M, Attia S, Blay JY, et al. Afamitresgene autoleucel for advanced synovial sarcoma and myxoid round cell liposarcoma (SPEARHEAD-1): an international, open-label, phase 2 trial. Lancet. 2024;403(10435):1460-71.
12. Zheng Z, Li S, Liu M, Chen C, Zhang L, Zhou D. Fine-Tuning through Generations: Advances in Structure and Production of CAR-T Therapy. Cancers (Basel). 2023;15(13).
13. Ran T, Eichmüller SB, Schmidt P, Schlander M. Cost of decentralized CAR T-cell production in an academic nonprofit setting. International journal of cancer. 2020;147(12):3438–45.
14. Zhang M, Jin X, Sun R, Xiong X, Wang J, Xie D, et al. Optimization of metabolism to improve efficacy during CAR-T cell manufacturing. Journal of translational medicine. 2021;19(1):499.
15. Bersenev A. CAR-T cell manufacturing: time to put it in gear. Transfusion. 2017;57(5):1104–6.
16. Depil S, Duchateau P, Grupp SA, Mufti G, Poirot L. 'Off-the-shelf' allogeneic CAR T cells: development and challenges. Nature reviews Drug discovery. 2020;19(3):185–99.

17. Stenger D, Stief TA, Kaeuferle T, Willier S, Rataj F, Schober K, et al. Endogenous TCR promotes in vivo persistence of CD19-CAR-T cells compared to a CRISPR/Cas9-mediated TCR knockout CAR. Blood. 2020;136(12):1407–18.
18. Winterhalter PM, Warmuth L, Hilgendorf P, Schutz JM, Dotsch S, Tonn T, et al. HLA reduction of human T cells facilitates generation of immunologically multicompatible cellular products. Blood Adv. 2024;8(13):3416-26.
19. Li YR, Zhu Y, Fang Y, Lyu Z, Yang L. Emerging trends in clinical allogeneic CAR cell therapy. Med. 2025;6(8):100677.
20. Guedan S, Calderon H, Posey AD, Jr., Maus MV. Engineering and Design of Chimeric Antigen Receptors. Mol Ther Methods Clin Dev. 2019;12:145-56.
21. Fujiwara K, Tsunei A, Kusabuka H, Ogaki E, Tachibana M, Okada N. Hinge and Transmembrane Domains of Chimeric Antigen Receptor Regulate Receptor Expression and Signaling Threshold. Cells. 2020;9(5).
22. Eshhar Z, Waks T, Gross G, Schindler DG. Specific activation and targeting of cytotoxic lymphocytes through chimeric single chains consisting of antibody-binding domains and the gamma or zeta subunits of the immunoglobulin and T-cell receptors. Proc Natl Acad Sci U S A. 1993;90(2):720-4.
23. Thistlethwaite FC, Gilham DE, Guest RD, Rothwell DG, Pillai M, Burt DJ, et al. The clinical efficacy of first-generation carcinoembryonic antigen (CEACAM5)-specific CAR T cells is limited by poor persistence and transient pre-conditioning-dependent respiratory toxicity. Cancer Immunol Immunother. 2017;66(11):1425-36.
24. van der Stegen SJ, Hamieh M, Sadelain M. The pharmacology of second-generation chimeric antigen receptors. Nat Rev Drug Discov. 2015;14(7):499-509.
25. Gomes da Silva D, Mukherjee M, Srinivasan M, Dakhova O, Liu H, Grilley B, et al. Direct Comparison of In Vivo Fate of Second and Third-Generation CD19-Specific Chimeric Antigen Receptor (CAR)-T Cells in Patients with B-Cell Lymphoma: Reversal of Toxicity from Tonic Signaling. Blood. 2016;128(22):1851-.
26. Chmielewski M, Abken H. TRUCKS, the fourth-generation CAR T cells: Current developments and clinical translation. ADVANCES IN CELL AND GENE THERAPY. 2020;3(3):e84.
27. Tang L, Pan S, Wei X, Xu X, Wei Q. Arming CAR-T cells with cytokines and more: Innovations in the fourth-generation CAR-T development. Mol Ther. 2023;31(11):3146-62.
28. Kagoya Y, Tanaka S, Guo T, Anczurowski M, Wang CH, Saso K, et al. A novel chimeric antigen receptor containing a JAK-STAT signaling domain mediates superior antitumor effects. Nat Med. 2018;24(3):352-9.
29. Yin H, Wei X. The design of retroviral vectors used in the CAR-T products, risk management, and future perspective. MedComm (2020). 2025;6(2):e70067.
30. Shao L, Shi R, Zhao Y, Liu H, Lu A, Ma J, et al. Genome-wide profiling of retroviral DNA integration and its effect on clinical pre-infusion CAR T-cell products. J Transl Med. 2022;20(1):514.
31. Ozdemirli M, Loughney TM, Deniz E, Chahine JJ, Albitar M, Pittaluga S, et al. Indolent CD4+ CAR T-Cell Lymphoma after Cilta-cel CAR T-Cell Therapy. N Engl J Med. 2024;390(22):2074-82.
32. Hamilton MP, Miklos DB, Alizadeh AA. Risk of Second Tumors and T-Cell Lymphoma after CAR T-Cell Therapy. Reply. N Engl J Med. 2024;391(9):870-1.
33. Eisenman D, Swindle S. Food and Drug Administration Guidance on Design of Clinical Trials for Gene Therapy Products with Potential for Genome Integration or Genome Editing and Associated Long-Term Follow-Up of Research Subjects. Appl Biosaf. 2022;27(4):201-9.

34. Beatty GL, O'Hara MH, Lacey SF, Torigian DA, Nazimuddin F, Chen F, et al. Activity of Mesothelin-Specific Chimeric Antigen Receptor T Cells Against Pancreatic Carcinoma Metastases in a Phase 1 Trial. Gastroenterology. 2018;155(1):29-32.
35. Panjwani MK, Smith JB, Schutsky K, Gnanandarajah J, O'Connor CM, Powell DJ, et al. Feasibility and Safety of RNA-transfected CD20-specific Chimeric Antigen Receptor T Cells in Dogs with Spontaneous B Cell Lymphoma. Molecular therapy : the journal of the American Society of Gene Therapy. 2016;24(9):1602–14.
36. Wiesinger M, März J, Kummer M, Schuler G, Dörrie J, Schuler-Thurner B, et al. Clinical-Scale Production of CAR-T Cells for the Treatment of Melanoma Patients by mRNA Transfection of a CSPG4-Specific CAR under Full GMP Compliance. Cancers. 2019;11(8).
37. Zhang Z, Qiu S, Zhang X, Chen W. Optimized DNA electroporation for primary human T cell engineering. BMC biotechnology. 2018;18(1):4.
38. Lukjanov V, Koutná I, Šimara P. CAR T-Cell Production Using Nonviral Approaches. Journal of immunology research. 2021;2021:6644685.
39. Wilson MH, Coates CJ, George AL. PiggyBac transposon-mediated gene transfer in human cells. Molecular therapy : the journal of the American Society of Gene Therapy. 2007;15(1):139–45.
40. Geurts AM, Yang Y, Clark KJ, Liu G, Cui Z, Dupuy AJ, et al. Gene transfer into genomes of human cells by the sleeping beauty transposon system. Molecular Therapy. 2003;8(1):108–17.
41. Huang X, Guo H, Kang J, Choi S, Zhou TC, Tammana S, et al. Sleeping Beauty transposon-mediated engineering of human primary T cells for therapy of CD19+ lymphoid malignancies. Molecular therapy : the journal of the American Society of Gene Therapy. 2008;16(3):580–9.
42. Micklethwaite KP, Gowrishankar K, Gloss BS, Li Z, Street JA, Moezzi L, et al. Investigation of product-derived lymphoma following infusion of piggyBac-modified CD19 chimeric antigen receptor T cells. Blood. 2021;138(16):1391-405.
43. Rurik JG, Tombácz I, Yadegari A, Méndez Fernández PO, Shewale SV, Li L, et al. CAR T cells produced in vivo to treat cardiac injury. Science (New York, NY). 2022;375(6576):91–6.
44. Billingsley MM, Singh N, Ravikumar P, Zhang R, June CH, Mitchell MJ. Ionizable Lipid Nanoparticle-Mediated mRNA Delivery for Human CAR T Cell Engineering. Nano letters. 2020;20(3):1578–89.
45. Billingsley MM, Hamilton AG, Mai D, Patel SK, Swingle KL, Sheppard NC, et al. Orthogonal Design of Experiments for Optimization of Lipid Nanoparticles for mRNA Engineering of CAR T Cells. Nano letters. 2022;22(1):533–42.
46. Pardi N, Tuyishime S, Muramatsu H, Kariko K, Mui BL, Tam YK, et al. Expression kinetics of nucleoside-modified mRNA delivered in lipid nanoparticles to mice by various routes. Journal of controlled release : official journal of the Controlled Release Society. 2015;217:345–51.
47. Hunter TL, Bao Y, Zhang Y, Matsuda D, Riener R, Wang A, et al. In vivo CAR T cell generation to treat cancer and autoimmune disease. Science. 2025;388(6753):1311-7.
48. Mukherjee M, Mace EM, Carisey AF, Ahmed N, Orange JS. Quantitative Imaging Approaches to Study the CAR Immunological Synapse. Molecular therapy : the journal of the American Society of Gene Therapy. 2017:1757–68.
49. Davenport AJ, Cross RS, Watson KA, Liao Y, Shi W, Prince HM, et al. Chimeric antigen receptor T cells form nonclassical and potent immune synapses driving rapid cytotoxicity. Proceedings of the National Academy of Sciences of the United States of America. 2018:E2068-E76.

50. James JR, Vale RD. Biophysical mechanism of T-cell receptor triggering in a reconstituted system. Nature. 2012;487(7405):64–9.
51. Bridgeman JS, Ladell K, Sheard VE, Miners K, Hawkins RE, Price DA, et al. CD3ζ-based chimeric antigen receptors mediate T cell activation via cis- and trans-signalling mechanisms: implications for optimization of receptor structure for adoptive cell therapy. Clinical and experimental immunology. 2014;175(2):258–67.
52. Salter AI, Ivey RG, Kennedy JJ, Voillet V, Rajan A, Alderman EJ, et al. Phosphoproteomic analysis of chimeric antigen receptor signaling reveals kinetic and quantitative differences that affect cell function. Science signaling. 2018.
53. Ramello MC, Benzaïd I, Kuenzi BM, Lienlaf-Moreno M, Kandell WM, Santiago DN, et al. An immunoproteomic approach to characterize the CAR interactome and signalosome. Science signaling. 2019;12(568).
54. Karlsson H, Svensson E, Gigg C, Jarvius M, Olsson-Strömberg U, Savoldo B, et al. Evaluation of Intracellular Signaling Downstream Chimeric Antigen Receptors. PloS one. 2015;10(12):e0144787.
55. Li G, Boucher JC, Kotani H, Park K, Zhang Y, Shrestha B, et al. 4-1BB enhancement of CAR T function requires NF-κB and TRAFs. JCI insight. 2018.
56. Kawalekar OU, O'Connor RS, Fraietta JA, Guo L, McGettigan SE, Posey AD, et al. Distinct Signaling of Coreceptors Regulates Specific Metabolism Pathways and Impacts Memory Development in CAR T Cells. Immunity. 2016;44(2):380–90.
57. Ying Z, He T, Wang X, Zheng W, Lin N, Tu M, et al. Parallel Comparison of 4-1BB or CD28 Co-stimulated CD19-Targeted CAR-T Cells for B Cell Non-Hodgkin's Lymphoma. Molecular therapy oncolytics. 2019:60–8.
58. Benmebarek M-R, Karches CH, Cadilha BL, Lesch S, Endres S, Kobold S. Killing Mechanisms of Chimeric Antigen Receptor (CAR) T Cells. International journal of molecular sciences. 2019.
59. Hombach A, Köhler H, Rappl G, Abken H. Human CD4+ T cells lyse target cells via granzyme/perforin upon circumvention of MHC class II restriction by an antibody-like immunoreceptor. Journal of immunology (Baltimore, Md : 1950). 2006;177(8):5668–75.
60. Hombach AA, Abken H. Most Do, but Some Do Not: $CD4^{+}CD25$- T Cells, but Not $CD4^{+}CD25^{+}$ Treg Cells, Are Cytolytic When Redirected by a Chimeric Antigen Receptor (CAR). Cancers. 2017.
61. Liadi I, Singh H, Romain G, Rey-Villamizar N, Merouane A, Adolacion JRT, et al. Individual Motile CD4(+) T Cells Can Participate in Efficient Multikilling through Conjugation to Multiple Tumor Cells. Cancer immunology research. 2015:473–82.
62. Adusumilli PS, Cherkassky L, Villena-Vargas J, Colovos C, Servais E, Plotkin J, et al. Regional delivery of mesothelin-targeted CAR T cell therapy generates potent and long-lasting CD4-dependent tumor immunity. Sci Transl Med. 2014;6(261):261ra151.
63. Sommermeyer D, Hudecek M, Kosasih PL, Gogishvili T, Maloney DG, Turtle CJ, et al. Chimeric antigen receptor-modified T cells derived from defined CD8+ and CD4+ subsets confer superior antitumor reactivity in vivo. Leukemia. 2016;30(2):492-500.
64. Tschumi BO, Dumauthioz N, Marti B, Zhang L, Lanitis E, Irving M, et al. CART cells are prone to Fas- and DR5-mediated cell death. Journal for immunotherapy of cancer. 2018:71.
65. Künkele A, Johnson AJ, Rolczynski LS, Chang CA, Hoglund V, Kelly-Spratt KS, et al. Functional Tuning of CARs Reveals Signaling Threshold above Which CD8+ CTL Antitumor Potency Is Attenuated due to Cell Fas-FasL-Dependent AICD. Cancer immunology research. 2015:368–79.

66. Singh N, Lee YG, Shestova O, Ravikumar P, Hayer KE, Hong SJ, et al. Impaired Death Receptor Signaling in Leukemia Causes Antigen-Independent Resistance by Inducing CAR T-cell Dysfunction. Cancer discovery. 2020:552–67.
67. Watanabe K, Terakura S, Martens AC, van Meerten T, Uchiyama S, Imai M, et al. Target antigen density governs the efficacy of anti-CD20-CD28-CD3 ζ chimeric antigen receptor-modified effector CD8+ T cells. Journal of immunology (Baltimore, Md : 1950). 2015;194(3):911–20.
68. Majzner RG, Rietberg SP, Sotillo E, Dong R, Vachharajani VT, Labanieh L, et al. Tuning the Antigen Density Requirement for CAR T-cell Activity. Cancer discovery. 2020:702–23.
69. Kagoya Y. Cytokine signaling in chimeric antigen receptor T-cell therapy. Int Immunol. 2024;36(2):49-56.
70. Morgan DA, Ruscetti FW, Gallo R. Selective in vitro growth of T lymphocytes from normal human bone marrows. Science (New York, NY). 1976;193(4257):1007–8.
71. Mehta AK, Gracias DT, Croft M. TNF activity and T cells. Cytokine. 2018;101:14-8.
72. Larson RC, Kann MC, Bailey SR, Haradhvala NJ, Llopis PM, Bouffard AA, et al. CAR T cell killing requires the IFNgammaR pathway in solid but not liquid tumours. Nature. 2022;604(7906):563-70.
73. Textor A, Listopad JJ, Wuhrmann LL, Perez C, Kruschinski A, Chmielewski M, et al. Efficacy of CAR T-cell therapy in large tumors relies upon stromal targeting by IFNgamma. Cancer Res. 2014;74(23):6796-805.
74. Xue Q, Bettini E, Paczkowski P, Ng C, Kaiser A, McConnell T, et al. Single-cell multiplexed cytokine profiling of CD19 CAR-T cells reveals a diverse landscape of polyfunctional antigen-specific response. Journal for immunotherapy of cancer. 2017;5(1):85.
75. Turcotte S, Donia M, Gastman B, Besser M, Brown R, Coukos G, et al. Art of TIL immunotherapy: SITC's perspective on demystifying a complex treatment. J Immunother Cancer. 2025;13(1).
76. Betof Warner A, Corrie PG, Hamid O. Tumor-Infiltrating Lymphocyte Therapy in Melanoma: Facts to the Future. Clin Cancer Res. 2023;29(10):1835-54.
77. Coman MM, Pusztai L, Hooley R, Andreveja L, Kim L, Joshi N, et al. Core Needle Biopsies as an Alternative Source for Ex Vivo Expanded TIL for Adoptive Cell Therapy in Triple-Negative Breast Cancer. J Immunother. 2024;47(2):49-53.
78. Simpson-Abelson MC-C, C, inventorTil expansion from fine needle aspirates and small biopsies. Worldwide2019 23 May 2019.
79. Kirane A, Lee D, Ariyan C. Surgical Considerations in Tumor-Infiltrating Lymphocyte Therapy: Challenges and Opportunities. Transplant Cell Ther. 2025;31(3S):S591-S8.
80. Amaria R, Knisely A, Vining D, Kopetz S, Overman MJ, Javle M, et al. Efficacy and safety of autologous tumor-infiltrating lymphocytes in recurrent or refractory ovarian cancer, colorectal cancer, and pancreatic ductal adenocarcinoma. J Immunother Cancer. 2024;12(2).
81. Crompton JG, Klemen N, Kammula US. Metastasectomy for Tumor-Infiltrating Lymphocytes: An Emerging Operative Indication in Surgical Oncology. Ann Surg Oncol. 2018;25(2):565-72.
82. Gotti E, Tettamanti S, Zaninelli S, Cuofano C, Cattaneo I, Rotiroti MC, et al. Optimization of therapeutic T cell expansion in G-Rex device and applicability to large-scale production for clinical use. Cytotherapy. 2022;24(3):334-43.
83. Wardell SM, ML, inventorProcesses for production of tumour infiltrating lymphocytes and uses of the same in immunotherapy. Worldwide2020 14/05/2020.

84. Brook AM, S; Lanzi, K, inventorSystems and methods for coordinating manufacturing of cells for patient-specific immunotherapy. Worldwide2021 28/10/2021.
85. Gettinger S, Kluger H, Schoenfeld A, Warner AB, He K, Sukari A, et al. P14. 05 Phase 2, Study of Iovance Autologous Tumor Infiltrating Lymphocytes (Lifileucel, LN-144, LN-145, LN-145-S1) In Patients With Solid Tumors. Journal of Thoracic Oncology. 2021;16(10):S1012-S3.
86. Dudley ME, Wunderlich JR, Shelton TE, Even J, Rosenberg SA. Generation of tumor-infiltrating lymphocyte cultures for use in adoptive transfer therapy for melanoma patients. J Immunother. 2003;26(4):332-42.
87. Baldan V, Griffiths R, Hawkins RE, Gilham DE. Efficient and reproducible generation of tumour-infiltrating lymphocytes for renal cell carcinoma. Br J Cancer. 2015;112(9):1510-8.
88. Jin J, Sabatino M, Somerville R, Wilson JR, Dudley ME, Stroncek DF, et al. Simplified method of the growth of human tumor infiltrating lymphocytes in gas-permeable flasks to numbers needed for patient treatment. J Immunother. 2012;35(3):283-92.
89. Tran KQ, Zhou J, Durflinger KH, Langhan MM, Shelton TE, Wunderlich JR, et al. Minimally cultured tumor-infiltrating lymphocytes display optimal characteristics for adoptive cell therapy. J Immunother. 2008;31(8):742-51.
90. Ye Q, Loisiou M, Levine BL, Suhoski MM, Riley JL, June CH, et al. Engineered artificial antigen presenting cells facilitate direct and efficient expansion of tumor infiltrating lymphocytes. J Transl Med. 2011;9:131.
91. Lowery FJ, Goff SL, Gasmi B, Parkhurst MR, Ratnam NM, Halas HK, et al. Neoantigen-specific tumor-infiltrating lymphocytes in gastrointestinal cancers: a phase 2 trial. Nat Med. 2025.
92. Gros A, Robbins PF, Yao X, Li YF, Turcotte S, Tran E, et al. PD-1 identifies the patient-specific CD8(+) tumor-reactive repertoire infiltrating human tumors. J Clin Invest. 2014;124(5):2246-59.
93. Fernandez-Poma SM, Salas-Benito D, Lozano T, Casares N, Riezu-Boj JI, Mancheno U, et al. Expansion of Tumor-Infiltrating CD8(+) T cells Expressing PD-1 Improves the Efficacy of Adoptive T-cell Therapy. Cancer Res. 2017;77(13):3672-84.
94. Inozume T, Hanada K, Wang QJ, Ahmadzadeh M, Wunderlich JR, Rosenberg SA, et al. Selection of CD8+PD-1+ lymphocytes in fresh human melanomas enriches for tumor-reactive T cells. J Immunother. 2010;33(9):956-64.
95. Duhen T, Duhen R, Montler R, Moses J, Moudgil T, de Miranda NF, et al. Co-expression of CD39 and CD103 identifies tumor-reactive CD8 T cells in human solid tumors. Nat Commun. 2018;9(1):2724.
96. Kortekaas KE, Santegoets SJ, Sturm G, Ehsan I, van Egmond SL, Finotello F, et al. CD39 Identifies the CD4(+) Tumor-Specific T-cell Population in Human Cancer. Cancer Immunol Res. 2020;8(10):1311-21.
97. Ye Q, Song DG, Poussin M, Yamamoto T, Best A, Li C, et al. CD137 accurately identifies and enriches for naturally occurring tumor-reactive T cells in tumor. Clin Cancer Res. 2014;20(1):44-55.
98. Seliktar-Ofir S, Merhavi-Shoham E, Itzhaki O, Yunger S, Markel G, Schachter J, et al. Selection of Shared and Neoantigen-Reactive T Cells for Adoptive Cell Therapy Based on CD137 Separation. Front Immunol. 2017;8:1211.
99. Volzke C, Ehrhardt L, Fischer L, Maul P, Wenzel C, Riabinska A, et al. Clinical-scale, modular manufacturing of tumor-reactive TILs using a closed and automated culture system. Front Immunol. 2024;15:1483254.

100. Tavera RJ, Forget MA, Kim YU, Sakellariou-Thompson D, Creasy CA, Bhatta A, et al. Utilizing T-cell Activation Signals 1, 2, and 3 for Tumor-infiltrating Lymphocytes (TIL) Expansion: The Advantage Over the Sole Use of Interleukin-2 in Cutaneous and Uveal Melanoma. J Immunother. 2018;41(9):399-405.
101. Yossef R, Tran E, Deniger DC, Gros A, Pasetto A, Parkhurst MR, et al. Enhanced detection of neoantigen-reactive T cells targeting unique and shared oncogenes for personalized cancer immunotherapy. JCI Insight. 2018;3(19).
102. van Asten SD, de Groot R, van Loenen MM, Castenmiller SM, de Jong J, Monkhorst K, et al. T cells expanded from renal cell carcinoma display tumor-specific CD137 expression but lack significant IFN-gamma, TNF-alpha or IL-2 production. Oncoimmunology. 2021;10(1):1860482.
103. Stevanovic S, Helman SR, Wunderlich JR, Langhan MM, Doran SL, Kwong MLM, et al. A Phase II Study of Tumor-infiltrating Lymphocyte Therapy for Human Papillomavirus-associated Epithelial Cancers. Clin Cancer Res. 2019;25(5):1486-93.
104. Lou E, Choudhry MS, Starr TK, Folsom TD, Bell J, Rathmann B, et al. Targeting the intracellular immune checkpoint CISH with CRISPR-Cas9-edited T cells in patients with metastatic colorectal cancer: a first-in-human, single-centre, phase 1 trial. Lancet Oncol. 2025;26(5):559-70.
105. Levin N, Kim SP, Marquardt CA, Vale NR, Yu Z, Sindiri S, et al. Neoantigen-specific stimulation of tumor-infiltrating lymphocytes enables effective TCR isolation and expansion while preserving stem-like memory phenotypes. J Immunother Cancer. 2024;12(5).
106. Lu YC, Yao X, Crystal JS, Li YF, El-Gamil M, Gross C, et al. Efficient identification of mutated cancer antigens recognized by T cells associated with durable tumor regressions. Clin Cancer Res. 2014;20(13):3401-10.
107. Forget MA, Haymaker C, Dennison JB, Toth C, Maiti S, Fulbright OJ, et al. The beneficial effects of a gas-permeable flask for expansion of Tumor-Infiltrating lymphocytes as reflected in their mitochondrial function and respiration capacity. Oncoimmunology. 2016;5(2):e1057386.
108. Forget MA, Malu S, Liu H, Toth C, Maiti S, Kale C, et al. Activation and propagation of tumor-infiltrating lymphocytes on clinical-grade designer artificial antigen-presenting cells for adoptive immunotherapy of melanoma. J Immunother. 2014;37(9):448-60.
109. Wang K, Wei G, Liu D. CD19: a biomarker for B cell development, lymphoma diagnosis and therapy. Exp Hematol Oncol. 2012;1(1):36.
110. Wei J, Han X, Bo J, Han W. Target selection for CAR-T therapy. J Hematol Oncol. 2019;12(1):62.
111. Piccaluga PP, Arpinati M, Candoni A, Laterza C, Paolini S, Gazzola A, et al. Surface antigens analysis reveals significant expression of candidate targets for immunotherapy in adult acute lymphoid leukemia. Leuk Lymphoma. 2011;52(2):325-7.
112. Davila ML, Brentjens RJ. CD19-Targeted CAR T cells as novel cancer immunotherapy for relapsed or refractory B-cell acute lymphoblastic leukemia. Clin Adv Hematol Oncol. 2016;14(10):802-8.
113. Morgan RA, Yang JC, Kitano M, Dudley ME, Laurencot CM, Rosenberg SA. Case report of a serious adverse event following the administration of T cells transduced with a chimeric antigen receptor recognizing ERBB2. Mol Ther. 2010;18(4):843-51.
114. Shabaneh TB, Stevens AR, Stull SM, Shimp KR, Seaton BW, Gad EA, et al. Systemically administered low-affinity HER2 CAR T cells mediate antitumor efficacy without toxicity. Journal for ImmunoTherapy of Cancer. 2024;12(2):e008566.

115. Tony LT, Stabile A, Schauer MP, Hudecek M, Weber J. CAR-T Cell Therapy for Solid Tumors. Transfusion Medicine and Hemotherapy. 2025;52(1):96-108.
116. Chang K, Pastan I, Willingham MC. Isolation and characterization of a monoclonal antibody, K1, reactive with ovarian cancers and normal mesothelium. Int J Cancer. 1992;50(3):373-81.
117. Weidemann S, Gagelmann P, Gorbokon N, Lennartz M, Menz A, Luebke AM, et al. Mesothelin Expression in Human Tumors: A Tissue Microarray Study on 12,679 Tumors. Biomedicines. 2021;9(4).
118. Bera TK, Pastan I. Mesothelin is not required for normal mouse development or reproduction. Mol Cell Biol. 2000;20(8):2902-6.
119. Bharadwaj U, Li M, Chen C, Yao Q. Mesothelin-induced pancreatic cancer cell proliferation involves alteration of cyclin E via activation of signal transducer and activator of transcription protein 3. Mol Cancer Res. 2008;6(11):1755-65.
120. Bharadwaj U, Marin-Muller C, Li M, Chen C, Yao Q. Mesothelin confers pancreatic cancer cell resistance to TNF-alpha-induced apoptosis through Akt/PI3K/NF-kappaB activation and IL-6/Mcl-1 overexpression. Mol Cancer. 2011;10:106.
121. Bharadwaj U, Marin-Muller C, Li M, Chen C, Yao Q. Mesothelin overexpression promotes autocrine IL-6/sIL-6R trans-signaling to stimulate pancreatic cancer cell proliferation. Carcinogenesis. 2011;32(7):1013-24.
122. Lurie E, Liu D, LaPlante EL, Thistlethwaite LR, Yao Q, Milosavljevic A. Histoepigenetic analysis of the mesothelin network within pancreatic ductal adenocarcinoma cells reveals regulation of retinoic acid receptor gamma and AKT by mesothelin. Oncogenesis. 2020;9(7):62.
123. Shimizu A, Hirono S, Tani M, Kawai M, Okada K, Miyazawa M, et al. Coexpression of MUC16 and mesothelin is related to the invasion process in pancreatic ductal adenocarcinoma. Cancer Sci. 2012;103(4):739-46.
124. Chen SH, Hung WC, Wang P, Paul C, Konstantopoulos K. Mesothelin binding to CA125/MUC16 promotes pancreatic cancer cell motility and invasion via MMP-7 activation. Sci Rep. 2013;3:1870.
125. Kojima T, Oh-eda M, Hattori K, Taniguchi Y, Tamura M, Ochi N, et al. Molecular cloning and expression of megakaryocyte potentiating factor cDNA. J Biol Chem. 1995;270(37):21984-90.
126. Lanitis E, Poussin M, Hagemann IS, Coukos G, Sandaltzopoulos R, Scholler N, et al. Redirected antitumor activity of primary human lymphocytes transduced with a fully human anti-mesothelin chimeric receptor. Mol Ther. 2012;20(3):633-43.
127. Bergan L, Gross JA, Nevin B, Urban N, Scholler N. Development and in vitro validation of anti-mesothelin biobodies that prevent CA125/Mesothelin-dependent cell attachment. Cancer Lett. 2007;255(2):263-74.
128. Liu X, Chan A, Tai CH, Andresson T, Pastan I. Multiple proteases are involved in mesothelin shedding by cancer cells. Commun Biol. 2020;3(1):728.
129. Sapede C, Gauvrit A, Barbieux I, Padieu M, Cellerin L, Sagan C, et al. Aberrant splicing and protease involvement in mesothelin release from epithelioid mesothelioma cells. Cancer Sci. 2008;99(3):590-4.
130. Rupert PB, Buerger M, Friend DJ, Strong RK. Structural elucidation of the mesothelin-mucin-16/CA125 interaction. Structure. 2024;32(8):1049-54 e2.
131. Kaneko O, Gong L, Zhang J, Hansen JK, Hassan R, Lee B, et al. A binding domain on mesothelin for CA125/MUC16. J Biol Chem. 2009;284(6):3739-49.

132. Baldo P, Cecco S. Amatuximab and novel agents targeting mesothelin for solid tumors. Onco Targets Ther. 2017;10:5337-53.
133. Carpenito C, Milone MC, Hassan R, Simonet JC, Lakhal M, Suhoski MM, et al. Control of large, established tumor xenografts with genetically retargeted human T cells containing CD28 and CD137 domains. Proc Natl Acad Sci U S A. 2009;106(9):3360-5.
134. Maus MV, Haas AR, Beatty GL, Albelda SM, Levine BL, Liu X, et al. T cells expressing chimeric antigen receptors can cause anaphylaxis in humans. Cancer Immunol Res. 2013;1(1):26-31.
135. Haas AR, Tanyi JL, O'Hara MH, Gladney WL, Lacey SF, Torigian DA, et al. Phase I Study of Lentiviral-Transduced Chimeric Antigen Receptor-Modified T Cells Recognizing Mesothelin in Advanced Solid Cancers. Mol Ther. 2019;27(11):1919-29.
136. Liu X, Onda M, Watson N, Hassan R, Ho M, Bera TK, et al. Highly active CAR T cells that bind to a juxtamembrane region of mesothelin and are not blocked by shed mesothelin. Proc Natl Acad Sci U S A. 2022;119(19):e2202439119.
137. Wang Z, Li N, Feng K, Chen M, Zhang Y, Liu Y, et al. Phase I study of CAR-T cells with PD-1 and TCR disruption in mesothelin-positive solid tumors. Cell Mol Immunol. 2021;18(9):2188-98.
138. Zhang X, Zhang C, Qiao M, Cheng C, Tang N, Lu S, et al. Depletion of BATF in CAR-T cells enhances antitumor activity by inducing resistance against exhaustion and formation of central memory cells. Cancer Cell. 2022;40(11):1407-22 e7.
139. Lanitis E, Poussin M, Klattenhoff AW, Song D, Sandaltzopoulos R, June CH, et al. Chimeric antigen receptor T Cells with dissociated signaling domains exhibit focused antitumor activity with reduced potential for toxicity in vivo. Cancer Immunol Res. 2013;1(1):43-53.
140. Liang Z, Dong J, Yang N, Li SD, Yang ZY, Huang R, et al. Tandem CAR-T cells targeting FOLR1 and MSLN enhance the antitumor effects in ovarian cancer. Int J Biol Sci. 2021;17(15):4365-76.
141. Feng Y, Xiao X, Zhu Z, Streaker E, Ho M, Pastan I, et al. A novel human monoclonal antibody that binds with high affinity to mesothelin-expressing cells and kills them by antibody-dependent cell-mediated cytotoxicity. Mol Cancer Ther. 2009;8(5):1113-8.
142. Chu GJ, Bailey CG, Nagarajah R, Liang O, Metierre C, Sagnella SM, et al. Mesothelin antigen density influences anti-mesothelin chimeric antigen receptor T cell cytotoxicity. Cytotherapy. 2024.
143. Adusumilli PS, Zauderer MG, Rivière I, Solomon SB, Rusch VW, O'Cearbhaill RE, et al. A phase I trial of regional mesothelin-targeted CAR T-cell therapy in patients with malignant pleural disease, in combination with the anti–PD-1 agent pembrolizumab. Cancer discovery. 2021;11(11):2748-63.
144. Haas AR, Golden RJ, Litzky LA, Engels B, Zhao L, Xu F, et al. Two cases of severe pulmonary toxicity from highly active mesothelin-directed CAR T cells. Mol Ther. 2023;31(8):2309-25.
145. Tanyi J, Haas A, Aggarwal C, O'Hara M, Lacey S, Golden R, et al. Phase I study of autologous T cells bearing fully-humanized chimeric antigen receptors targeting mesothelin in mesothelin- expressing cancers (314). Gynecologic Oncology. 2022;166:S164-S5.
146. Aznar MA, Good CR, Barber-Rotenberg JS, Agarwal S, Wilson W, Watts A, et al. Clinical and molecular dissection of CAR T cell resistance in pancreatic cancer. Cell Rep Med. 2025:102301.

147. Liu XF, Onda M, Schlomer J, Bassel L, Kozlov S, Tai CH, et al. Tumor resistance to anti-mesothelin CAR-T cells caused by binding to shed mesothelin is overcome by targeting a juxtamembrane epitope. Proc Natl Acad Sci U S A. 2024;121(4):e2317283121.
148. Tomar S, Zhang J, Khanal M, Hong J, Venugopalan A, Jiang Q, et al. Development of Highly Effective Anti-Mesothelin hYP218 Chimeric Antigen Receptor T Cells With Increased Tumor Infiltration and Persistence for Treating Solid Tumors. Mol Cancer Ther. 2022;21(7):1195-206.
149. Mir S, Venugopalan A, Zhang J, Nair NU, Sengupta M, Khanal M, et al. Persistence of activated anti-mesothelin hYP218 chimeric antigen receptor T cells in the tumour is associated with efficacy in gastric and colorectal carcinomas. Clin Transl Med. 2024;14(11):e70057.
150. Lan Y, Ni W, Tai G. Expression of MUC1 in different tumours and its clinical significance (Review). Mol Clin Oncol. 2022;17(6):161.
151. Chen W, Zhang Z, Zhang S, Zhu P, Ko JK, Yung KK. MUC1: Structure, Function, and Clinic Application in Epithelial Cancers. Int J Mol Sci. 2021;22(12).
152. Dhar P, McAuley J. The Role of the Cell Surface Mucin MUC1 as a Barrier to Infection and Regulator of Inflammation. Front Cell Infect Microbiol. 2019;9:117.
153. Yu LG. Cancer cell resistance to anoikis: MUC1 glycosylation comes to play. Cell Death Dis. 2017;8(7):e2962.
154. Beckwith DM, Cudic M. Tumor-associated O-glycans of MUC1: Carriers of the glyco-code and targets for cancer vaccine design. Semin Immunol. 2020;47:101389.
155. Thathiah A, Blobel CP, Carson DD. Tumor necrosis factor-alpha converting enzyme/ADAM 17 mediates MUC1 shedding. J Biol Chem. 2003;278(5):3386-94.
156. Maher J, Wilkie S, Davies DM, Arif S, Picco G, Julien S, et al. Targeting of Tumor-Associated Glycoforms of MUC1 with CAR T Cells. Immunity. 2016;45(5):945-6.
157. Wilkie S, Picco G, Foster J, Davies DM, Julien S, Cooper L, et al. Retargeting of human T cells to tumor-associated MUC1: the evolution of a chimeric antigen receptor. J Immunol. 2008;180(7):4901-9.
158. Lin Y, Chen S, Zhong S, An H, Yin H, McGowan E. 35O - Phase I clinical trial of PD-1 knockout anti-MUC1 CAR-T cells in the treatment of patients with non-small cell lung cancer. Annals of Oncology. 2019;30:xi12.
159. Chen S, Lin Y. Phase I clinical trial using a unique immunotherapeutic combination of MUC1-targeted CAR-T cells with PD-1-knockout in the treatment of patients with advanced esophageal cancer. Journal of Clinical Oncology. 2023;41(16_suppl):e16061-e.
160. You F, Jiang L, Zhang B, Lu Q, Zhou Q, Liao X, et al. Phase 1 clinical trial demonstrated that MUC1 positive metastatic seminal vesicle cancer can be effectively eradicated by modified Anti-MUC1 chimeric antigen receptor transduced T cells. Sci China Life Sci. 2016;59(4):386-97.
161. Burchell J, Gendler S, Taylor-Papadimitriou J, Girling A, Lewis A, Millis R, et al. Development and characterization of breast cancer reactive monoclonal antibodies directed to the core protein of the human milk mucin. Cancer Res. 1987;47(20):5476-82.
162. Posey AD, Jr., Schwab RD, Boesteanu AC, Steentoft C, Mandel U, Engels B, et al. Engineered CAR T Cells Targeting the Cancer-Associated Tn-Glycoform of the Membrane Mucin MUC1 Control Adenocarcinoma. Immunity. 2016;44(6):1444-54.
163. Macias-Leon J, Bermejo IA, Asin A, Garcia-Garcia A, Companon I, Jimenez-Moreno E, et al. Structural characterization of an unprecedented lectin-like antitumoral anti-MUC1 antibody. Chem Commun (Camb). 2020;56(96):15137-40.

164. Mao L, Su S, Li J, Yu S, Gong Y, Chen C, et al. Development of Engineered CAR T Cells Targeting Tumor-Associated Glycoforms of MUC1 for the Treatment of Intrahepatic Cholangiocarcinoma. J Immunother. 2023;46(3):89-95.
165. Ranoa DRE, Sharma P, Schane CP, Lewis AN, Valdez E, Marada V, et al. Single CAR-T cell treatment controls disseminated ovarian cancer in a syngeneic mouse model. J Immunother Cancer. 2023;11(5).
166. Lin Y, Yin H, Zhou C, Zhou L, Zeng Y, Yao H. Phase I clinical trial of MUC1-targeted CAR-T cells with PD-1-knockout in the treatment of advanced breast cancer. Journal of Clinical Oncology. 2024;42(16_suppl):1089-.
167. Smagghe BJ, Carter MG, Yi KR, Nash JSS, Grant TJ, Miller DS, et al. Effective CAR T-cell targeting of an MUC1 cleavage product. J Immunother Cancer. 2025;13(5).
168. Bamdad C, Stewart AK, Smagghe BJ, Glennie ND, Huang P, Moe S, et al. First-in-human CAR T for solid tumors targets the MUC1 transmembrane cleavage product. Cytotherapy. 2019;21(5, Supplement):S9.
169. Specht JM, Maloney DG, Yeung C, Wu V, Bamdad C. Phase I study of adoptive immunotherapy for advanced MUC1* positive breast cancer with autologous T cells engineered to express a chimeric antigen receptor, huMNC2-CAR44 specific for a cleaved form of MUC1 (MUC1*). Journal of Clinical Oncology. 2021;39(15_suppl):TPS2663-TPS.
170. Bamdad CC, Yuan Y, Specht JM, Stewart AK, Smagghe BJ, Lin SC-M, et al. Phase I/II first-in-human CAR T–targeting MUC1 transmembrane cleavage product (MUC1*) in patients with metastatic breast cancer. Journal of Clinical Oncology. 2022;40(16_suppl):TPS1130-TPS.
171. Eberlein TJ, Rosenstein M, Rosenberg SA. Regression of a disseminated syngeneic solid tumor by systemic transfer of lymphoid cells expanded in interleukin 2. J Exp Med. 1982;156(2):385-97.
172. Rosenberg SA, Packard BS, Aebersold PM, Solomon D, Topalian SL, Toy ST, et al. Use of tumor-infiltrating lymphocytes and interleukin-2 in the immunotherapy of patients with metastatic melanoma. A preliminary report. N Engl J Med. 1988;319(25):1676-80.
173. Betof Warner A, Hamid O, Komanduri K, Amaria R, Butler MO, Haanen J, et al. Expert consensus guidelines on management and best practices for tumor-infiltrating lymphocyte cell therapy. J Immunother Cancer. 2024;12(2).
174. Hong H, He Y, Li Y, Shen Y, Qu Y. Clinical trial landscape for TIL therapy: emerging insights and future directions in oncology. J Transl Med. 2024;22(1):1008.
175. Rosenberg SA, Yannelli JR, Yang JC, Topalian SL, Schwartzentruber DJ, Weber JS, et al. Treatment of patients with metastatic melanoma with autologous tumor-infiltrating lymphocytes and interleukin 2. J Natl Cancer Inst. 1994;86(15):1159-66.
176. Besser MJ, Itzhaki O, Ben-Betzalel G, Zippel DB, Zikich D, Kubi A, et al. Comprehensive single institute experience with melanoma TIL: Long term clinical results, toxicity profile, and prognostic factors of response. Mol Carcinog. 2020;59(7):736-44.
177. Dudley ME, Gross CA, Langhan MM, Garcia MR, Sherry RM, Yang JC, et al. CD8+ enriched "young" tumor infiltrating lymphocytes can mediate regression of metastatic melanoma. Clin Cancer Res. 2010;16(24):6122-31.
178. Olson D, Hong Y, Thomas SS, Martin-Liberal J, Finckenstein FG, Wu RX, et al. A phase 3 study (TILVANCE-301) to assess the efficacy and safety of lifileucel, an autologous tumor-infiltrating lymphocyte cell therapy, in combination with pembrolizumab compared with pembrolizumab alone in patients with untreated unresectable or metastatic melanoma. Journal of Clinical Oncology. 2023;41(16_suppl):TPS9607-TPS.

179. O'Malley D, Lee S, Psyrri A, Sukari A, Thomas S, Wenham R, et al. 492 Phase 2 efficacy and safety of autologous tumor-infiltrating lymphocyte (TIL) cell therapy in combination with pembrolizumab in immune checkpoint inhibitor-naïve patients with advanced cancers. Journal for ImmunoTherapy of Cancer. 2021;9(Suppl 2):A523-A4.
180. Rohaan MW, Borch TH, van den Berg JH, Met O, Kessels R, Geukes Foppen MH, et al. Tumor-Infiltrating Lymphocyte Therapy or Ipilimumab in Advanced Melanoma. N Engl J Med. 2022;387(23):2113-25.
181. Schoenfeld AJ, Lee SM, Doger de Speville B, Gettinger SN, Hafliger S, Sukari A, et al. Lifileucel, an Autologous Tumor-Infiltrating Lymphocyte Monotherapy, in Patients with Advanced Non-Small Cell Lung Cancer Resistant to Immune Checkpoint Inhibitors. Cancer Discov. 2024;14(8):1389-402.
182. Stevanovic S, Draper LM, Langhan MM, Campbell TE, Kwong ML, Wunderlich JR, et al. Complete regression of metastatic cervical cancer after treatment with human papillomavirus-targeted tumor-infiltrating T cells. J Clin Oncol. 2015;33(14):1543-50.
183. Anand J. Incidence and management of Cytokine release syndrome in CAR-T cell therapy for solid tumors: A systematic review of phase I trials. J Cancer Immunol Ther 2024; 7 (5): 235 1 J Cancer Immunol Ther 2024 Volume 7 Issue 5 Review Article https://www alliedacademies org/journal-cancer-immunology-therapy.
184. Olivera I, Etxeberria I, Luri-Rey C, Molero-Glez P, Melero I. Regional and intratumoral adoptive T-cell therapy. Immunooncol Technol. 2024;24:100715.
185. Sagnella SM, White AL, Yeo D, Saxena P, van Zandwijk N, Rasko JEJ. Locoregional delivery of CAR-T cells in the clinic. Pharmacol Res. 2022;182:106329.
186. Monje M, Mahdi J, Majzner R, Yeom KW, Schultz LM, Richards RM, et al. Intravenous and intracranial GD2-CAR T cells for H3K27M(+) diffuse midline gliomas. Nature. 2025;637(8046):708-15.
187. Choi BD, Gerstner ER, Frigault MJ, Leick MB, Mount CW, Balaj L, et al. Intraventricular CARv3-TEAM-E T Cells in Recurrent Glioblastoma. N Engl J Med. 2024;390(14):1290-8.
188. Vitanza NA, Johnson AJ, Wilson AL, Brown C, Yokoyama JK, Kunkele A, et al. Locoregional infusion of HER2-specific CAR T cells in children and young adults with recurrent or refractory CNS tumors: an interim analysis. Nat Med. 2021;27(9):1544-52.
189. Brown CE, Hibbard JC, Alizadeh D, Blanchard MS, Natri HM, Wang D, et al. Locoregional delivery of IL-13Ralpha2-targeting CAR-T cells in recurrent high-grade glioma: a phase 1 trial. Nat Med. 2024;30(4):1001-12.
190. Bagley SJ, Logun M, Fraietta JA, Wang X, Desai AS, Bagley LJ, et al. Intrathecal bivalent CAR T cells targeting EGFR and IL13Ralpha2 in recurrent glioblastoma: phase 1 trial interim results. Nat Med. 2024;30(5):1320-9.
191. Tchou J, Zhao Y, Levine BL, Zhang PJ, Davis MM, Melenhorst JJ, et al. Safety and Efficacy of Intratumoral Injections of Chimeric Antigen Receptor (CAR) T Cells in Metastatic Breast Cancer. Cancer Immunol Res. 2017;5(12):1152-61.
192. Uslu U, Castelli S, June CH. CAR T cell combination therapies to treat cancer. Cancer Cell. 2024;42(8):1319-25.
193. Bagley SJ, Binder ZA, Lamrani L, Marinari E, Desai AS, Nasrallah MP, et al. Repeated peripheral infusions of anti-EGFRvIII CAR T cells in combination with pembrolizumab show no efficacy in glioblastoma: a phase 1 trial. Nat Cancer. 2024;5(3):517-31.
194. Heczey A, Louis CU, Savoldo B, Dakhova O, Durett A, Grilley B, et al. CAR T Cells Administered in Combination with Lymphodepletion and PD-1 Inhibition to Patients with Neuroblastoma. Mol Ther. 2017;25(9):2214-24.

195. Ponterio E, Haas TL, De Maria R. Oncolytic virus and CAR-T cell therapy in solid tumors. Front Immunol. 2024;15:1455163.
196. Li YR, Lyu Z, Shen X, Fang Y, Yang L. Boosting CAR-T cell therapy through vaccine synergy. Trends Pharmacol Sci. 2025;46(2):180-99.
197. Tanyi JL, O'Hara MH, Hexner E, Marshall A, Jadlowsky J, Ferrara M, et al. 671 Phase 1 trial of human chimeric antigen receptor modified T cells (huCART-meso) administered in combination with oncolytic virus VCN-01 in patients with pancreatic and ovarian cancer. Journal for ImmunoTherapy of Cancer. 2023;11(Suppl 1):A760-A1.
198. Makawita S, Gibbs JM, McFadden DR, Porter C, Shaw AR, Robertson C, et al. Binary oncolytic adenovirus in combination with HER2-specific autologous CAR VST for treatment of advanced HER2-positive solid tumors (VISTA). Journal of Clinical Oncology. 2024;42(16_suppl):TPS2679-TPS.
199. Mackensen A, Haanen J, Koenecke C, Alsdorf W, Wagner-Drouet E, Borchmann P, et al. CLDN6-specific CAR-T cells plus amplifying RNA vaccine in relapsed or refractory solid tumors: the phase 1 BNT211-01 trial. Nat Med. 2023;29(11):2844-53.
200. Zhong XS, Matsushita M, Plotkin J, Riviere I, Sadelain M. Chimeric antigen receptors combining 4-1BB and CD28 signaling domains augment PI3kinase/AKT/Bcl-XL activation and CD8+ T cell-mediated tumor eradication. Mol Ther. 2010;18(2):413-20.
201. Guercio M, Orlando D, Di Cecca S, Sinibaldi M, Boffa I, Caruso S, et al. CD28.OX40 co-stimulatory combination is associated with long in vivo persistence and high activity of CAR.CD30 T-cells. Haematologica. 2021;106(4):987-99.
202. Goff SL, Morgan RA, Yang JC, Sherry RM, Robbins PF, Restifo NP, et al. Pilot Trial of Adoptive Transfer of Chimeric Antigen Receptor-transduced T Cells Targeting EGFRvIII in Patients With Glioblastoma. J Immunother. 2019;42(4):126-35.
203. Kaczanowska S, Murty T, Alimadadi A, Contreras CF, Duault C, Subrahmanyam PB, et al. Immune determinants of CAR-T cell expansion in solid tumor patients receiving GD2 CAR-T cell therapy. Cancer Cell. 2024;42(1):35-51 e8.
204. Pang N, Shi J, Qin L, Chen A, Tang Y, Yang H, et al. IL-7 and CCL19-secreting CAR-T cell therapy for tumors with positive glypican-3 or mesothelin. J Hematol Oncol. 2021;14(1):118.
205. Adachi K, Kano Y, Nagai T, Okuyama N, Sakoda Y, Tamada K. IL-7 and CCL19 expression in CAR-T cells improves immune cell infiltration and CAR-T cell survival in the tumor. Nat Biotechnol. 2018;36(4):346-51.
206. McGowan E, Lin Q, Ma G, Yin H, Chen S, Lin Y. PD-1 disrupted CAR-T cells in the treatment of solid tumors: Promises and challenges. Biomed Pharmacother. 2020;121:109625.
207. Foeng J, Comerford I, McColl SR. Harnessing the chemokine system to home CAR-T cells into solid tumors. Cell Rep Med. 2022;3(3):100543.
208. Grover N, Moore D, Ivanova A, Beaven AW, Dittus C, Cheng CJA, et al. CD30.CAR-T Cells Co-Expressing the CCR4 Chemokine Receptor in Relapsed/Refractory Hodgkin Lymphoma. Blood. 2024;144(Supplement 1):919-.
209. Flugel CL, Majzner RG, Krenciute G, Dotti G, Riddell SR, Wagner DL, et al. Overcoming on-target, off-tumour toxicity of CAR T cell therapy for solid tumours. Nat Rev Clin Oncol. 2023;20(1):49-62.
210. Gargett T, Brown MP. The inducible caspase-9 suicide gene system as a "safety switch" to limit on-target, off-tumor toxicities of chimeric antigen receptor T cells. Front Pharmacol. 2014;5:235.
211. Foster MC, Savoldo B, Lau W, Rubinos C, Grover N, Armistead P, et al. Utility of a safety switch to abrogate CD19.CAR T-cell-associated neurotoxicity. Blood. 2021;137(23):3306-9.

212. Hopewell EL, Cox C, Pilon-Thomas S, Kelley LL. Tumor-infiltrating lymphocytes: Streamlining a complex manufacturing process. Cytotherapy. 2019;21(3):307-14.
213. Turcotte S, Gros A, Hogan K, Tran E, Hinrichs CS, Wunderlich JR, et al. Phenotype and function of T cells infiltrating visceral metastases from gastrointestinal cancers and melanoma: implications for adoptive cell transfer therapy. J Immunol. 2013;191(5):2217-25.
214. Albarran Fernandez V, Ballestin Martinez P, Stoltenborg Granhoj J, Borch TH, Donia M, Marie Svane I. Biomarkers for response to TIL therapy: a comprehensive review. J Immunother Cancer. 2024;12(3).
215. Fix SM, Forget MA, Sakellariou-Thompson D, Wang Y, Griffiths TM, Lee M, et al. CRISPR-mediated TGFBR2 knockout renders human ovarian cancer tumor-infiltrating lymphocytes resistant to TGF-beta signaling. J Immunother Cancer. 2022;10(7).
216. Chamberlain CA, Bennett EP, Kverneland AH, Svane IM, Donia M, Met O. Highly efficient PD-1-targeted CRISPR-Cas9 for tumor-infiltrating lymphocyte-based adoptive T cell therapy. Mol Ther Oncolytics. 2022;24:417-28.
217. Palmer DC, Webber BR, Patel Y, Johnson MJ, Kariya CM, Lahr WS, et al. Internal checkpoint regulates T cell neoantigen reactivity and susceptibility to PD1 blockade. Med. 2022;3(10):682-704 e8.
218. Mills JK, Henderson MA, Giuffrida L, Petrone P, Westwood JA, Darcy PK, et al. Generating CAR T cells from tumor-infiltrating lymphocytes. Ther Adv Vaccines Immunother. 2021;9:25151355211017119.
219. Zhu C, Zhao Y, He J, Zhao H, Ni L, Cheng X, et al. TIL-Derived CAR T Cells Improve Immune Cell Infiltration and Survival in the Treatment of CD19-Humanized Mouse Colorectal Cancer. Cancers (Basel). 2023;15(23).
220. Etxeberria I, Bolanos E, Quetglas JI, Gros A, Villanueva A, Palomero J, et al. Intratumor Adoptive Transfer of IL-12 mRNA Transiently Engineered Antitumor CD8(+) T Cells. Cancer Cell. 2019;36(6):613-29 e7.
221. Zhang L, Morgan RA, Beane JD, Zheng Z, Dudley ME, Kassim SH, et al. Tumor-infiltrating lymphocytes genetically engineered with an inducible gene encoding interleukin-12 for the immunotherapy of metastatic melanoma. Clin Cancer Res. 2015;21(10):2278-88.
222. Forget MA, Tavera RJ, Haymaker C, Ramachandran R, Malu S, Zhang M, et al. A Novel Method to Generate and Expand Clinical-Grade, Genetically Modified, Tumor-Infiltrating Lymphocytes. Front Immunol. 2017;8:908.
223. Amaria RN, Haymaker CL, Bernatchez C, Forget M-A, Patel V, Hwu W-J, et al. A phase I/II study of lymphodepletion plus adoptive cell transfer (ACT) with T cells transduced with CXCR2 and NGFR followed by high dose interleukin-2 (IL-2) in patients with metastatic melanoma (MM). Journal of Clinical Oncology. 2016;34(15_suppl):TPS9594-TPS.
224. Ilic I, Ilic M. International patterns in incidence and mortality trends of pancreatic cancer in the last three decades: A joinpoint regression analysis. World J Gastroenterol. 2022;28(32):4698-715.
225. Loveday BPT, Lipton L, Thomson BN. Pancreatic cancer: An update on diagnosis and management. Aust J Gen Pract. 2019;48(12):826-31.
226. Sarantis P, Koustas E, Papadimitropoulou A, Papavassiliou AG, Karamouzis MV. Pancreatic ductal adenocarcinoma: Treatment hurdles, tumor microenvironment and immunotherapy. World J Gastrointest Oncol. 2020;12(2):173-81.
227. Hruban RH, Adsay NV, Albores-Saavedra J, Compton C, Garrett ES, Goodman SN, et al. Pancreatic intraepithelial neoplasia: a new nomenclature and classification system for pancreatic duct lesions. Am J Surg Pathol. 2001;25(5):579-86.

228. Muraki T, Jang KT, Reid MD, Pehlivanoglu B, Memis B, Basturk O, et al. Pancreatic ductal adenocarcinomas associated with intraductal papillary mucinous neoplasms (IPMNs) versus pseudo-IPMNs: relative frequency, clinicopathologic characteristics and differential diagnosis. Mod Pathol. 2022;35(1):96-105.
229. Bengtsson A, Andersson R, Ansari D. The actual 5-year survivors of pancreatic ductal adenocarcinoma based on real-world data. Sci Rep. 2020;10(1):16425.
230. Elbanna KY, Jang HJ, Kim TK. Imaging diagnosis and staging of pancreatic ductal adenocarcinoma: a comprehensive review. Insights Imaging. 2020;11(1):58.
231. Ansari D, Gustafsson A, Andersson R. Update on the management of pancreatic cancer: surgery is not enough. World J Gastroenterol. 2015;21(11):3157-65.
232. Kolbeinsson HM, Chandana S, Wright GP, Chung M. Pancreatic Cancer: A Review of Current Treatment and Novel Therapies. J Invest Surg. 2023;36(1):2129884.
233. Janssen QP, O'Reilly EM, van Eijck CHJ, Groot Koerkamp B. Neoadjuvant Treatment in Patients With Resectable and Borderline Resectable Pancreatic Cancer. Front Oncol. 2020;10:41.
234. Jan IS, Ch'ang HJ. Selection of patients with pancreatic adenocarcinoma who may benefit from radiotherapy. Radiat Oncol. 2023;18(1):137.
235. Cannone S, Greco MR, Carvalho TMA, Guizouarn H, Soriani O, Di Molfetta D, et al. Cancer Associated Fibroblast (CAF) Regulation of PDAC Parenchymal (CPC) and CSC Phenotypes Is Modulated by ECM Composition. Cancers (Basel). 2022;14(15).
236. Zhao J, Xiao Z, Li T, Chen H, Yuan Y, Wang YA, et al. Stromal Modulation Reverses Primary Resistance to Immune Checkpoint Blockade in Pancreatic Cancer. ACS Nano. 2018;12(10):9881-93.
237. Khan S, Ebeling MC, Chauhan N, Thompson PA, Gara RK, Ganju A, et al. Ormeloxifene suppresses desmoplasia and enhances sensitivity of gemcitabine in pancreatic cancer. Cancer Res. 2015;75(11):2292-304.
238. Perez VM, Kearney JF, Yeh JJ. The PDAC Extracellular Matrix: A Review of the ECM Protein Composition, Tumor Cell Interaction, and Therapeutic Strategies. Front Oncol. 2021;11:751311.
239. Mollenhauer J, Roether I, Kern HF. Distribution of extracellular matrix proteins in pancreatic ductal adenocarcinoma and its influence on tumor cell proliferation in vitro. Pancreas. 1987;2(1):14-24.
240. Ohlund D, Handly-Santana A, Biffi G, Elyada E, Almeida AS, Ponz-Sarvise M, et al. Distinct populations of inflammatory fibroblasts and myofibroblasts in pancreatic cancer. J Exp Med. 2017;214(3):579-96.
241. Huang H, Wang Z, Zhang Y, Pradhan RN, Ganguly D, Chandra R, et al. Mesothelial cell-derived antigen-presenting cancer-associated fibroblasts induce expansion of regulatory T cells in pancreatic cancer. Cancer Cell. 2022;40(6):656-73 e7.
242. Ozdemir BC, Pentcheva-Hoang T, Carstens JL, Zheng X, Wu CC, Simpson TR, et al. Depletion of carcinoma-associated fibroblasts and fibrosis induces immunosuppression and accelerates pancreas cancer with reduced survival. Cancer Cell. 2014;25(6):719-34.
243. Datta J, Dai X, Bianchi A, De Castro Silva I, Mehra S, Garrido VT, et al. Combined MEK and STAT3 Inhibition Uncovers Stromal Plasticity by Enriching for Cancer-Associated Fibroblasts With Mesenchymal Stem Cell-Like Features to Overcome Immunotherapy Resistance in Pancreatic Cancer. Gastroenterology. 2022;163(6):1593-612.

244. Provenzano PP, Cuevas C, Chang AE, Goel VK, Von Hoff DD, Hingorani SR. Enzymatic targeting of the stroma ablates physical barriers to treatment of pancreatic ductal adenocarcinoma. Cancer Cell. 2012;21(3):418-29.
245. Goulart MR, Stasinos K, Fincham REA, Delvecchio FR, Kocher HM. T cells in pancreatic cancer stroma. World J Gastroenterol. 2021;27(46):7956-68.
246. Siret C, Collignon A, Silvy F, Robert S, Cheyrol T, Andre P, et al. Deciphering the Crosstalk Between Myeloid-Derived Suppressor Cells and Regulatory T Cells in Pancreatic Ductal Adenocarcinoma. Front Immunol. 2019;10:3070.
247. Kemp SB, Carpenter ES, Steele NG, Donahue KL, Nwosu ZC, Pacheco A, et al. Apolipoprotein E Promotes Immune Suppression in Pancreatic Cancer through NF-kappaB-Mediated Production of CXCL1. Cancer Res. 2021;81(16):4305-18.
248. Xia Q, Jia J, Hu C, Lu J, Li J, Xu H, et al. Tumor-associated macrophages promote PD-L1 expression in tumor cells by regulating PKM2 nuclear translocation in pancreatic ductal adenocarcinoma. Oncogene. 2022;41(6):865-77.
249. Poh AR, Ernst M. Tumor-Associated Macrophages in Pancreatic Ductal Adenocarcinoma: Therapeutic Opportunities and Clinical Challenges. Cancers (Basel). 2021;13(12).
250. Luo H, Ikenaga N, Nakata K, Higashijima N, Zhong P, Kubo A, et al. Tumor-associated neutrophils upregulate Nectin2 expression, creating the immunosuppressive microenvironment in pancreatic ductal adenocarcinoma. J Exp Clin Cancer Res. 2024;43(1):258.
251. Zhang Y, Chandra V, Riquelme Sanchez E, Dutta P, Quesada PR, Rakoski A, et al. Interleukin-17-induced neutrophil extracellular traps mediate resistance to checkpoint blockade in pancreatic cancer. J Exp Med. 2020;217(12).
252. Apiz Saab JJ, Dzierozynski LN, Jonker PB, AminiTabrizi R, Shah H, Menjivar RE, et al. Pancreatic tumors exhibit myeloid-driven amino acid stress and upregulate arginine biosynthesis. Elife. 2023;12.
253. Geiger R, Rieckmann JC, Wolf T, Basso C, Feng Y, Fuhrer T, et al. L-Arginine Modulates T Cell Metabolism and Enhances Survival and Anti-tumor Activity. Cell. 2016;167(3):829-42 e13.
254. Mirlekar B, Michaud D, Lee SJ, Kren NP, Harris C, Greene K, et al. B cell-Derived IL35 Drives STAT3-Dependent CD8(+) T-cell Exclusion in Pancreatic Cancer. Cancer Immunol Res. 2020;8(3):292-308.
255. Mirlekar B, Michaud D, Searcy R, Greene K, Pylayeva-Gupta Y. IL35 Hinders Endogenous Antitumor T-cell Immunity and Responsiveness to Immunotherapy in Pancreatic Cancer. Cancer Immunol Res. 2018;6(9):1014-24.
256. Nicholl MB, Ledgewood CL, Chen X, Bai Q, Qin C, Cook KM, et al. IL-35 promotes pancreas cancer growth through enhancement of proliferation and inhibition of apoptosis: evidence for a role as an autocrine growth factor. Cytokine. 2014;70(2):126-33.
257. Tong DN, Guan J, Sun JH, Zhao CY, Chen SG, Zhang ZY, et al. Characterization of B cell-mediated PD-1/PD-L1 interaction in pancreatic cancer patients. Clin Exp Pharmacol Physiol. 2020;47(8):1342-9.
258. Gunderson AJ, Kaneda MM, Tsujikawa T, Nguyen AV, Affara NI, Ruffell B, et al. Bruton Tyrosine Kinase-Dependent Immune Cell Cross-talk Drives Pancreas Cancer. Cancer Discov. 2016;6(3):270-85.

259. Hiraoka N, Onozato K, Kosuge T, Hirohashi S. Prevalence of FOXP3+ regulatory T cells increases during the progression of pancreatic ductal adenocarcinoma and its premalignant lesions. Clin Cancer Res. 2006;12(18):5423-34.
260. Jang JE, Hajdu CH, Liot C, Miller G, Dustin ML, Bar-Sagi D. Crosstalk between Regulatory T Cells and Tumor-Associated Dendritic Cells Negates Anti-tumor Immunity in Pancreatic Cancer. Cell Rep. 2017;20(3):558-71.
261. Sivakumar S, Abu-Shah E, Ahern DJ, Arbe-Barnes EH, Jainarayanan AK, Mangal N, et al. Activated Regulatory T-Cells, Dysfunctional and Senescent T-Cells Hinder the Immunity in Pancreatic Cancer. Cancers (Basel). 2021;13(8).
262. Waddell N, Pajic M, Patch AM, Chang DK, Kassahn KS, Bailey P, et al. Whole genomes redefine the mutational landscape of pancreatic cancer. Nature. 2015;518(7540):495-501.
263. Kerepesi C, Bakacs T, Moss RW, Slavin S, Anderson CC. Significant association between tumor mutational burden and immune-related adverse events during immune checkpoint inhibition therapies. Cancer Immunol Immunother. 2020;69(5):683-7.
264. Hu HF, Ye Z, Qin Y, Xu XW, Yu XJ, Zhuo QF, et al. Mutations in key driver genes of pancreatic cancer: molecularly targeted therapies and other clinical implications. Acta Pharmacol Sin. 2021;42(11):1725-41.
265. Aoki H, Shichino S, Matsushima K, Ueha S. Revealing Clonal Responses of Tumor-Reactive T-Cells Through T Cell Receptor Repertoire Analysis. Front Immunol. 2022;13:807696.
266. Pandha H, Rigg A, John J, Lemoine N. Loss of expression of antigen-presenting molecules in human pancreatic cancer and pancreatic cancer cell lines. Clin Exp Immunol. 2007;148(1):127-35.
267. Lahusen A, Minhofer N, Lohse KA, Blechner C, Lindenmayer J, Eiseler T, et al. Pancreatic cancer cell-intrinsic transglutaminase-2 promotes T cell suppression through microtubule-dependent secretion of immunosuppressive cytokines. J Immunother Cancer. 2025;13(1).
268. Hamacher R, Schmid RM, Saur D, Schneider G. Apoptotic pathways in pancreatic ductal adenocarcinoma. Mol Cancer. 2008;7:64.
269. Joseph AM, Al Aiyan A, Al-Ramadi B, Singh SK, Kishore U. Innate and adaptive immune-directed tumour microenvironment in pancreatic ductal adenocarcinoma. Front Immunol. 2024;15:1323198.
270. Hassan R, Cohen SJ, Phillips M, Pastan I, Sharon E, Kelly RJ, et al. Phase I clinical trial of the chimeric anti-mesothelin monoclonal antibody MORAb-009 in patients with mesothelin-expressing cancers. Clin Cancer Res. 2010;16(24):6132-8.
271. Fujisaka Y, Kurata T, Tanaka K, Kudo T, Okamoto K, Tsurutani J, et al. Phase I study of amatuximab, a novel monoclonal antibody to mesothelin, in Japanese patients with advanced solid tumors. Invest New Drugs. 2015;33(2):380-8.
272. Lindenberg L, Thomas A, Adler S, Mena E, Kurdziel K, Maltzman J, et al. Safety and biodistribution of 111In-amatuximab in patients with mesothelin expressing cancers using single photon emission computed tomography-computed tomography (SPECT-CT) imaging. Oncotarget. 2015;6(6):4496-504.
273. Hassan R, Bullock S, Premkumar A, Kreitman RJ, Kindler H, Willingham MC, et al. Phase I study of SS1P, a recombinant anti-mesothelin immunotoxin given as a bolus I.V. infusion to patients with mesothelin-expressing mesothelioma, ovarian, and pancreatic cancers. Clin Cancer Res. 2007;13(17):5144-9.
274. Rottey S, Clarke J, Aung K, Machiels JP, Markman B, Heinhuis KM, et al. Phase I/IIa Trial of BMS-986148, an Anti-mesothelin Antibody-drug Conjugate, Alone or in Combination with Nivolumab in Patients with Advanced Solid Tumors. Clin Cancer Res. 2022;28(1):95-105.

275. Klampatsa A, Dimou V, Albelda SM. Mesothelin-targeted CAR-T cell therapy for solid tumors. Expert Opin Biol Ther. 2021;21(4):473-86.
276. Chu Q. Targeting Mesothelin in Solid Tumours: Anti-mesothelin Antibody and Drug Conjugates. Curr Oncol Rep. 2023;25(4):309-23.
277. Sherpally D, Manne A. Advancing Immunotherapy in Pancreatic Cancer: A Brief Review of Emerging Adoptive Cell Therapies. Cancers (Basel). 2025;17(4).
278. Hoehn RS, Rieser CJ, Choudry MH, Melnitchouk N, Hechtman J, Bahary N. Current Management of Appendiceal Neoplasms. Am Soc Clin Oncol Educ Book. 2021;41:1-15.
279. Holowatyj AN, Washington MK, Goldberg RM, Murphy CC. Birth Cohort Effects in Appendiceal Adenocarcinoma Incidence Across the United States. Ann Intern Med. 2025;178(7):957-62.
280. Chawrylak K, Lesniewska M, Mielniczek K, Sedlak K, Pelc Z, Kobialka S, et al. Current Status of Treatment among Patients with Appendiceal Tumors-Old Challenges and New Solutions? Cancers (Basel). 2024;16(5).
281. Strach MC, Sutherland S, Horvath LG, Mahon K. The role of chemotherapy in the treatment of advanced appendiceal cancers: summary of the literature and future directions. Ther Adv Med Oncol. 2022;14:17588359221112478.
282. Roxburgh CS, Fenig YM, Cercek A, Shia J, Rassam RM, Paty PB, et al. Outcomes of Low-Grade Appendiceal Mucinous Neoplasms with Remote Acellular Mucinous Peritoneal Deposits. Ann Surg Oncol. 2019;26(1):118-24.
283. Votanopoulos KI, Shen P, Skardal A, Levine EA. Peritoneal Metastases from Appendiceal Cancer. Surg Oncol Clin N Am. 2018;27(3):551-61.
284. Andjelkovic B, Stojanovic B, Stojanovic MD, Milosevic B, Cvetkovic A, Spasic M, et al. Appendiceal Signet Ring Cell Carcinoma: An Atypical Cause of Acute Appendicitis-A Case Study and Review of Current Knowledge. Diagnostics (Basel). 2023;13(14).
285. Palmer K, Weerasuriya S, Chandrakumaran K, Rous B, White BE, Paisey S, et al. Goblet Cell Adenocarcinoma of the Appendix: A Systematic Review and Incidence and Survival of 1,225 Cases From an English Cancer Registry. Front Oncol. 2022;12:915028.
286. Constantin M, Matanie C, Petrescu L, Bolocan A, Andronic O, Bleotu C, et al. Landscape of Genetic Mutations in Appendiceal Cancers. Cancers (Basel). 2023;15(14).
287. Raghav K, Shen JP, Jacome AA, Guerra JL, Scally CP, Taggart MW, et al. Integrated clinico-molecular profiling of appendiceal adenocarcinoma reveals a unique grade-driven entity distinct from colorectal cancer. Br J Cancer. 2020;123(8):1262-70.
288. Holowatyj AN, Eng C, Wen W, Idrees K, Guo X. Spectrum of Somatic Cancer Gene Variations Among Adults With Appendiceal Cancer by Age at Disease Onset. JAMA Netw Open. 2020;3(12):e2028644.
289. Ang CS, Shen JP, Hardy-Abeloos CJ, Huang JK, Ross JS, Miller VA, et al. Genomic Landscape of Appendiceal Neoplasms. JCO Precis Oncol. 2018;2.
290. Taggart MW, Galbincea J, Mansfield PF, Fournier KF, Royal RE, Overman MJ, et al. High-level microsatellite instability in appendiceal carcinomas. Am J Surg Pathol. 2013;37(8):1192-200.
291. Gunes BB, Hornstein NJ, Wang M, Yousef M, Fanaeian MM, Yousef A, et al. Single-cell RNA sequencing of appendiceal adenocarcinoma reveals a low proportion of epithelial cells and a fibroblast enriched tumor microenvironment. ESMO Gastrointestinal Oncology. 2024;6.
292. Ayala C, Sathe A, Bai X, Grimes SM, Shen J, Poultsides GA, et al. Distinct gene signatures define the epithelial cell features of mucinous appendiceal neoplasms and pseudomyxoma metastases. Front Genet. 2025;16:1536982.

293. Borazanci E, Millis SZ, Kimbrough J, Doll N, Von Hoff D, Ramanathan RK. Potential actionable targets in appendiceal cancer detected by immunohistochemistry, fluorescent in situ hybridization, and mutational analysis. J Gastrointest Oncol. 2017;8(1):164-72.
294. Yoon DH, Ibrahim A, Tatishchev S, Duldulao MPN, Lee SW, Shin J. Prevalence of mesothelin expression in peritoneal disease from colorectal and appendiceal cancers. J Surg Oncol. 2021;124(7):1091-7.
295. Yoon SO, Kim BH, Lee HS, Kang GH, Kim WH, Kim YA, et al. Differential protein immunoexpression profiles in appendiceal mucinous neoplasms: a special reference to classification and predictive factors. Mod Pathol. 2009;22(8):1102-12.
296. Shibahara H, Higashi M, Yokoyama S, Rousseau K, Kitazono I, Osako M, et al. A comprehensive expression analysis of mucins in appendiceal carcinoma in a multicenter study: MUC3 is a novel prognostic factor. PLoS One. 2014;9(12):e115613.
297. Holowatyj AN, Overman MJ, Votanopoulos KI, Lowy AM, Wagner P, Washington MK, et al. Defining a 'cells to society' research framework for appendiceal tumours. Nat Rev Cancer. 2025;25(4):293-315.
298. Bignell M, Carr NJ, Mohamed F. Pathophysiology and classification of pseudomyxoma peritonei. Pleura Peritoneum. 2016;1(1):3-13.
299. Strach MC, Yeung N, Lin H-M, Ansari N, Koh C, Shin J-S, et al. Characteristics of immune-infiltrating cells in the tumor microenvironment of appendiceal cancer with peritoneal disease. Journal of Clinical Oncology. 2023;41(4_suppl):217-.
300. Sagor MS, Islam T, Tamanna NT, Bappy MKI, Danishuddin, Haque MA, et al. The functional landscape of the appendix microbiome under conditions of health and disease. Gut Pathog. 2025;17(1):38.
301. Knotts C, Park H, Sherry C, Blodgett R, Lewis C, Omstead A, et al. Intra-Tumoral CD8+:CD3+ Lymphocyte Density Ratio in Appendix Cancer Is a Tumor Volume- and Grade-Independent Predictor of Survival. Cancers (Basel). 2025;17(3).
302. Ghelardi F, Raimondi A, Morano F, Randon G, Pannone A, Guaglio M, et al. Mytomicin-C, Metronomic Capecitabine, and Bevacizumab in Patients With Unresectable or Relapsed Pseudomyxoma Peritonei of Appendiceal Origin. Clin Colorectal Cancer. 2023;22(4):450-6 e1.
303. Shen JP, Yousef AM, Zeineddine FA, Zeineddine MA, Tidwell RS, Beaty KA, et al. Efficacy of Systemic Chemotherapy in Patients With Low-grade Mucinous Appendiceal Adenocarcinoma: A Randomized Crossover Trial. JAMA Netw Open. 2023;6(6):e2316161.
304. Pattalachinti VK, Haque E, Yousef M, Yousef A, Chowdhury S, Overman M, et al. BRAF mutant appendiceal adenocarcinoma differs from colorectal cancer but responds to BRAF-targeted therapy. NPJ Precis Oncol. 2025;9(1):38.
305. Weitz J, Nishizaki D, Liau J, Patel J, Ng I, Sun S, et al. Cyclin-Dependent Kinase 4/6 Inhibition as a Novel Therapy for Peritoneal Mucinous Carcinomatosis With GNAS Mutations. J Clin Oncol. 2025;43(6):705-15.
306. Ramanathan R, Choudry H, Jones H, Girgis M, Gooding W, Kalinski P, et al. Phase II Trial of Adjuvant Dendritic Cell Vaccine in Combination with Celecoxib, Interferon-alpha, and Rintatolimod in Patients Undergoing Cytoreductive Surgery and Hyperthermic Intraperitoneal Chemotherapy for Peritoneal Metastases. Ann Surg Oncol. 2021;28(8):4637-46.
307. Forsythe SD, Erali RA, Sasikumar S, Laney P, Shelkey E, D'Agostino R, Jr., et al. Organoid Platform in Preclinical Investigation of Personalized Immunotherapy Efficacy in Appendiceal Cancer: Feasibility Study. Clin Cancer Res. 2021;27(18):5141-50.
308. Votanopoulos KI, Mazzocchi A, Sivakumar H, Forsythe S, Aleman J, Levine EA, et al. Appendiceal Cancer Patient-Specific Tumor Organoid Model for Predicting Chemotherapy

Efficacy Prior to Initiation of Treatment: A Feasibility Study. Ann Surg Oncol. 2019;26(1):139-47.
309. Liu G, Xiao X, Xia Y, Huang W, Chen W, Xu J, et al. Organoids From Mucinous Appendiceal Adenocarcinomas as High-Fidelity Models for Individual Therapy. Front Med (Lausanne). 2022;9:829033.
310. Thapa R, Wilson GD. The Importance of CD44 as a Stem Cell Biomarker and Therapeutic Target in Cancer. Stem Cells Int. 2016;2016:2087204.
311. Yu G, Wang LG, Han Y, He QY. clusterProfiler: an R package for comparing biological themes among gene clusters. OMICS. 2012;16(5):284-7.
312. Love MI, Huber W, Anders S. Moderated estimation of fold change and dispersion for RNA-seq data with DESeq2. Genome Biol. 2014;15(12):550.
313. Hanzelmann S, Castelo R, Guinney J. GSVA: gene set variation analysis for microarray and RNA-seq data. BMC Bioinformatics. 2013;14:7.
314. Andreatta M, Corria-Osorio J, Müller S, Cubas R, Coukos G, Carmona SJ. Interpretation of T cell states from single-cell transcriptomics data using reference atlases. Nature Communications. 2021;12(1):2965.
315. Jiang P, Zhang Y, Ru B, Yang Y, Vu T, Paul R, et al. Systematic investigation of cytokine signaling activity at the tissue and single-cell levels. Nature Methods. 2021;18(10):1181-91.
316. Zhang Z, Luo D, Zhong X, Choi JH, Ma Y, Wang S, et al. SCINA: A Semi-Supervised Subtyping Algorithm of Single Cells and Bulk Samples. Genes (Basel). 2019;10(7).
317. Hao Y, Hao S, Andersen-Nissen E, Mauck WM, 3rd, Zheng S, Butler A, et al. Integrated analysis of multimodal single-cell data. Cell. 2021;184(13):3573-87 e29.
318. Andreatta M, Carmona SJ. UCell: Robust and scalable single-cell gene signature scoring. Computational and Structural Biotechnology Journal. 2021;19:3796-8.
319. Quinlan AR, Hall IM. BEDTools: a flexible suite of utilities for comparing genomic features. Bioinformatics. 2010;26(6):841-2.
320. Dobin A, Davis CA, Schlesinger F, Drenkow J, Zaleski C, Jha S, et al. STAR: ultrafast universal RNA-seq aligner. Bioinformatics. 2013;29(1):15-21.
321. Liao Y, Smyth GK, Shi W. featureCounts: an efficient general purpose program for assigning sequence reads to genomic features. Bioinformatics. 2014;30(7):923-30.
322. Leek JT, Johnson WE, Parker HS, Jaffe AE, Storey JD. The sva package for removing batch effects and other unwanted variation in high-throughput experiments. Bioinformatics. 2012;28(6):882-3.
323. Li J, Byrne KT, Yan F, Yamazoe T, Chen Z, Baslan T, et al. Tumor Cell-Intrinsic Factors Underlie Heterogeneity of Immune Cell Infiltration and Response to Immunotherapy. Immunity. 2018;49(1):178-93 e7.
324. Yan M, Hu J, Ping Y, Xu L, Liao G, Jiang Z, et al. Single-Cell Transcriptomic Analysis Reveals a Tumor-Reactive T Cell Signature Associated With Clinical Outcome and Immunotherapy Response In Melanoma. Front Immunol. 2021;12:758288.
325. Li T, Fu J, Zeng Z, Cohen D, Li J, Chen Q, et al. TIMER2.0 for analysis of tumor-infiltrating immune cells. Nucleic Acids Res. 2020;48(W1):W509-W14.
326. Peng J, Sun BF, Chen CY, Zhou JY, Chen YS, Chen H, et al. Single-cell RNA-seq highlights intra-tumoral heterogeneity and malignant progression in pancreatic ductal adenocarcinoma. Cell Res. 2019;29(9):725-38.
327. Cheng S, Li Z, Gao R, Xing B, Gao Y, Yang Y, et al. A pan-cancer single-cell transcriptional atlas of tumor infiltrating myeloid cells. Cell. 2021;184(3):792-809.e23.

328. Chu GJ, Linton A, Kao S, Klebe S, Adelstein S, Yeo D, et al. High mesothelin expression by immunohistochemistry predicts improved survival in pleural mesothelioma. Histopathology. 2023;83(2):202-10.
329. Hendry S, Salgado R, Gevaert T, Russell PA, John T, Thapa B, et al. Assessing Tumor-infiltrating Lymphocytes in Solid Tumors: A Practical Review for Pathologists and Proposal for a Standardized Method From the International Immunooncology Biomarkers Working Group: Part 1: Assessing the Host Immune Response, TILs in Invasive Breast Carcinoma and Ductal Carcinoma In Situ, Metastatic Tumor Deposits and Areas for Further Research. Adv Anat Pathol. 2017;24(5):235-51.
330. Cattaneo CM, Dijkstra KK, Fanchi LF, Kelderman S, Kaing S, van Rooij N, et al. Tumor organoid-T-cell coculture systems. Nat Protoc. 2020;15(1):15-39.
331. Cerignoli F, Abassi YA, Lamarche BJ, Guenther G, Santa Ana D, Guimet D, et al. In vitro immunotherapy potency assays using real-time cell analysis. PLoS One. 2018;13(3):e0193498.
332. Limame R, Wouters A, Pauwels B, Fransen E, Peeters M, Lardon F, et al. Comparative analysis of dynamic cell viability, migration and invasion assessments by novel real-time technology and classic endpoint assays. PLoS One. 2012;7(10):e46536.
333. Hothorn T, Lausen B. On the exact distribution of maximally selected rank statistics. Comput Stat Data Anal. 2003;43(2):121–37.
334. Nagata K, Shinto E, Shiraishi T, Yamadera M, Kajiwara Y, Mochizuki S, et al. Mesothelin Expression is Correlated with Chemoresistance in Stage IV Colorectal Cancer. Ann Surg Oncol. 2021;28(13):8579-86.
335. Shiraishi T, Shinto E, Mochizuki S, Tsuda H, Kajiwara Y, Okamoto K, et al. Mesothelin expression has prognostic value in stage IotaIota/IotaIotaIota colorectal cancer. Virchows Arch. 2019;474(3):297-307.
336. Magalhaes I, Fernebro J, Abd Own S, Glaessgen D, Corvigno S, Remberger M, et al. Mesothelin Expression in Patients with High-Grade Serous Ovarian Cancer Does Not Predict Clinical Outcome But Correlates with CD11c(+) Expression in Tumor. Adv Ther. 2020;37(12):5023-31.
337. Cheng WF, Huang CY, Chang MC, Hu YH, Chiang YC, Chen YL, et al. High mesothelin correlates with chemoresistance and poor survival in epithelial ovarian carcinoma. Br J Cancer. 2009;100(7):1144-53.
338. Li YR, Xian RR, Ziober A, Conejo-Garcia J, Perales-Puchalt A, June CH, et al. Mesothelin expression is associated with poor outcomes in breast cancer. Breast Cancer Res Treat. 2014;147(3):675-84.
339. Parinyanitikul N, Blumenschein GR, Wu Y, Lei X, Chavez-Macgregor M, Smart M, et al. Mesothelin expression and survival outcomes in triple receptor negative breast cancer. Clin Breast Cancer. 2013;13(5):378-84.
340. Baba K, Ishigami S, Arigami T, Uenosono Y, Okumura H, Matsumoto M, et al. Mesothelin expression correlates with prolonged patient survival in gastric cancer. J Surg Oncol. 2012;105(2):195-9.
341. Han SH, Joo M, Kim H, Chang S. Mesothelin Expression in Gastric Adenocarcinoma and Its Relation to Clinical Outcomes. J Pathol Transl Med. 2017;51(2):122-8.
342. Thomas A, Chen Y, Steinberg SM, Luo J, Pack S, Raffeld M, et al. High mesothelin expression in advanced lung adenocarcinoma is associated with KRAS mutations and a poor prognosis. Oncotarget. 2015;6(13):11694-703.
343. Kachala SS, Bograd AJ, Villena-Vargas J, Suzuki K, Servais EL, Kadota K, et al. Mesothelin overexpression is a marker of tumor aggressiveness and is associated with reduced

recurrence-free and overall survival in early-stage lung adenocarcinoma. Clin Cancer Res. 2014;20(4):1020-8.
344. Roe OD, Creaney J, Lundgren S, Larsson E, Sandeck H, Boffetta P, et al. Mesothelin-related predictive and prognostic factors in malignant mesothelioma: a nested case-control study. Lung Cancer. 2008;61(2):235-43.
345. Montemagno C, Cassim S, Trichanh D, Savary C, Pouyssegur J, Pages G, et al. (99m)Tc-A1 as a Novel Imaging Agent Targeting Mesothelin-Expressing Pancreatic Ductal Adenocarcinoma. Cancers (Basel). 2019;11(10).
346. Hagerty BL, Oshi M, Endo I, Takabe K. High Mesothelin expression in pancreatic adenocarcinoma is associated with aggressive tumor features but not prognosis. Am J Cancer Res. 2023;13(9):4235-45.
347. Einama T, Kamachi H, Nishihara H, Homma S, Kanno H, Takahashi K, et al. Co-expression of mesothelin and CA125 correlates with unfavorable patient outcome in pancreatic ductal adenocarcinoma. Pancreas. 2011;40(8):1276-82.
348. Winter JM, Tang LH, Klimstra DS, Brennan MF, Brody JR, Rocha FG, et al. A novel survival-based tissue microarray of pancreatic cancer validates MUC1 and mesothelin as biomarkers. PLoS One. 2012;7(7):e40157.
349. Le K, Wang J, Zhang T, Guo Y, Chang H, Wang S, et al. Overexpression of Mesothelin in Pancreatic Ductal Adenocarcinoma (PDAC). Int J Med Sci. 2020;17(4):422-7.
350. Li Y, Tian W, Zhang H, Zhang Z, Zhao Q, Chang L, et al. MSLN Correlates With Immune Infiltration and Chemoresistance as a Prognostic Biomarker in Ovarian Cancer. Front Oncol. 2022;12:830570.
351. Malla M, Deshmukh SK, Wu S, Samec T, Olevian DC, El Naili R, et al. Mesothelin expression correlates with elevated inhibitory immune activity in patients with colorectal cancer. Cancer Gene Ther. 2024;31(10):1547-58.
352. LaPlante EL, Liu D, Petrosyan V, Yao Q, Milosavljevic A. XDec-CHI reveals immunosuppressive interactions in pancreatic ductal adenocarcinoma. iScience. 2022;25(10):105249.
353. Chan-Seng-Yue M, Kim JC, Wilson GW, Ng K, Figueroa EF, O'Kane GM, et al. Transcription phenotypes of pancreatic cancer are driven by genomic events during tumor evolution. Nat Genet. 2020;52(2):231-40.
354. Sun D, Tan L, Chen Y, Yuan Q, Jiang K, Liu Y, et al. CXCL5 impedes CD8(+) T cell immunity by upregulating PD-L1 expression in lung cancer via PXN/AKT signaling phosphorylation and neutrophil chemotaxis. J Exp Clin Cancer Res. 2024;43(1):202.
355. Chistiakov DA, Killingsworth MC, Myasoedova VA, Orekhov AN, Bobryshev YV. CD68/macrosialin: not just a histochemical marker. Lab Invest. 2017;97(1):4-13.
356. Inaguma S, Wang Z, Lasota J, Onda M, Czapiewski P, Langfort R, et al. Comprehensive immunohistochemical study of mesothelin (MSLN) using different monoclonal antibodies 5B2 and MN-1 in 1562 tumors with evaluation of its prognostic value in malignant pleural mesothelioma. Oncotarget. 2017;8(16):26744-54.
357. Meyerhoff RR, Yang CF, Speicher PJ, Gulack BC, Hartwig MG, D'Amico TA, et al. Impact of mesothelioma histologic subtype on outcomes in the Surveillance, Epidemiology, and End Results database. J Surg Res. 2015;196(1):23-32.
358. Johnston FM, Tan MC, Tan BR, Jr., Porembka MR, Brunt EM, Linehan DC, et al. Circulating mesothelin protein and cellular antimesothelin immunity in patients with pancreatic cancer. Clin Cancer Res. 2009;15(21):6511-8.

359. Staveley-O'Carroll K, Sotomayor E, Montgomery J, Borrello I, Hwang L, Fein S, et al. Induction of antigen-specific T cell anergy: An early event in the course of tumor progression. Proc Natl Acad Sci U S A. 1998;95(3):1178-83.
360. Sun C, Mezzadra R, Schumacher TN. Regulation and Function of the PD-L1 Checkpoint. Immunity. 2018;48(3):434-52.
361. Rantakari P, Auvinen K, Jappinen N, Kapraali M, Valtonen J, Karikoski M, et al. The endothelial protein PLVAP in lymphatics controls the entry of lymphocytes and antigens into lymph nodes. Nat Immunol. 2015;16(4):386-96.
362. Keuschnigg J, Henttinen T, Auvinen K, Karikoski M, Salmi M, Jalkanen S. The prototype endothelial marker PAL-E is a leukocyte trafficking molecule. Blood. 2009;114(2):478-84.
363. Denzer L, Muranyi W, Schroten H, Schwerk C. The role of PLVAP in endothelial cells. Cell Tissue Res. 2023;392(2):393-412.
364. Zhong Y, Wang Y, Wang C, Cao K, Wang X, Xu X, et al. Targeting mesothelin-CD24 axis repolarizes tumor-associated macrophages to potentiate PD-1 blockade therapy in high-grade serous ovarian cancer. J Immunother Cancer. 2025;13(2).
365. Aran D, Hu Z, Butte AJ. xCell: digitally portraying the tissue cellular heterogeneity landscape. Genome Biol. 2017;18(1):220.
366. Qualiotto AN, Baldavira CM, Balancin M, Ab'Saber A, Takagaki T, Capelozzi VL. Mesothelin expression remodeled the immune-matrix tumor microenvironment predicting the risk of death in patients with malignant pleural mesothelioma. Front Immunol. 2023;14:1268927.
367. Malla M, Deshkmukh SK, Wu S, Samec T, Olevian D, Naili R, et al. Mesothelin expression correlates with elevated inhibitory immune activity in patients with colorectal cancer. 2023.
368. Adusumilli PS, Zauderer MG, Riviere I, Solomon SB, Rusch VW, O'Cearbhaill RE, et al. A Phase I Trial of Regional Mesothelin-Targeted CAR T-cell Therapy in Patients with Malignant Pleural Disease, in Combination with the Anti-PD-1 Agent Pembrolizumab. Cancer Discov. 2021;11(11):2748-63.
369. Adusumilli PS, Cherkassky L, Villena-Vargas J, Colovos C, Servais E, Plotkin J, et al. Regional delivery of mesothelin-targeted CAR T cell therapy generates potent and long-lasting CD4-dependent tumor immunity. Science translational medicine. 2014;6(261):261ra151.
370. Kaur J, Jaruvongvanich V, Chandrasekhara V. Endoscopic ultrasound-guided injectable therapy for pancreatic cancer: A systematic review. World J Gastroenterol. 2022;28(21):2383-95.
371. Chang KJ, Nguyen PT, Thompson JA, Kurosaki TT, Casey LR, Leung EC, et al. Phase I clinical trial of allogeneic mixed lymphocyte culture (cytoimplant) delivered by endoscopic ultrasound-guided fine-needle injection in patients with advanced pancreatic carcinoma. Cancer. 2000;88(6):1325-35.
372. Beatty GL, Haas AR, Maus MV, Torigian DA, Soulen MC, Plesa G, et al. Mesothelin-specific chimeric antigen receptor mRNA-engineered T cells induce anti-tumor activity in solid malignancies. Cancer Immunol Res. 2014;2(2):112-20.
373. Lesch S, Blumenberg V, Stoiber S, Gottschlich A, Ogonek J, Cadilha BL, et al. T cells armed with C-X-C chemokine receptor type 6 enhance adoptive cell therapy for pancreatic tumours. Nat Biomed Eng. 2021;5(11):1246-60.
374. Li XN, Wang F, Chen K, Wu Z, Zhang R, Xiao C, et al. XCL1-secreting CEA CAR-T cells enhance endogenous CD8(+) T cell responses to tumor neoantigens to confer a long-term antitumor immunity. J Immunother Cancer. 2025;13(1).

375. Yamaguchi Y, Gibson J, Ou K, Lopez LS, Ng RH, Leggett N, et al. PD-L1 blockade restores CAR T cell activity through IFN-gamma-regulation of CD163+ M2 macrophages. J Immunother Cancer. 2022;10(6).
376. Zhu Y, Knolhoff BL, Meyer MA, Nywening TM, West BL, Luo J, et al. CSF1/CSF1R blockade reprograms tumor-infiltrating macrophages and improves response to T-cell checkpoint immunotherapy in pancreatic cancer models. Cancer Res. 2014;74(18):5057-69.
377. Chmielewski M, Kopecky C, Hombach AA, Abken H. IL-12 release by engineered T cells expressing chimeric antigen receptors can effectively Muster an antigen-independent macrophage response on tumor cells that have shut down tumor antigen expression. Cancer Res. 2011;71(17):5697-706.
378. Hou AJ, Shih RM, Uy BR, Shafer A, Chang ZL, Comin-Anduix B, et al. IL-13Ralpha2/TGF-beta bispecific CAR-T cells counter TGF-beta-mediated immune suppression and potentiate anti-tumor responses in glioblastoma. Neuro Oncol. 2024;26(10):1850-66.
379. Joseph RW, Peddareddigari VR, Liu P, Miller PW, Overwijk WW, Bekele NB, et al. Impact of clinical and pathologic features on tumor-infiltrating lymphocyte expansion from surgically excised melanoma metastases for adoptive T-cell therapy. Clin Cancer Res. 2011;17(14):4882-91.
380. Choi S, Hossain M, Lee H, Baek J, Park HS, Lim CL, et al. Expansion of tumor-infiltrating lymphocytes from head and neck squamous cell carcinoma to assess the potential of adoptive cell therapy. Cancer Immunol Immunother. 2024;73(6):101.
381. Lee HJ, Kim YA, Sim CK, Heo SH, Song IH, Park HS, et al. Expansion of tumor-infiltrating lymphocytes and their potential for application as adoptive cell transfer therapy in human breast cancer. Oncotarget. 2017;8(69):113345-59.
382. Poschke IC, Hassel JC, Rodriguez-Ehrenfried A, Lindner KAM, Heras-Murillo I, Appel LM, et al. The Outcome of Ex Vivo TIL Expansion Is Highly Influenced by Spatial Heterogeneity of the Tumor T-Cell Repertoire and Differences in Intrinsic In Vitro Growth Capacity between T-Cell Clones. Clin Cancer Res. 2020;26(16):4289-301.
383. Kvistborg P, Shu CJ, Heemskerk B, Fankhauser M, Thrue CA, Toebes M, et al. TIL therapy broadens the tumor-reactive CD8(+) T cell compartment in melanoma patients. Oncoimmunology. 2012;1(4):409-18.
384. Hall M, Liu H, Malafa M, Centeno B, Hodul PJ, Pimiento J, et al. Expansion of tumor-infiltrating lymphocytes (TIL) from human pancreatic tumors. J Immunother Cancer. 2016;4:61.
385. Niedergang F, Hemar A, Hewitt CR, Owen MJ, Dautry-Varsat A, Alcover A. The Staphylococcus aureus enterotoxin B superantigen induces specific T cell receptor down-regulation by increasing its internalization. J Biol Chem. 1995;270(21):12839-45.
386. Chang K, Pastan I. Molecular cloning of mesothelin, a differentiation antigen present on mesothelium, mesotheliomas, and ovarian cancers. Proc Natl Acad Sci U S A. 1996;93(1):136-40.
387. Chowdhury PS, Pastan I. Improving antibody affinity by mimicking somatic hypermutation in vitro. Nat Biotechnol. 1999;17(6):568-72.
388. Li F, Choudhuri K. Membrane positioning across antigen-induced synaptic contacts tunes CAR-T cell signaling and effector responses. bioRxiv. 2023.
389. Watanabe K, Terakura S, Martens AC, van Meerten T, Uchiyama S, Imai M, et al. Target antigen density governs the efficacy of anti-CD20-CD28-CD3 zeta chimeric antigen receptor-modified effector CD8+ T cells. J Immunol. 2015;194(3):911-20.

390. Mavanur AA, Parimi V, O'Malley M, Nikiforova M, Bartlett DL, Davison JM. Establishment and characterization of a murine xenograft model of appendiceal mucinous adenocarcinoma. Int J Exp Pathol. 2010;91(4):357-67.
391. Dohan A, Lousquy R, Eveno C, Goere D, Broqueres-You D, Kaci R, et al. Orthotopic animal model of pseudomyxoma peritonei: An in vivo model to test anti-angiogenic drug effects. Am J Pathol. 2014;184(7):1920-9.
392. Martinez-Quintanilla J, Cabot D, Sabia D, Arques O, Group PM, Verges J, et al. Precision Oncology and Systemic Targeted Therapy in Pseudomyxoma Peritonei. Clin Cancer Res. 2024;30(18):4082-99.
393. Flatmark K, Reed W, Halvorsen T, Sorensen O, Wiig JN, Larsen SG, et al. Pseudomyxoma peritonei--two novel orthotopic mouse models portray the PMCA-I histopathologic subtype. BMC Cancer. 2007;7:116.
394. Dilly AK, Honick BD, Lee YJ, Guo ZS, Zeh HJ, Bartlett DL, et al. Targeting G-protein coupled receptor-related signaling pathway in a murine xenograft model of appendiceal pseudomyxoma peritonei. Oncotarget. 2017;8(63):106888-900.
395. Duggan WP, Kisakol B, O'Connell E, Matveeva A, O'Grady T, McDonough E, et al. Multiplexed Immunofluorescence Imaging Reveals an Immune-Rich Tumor Microenvironment in Mucinous Rectal Cancer Characterized by Increased Lymphocyte Infiltration and Enhanced Programmed Cell Death Protein 1 Expression. Dis Colon Rectum. 2023;66(7):914-22.
396. Tokatlian T, Asuelime GE, Mock J-Y, DiAndreth B, Sharma S, Toledo Warshaviak D, et al. Mesothelin-specific CAR-T cell therapy that incorporates an HLA-gated safety mechanism selectively kills tumor cells. Journal for immunotherapy of cancer. 2022;10(1).
397. Lee DH, Choi S, Park Y, Jin HS. Mucin1 and Mucin16: Therapeutic Targets for Cancer Therapy. Pharmaceuticals (Basel). 2021;14(10).
398. Wajih N, Erali RA, Forsythe SD, Schaaf CR, Shen P, Levine EA, et al. Enhancing the Efficacy of HIPEC Through Bromelain: A Preclinical Investigation in Appendiceal Cancer. Ann Surg Oncol. 2024;31(8):5377-89.
399. Dilly AK, Honick BD, Frederick R, Elapavaluru A, Velankar S, Makala H, et al. Improved chemosensitivity following mucolytic therapy in patient-derived models of mucinous appendix cancer. Transl Res. 2021;229:100-14.
400. Kongkaew T, Thaiwong R, Tudsamran S, Sae-Jung T, Sengprasert P, Vasuratna A, et al. TIL expansion with high dose IL-2 or low dose IL-2 with anti-CD3/anti-CD28 stimulation provides different quality of TIL-expanded T cell clones. J Immunol Methods. 2022;503:113229.
401. Khamzina Y, King MC, Nieroda C, Merrell DS, Sardi A, Gushchin V. The Role of Microorganisms in Appendiceal Pseudomyxoma Peritonei: A Review. Curr Oncol. 2022;29(5):3576-84.
402. Liang F, Rezapour A, Falk P, Angenete E, Yrlid U. Cryopreservation of Whole Tumor Biopsies from Rectal Cancer Patients Enable Phenotypic and In Vitro Functional Evaluation of Tumor-Infiltrating T Cells. Cancers (Basel). 2021;13(10).
403. Onimus K, Wells A, Herman C, Tawashi A, Long G, Scolyer R, et al. Successful Manufacturing of Tumor-Infiltrating Lymphocyte (TIL) Cell Therapy from Cryopreserved Melanoma Tumors Shipped from Australia. Transplantation and Cellular Therapy. 2022;28:S226-S7.
404. Li R, Johnson R, Yu G, McKenna DH, Hubel A. Preservation of cell-based immunotherapies for clinical trials. Cytotherapy. 2019;21(9):943-57.

405. Wang S, Sun J, Chen K, Ma P, Lei Q, Xing S, et al. Perspectives of tumor-infiltrating lymphocyte treatment in solid tumors. BMC Med. 2021;19(1):140.
406. Liu Y, Zhou N, Zhou L, Wang J, Zhou Y, Zhang T, et al. IL-2 regulates tumor-reactive CD8(+) T cell exhaustion by activating the aryl hydrocarbon receptor. Nat Immunol. 2021;22(3):358-69.
407. Thomas D, Dauwalder O, Brun V, Badiou C, Ferry T, Etienne J, et al. Staphylococcus aureus superantigens elicit redundant and extensive human Vbeta patterns. Infect Immun. 2009;77(5):2043-50.
408. Ai W, Li H, Song N, Li L, Chen H. Optimal method to stimulate cytokine production and its use in immunotoxicity assessment. Int J Environ Res Public Health. 2013;10(9):3834-42.
409. Mirlekar B. Tumor promoting roles of IL-10, TGF-beta, IL-4, and IL-35: Its implications in cancer immunotherapy. SAGE Open Med. 2022;10:20503121211069012.
410. Amicarella F, Muraro MG, Hirt C, Cremonesi E, Padovan E, Mele V, et al. Dual role of tumour-infiltrating T helper 17 cells in human colorectal cancer. Gut. 2017;66(4):692-704.
411. Jost E, Mack LA, Sideris L, Dube P, Temple W, Bouchard-Fortier A. Evaluation of repeat cytoreductive surgery and heated intraperitoneal chemotherapy for patients with recurrent peritoneal carcinomatosis from appendiceal and colorectal cancers: a multicentre Canadian study. Can J Surg. 2020;63(1):E71-E9.
412. Navarro Rodrigo B, Ortiz Miranda Y, Corria-Osorio J, Coukos G, Harari A. Immune correlates and mechanisms of TIL therapy efficacy: current insights and knowledge gaps. Trends Cancer. 2025.
413. Jacob F, Ming GL, Song H. Generation and biobanking of patient-derived glioblastoma organoids and their application in CAR T cell testing. Nat Protoc. 2020;15(12):4000-33.
414. Zhou G, Lieshout R, van Tienderen GS, de Ruiter V, van Royen ME, Boor PPC, et al. Modelling immune cytotoxicity for cholangiocarcinoma with tumour-derived organoids and effector T cells. Br J Cancer. 2022;127(4):649-60.
415. Strijker JGM, Pscheid R, Drent E, van der Hoek JJF, Koopmans B, Ober K, et al. alphabeta-T Cells Engineered to Express gammadelta-T Cell Receptors Can Kill Neuroblastoma Organoids Independent of MHC-I Expression. J Pers Med. 2021;11(9).
416. Zhou Z, Van der Jeught K, Li Y, Sharma S, Yu T, Moulana I, et al. A T Cell-Engaging Tumor Organoid Platform for Pancreatic Cancer Immunotherapy. Adv Sci (Weinh). 2023;10(23):e2300548.
417. Yeo D, Giardina C, Saxena P, Rasko JEJ. The next wave of cellular immunotherapies in pancreatic cancer. Mol Ther Oncolytics. 2022;24:561-76.
418. Wu G, Standring OJ, King DA, Gholami S, Devoe CE, Thiels CA, et al. Management of Peritoneal Metastasis in Patients with Pancreatic Ductal Adenocarcinoma. Curr Oncol. 2025;32(2).

Appendix

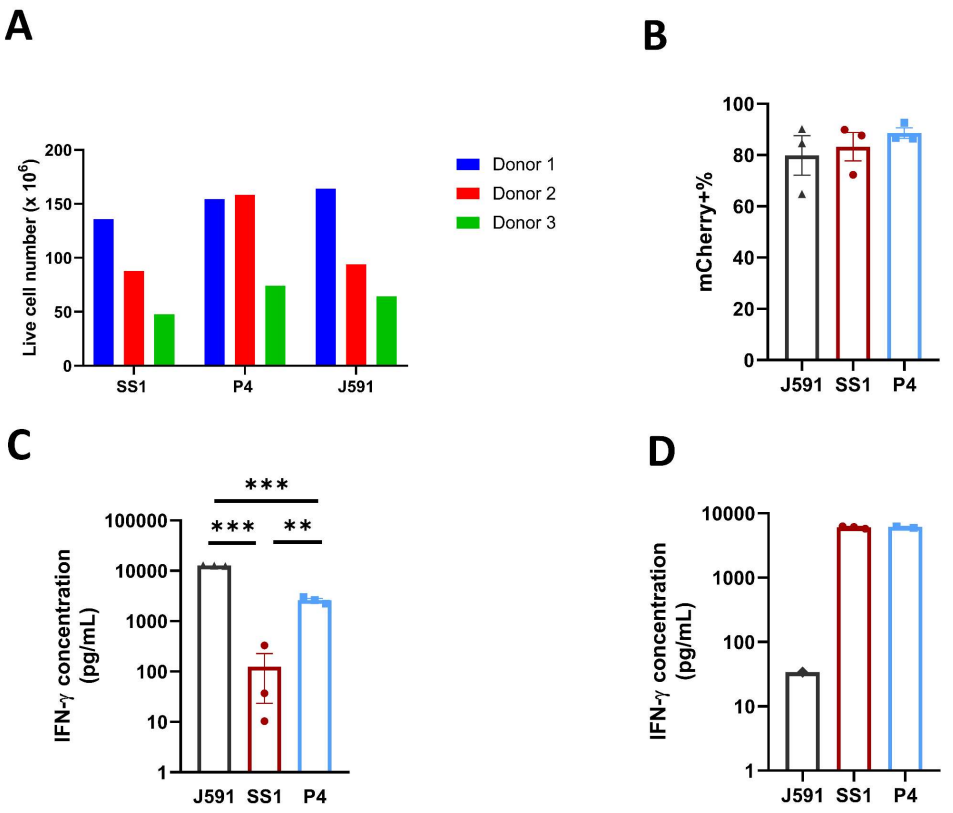

Supplementary Figure 1 Chimeric antigen receptor (CAR) T cell expansion and *in vitro* validation. CAR T cells were generated from peripheral blood mononuclear cells from three healthy independent donors. **(A)** Live cell number at the end of each CAR T cell expansion. **(B)** Transduction efficiency, assessed by mCherry expression, from each CAR T cell product. **(C)** Interferon-γ (IFN-γ) release assessed by CAR T cells co-cultured with the prostate cancer cell line LnCaP, which expresses prostate-specific membrane antigen. **(D)** IFN-γ release assessed by CAR T cells co-cultured with the mesothelin-transduced pancreatic cancer cell line MiaPaCa-2. Statistical testing was performed via repeated measures one-way ANOVA (matched based on CAR T cell donors) followed by Turkey's post hoc test for multiple comparisons, with significance indicated (**p < 0.01; ***p < 0.001).

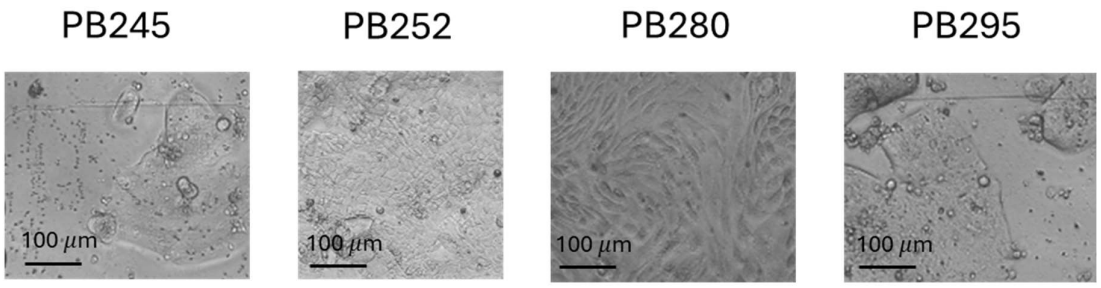

Supplementary Figure 2 Adherence of appendiceal cancer organoid-derived monolayer on the xCELLigence Real-Time Cell Analysis (RTCA) E-plate. Appendiceal cancer organoids were seeded as single cell suspensions in organoid culture media and incubated for 96 hours to allow for cell adherence as a monolayer. Organoid adherence was microscopically visualised. Scale bars were indicated.

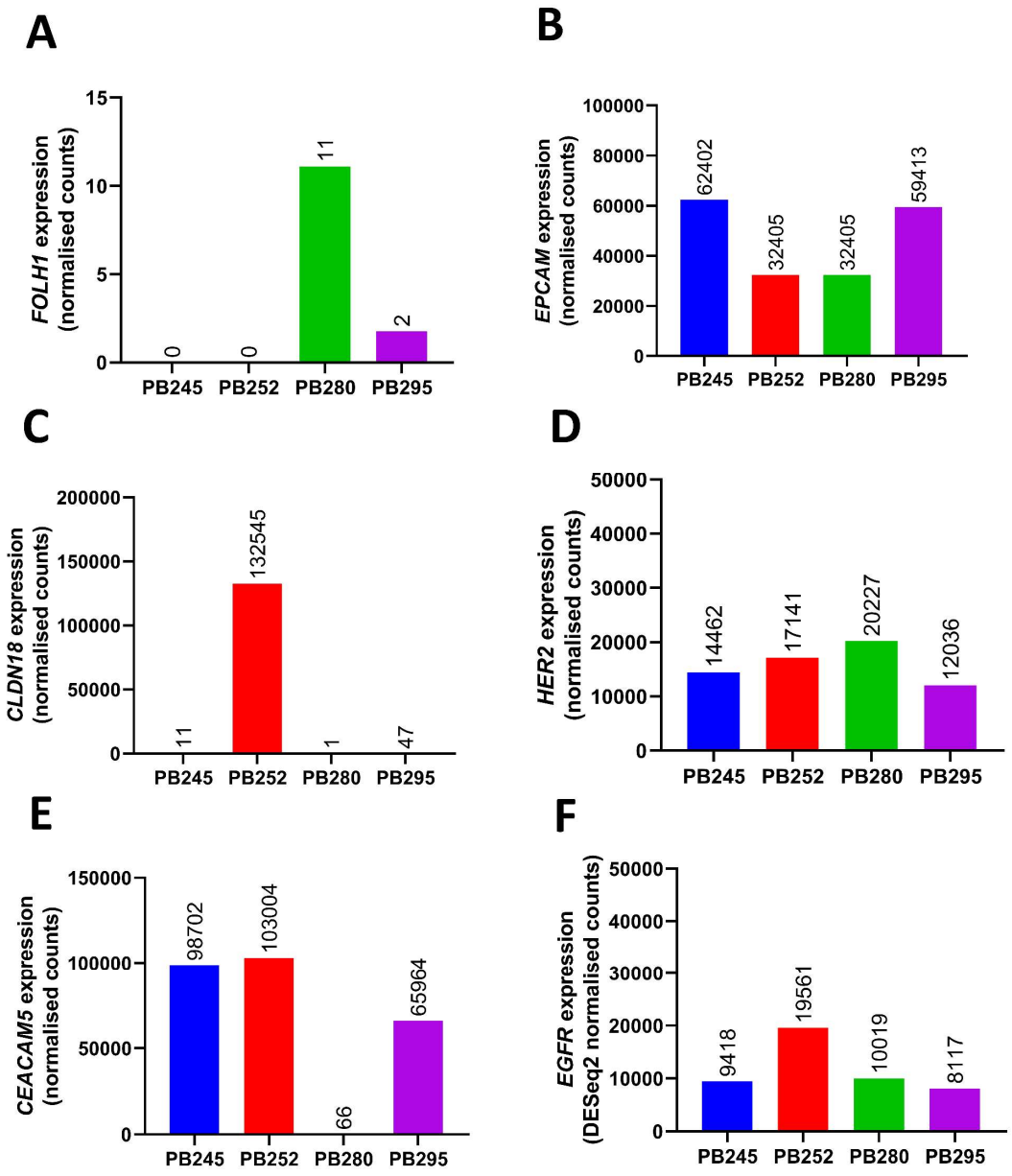

Supplementary Figure 3 Transcriptomic expression of tumour antigens in appendiceal cancer organoids. Expression of tumour antigens *FOLH1* (encodes PSMA) **(A)**, *EPCAM* **(B)**, *CLDN18* **(C)**, *HER2* **(D)**, *CEACAM5* **(E)**, and *EGFR* **(F)** were evaluated on appendiceal cancer PDOs via RNA-sequencing analysis. Normalised counts were quantified via DESeq2. PSMA, prostate-specific membrane antigen.